SURF ZONE PROPERTIES AND ON/OFFSHORE SEDIMENT TRANSPORT

By

Wei-Chong Yang and Hsiang Wang

Technical Report No. 12

Contract No. N00014-81-K-0297

with the Office of Naval Research, Geography Programs

RESEARCH REPORT CE-82-25

June 1982

Ocean Engineering Program

Department of Civil Engineering

University of Delaware

Newark, Delaware

19711

ABSTRACT

The surf zone properties and the on/offshore sediment transport rate were studied. A non-dimensional surf zone parameter was obtained by taking the ratio of natural swash period to wave period. This parameter, in addition to its wide application in describing the breaker types, was pertinent to describing the flow patterns in surf zone and defining the region of validity of the similarity solutions. A similarity model was applied to describe the flow field of breaking waves in surf zone. Laboratory results from other investigators and those obtained in the present study were used to test the validity of the proposed model. The results showed that if the wave was of the spilling type and in the region of $I_w > 0.9$ and $d/d_b < 0.6$, where I_w is the surf zone parameter defined as $I_w = \frac{H_b^{1/2}}{g^{1/2} T \tan\alpha}$, the similarity solution was suitable. A numerical model was presented to predict the on/offshore sediment transport rate. This model was based on a suspended load transport equation derived through the application of flow field and sediment suspension in surf zone. Due to limited knowledge of sediment suspension in surf zone, the present model is only able to predict the offshore transport rate. Several numerical

simulations were made to compare with the laboratory results of the author's and other investigators'. Fair to good agreement was observed.

TABLE OF CONTENTS

LIST OF FIGURES

LIST OF TABLES

NOTATION

A_o	Surface contact area of uprushing fluid element
a_n	n^{th} wave harmonic amplitude
a_ε	Constant controlling vertical profile of sediment concentration
b_n	Fourier constant ($b_n'/\overline{C}_c$)
b_n'	Fourier constant of sediment concentration
C	Wave celerity ($\sqrt{g(d+\bar{\eta})}$)
C_D	Drag coefficient
C_k	Constant controlling absolute value of sediment concentration
C_g	Wave group velocity
$\overline{C}_c$	Mean suspended sediment concentration
C_{max}	Maximum suspended sediment concentration
$C(t)$	Time function of suspended sediment concentration
$C_m(x)$	Sediment concentration measured at a reference point near bottom
$C_x(z)$	Vertical profile of sediment concentration

$C_x(z,t)$	Instantaneous sediment concentration in surf zone
c_p	Porosity factor
d	Still water depth
D_{50}	Median sediment grain size
E	Wave energy
$e_t(t)$	Turbulence energy density
f	Bottom frictional coefficient
g	Gravitational acceleration
h	Local water depth $(d+\bar{\eta})$
h_b	Breaking depth
h_i	Local water depth at i'th grid
H_b	Breaking wave height
H_c	Incident wave height
H_o	Deep water wave height
I_w	Non-dimensional surf zone parameter $\left(\frac{H_b^{1/2}}{g^{1/2}T\tan\alpha}\right)$
K	Proportional constant of swashing period $(K_1+K_2+K_3)$
K_1	Proportional constant of developing period
K_2	Proportional constant of uprushing period
K_3	Proportional constant of downwashing period
KE	Wave kinetic energy

k_1	Proportional constant of kinetic wave energy
k_2	Proportional constant of breaking wave energy
k_3	Proportional constant of potential wave energy
L	Wave length
L_o	Deep water wave length
M	Uprushing fluid element mass
$Q_x(t)$	Net sediment flux at a vertical water column
N^*	Number of waves in surf zone (T_n/T)
r	Reflection coefficient
R	Wave run-up height
Re	Reynolds number
s_1	Slope of potential energy line
s_2	Slope of total energy line
T	Wave period
T_n	Swash period
t_D	Fluid element traveling time at developing stage
t_d	Fluid element traveling time at downwashing stage
t_u	Fluid element traveling time at uprushing stage
t_h	Thickness of fluid element
t_n	Natural swash period

t'	Non-dimensional time (t/t_n)
$U(t)$	Horizontal fluid velocity in surf zone
$\overline{U}_R$	Mean return flow
V	Swash velocity of fluid element
V'	Non-dimensional velocity (V/V_o)
V_o	Initial uprush velocity at SWL
V_D	Fluid element velocity at developing stage
V_d	Fluid element velocity at downwash stage
V_u	Fluid element velocity at uprush stage
$V_{d(max)}$	Maximum downwash velocity at SWL
X	Fluid element traveling distance
X'	Non-dimensional distance (X/X_o)
X_o	Non-frictional traveling distance ($V^2/2g\sin\alpha$)
X_{max}	Maximum uprush distance
z_m	Reference coordinate of sediment concentration measurement
α	Beach slope angle
α_n	Wave harmonic amplitude coefficient
β	Bottom frictional factor ($\frac{fV_o^2}{4\pi g\sin\alpha}$)
β_n	Velocity harmonic amplitude coefficient
γ	Specific weight of fluid (ρg)

$\bar{\gamma}$	Mean of wave height to water depth ratio
ξ	Battjes' surf zone parameter
ξ_c	Incipient breaking criteria
ξ_b	Galvin's inshore parameter
ρ	Fluid density
ρ_s	Sediment density
ω	Particle falling velocity
κ	Breaking wave height to water depth ratio
η	Water elevation
$\bar{\eta}$	Wave set-up
σ	Fundamental wave frequency (2 /T)
ϵ	Kinematic eddy viscosity
τ	Bottom shear stress
$\sqrt{\tau/\rho}$	Shear velocity
λ_p	Void ratio
$\tan\alpha$	Beach slope
ϕ_n	n^{th} wave phase angle
ψ_n	n^{th} velocity phase angle
θ_n	n^{th} sediment concentration phase angle

CHAPTER 1

INTRODUCTION

The surf zone properties and the on/offshore sediment transport process were closely examined in this study to provide both theoretical and numerical predictions of breaking wave properties and sediment transport rate. The surf zone properties studied included the surf zone parameter and the breaking wave similarity. These properties were developed theoretically and calibrated with laboratory data. The laboratory experiments conducted included water elevation and mean horizontal velocity measurements of breaking waves and the instantaneous suspended sediment concentration measurements in surf zone. A numerical model was then developed based on the theoretical background to predict the on/offshore sediment transport rate.

In Chapter 2 a comprehensive review of all related previous works were presented; these included surf zone properties, on/offshore sediment transport process and a review of laboratory measuring techniques.

The theoretical background was introduced in Chapter 3. A non-dimensional surf zone parameter was developed first based on the swash mechanics of a single breaking wave. The physical implications of this parameter and its role in characterizing the breaking wave properties were discussed in detail. The breaking wave similarity, including the similar properties of water elevation and horizontal velocity, were developed based on the concept of harmonic transfer in shoaling waves. A sediment transport equation was developed based on the derived velocity field and empirical suspended sediment concentration. This transport equation was then applied to a numerical model for on/offshore sediment transport rate prediction.

The procedures and arrangements of laboratory experiments are discussed in Chapter 4. All tests were conducted in the wave tank located in the Civil Engineering Laboratory. Both plane and sand beaches were applied. There were 2 sets of tests conducted, including 10 runs of breaking wave similarity measurement and 4 runs of suspended sediment measurement. The air bubble releasing technique and photographic method were applied for velocity measurement and the Iowa Sediment Concentration Measuring System was used for suspended sediment measurement.

In Chapter 5 the results of analyzed laboratory data and the results of numerical prediction were presented. The technique of Fourier Analysis was applied to analyze the harmonic components of water elevation and horizontal velocity. The author's results were compared with the data from previous investigators and the region of applicability of similarity property were discussed. Spectral analysis and data averaging techniques were employed for suspended sediment study. The correlation of sediment concentration and breaking wave was studied based on the analyzed results of suspended sediment concentration and corresponding breaking wave property. Finally the simulated numerical results of the on/offshore sediment transport model were compared with the author's and the previous researchers' laboratory data. Sensitivity analysis and prototype simulation of the numerical model were also conducted.

Conclusions were presented in Chapter 6. It concluded the findings and the physical importance of theoretical, laboratory and numerical results of the surf zone properties and the on/offshore sediment transport process.

The measured water elevation and horizontal velocity data were presented in Appendix A in non-dimensional form. A theoretical analysis of the dynamics of air bubble in

unsteady wave field was presented in Appendix B to demonstrate the percentage error of the present velocity measuring technique. Appendix C summarized the field and laboratory results of suspended sediment concentration in surf zone. Both theoretical prediction and laboratory wave set-ups were shown in Appendix D. A list of computer program was presented in Appendix E.

CHAPTER 2

LITERATURE REVIEW

The previous research works in the fields of surf zone properties, on/offshore sediment transport, and laboratory measuring techniques were reviewed. The researchers who made important contributions were outlined and their findings were summarized. Among the research results, many empirical and experimental conclusions were found to be valuable towards the theoretical development of the present study. The following sections discuss the literature review in detail.

2.1 Surf Zone Properties

Due to the complicated nature of breaking wave induced turbulence in surf zone, few analytical solutions can be applied successfully in this region. However, many previous empirical formula and laboratory results indicated that there exist some important surf zone properties which would lead to a better understanding of the flow field in surf zone. The major surf zone properties include the flow pattern, the surf zone parameter, and the breaking wave

similarity. These properties are discussed in detail in the following sub-sections.

2.1.1 Flow Pattern in Surf Zone

The fluid flow in surf zone can be categorized into three conditions based on the degree of interference among breaking waves. Following Kemp (1968), the wave-beach relationship can be classified into three categories:

(1) Swash Condition: The broken wave is able to surge up to run up limit on beach and return as backwash to the breaking point before the succeeding wave had broken. The flow shoreward the breaker is distinctly oscillatory.

(2) Transition Condition: The backwash wave can not be completed before the next wave breaks. The condition involved interaction between the backwash wave and the next uprush wave, resulting in the interchange of water between the zones seaward and shoreward of breakers.

(3) Surf Condition: The transition flow give way to flow conditions in which successive lines of breakers continuously spills water into the surf zone, producing a seaward return flow.

The sequence of flow conditions is illustrated in Figure 2-1.

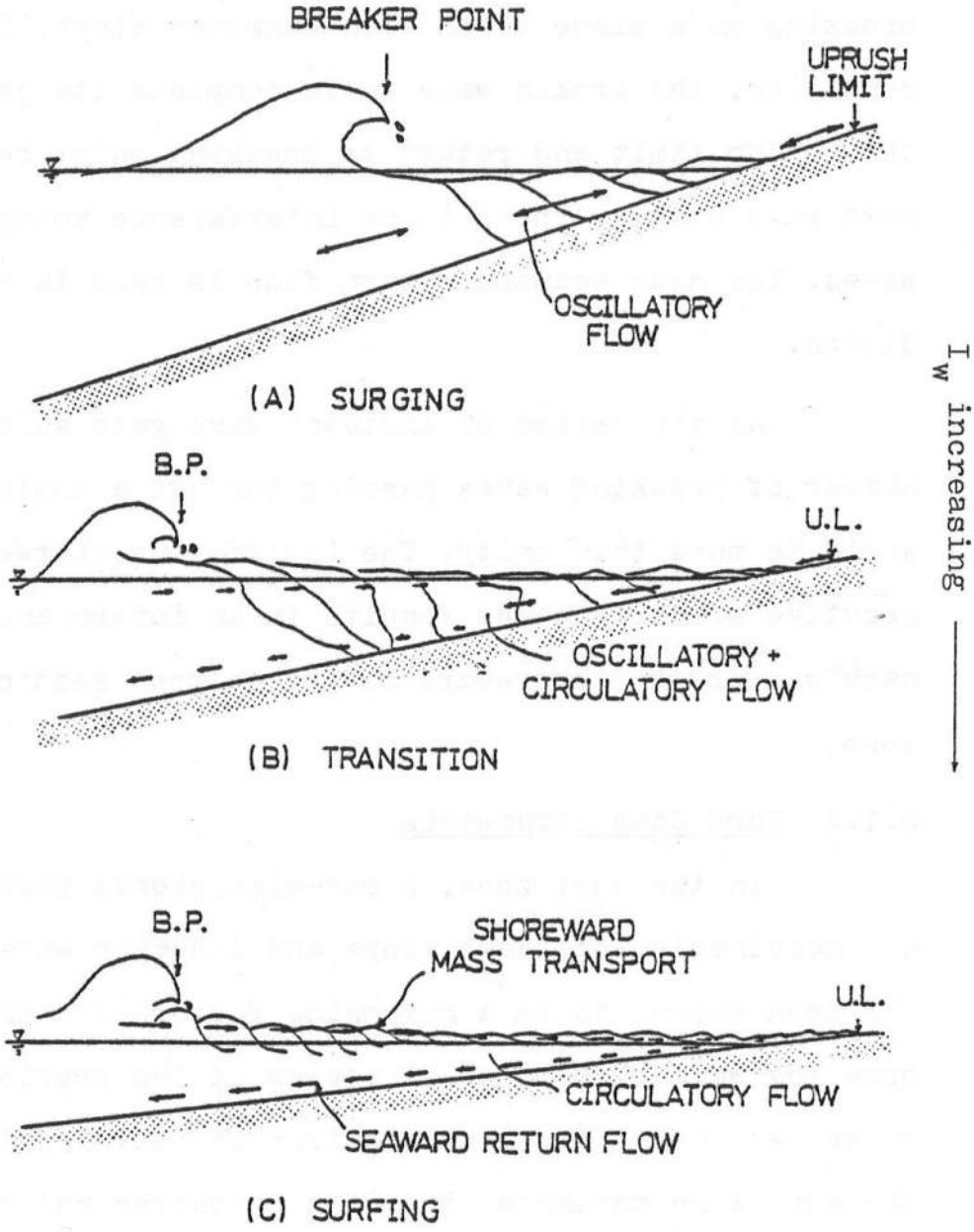

Figure 2-1 Breaker Classification Based on Surf Zone Parameter (I_w)

The degree of interference among breaking waves is also closely related to the flow pattern. Consider waves breaking on a plane beach with constant slope. During swash condition, the broken wave would complete its journey up to the run up limit and return to breaking point before the next wave breaks. There is no interference among breaking waves. The mean seaward return flow is zero in this condition.

As the period of incident wave gets shorter, the number of breaking waves passing through a control section would be more than unity. The interference between consecutive breaking waves results in an interchange of fluid mass seaward and shoreward of the control sections in surf zone.

2.1.2 Surf Zone Parameters

In the surf zone, a non-dimensional parameter, a combination of beach slope and incoming wave steepness has been shown to be a governing factor of characterizing breaking wave properties. A review of the previous related works was made. The investigators who developed and applied the surf zone parameter included Iribarren and Nogales, Hunt, Bowen et. al., Galvin, and Battjes. The various forms of the surf zone parameter proposed, how they were arrived at, and the breaking wave properties characterized by this parameter are summarized.

Iribarren and Nogales (1949) first used this parameter to determine whether wave breaking would occur. By applying the shallow water trochoidal theory for uniform, progressive waves, the condition of incipient breaking can be expressed as:

$$\frac{1}{2} H_c = d_c \qquad (2\text{-}1)$$

where H_c is the incident wave height, d_c is the still water depth, and "c" denotes the incipient breaking. The depth at breaking was expressed as:

$$d_c = \frac{1}{8} L_c \tan\alpha_c \qquad (2\text{-}2)$$

where L_c is the breaking wave length expressed as $L_c = T_c\sqrt{gd_c}$ and $\tan\alpha_c$ is the beach slope, T_c is the wave period. Therefore,

$$d_c = \frac{1}{8} T_c \sqrt{g d_c}\, \tan\alpha_c \qquad (2\text{-}3)$$

Elimination of d_c between (2-1) and (2-3) gives

$$\left(T\sqrt{\frac{g}{H}}\tan\alpha\right)_c = 4\sqrt{2} \qquad (2\text{-}4)$$

Substituting $L_o = \frac{gT^2}{2\pi}$ in (2-4) where L_o is the deep water wave length and rearranging gives

$$\xi_c = \left(\frac{\tan\alpha}{\sqrt{H/L_o}}\right)_c = \frac{4}{\sqrt{\pi}} \approx 2.3 \qquad (2\text{-}5)$$

The derivation given by Iribarren and Nogales suggested that the incipient breaking of periodic waves correspond to a critical value of the proposed surf zone parameter defined in Equation (2-5).

Hunt (1959) suggested that the wave run-up height is proportional to the surf zone parameter. By defining the run-up height "R" as the maximum elevation of the waterline above the undisturbed water level, he proposed the empirical theory for the run-up height of waves breaking on a smooth slope as:

$$\frac{R}{C_p H_o} = \frac{\tan\alpha}{(H_o/L_o)^{1/2}} \; ; \quad 0.1 < \frac{\tan\alpha}{(H_o/L_o)^{1/2}} < 2.3 \qquad (2\text{-}6)$$

where C_p is a porosity factor, approximately 1 for solid beaches, H_o is the deep water wave height, and L_o is the deep water wave length. This empirical formula was proved to be in good agreement with the observed laboratory results by Bowen et. al. (1968).

In addition to wave run-up, Bowen et. al. (1968) further pointed out that the maximum set-up is also governed by the surf zone parameter. The experimental results summarized by them indicated that the mean of the ratio of wave height to water depth in the surf zone ($\bar{\gamma}$) is a function of the surf zone parameter. Since the coefficient of proportionality of wave set-up is a function of $\bar{\gamma}$,

the maximum height of wave set-up is governed by the surf zone parameter.

Galvin (1968, 1972) proposed that the transition ranges of the main breaker types are also characterized by the surf zone parameter. By introducing the "Offshore Parameter", $H_o/(L_o \tan^2\alpha)$, the transition values separating the main breaker types were given:

Surging or Collapsing	if	$H_o/(L_o \tan^2\alpha) > 4.8$
Plunging	if	$0.09 < H_o/(L_o \tan^2\alpha) < 4.8$ (2-7)
Spilling	if	$H_o/(L_o \tan^2\alpha) < 0.09$

The "Inshore Parameter", $H_b/(gT^2 \tan\alpha)$, presented by Galvin is not equivalent to the surf zone parameter. However, a re-analysis of Galvin's data in terms of $\xi_b = \tan\alpha/(H_b/L_o)^{1/2}$ by Battjes (1974) showed that the classification of breaker types could be performed equally well with ξ_b as with Galvin's inshore parameter. The following approximate transition values were found:

Surging or Collapsing	if	$\xi_b > 2.0$
Plunging	if	$0.4 < \xi_b < 2.0$ (2-8)
Spilling	if	$\xi_b < 0.4$

Battjes (1974) re-derived this surf zone parameter through dimensional analysis and summarized all breaking wave properties characterized by this parameter. The

derivation was based on the flow parameters of a periodic, long-crested wave approaching a rigid, plane, impermeable beach. The motion of this periodic wave on beach was determined by a dimensionless dependent variable as:

$$\chi = f(\alpha, \frac{H}{L_o}, \frac{d}{L_o}, Re) \qquad (2\text{-}9)$$

where α is the beach slope angle, H is the incident wave height at the toe of the beach slope, d is the still water depth, L_o is the deep water wave length and Re is a typical Reynolds Number.

For breaking waves, the values of Reynolds Number and relative depth would not significantly affect the resultant motion. Therefore, he concluded that for many overall properties of breaking waves the dependent variables were reduced to:

$$\chi = f(\xi) \quad \text{or} \quad \chi = f(\xi_b) \qquad (2\text{-}10)$$

where $\xi = \frac{\tan\alpha}{(H_o/L_o)^{1/2}}$ and $\xi_b = \frac{\tan\alpha}{(H_b/L_o)^{1/2}}$

The characteristic values of the surf zone parameter corresponding to the overall properties of breaking waves in surf zone was summarized by him as shown in Table 2-1. Also, Battjes suggested that ξ^{-1} was approximately proportional to the number of wave lengths within surf zone.

In summary, the previously developed surf zone parameters were arrived empirically or through physical

Table 2-1 Summary of Breaking Wave Properties Based on Surf Zone Parameter

ξ	0.1	0.5	1.0	2.0	3.0	4.0	5.0
	breaking						no breaking
	spilling		plunging		collapsing/surging		
H_b/d_b	0.8	1.0	1.1	1.2			
N^*	6-7	2-3	1-2	0-1	0-1		
r	10^{-3}	10^{-2}	10^{-1}	4×10^{-1}	8×10^{-1}		
	absorption					reflection	
	progressive wave					standing wave	
	wave set-up predominant			wave run-up predominant			
*	high wave interference			no wave interference			
*	circulatory flow			oscillatory flow			
*	surf similarity exists						

Notes: ξ : Surf Zone Parameter Defined by Battjes
N* : Number of Waves in Surf Zone
r : Reflection Coefficient (Reflected Wave/Incident Wave)
* : Additional Properties Recommended by Author

modeling. Although presented in different forms, this parameter can be generalized as a ratio of the beach slope to the square root of the incident wave steepness. The breaking wave properties proved to be characterized by the surf zone parameter included the breaking wave criterion, the breaker type, the relative importance of wave run-up and set-up, the breaker height-to-depth ratio, the number of waves in surf zone, and the reflection coefficient on beach.

2.1.3 Breaking Wave Similarity

When a wave moves into shoaling water, it will grow in wave height until the water depth is shallow enough to initiation of breaking. The assumption made for a shoaling wave is that there is no loss of energy and no reflection. It is assumed that the wave period remains constant in water of any depth, whereas the wave length, velocity and height vary. A realistic wave form is better described by non-linear wave theories. For a single frequency laboratory wave shoaling on beach, its energy would be transformed from primary to higher harmonics.

It was shown by Flick (1978) that the transfer is well described by third order Stokes theory that conserves energy flux as long as the local Ursell Number remains less than 1. Depending upon the breaker type, more or less energy relative to the primary is transferred to the higher

harmonics in the shoaling process before breaking. The amplitude dispersion among harmonics together with phase lag due to differential shoaling of each harmonic component result in a highly asymmetric wave form upon wave breaking.

After wave breaking, the broken wave at seaward limit of surf zone remain asymmetric. This asymmetric property is a result of relative importance of higher harmonic amplitude and the introduction of harmonic phase due to wave breaking. The shape of a breaking wave is determined by the relative harmonic amplitudes and harmonic phases.

Flick (1978) measured the breaking wave height and made the harmonic analysis as well. It was shown that the harmonic amplitudes as well as the spilling wave heights decay at a constant rate with local water depth as shown in Figure 2-2. The result of harmonic analysis by Flick implies that the non-dimensional ratio of breaking wave height to local water depth is bearing a similar shape.

During shoaling process, the transfer of wave energy to higher harmonic components also introduces an asymmetric velocity profile. The corresponding asymmetric velocity profile was evidenced by Iwagaki (1970) and Flick (1978) as shown in Figures 2-3 and 2-4.

The bottom friction during breaking process plays an important role in energy dissipation. For higher harmonic

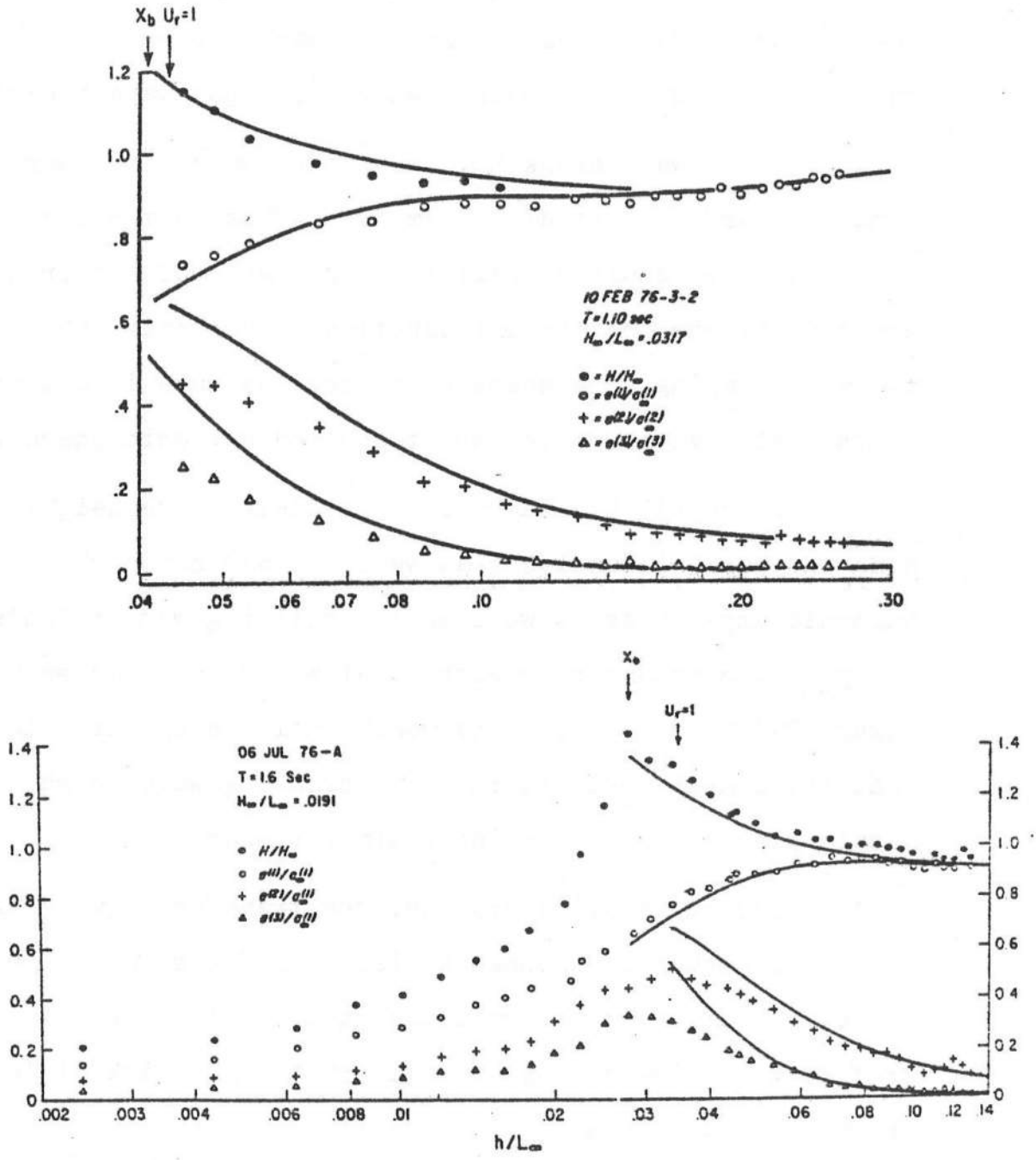

Figure 2-2 Harmonic Wave Height Decay as a Function of Local Water Depth after Flick (1978)

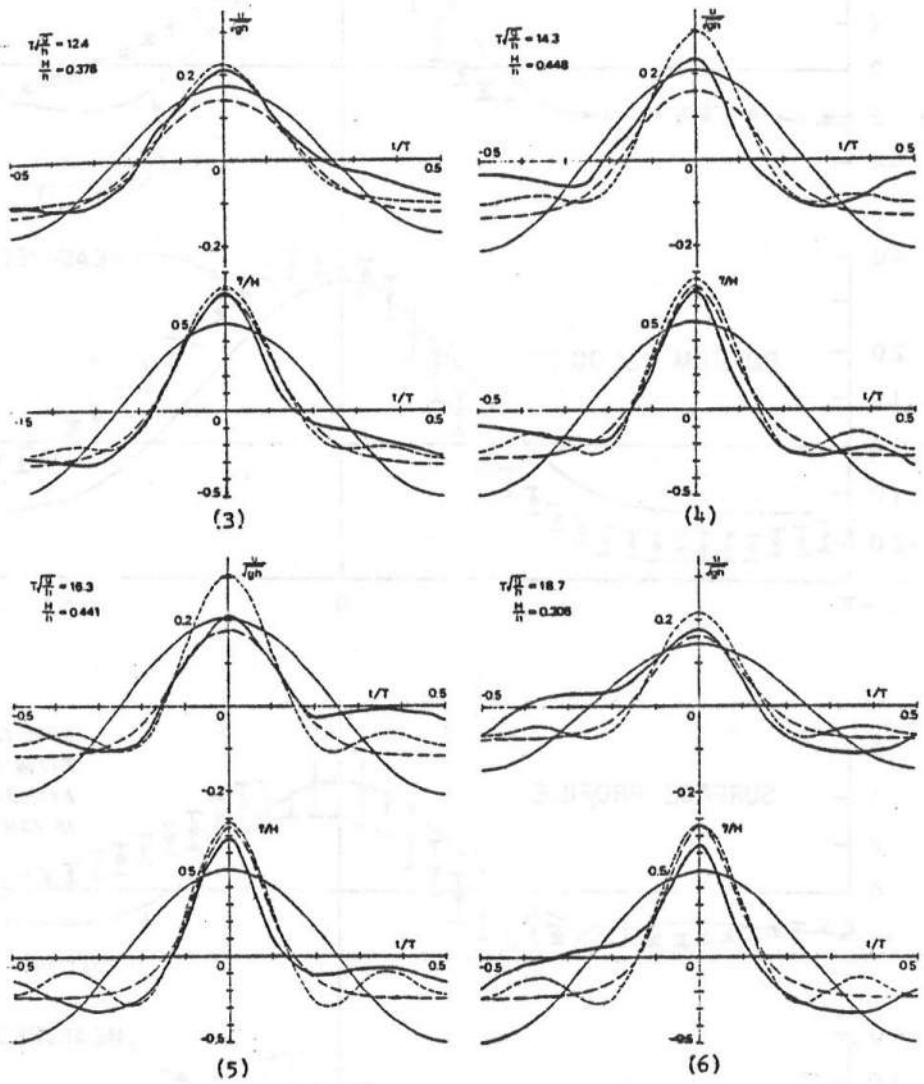

Note; $U/\sqrt{gh}$: non-dimensional horizontal velocity

η/H : non-dimensional water elevation

Figure 2-3 Asymmetric Water Elevation and Horizontal Velocity Profiles by Iwagaki (1970)

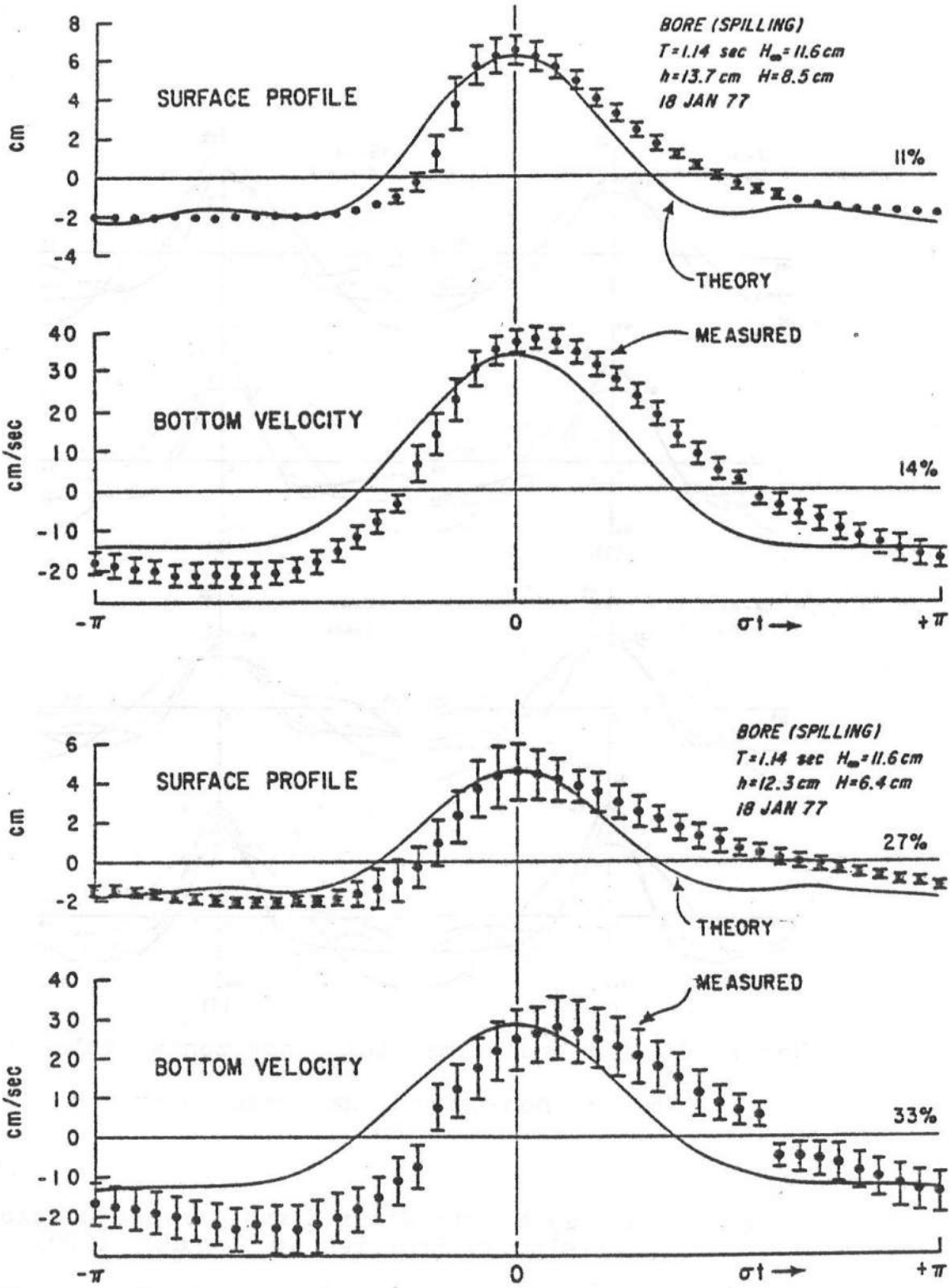

Figure 2-4 Asymmetric Water Elevation and Horizontal Velocity Profiles by Flick (1978)

velocity components with high oscillating frequency, the frictional dissipation is greater, resulting in less energy content in the higher harmonics. The smaller contribution of higher harmonic components results in a relatively more symmetric velocity profile than the corresponding wave profile.

Laboratory and field observations by Flick (1978) and Thornton (1976) both suggested that the shape of the horizontal velocity profile is more symmetric than the shape of the corresponding wave profile. Also, there exists a time lag between the velocity and wave profile.

2.2 On/offshore Sediment Transport

Sediment transport is the movement of sediment due to the interactions of sediment with wave, current, tide, wind and other causative forces in the surf zone. The direction of the sediment movement can be alongshore or on/offshore, which are known as longshore transport and on/offshore sediment transport, respectively.

The knowledge of on/offshore sediment transport criteria, transport mechanisms and modes, and the response of various beach materials is essential for the understanding of transport process. Previous laboratory experiments, field studies, and numerical models have provided some qualitative as well as quantitative results and empirical formula in describing the on/offshore transport

process. These works are discussed in the following sub-sections.

2.2.1 On/offshore Transport Criteria

It is well known that the seasonal variations of beach profiles are associated with seasonal variations in wave climate. Specifically, the idealized winter or storm profile is characterized by a mild foreshore slope and the presence of an offshore sand bar. The idealized summer or normal profile is of steeper foreshore slope and no offshore bar is present. These typical summer and winter profiles are illustrated in Figure 2-5. The transition of summer and winter profiles indicates the transition of on/offshore transport direction.

Laboratory measurements indicated that the wave steepness transition between summer and winter profiles is approximately 0.025. Field observations also suggested that the variation of profiles are due to the seasonal changes in deep water wave steepness defined as H_o/L_o. Saville (1957) noted that for large scale tests, steepness smaller than 0.025 may result in a storm profile too. Iwagaki and Noda (1962) found that the ratio of wave height to sand grain size was also an important parameter. Dean (1973) related the on/offshore transport criteria to both the deep water wave steepness and the sediment falling velocity.

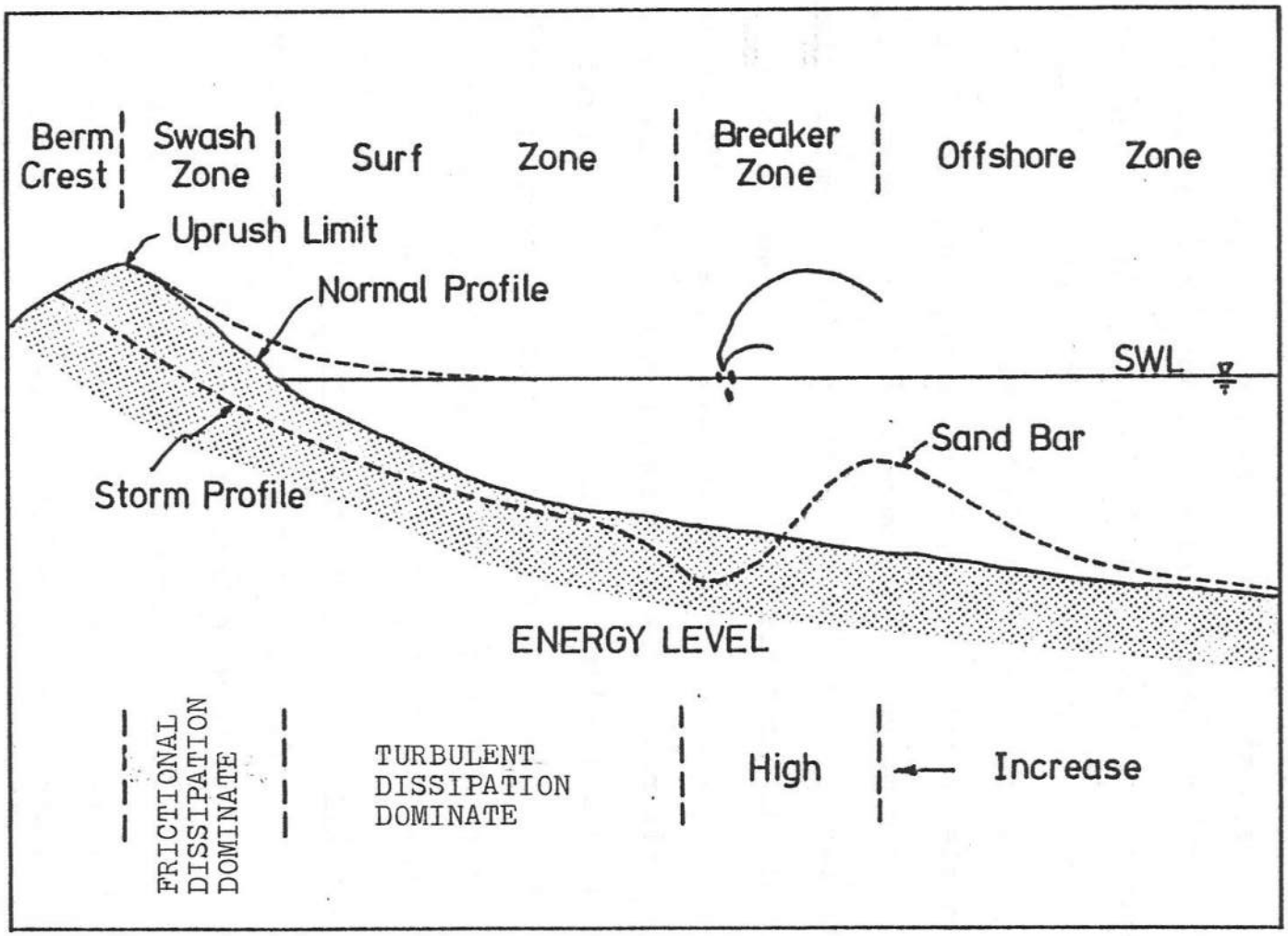

Figure 2-5 Typical Summer and Winter Profiles and the Definition of Energy Regions on Beach

In his transport model, Dean (1973) assumed that the action of breaking waves is sufficient to place sand into suspension over at least a portion of the water column. After the suspension phase, and during the return of the sediment particle to the bottom, the direction of net horizontal displacement depends on whether the sand particle is acted upon predominantly by onshore or offshore fluid particle velocities. If, on the other hand, the fall time is long compared to the wave period, the predominant sediment particle is directed offshore. The classification of normal and storm profiles proposed by Dean is shown in Figure 2-6. In an attempt to relate the on/offshore transport criteria to the surf zone parameter I_w, the author also compiled a similar normal and storm profiles classification curve as shown in Figure 2-7. It can be seen that the surf zone parameter also plays an important role in characterizing the on/offshore transport criteria.

2.2.2 Modes and Mechanism of Transport

Sediment on beach can be moved on/offshore by bottom friction due to wave induced bottom fluid particle velocity and/or on/offshore currents. Once the sediment is loosened by fluid particle, it can be transported on or offshore in the dominant force direction. This mode of sediment movement is usually called bed load transport.

Eagleson et. al. (1963) proposed a "null point"

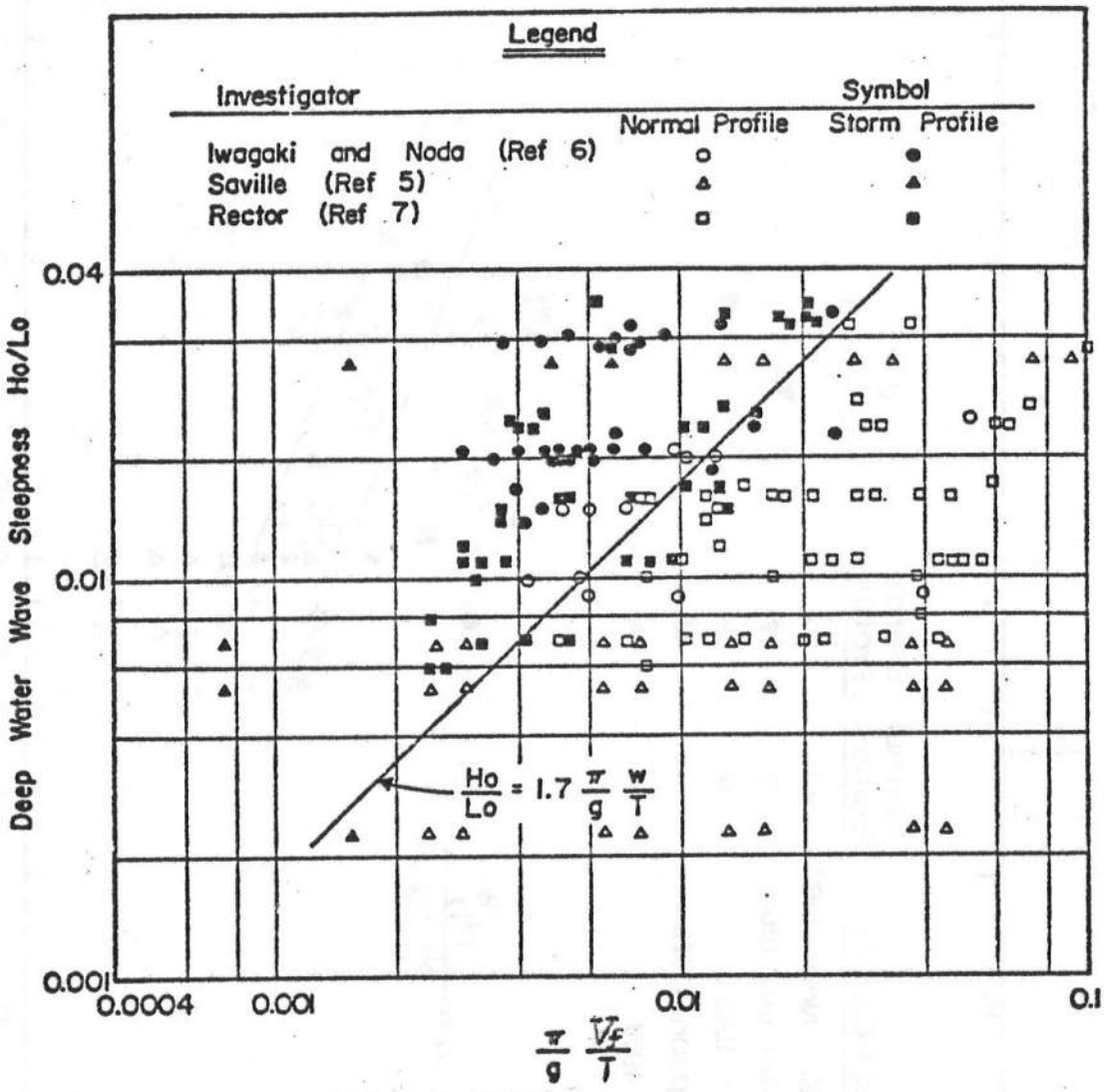

Figure 2-6 Classification of Normal and Storm Beach Profiles by Dean (1973)

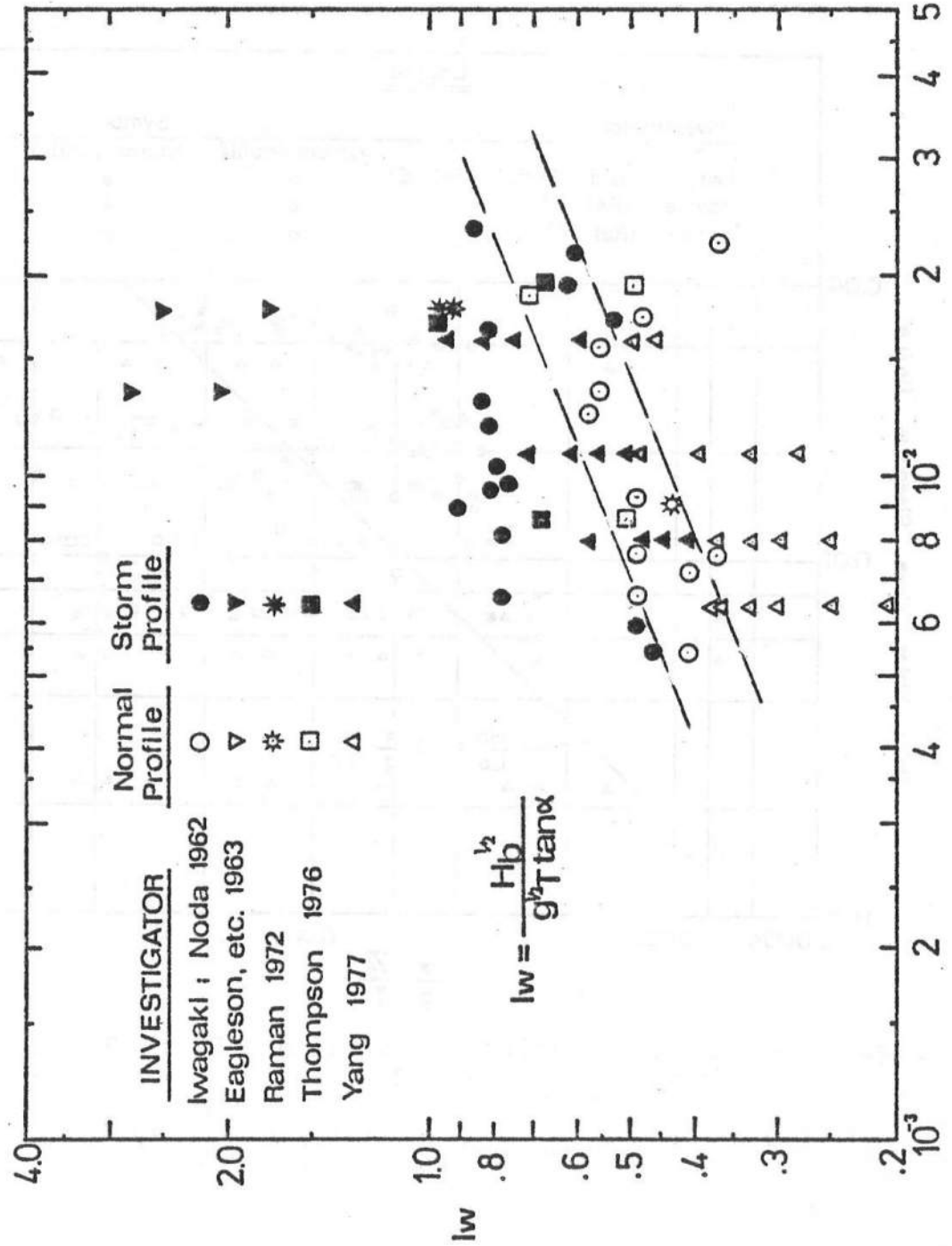

Figure 2-7 Classification of Normal and Storm beach profiles

analysis which involved the estimation of lift, drag and inertial forces on uniform sand size of spherical shape. The null point represents a balance point between wave forces and gravity. Shorewards of this point the sediments move onshore whereas seaward of it sediment moves offshore. This null point analysis renders no practical value, since the particles are actually irregular in shape.

Another mechanism of wave induced sediment motion can be explained by the asymmetric bottom shear stress due to the asymmetric fluid velocity field. The net on/offshore thrust would result in a net shoreward/seaward movement of sediments.

Sediments can also be carried on/offshore by currents as suspended load. This mode of transport includes the dynamic processes of sediment entrainment and transportation. The entrainment process requires force-producing near bottom fluid velocities and accelerations in excess of some threshold value, while transportation processes require the sediment particle moves with the fluid. This process can be approximated where the sediments are small enough to be in the Stokes range of settling with settling velocity Reynolds Number less than 1.

The major sediment carrying mechanism of suspended load transport is nearshore current. It was pointed out by Longuet-Higgins (1953) and Ippen (1966) that when waves

are approaching a straight and parallel shoreline, the continuity of mass necessitates a vertical distribution of mass transport foreward at the surface and near bottom, return flow near mid-depth before wave breaking. There were considerable laboratory evidences supporting the two-dimensional nearshore circulation model as illustrated in Figure 2-8(a). In breaker zone, the two-dimensional flow field can be described as oscillatory, transition and circulatory conditions. During circulatory flow condition the growing strength of near bottom return flow combined with sediment suspension due to breaking turbulence results in suspended load in offshore direction.

In the field, the near-shore current field is never restricted in two-dimensional. A longshore variation of energy density and/or an irregular nearshore bottom topography would induce high-energy concentrated rip currents.

Bowen (1969) developed a theoretical model using the concept of radiation stress. A three-dimensional nearshore circulation model was proposed by Shepard and Inman (1951) as shown in Figure 2-8(b). It was emphasized that the rips play a major role in carrying the suspended sediment further out of the offshore submarine bar.

2.2.3 Beach Materials

Sediment transport is the combined result of flow field in the nearshore region and the dynamic response of

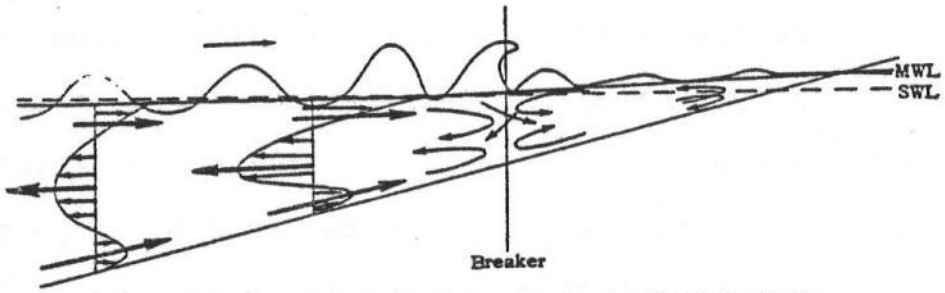

(a) Nearshore circulation pattern—two-dimensional case.

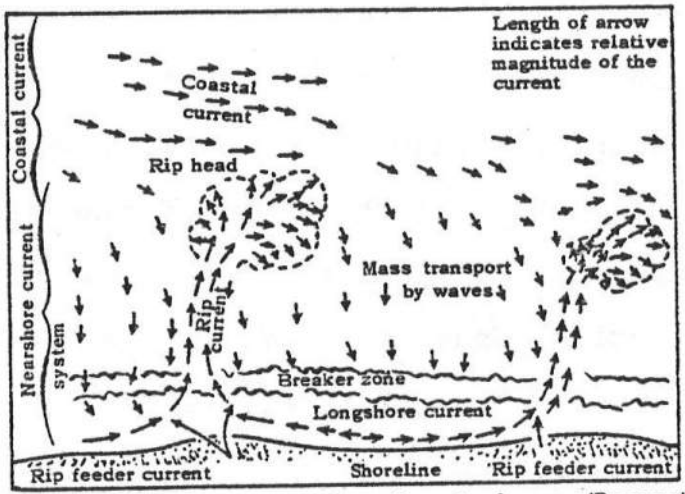

(b) Nearshore circulation pattern-three-dimensional case. (By permission from Shepard and Inman, Proc. First Conf. on Coastal Eng., Council on Wave Research, Berkeley, Calif., 1951.)

Figure 2-8 Two- and Three-dimensional Nearshore Circulation Model After Ippen(1966)

beach materials, therefore, the physical characteristics of beach materials also play an important role in the sediment transport process.

The properties of beach materials include their size, density, shape, and permeability. Large materials such as shingle and gravel is gradually rolled along the bottom. Finer material such as sand can be moved by suspension. The physical characteristics of sand important to its transport process are the grain size distribution, the submerged density in sea water, and the sphericity and roundness of grains. These three properties can be combined into one important physical parameter known as the particle falling velocity .

Dean (1973) suggested that this parameter is vital for on/offshore transport criteria. Sunamura and Horikawa (1974) indicated that the ratio of sand size to wave length is an important physical parameter controlling sand beach transportation. Under the same deep water wave condition and initial beach slope, their laboratory results showed erosion for beach with fine grain size and accretion for beach with coarse grain size.

2.2.4 Numerical Modeling

The knowledge of on/offshore transport rate as well as the beach profile evolution is essential for predicting the short term beach changes such as daily variation of

beach profile, the response under extreme wave condition, and the time needed to recover the eroded foreshore berm crest. It is also useful to other coastal engineering problems including beach nourishment, seawall design, etc.

In an attempt to model the on/offshore sediment transport process, the model developed should have the following capabilities to be qualified as "good" models (Dally and Dean, 1980) :

(1) Generate profiles of both the normal and storm types depending on the wave conditions and sediment characteristics.
(2) Predict the proper shape of these profiles; i.e., (a) the normal profile should be monotonic and concave upwards and (b) the bar of the storm profile should have the proper spacing and shape.
(3) Correctly predict the rate of profile evolution.
(4) Respond to changes in water level due to tides, storm surges, or long-term fluctuations.
(5) Approach an equilibrium if all the relevant parameters are held constant.

There has been plenty of information published on beach profiles, and a great number of studies undertaken to predict the condition for bar formation and profile erosion or accretion. However, there is still a lack of a good model

for prediction of profile evolution and rates of shoreline erosion, although there have been a few good models that were developed for limited use which require both calibration for each use and large data base for statistical analysis.

Fox and Davis (1973) assumed an arbitrary form for the beach profile and manipulated its coefficients empirically to change the bottom with time. The model requires substantial atmospheric data to calibrate and is extremely site specific, although they achieved good results. Swart (1974) developed a transport model which represents the sediment movement from the inshore region to the offshore region in a gross sense. The beach is divided into two horizontal layers with continuity being satisfied between the two. Suspended sediment transport is the dominant mechanism and the model can be adapted to various wave and sediment characteristics. Wang, Dalrymple and Shiau (1975) modeled sediment transport by dividing the nearshore region at the breaker line. Inside the surf zone, a gross longshore transport is proportioned across the region with the shape of the longshore current determined by Longuet-Higgins. Outside the surf zone, transport is determined by superimposing an exponential sediment concentration profile onto a mean flow profile, which gives good results for regions far from the breaker line.

Fleming and Hunt (1976), using both bed load and suspended load mechanics, formulated a three-dimensional transport model for a specific beach segment. Profile changes were caused by deviations in the longshore current much like the model by Wang et. al., (1975). Kana(1979) measured sediment concentration under fully plunging breakers on a stable monotonic beach. In the model, the nearshore region is artificially divided into sections where the transport is governed by different equations. The transport inside surf zone is coupled to the transport calculated just outside the breaker line using Wang's model which is valid only in regions far from the surf zone. The model does approach a state of equilibrium and is applicable to various sediments and wave characteristics which makes it attractive.

Winant, et. al. (1975) described the variability in a beach profile by means of empirical eigenfunctions with good results. However, the model is independent of wave and sediment characteristics, and, because it is a statistical method it requires a large data base for any site of interest used. Dean (1973) developed a heuristic model for the prediction of the presence or absence of bars which compared favorably with laboratory data. It does not describe beach profile evolution but does propose a realistic mechanism of suspended sediment transport in the surf

zone.

Dally and Dean (1980) developed a realistically based suspended sediment transport model for the surf zone and the nearshore region. The horizontal velocities responsible for sediment transport were found to be the first-order sinusoidal component and the second-order mean flow developed from radiation stress considerations. An exponential concentration profile governed by turbulent and wave-induced shear stress was developed and the net suspended sediment flux was found by integrating the product of the velocity and concentration profiles over depth. The results indicated reasonable quantitative and good qualitative agreement with experimental data.

2.3 Review of Laboratory Measuring Techniques

A review of the laboratory measuring experiences by former researchers was found helpful due to the extensive laboratory work in this study. In the following sub-sections the experimental techniques and apparatus involving water elevation, fluid velocity, and suspended sediment concentration measurements are discussed.

2.3.1 Water Elevation Measurement

In general, the surface water elevation measurement includes the using of capacitance and resistance type wave probe, pressure sensor and sonar system wave gauge. The pressure sensor and sonar system wave gauge are widely used

in the field study. They are not frequently adapted in the laboratory except for large wave tanks where big waves can be generated.

The capacitance and resistance wave probes are very commonly used in the wave flumes. The convenience of the probe is that they are more sensitive to small surface water disturbances, even in the capillary wave range. The wave probe is usually a thin steel rod which does not interfere the flow field significantly.

For surf zone measurement, some problems arise in the accuracy of output from these two types of wave probes. The turbulent water may splash on the wave probe causing an irregular peak on the output voltage. Also, the capillary force of water on probe will result in a mean water line drift. To avoid these sources of error, the photographic method offers a better solution, although it is more costly and time consuming.

2.3.2 Velocity Measurement

Velocity measurement is more complicated than the water elevation measurement, especially in the turbulent flow. In general, there are five types of measuring techniques being used with successful results. The instruments include propeller current meters, photographic method, hot film anemometers, ultrasonic doppler current meters and laser anemometer.

The propeller current meters are commonly used to measure quasi-steady flows. There are some differences in using them in the laboratory wave tanks because of its low dynamic response to high fluctuations. Besides, they are usually not very sensitive to low speed steady flow as pointed out by Goda (1964).

With photographic methods, the water particle motion can be clearly visualized with tracers such as neutrally buoyant particles or hydrogen bubble. The water particle velocity can be measured frame by frame with the aid of a high speed movie camera and a slow motion movie projector.

Although the newly improved hot film and hot wire anemometer can be operated in the water as well as in the air, it is still a sophisticated instrument. Its inconveniences include frequent failure of probe head due to overheating, zero velocity drift due to fluid temperature change and accumulation of dirty material on the sensor. It can not detect the flow direction when the velocity vector is in the plane perpendicular to the hot film axis. The draw backs also include the strong non-linearity in the correlation between the flow speed and the output voltage when the flow speed varies over a wide range and also the film is sensitive to flows that are parallel to the film axis.

Ultrasonic doppler current meter and laser doppler anemometers are most recently developed techniques.

Researchers such as Tsuchiya and Yamaguchi (1972), Lee et. al. (1974) had reported them as good instrument for periodic and random waves velocity measurement. However, they are still in a developing stage.

2.3.3 Suspended Sediment Measurement

Earlier researchers in the field of suspended sediment study were handicapped bythe lack of suitable measuring equipment. Shinohara, Tsubaki and Yoshitaki (1958) did some pioneering work in this field. Using a syphon type sediment sampler in a laboratory tank, they obtained a series of measurements of vertical distribution of the mean sediment concentration.

A very useful and simple technique for measuring the suspended sediment concentration in water was introduced by Hom-ma and Horikawa(1963). By utilizing a light source and light sensor placed at the two sides of a 10-cm wide glass wall wave tank, they measured the mean concentration and time-variztion of concentration in a wave period.

Hattori(1969) used an electrical resistance type instrument to count the number of sediment particles passing through a given section and from this he calculated the suspended sediment concentrations. Bhattacharya (1971) used an electro-optical instrument for in-situ measurements of sediment in suspension. The instrument was developed at the Iowa Institute of Hydraulic Research and is called Iowa

Sediment Concentration Measuring System (ISCMS).

CHAPTER 3

THEORETICAL FORMULATION

Two basic surf zone properties, the surf zone parameter and the breaking wave similarity, were developed theoretically in this chapter. The derivation of empirical formula and their physical implications were discussed in detail. Based on the theoretical background, a transport equation was developed for use in the on/offshore sediment transport model. Details of numerical modeling technique was also discussed.

3.1 Surf Zone Parameter

Consider a single long-crested wave breaking on a beach of constant slope, say, $\tan\alpha$, the cyclic breaking process can be approximately divided into three stages as illustrated in Figure 3-1. The developing stage include the period when the wave begins incipient breaking at the crest until it collapses on the beach in the vicinity of the water level unit. During this stage, the shape of the wave evolves from highly asymmetric curled form to a triangular form with numerous white caps. Its potential energy is converted into kinetic energy which in term is partially dissipated

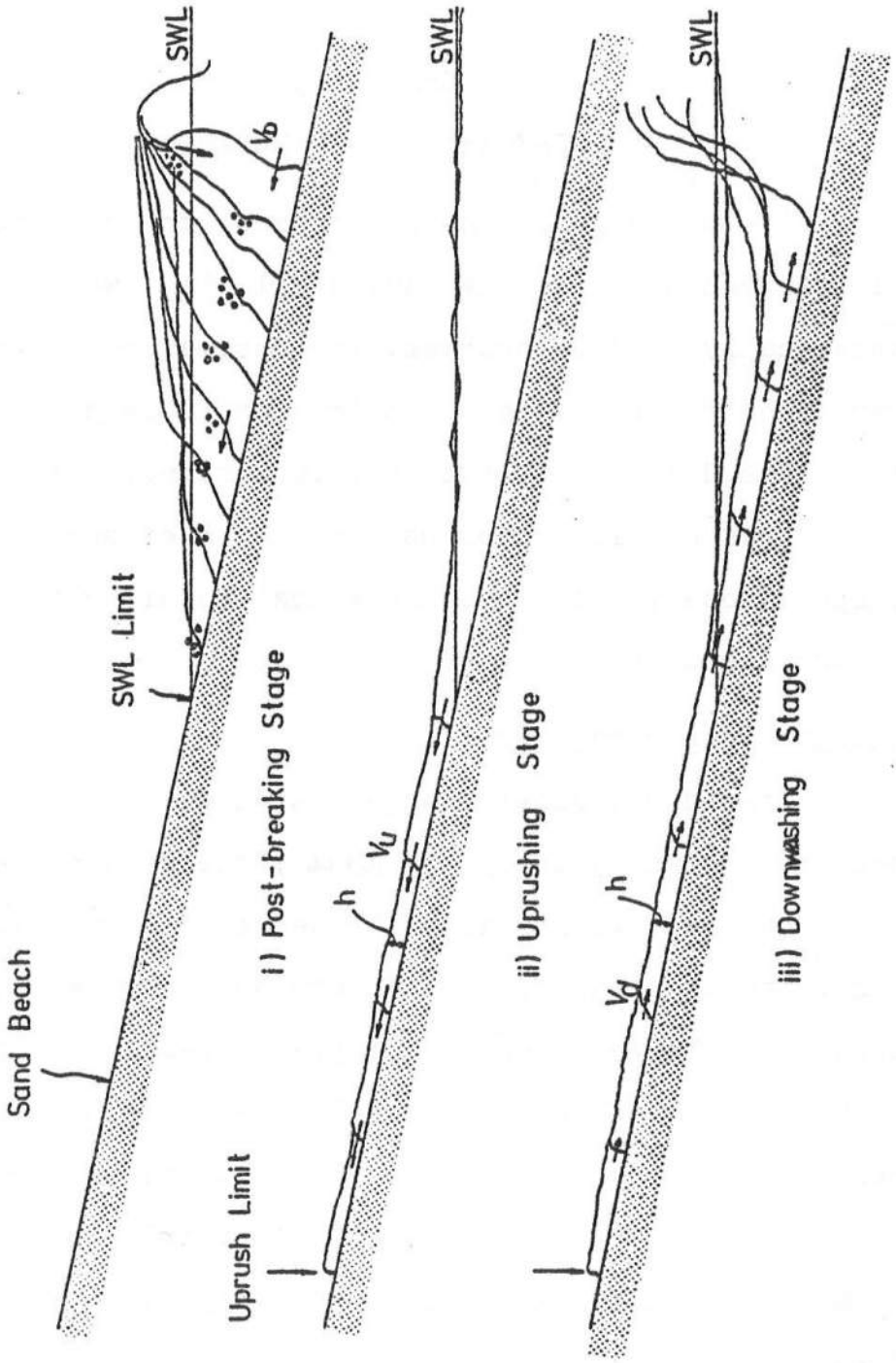

Figure 3-1 Illustration of Breaking Process

as the remaining portion preserved to stage the uprush.

In the second stage, the flow surges up to its runup limit similar to a solid element moving upslope while the kinetic energy is being converted back to potential energy. In the last stage, the flow washes down as a thin sheet to the breaking point to complete the cycle.

The time to complete each respective stage can be estimated based upon a simple energy model shown in Figure 3-2. This energy model is based on the premise that the fluid element at the crest of the wave during breaking remains at the crest and is the same element that reaches the runup limit. This condition is clearly observed from recorded slow-motion films.

If the kinetic energy of the fluid element at the wave crest at the breaking point is assumed to be proportional to the breaking height, say $k_1 H_b$, then the kinetic energy in the developing stage can be expressed as

$$KE(x) = k_1 H_b + (S_2 - S_1)x \qquad (3\text{-}1)$$

where S_2 and S_1 are the slopes of the total energy line and potential energy line, respectively. The velocity of the fluid element is

$$V_0(x) = \sqrt{2g\left[k_1 H_b + (S_2 - S_1)x\right]} \qquad (3\text{-}2)$$

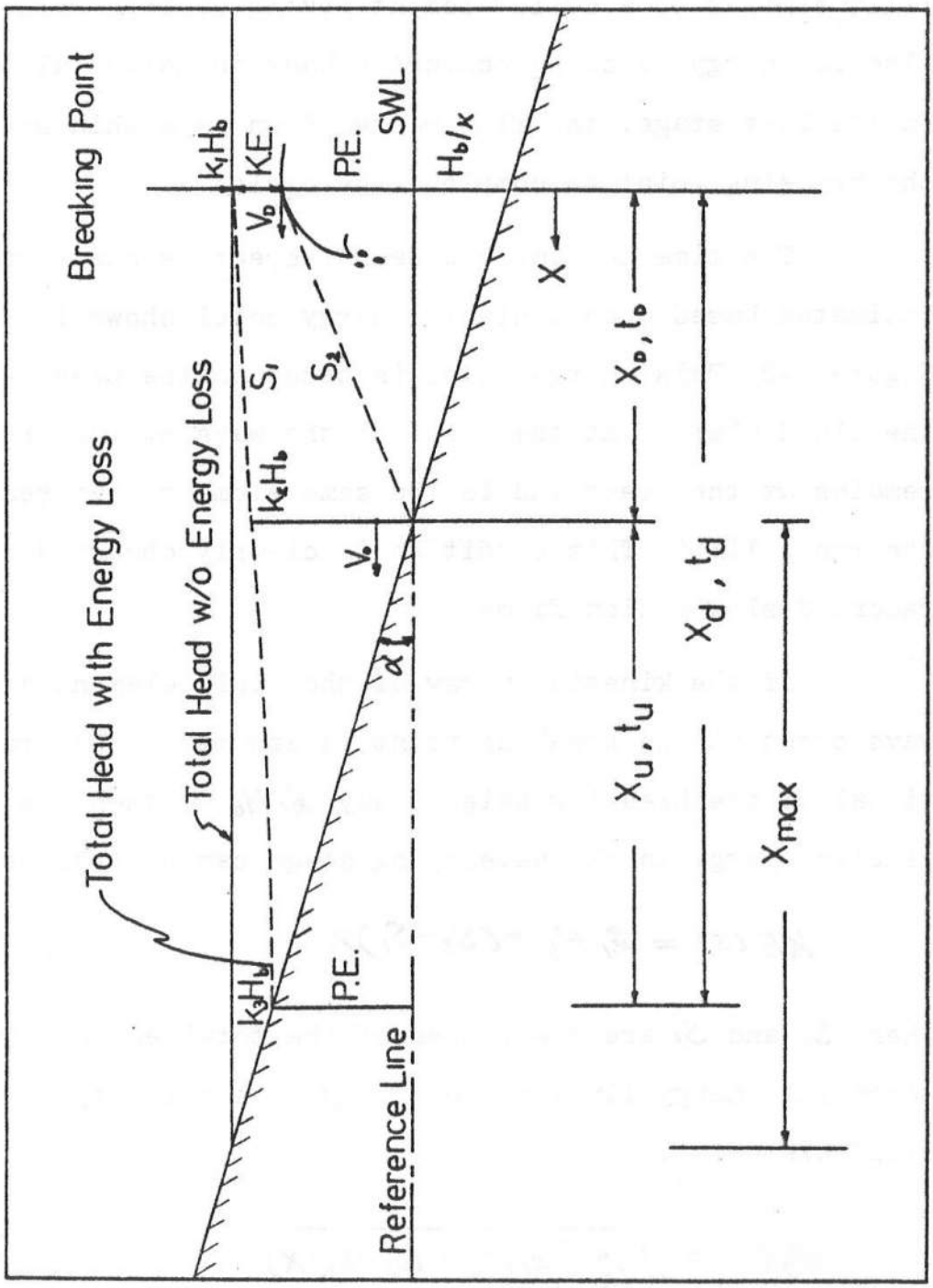

Figure 3-2 Energy Consideration of Breaking Wave

where $S_2 - S_1 = k(k_2 - k_1)\tan\alpha$ and the corresponding time required for the element traveling from the breaking point to the water level limit is

$$t_D = \int_0^{x_D} \frac{dx}{V_0(x)} = \frac{\sqrt{2}\,(\sqrt{k_2'} - \sqrt{k_1'})}{k(k_2 - k_1)} \cdot \frac{H_b^{1/2}}{g^{1/2}\tan\alpha} \qquad (3\text{-}3)$$

where k_2 and k are constants of proportionality as defined in Figure 3-2.

During the uprush and downwash stages, the crest element can be treated as a solid body moving on a sloped plan. In such cases, we have the following relationship on the basis of Newton's second law:

$$\mp Mg\sin\alpha - \rho f A_0 \frac{V|V|}{8} = M\frac{dV}{dt} \qquad (3\text{-}4)$$

where f is a frictional coefficient and A_0 is the contact surface area; the "-" sign corresponds to the uprush condition and the "+" sign the downwash case. If we let $M = \rho t_h A_0$, the above equation simplifies to

$$\mp g\sin\alpha - \rho f \frac{V|V|}{8 t_h} = \frac{dV}{dt}$$

where t_h is the thickness of the runup water sheet.

The free swash period in the region between the still water limit and the runup limit can be obtained by integrating Equation 3-5 without the friction term, $\rho f \frac{V|V|}{8 t_h}$,

which yields,

$$t_n = \frac{2V_0}{g \sin\alpha} \tag{3-6}$$

where V_0 is the initial uprushing velocity at the still water limit. By letting $t' = t/t_n$ and $V' = V/V_0$, Equation (3-5) can be non-dimensionalized as

$$\frac{dV'}{dt'} = \mp 2 - \beta |V'| V' \tag{3-7}$$

where $\beta = \frac{f V_0^2}{4 t_n g \sin\alpha}$

Equation (3-7) can be integrated to obtain the uprush and downwash periods which are, respectively,

$$t_u = \left(2\sqrt{\frac{k_2}{\beta}} \tan^{-1}\sqrt{\frac{\beta}{2}}\right) \frac{H_b^{1/2}}{g^{1/2} \tan\alpha} \tag{3-8}$$

and

$$t_d = 2\sqrt{\frac{k_2}{\beta}} \, EXP\left(\frac{\beta}{4} \cdot \frac{k_3 + k_2}{k_2}\right) \frac{H_b^{1/2}}{g^{1/2} \tan\alpha} \tag{3-9}$$

where we assume $\sin\alpha \approx \tan\alpha$ for mild beach slope and K_3 is a runup coefficient as shown in Figure 3-2.

Based upon Equations (3-3), (3-8), (3-9), the swash period of a single wave can be determined:

$$T_n = K \frac{H_b^{1/2}}{g^{1/2} \tan\alpha} \tag{3-10}$$

where $K = K_1 + K_2 + K_3$

with

$$K_1 = \frac{\sqrt{2}\left(\sqrt{k_2'} - \sqrt{k_1'}\right)}{k\left(k_2 - k_1\right)}$$

$$K_2 = 2\sqrt{\frac{k_2'}{\beta}}\tan^{-1}\sqrt{\frac{\beta}{2}}$$

$$K_3 = 2\sqrt{\frac{k_2'}{\beta}}\,EXP\left(\frac{\beta}{4}\,\frac{k_3 + \frac{1}{k}}{k_2}\right)$$

Therefore, the natural swash period is found to be a function of $\frac{H_b^{1/2}}{g^{1/2}\tan\alpha}$.

To obtain the numerical results of natural swash period, the friction coefficient β and the proportional constants K, K_1, K_2, K_3 were evaluated. The friction coefficient, β, by definition, is a function of the bottom frictional factor, the initial uprushing velocity, the fluid element thickness and the beach slope. For a typical breaking wave, V_0 = 8.0 fps, t_h = 0.3 ft, $\sin\alpha$ =0.05, and assuming f = 0.06, the typical friction coefficient is 2.0. To investigate the effect of bottom friction, Equation (3-7) was integrated in the swashing region from Sea Water Level to Uprush Limit. The equations obtained for analysis are:

Uprush

$$V' = 1 - \sqrt{\frac{2}{\beta}}\tan\left(2\sqrt{\frac{\beta}{2}}\,t'\right) \qquad (3\text{-}11)$$

$$V'^2 = -\frac{2}{\beta} + \left(1 + \frac{2}{\beta}\right)EXP\left[-\frac{\beta}{2}x'\right] \qquad (3\text{-}12)$$

Downwash

$$V' = -\sqrt{\frac{2}{\beta}} \tanh\left[2\sqrt{\frac{\beta}{2}}(t' - t'_{max})\right] \qquad (3\text{-}13)$$

$$V'^2 = \frac{2}{\beta}\left\{1 - EXP\left[-\frac{\beta}{2}(x'_{max} - x')\right]\right\} \qquad (3\text{-}14)$$

The non-dimensional period, velocity, and distance are defined as:

$$t' = t/t_n \;,\; V' = V/V_0 \;,\; \text{and } x' = x/x_0$$

where $x_0 = V_0^2/2g\sin\alpha$, X_{max} is the maximum uprush distance and $(V_d)_{max}$ is the downwash velocity at Sea Water Level. The non-dimensional swash period, velocity and distance are plotted against a wide range of the friction coefficient as shown in Figure 3-3.

Figure 3-3 indicated that all three quantities are decreasing with increasing bottom friction effect. Compared with the Friction-free condition, the swash period of the typical breaking wave (β = 2.0) is reduced to 83%, the downwashing velocity at Sea Water Level is reduced to 71% and the maximum uprush distance is reduced to 69%. The Eulerian swash velocities both without friction and with β = 2.0 are shown in Figure 3-4. The fluctuating velocity vectors at each station are assumed to be a cosine function. It can be seen that the downwash velocity is lower in strength than the uprush velocity if there is bottom friction. The Lagrangian swash velocities for β = 0 to 10

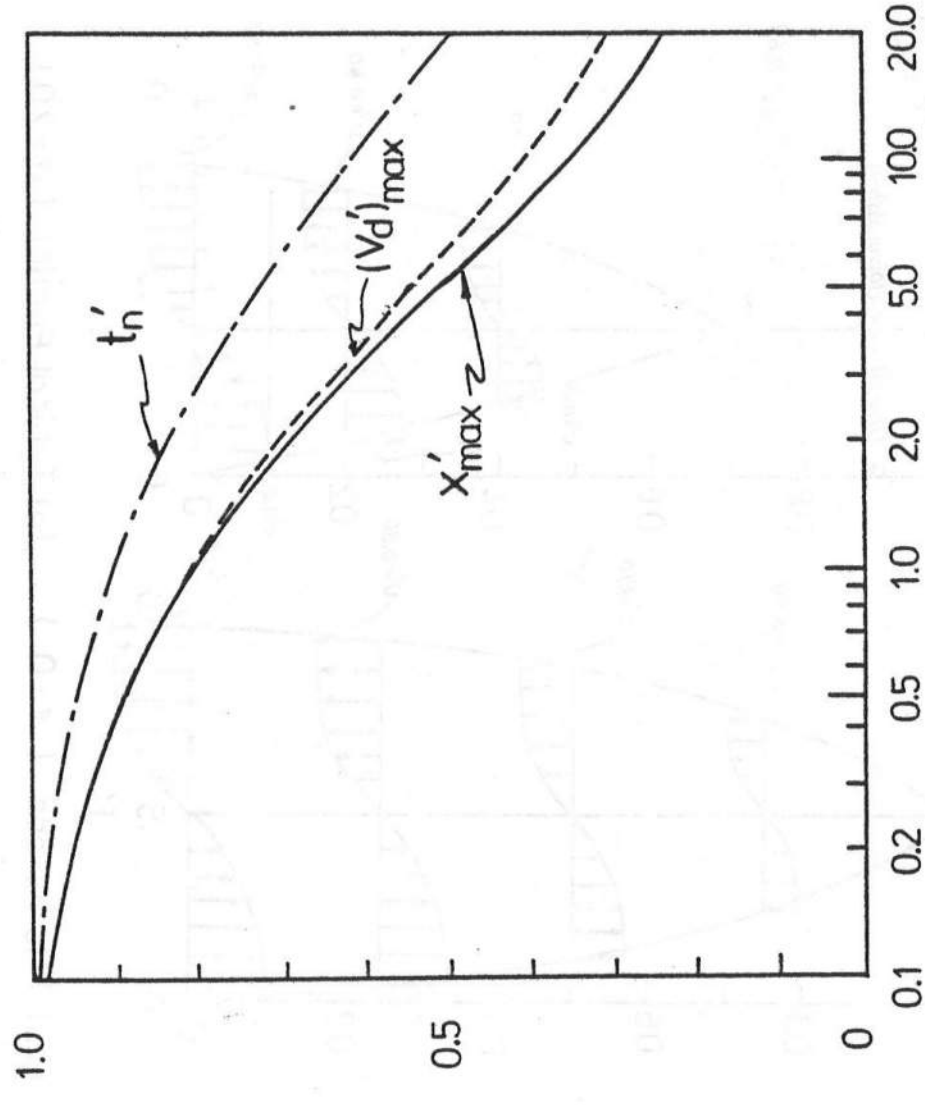

Figure 3-3 Non-dimensional Swash Period, Velocity and Distance vs. β

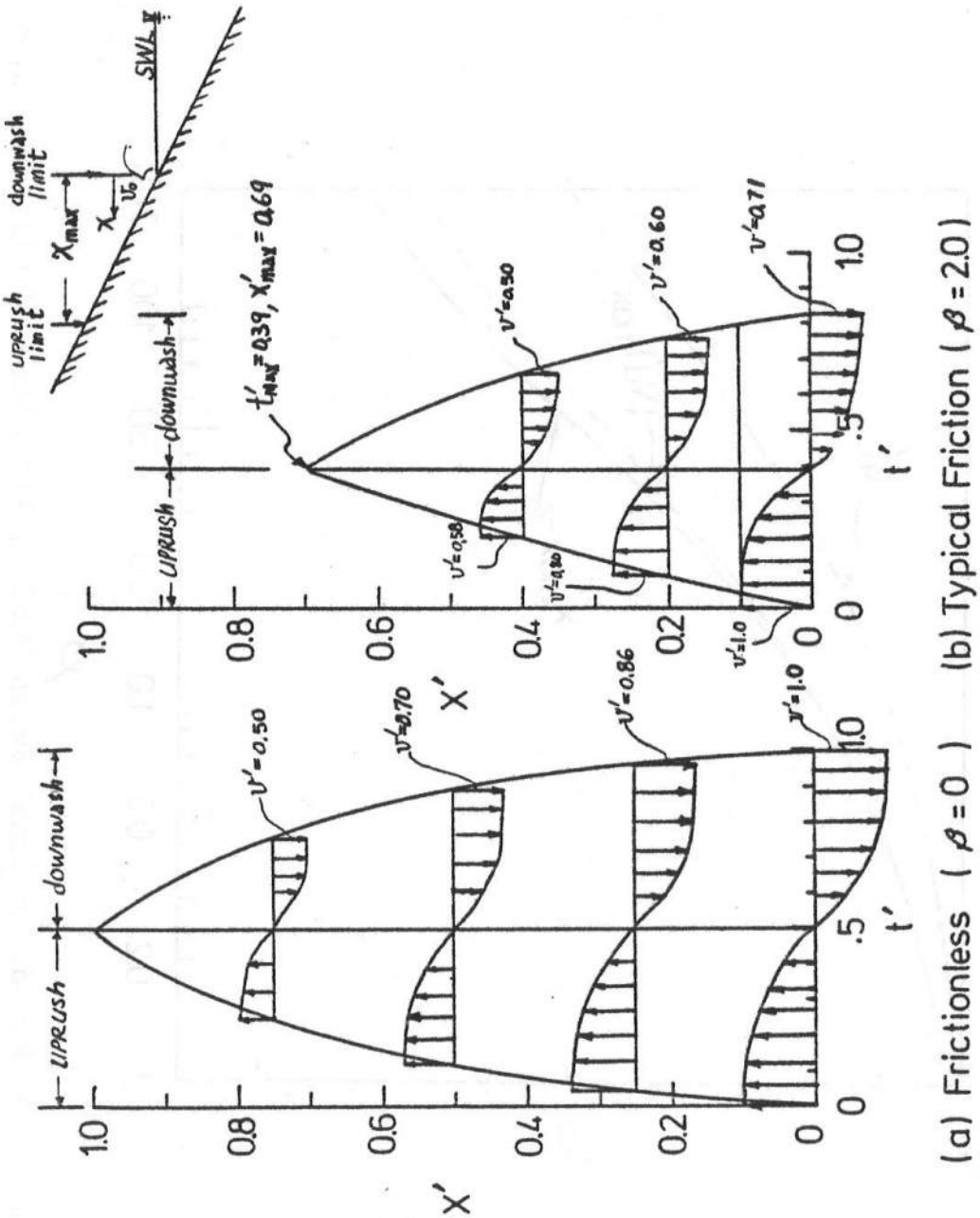

(a) Frictionless ($\beta = 0$) (b) Typical Friction ($\beta = 2.0$)

Figure 3-4 Eulerian Swash Velocity

are shown in Figure 3-5.

The proportional constants were evaluated based on a typical plunging breaker. The constant K_1 is 1.64 for the typical wave height-to-depth ratio, K = 1.0, and the typical crest elevation to height ratio is 0.75. The breaking wave height to depth ratio is the average value of 12 typical laboratory plunging breakers conducted on sand beach as summarized on Table 3-1.

The proportional constants K_2 and K_3 are related with the following equation:

$$K_2 = \frac{K_3}{4}\left(\frac{1}{\sqrt{\beta'}}\tan^{-1}\sqrt{\frac{\beta'}{2}} - \frac{1}{\beta}\ln\left|\sec\tan^{-1}\sqrt{\frac{\beta'}{2}}\right|\right)^{-1} \qquad (3\text{-}15)$$

This equation was derived based on the uprushing equations and the energy model shown in Figure 3-2.

The maximum runups on sand beach of 12 typical plunging breakers are also shown On Table 3-1. The results indicated that the average maximum runup to breaking wave height ratio, K_3, is 1.40. Since the sand beach was well compacted and fully saturated during experiment, the effect of bottom percolation was neglected. Based on the definition of friction coefficient and the knowledge of the proportional constants, the swash coefficients in Equation (3-11) were evaluated for β ranging from 0.1 to 2.5, which is the maximum frictional range of plunging breaker.

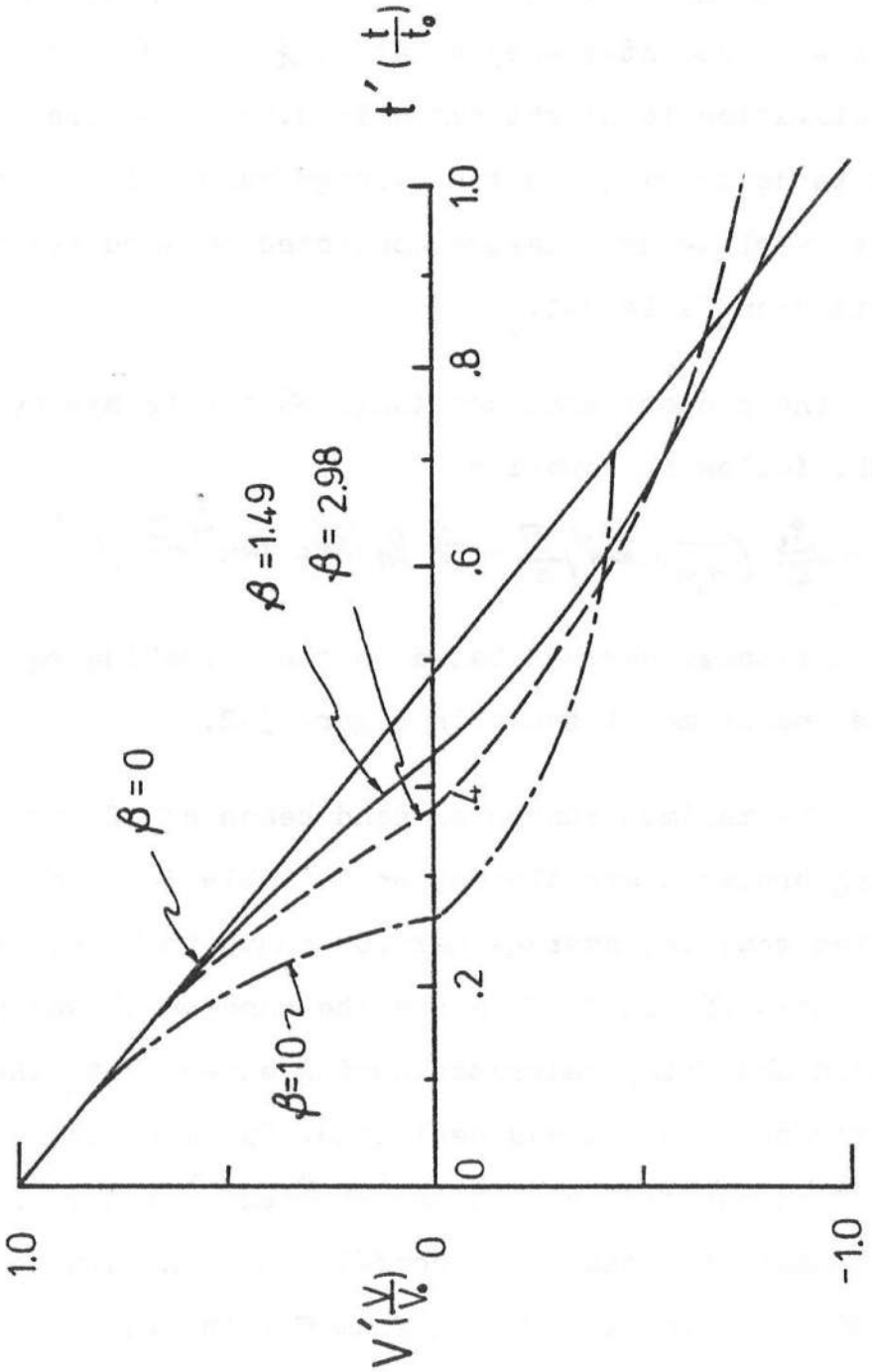

Figure 3-5 Lagrangian Swash Velocity vs. β

Table 3-1 Laboratory Experiments[1] of Maximum Runups

Run No	T (sec)	H_b (cm)	d_b (cm)	R_{max}[2] (cm)	$\tan\alpha$[3]	I_w	$\frac{H_b}{d_b}$	$\frac{R_{max}}{H_b}$
1	0.8	2.0	1.9	2.5	0.19	0.30	1.05	1.25
2	0.8	2.5	2.5	3.0	0.20	0.32	1.00	1.20
3	1.2	2.2	2.0	3.6	0.22	0.18	1.10	1.64
4	1.2	3.3	3.5	4.1	0.21	0.23	0.94	1.24
5	1.2	4.6	4.5	5.3	0.18	0.32	1.02	1.15
6	1.6	4.1	4.0	6.5	0.19	0.21	1.03	1.59
7	1.6	4.5	4.7	7.0	0.17	0.25	0.96	1.56
8	1.6	5.8	5.6	8.5	0.16	0.30	1.04	1.47
9	1.6	7.5	7.8	10.0	0.16	0.34	0.96	1.33
10	2.0	7.0	7.2	10.7	0.20	0.21	0.97	1.53
11	2.0	8.0	8.1	11.6	0.20	0.23	0.98	1.45
12	2.0	11.5	11.5	16.0	0.21	0.26	1.00	1.39
					Average:	0.26	1.00	1.40

Notes:

(1) Conducted in Civil Engineering Lab. wave tank with sand beach
(2) Maximum runup measured vertically from SWL to uprush limit
(3) average foreshore slope

The numerical swash coefficients are shown on Table 3-2 and plotted against β as shown in Figure 3-6. The results indicate that with increasing bottom friction effect, the uprushing period decreases and the downwashing period increases, while the breaking period and the total natural swashing period remain unchanged. The average swashing constant, K, is 4.81. The numerical results imply that the total natural swash period of a plunging breaker is primarily a function of breaking wave height and beach slope, if the bottom percolation effect can be neglected.

Having evaluated the swash coefficients, we now define a non-dimensional surf zone parameter as the ratio of natural swash period to the incoming wave period (T) :

$$I_w = \frac{T_n}{KT} = \frac{H_b^{1/2}}{g^{1/2} T \tan\alpha} \qquad (3\text{-}16)$$

This non-dimensional parameter is similar to Equation (2-10), the general formula of previously proposed parameter, with the following relation:

$$I_w = \frac{1}{\sqrt{2\pi}} \left(\frac{H_b}{H}\right)^{1/2} \xi^{-1}$$

$$\text{or,} \quad I_w = \frac{1}{\sqrt{2\pi}} \xi_b^{-1} \qquad (3\text{-}17)$$

where H is the wave height at the toe of sloping beach and H_b is the breaking wave height.

Table 3-2 Swash Coefficients

β	0.10	0.20	0.40	0.50	0.70	0.90	1.10	1.40	1.60	1.80	2.10	2.30	2.50
K_2	1.40	1.42	1.44	1.46	1.48	1.50	1.52	1.54	1.56	1.58	1.60	1.62	1.64
K_1	.84	.83	.83	.83	.83	.82	.82	.82	.81	.81	.81	.80	.80
K_2	1.61	1.60	1.56	1.55	1.52	1.50	1.47	1.43	1.41	1.39	1.36	1.35	1.34
K_3	2.33	2.38	2.40	2.41	2.43	2.45	2.50	2.54	2.58	2.62	2.67	2.69	2.73
K	4.78	4.81	4.79	4.79	4.79	4.77	4.79	4.79	4.80	4.82	4.84	4.84	4.87

Notes:

1. $\beta = \dfrac{f V_0^2}{4 t_h g \tan\alpha}$

2. $K_2 = \dfrac{K_3}{4}\left(\dfrac{1}{\sqrt{2\beta}} \tan^{-1}\sqrt{\dfrac{\beta}{2}} - \dfrac{1}{\beta} \ln \left| \sec \tan^{-1}\sqrt{\dfrac{\beta}{2}} \right| \right)^{-1}$, $K_3 = 1.40$

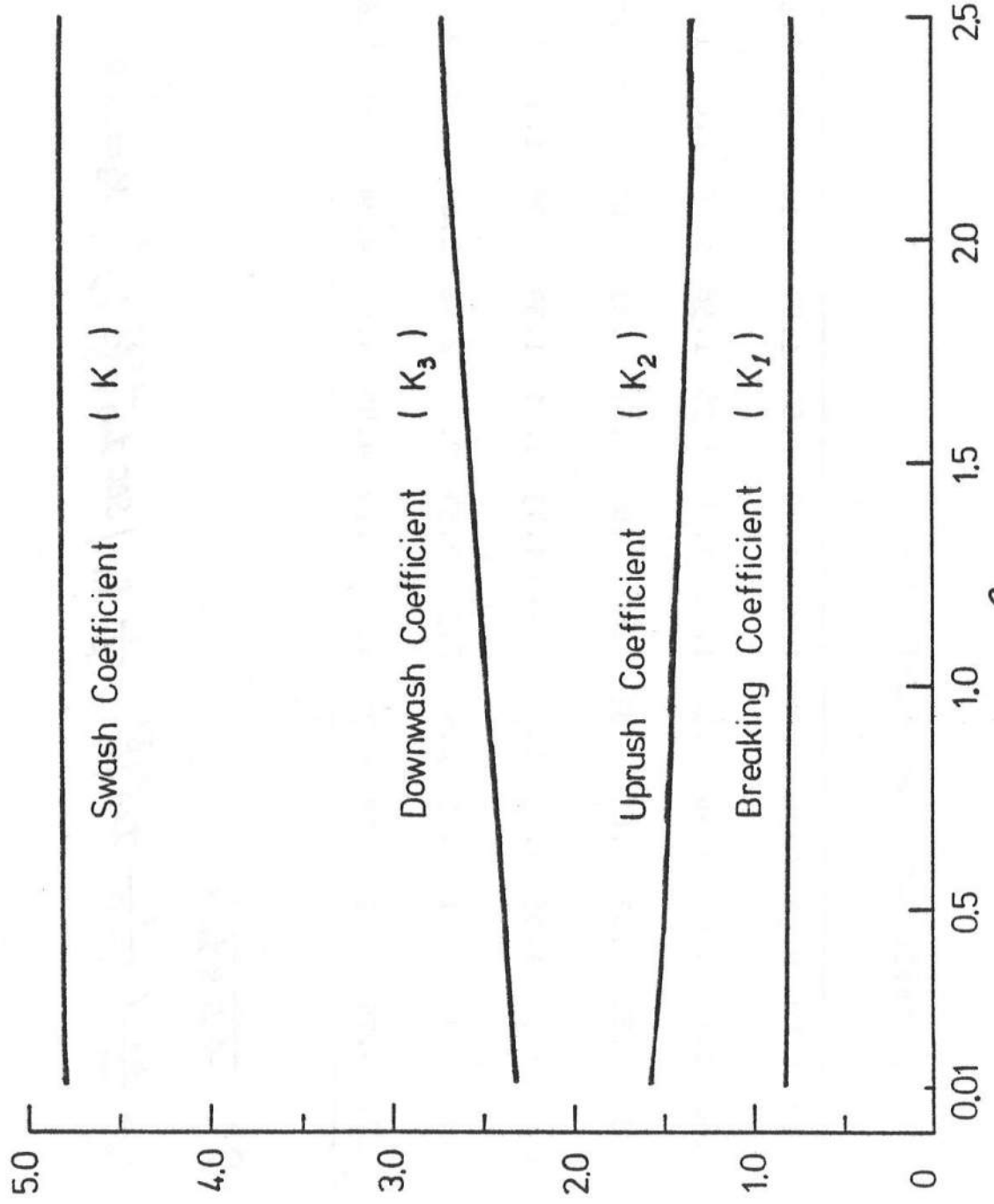

Figure 3-6 Swash Coefficients vs. β

The physical implication of I_w can be explained as follows. The I_w is the surf zone interference index. When I_w is small, each individual wave will complete the swash cycle with little or no interference from the successive waves. The flow in swash zone is mainly oscillating and the breaker is of the plunging type. When I_w increases, the degree of interference from successive waves also increases; a circulatory motion is gradually developing which will result in a return flow in the main water column; the breaking phenomenon gradually transforms from plunging to spilling. This sequence of events was illustrated in Figure 2-1.

The number of breaking waves in surf zone is less than unity for surging or collapsing breakers. When the breaking waves increases more than unity, the breaker type changes gradually from plunging to spilling. Therefore, by setting $N^* = T_n/T = 1.0$, the transition value of I_w for pure plunging is 0.21. The N^* denotes the number of breaking waves in surf zone. The transition value of plunging breaker is equivalent to $\xi_b = 1.92$, based on Equation (3-17) which is in the neighborhood of the transition value suggested by Battjes (Equation 2-8).

For I_w less than 0.21, the broken wave is able to surge up the slope to the uprush limit and return as downwash to the breaking point before the next wave breaks. There is no wave interference and energy loss is primarily due to

bottom friction, if the percolation effect is neglegible. For this I_w value, the breaking wave in surf zone is runup dominant and a large portion of wave energy is reflected resulting in a partial standing wave condition.

With the value of I_w increasing, the number of breaking waves in surf zone increases proportionally. The broken wave is not able to return to the breaking point before the next wave breaks. The increasing wave interference causes greater energy gradient throughout surf zone due to internal friction and successive breaking. The flow is set-up predominant and a large portion of wave energy is absorbed in surf zone with little reflection.

In addition to the breaking wave properties stated above, the I_w plays an important role in characterizing the breaking wave similarity which will be discussed in detail in the following section.

3.2 Breaking Wave Similarity

For a wave train of single frequency shoaling on a beach, a more or less energy is being transferred from the primary wave component to its higher harmonics. The amplitude dispersing among harmonics coupled with phase lags due to differential shoaling of each harmonic component results in a highly asymmetric wave form upon breaking.

After breaking, as the wave travels further inshore, the wave form tends to stabilize although it remains asymmetrical. The conventional higher order wave theories are no longer adequate to describe these asymmetrical wave forms. A variation would be the introduction of phase angles among harmonic components such that the water surface fluctuation is expressed as:

$$\eta(t) = \sum_{n=1}^{\infty} a_n \sin(n\sigma t + \phi_n') \qquad (3\text{-}18)$$

where a_n is the n^{th} harmonic amplitude, ϕ_n' is the n^{th} harmonic phase and σ is the fundamental frequency.

Equation (3-18) most certainly can be used to prescribe the wave form of any particular set of breaking waves. Yet, it serves little useful engineering purpose if the solution can not be generalized. If we assume that

(1) Each harmonic amplitude is limited by the local water depth, and,

(2) The phase velocity of each harmonic is also depth limited,

then, we have,

$$a_n = \alpha_n (d + \bar{\eta}) \qquad (3\text{-}19)$$

and

$$C_n \propto \sqrt{g(d+\bar{\eta})} \qquad (3\text{-}20)$$

where $\bar{\eta}$ is wave setup. Equation (3-18) can now be expressed as:

$$\frac{\eta(t)}{d+\bar{\eta}} = \sum_{n=1}^{\infty} \alpha_n \sin(n\sigma t + \phi_n) \qquad (3\text{-}21)$$

where α_n's are non-dimensional coefficients and ϕ_n's are constant phase angles. Thus, the wave profile remains similar and its magnitude is affected only by local parameter ($d+\bar{\eta}$).

In shallow water, the horizontal fluid particle velocity can be described by Stokes' higher order theory as:

$$U(t) = \frac{C\eta(t)}{d} + (\text{higher order terms}) \qquad (3\text{-}22)$$

The depth averaged velocity term can be expressed as:

$$U(t) = \frac{1}{d}\int_{-d}^{0} u(t)\,dz = \frac{C\eta(t)}{d} + \frac{1}{d}\int_{-d}^{0} (\text{higher order terms}) \qquad (3\text{-}23)$$

Recognizing that the contribution of the depth averaged higher order terms is a mean return flow in the water column as shown schematically in Figure 3-7, Equation (3-23) becomes:

$$U(t) = \frac{C\eta(t)}{d} - \bar{U}_R \qquad (3\text{-}24)$$

The fact of having a similarity solution of $\eta(t)$, leads to the following similarity solution for $U(t)$:

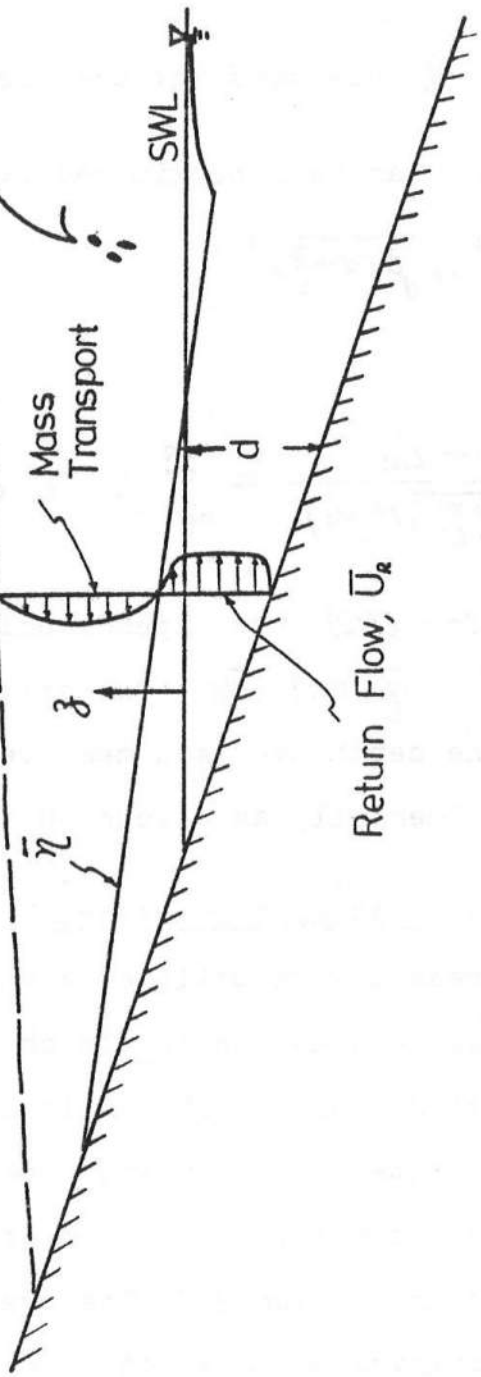

Figure 3-7 Schematic of Mass Transport and Return Flow in Surf Zone

$$\frac{U(t)+\bar{U}_R}{C(1+\bar{\eta}/d)} = \sum_{n=1}^{\infty} \beta_n \sin(n\sigma t + \gamma_n) \qquad (3\text{-}25)$$

where β_n and γ_n are constant coefficients.

Since C can be approximated by

$$C = k\sqrt{g(d+\bar{\eta})} \qquad (3\text{-}26)$$

we have

$$\frac{U(t)+\bar{U}_R}{k\sqrt{g(d+\bar{\eta})}(1+\bar{\eta}/d)} = \sum_{n=1}^{\infty} \beta_n \sin(n\sigma t + \gamma_n) \qquad (3\text{-}27)$$

The solution for $U(t)$ now depends only upon certain local parameters d, $\bar{\eta}$ and $\bar{U}_R$. The similarity constants α_n, β_n, ϕ_n, γ_n, and the depth averaged mean return flow $\bar{U}_R$ would be obtained experimentally as discussed in Chapters 4 and 5.

3.3 On/offshore Sediment Transport Model

The present work utilized a suspended sediment transport model to simulate the beach profile evolution and the rate of beach erosion. The horizontal sediment velocity, expressed as a time mean term and a periodic term, was developed based on the similarity model of breaking wave in surf zone presented in Section 3.2. The predominant sediment suspension mechanism was assumed to be turbulent induced shear stress. The sediment concentration equation used was based on the results by previous researchers and was assumed

to be composed of a time-mean term and a periodic term. The net suspended sediment flux was found by integrating the product of the suspended sediment horizontal velocity and concentration over depth and time-averaged in a wave period.

Based on the derived transport equation, a numerical model was developed to predict the foreshore slope evolution as well as the erosion rate. To start the model, the initial beach slope, water level, sediment characteristics and breaking wave condition would have to be furnished. The suspended sediment concentration coefficients were calibrated with both laboratory and field data.

3.3.1 Problem Formulation

Consider a vertical section of water in the surf zone where sediment is entrained from the bottom by passing breaking waves. The suspended sediment moves with the fluid velocity in this section on or offshore till it falls down on the bottom. The net suspended sediment flux past this section can be found by integrating the product of the horizontal fluid velocity and the sediment concentration profile over depth, which can be expressed as:

$$Q_x(t) = \int_d^{\eta} u_x(z,t)\, C_x(z,t)\, dz \qquad (3\text{-}28)$$

where d is the water depth measured from sea water level to bottom, η is the water elevation at wave crest,

$u_x(z,t)$ is the horizontal sediment particle velocity, and $C_x(z,t)$ is the suspended sediment concentration. The coordinate system and expressions of water depth are shown schematically in Figure (3-8)

The suspended sediment transport equation is based on the knowledge of fluid particle velocity and suspended sediment concentration. Due to the great turbulence in surf zone, the conventional linear and higher order wave theories no longer apply in this region, neither does the suspended sediment profiles developed for use in the offshore region. In this model, both equations are based on the empirical formula proposed by the author and the previous researchers.

In the following paragraphs the horizontal velocity, suspended sediment concentration, transport equation and continuity equation used in the transport model are discussed.

HORIZONTAL VELOCITY

The horizontal velocity of the sediment particle, once suspended in the water column by breaking waves, is assumed to be the same as the fluid velocity. The horizontal fluid velocity in surf zone was obtained based on the similarity model for breaking waves in surf zone presented in Section 3.2. Based on Equation (3-27), the velocity can be expressed as:

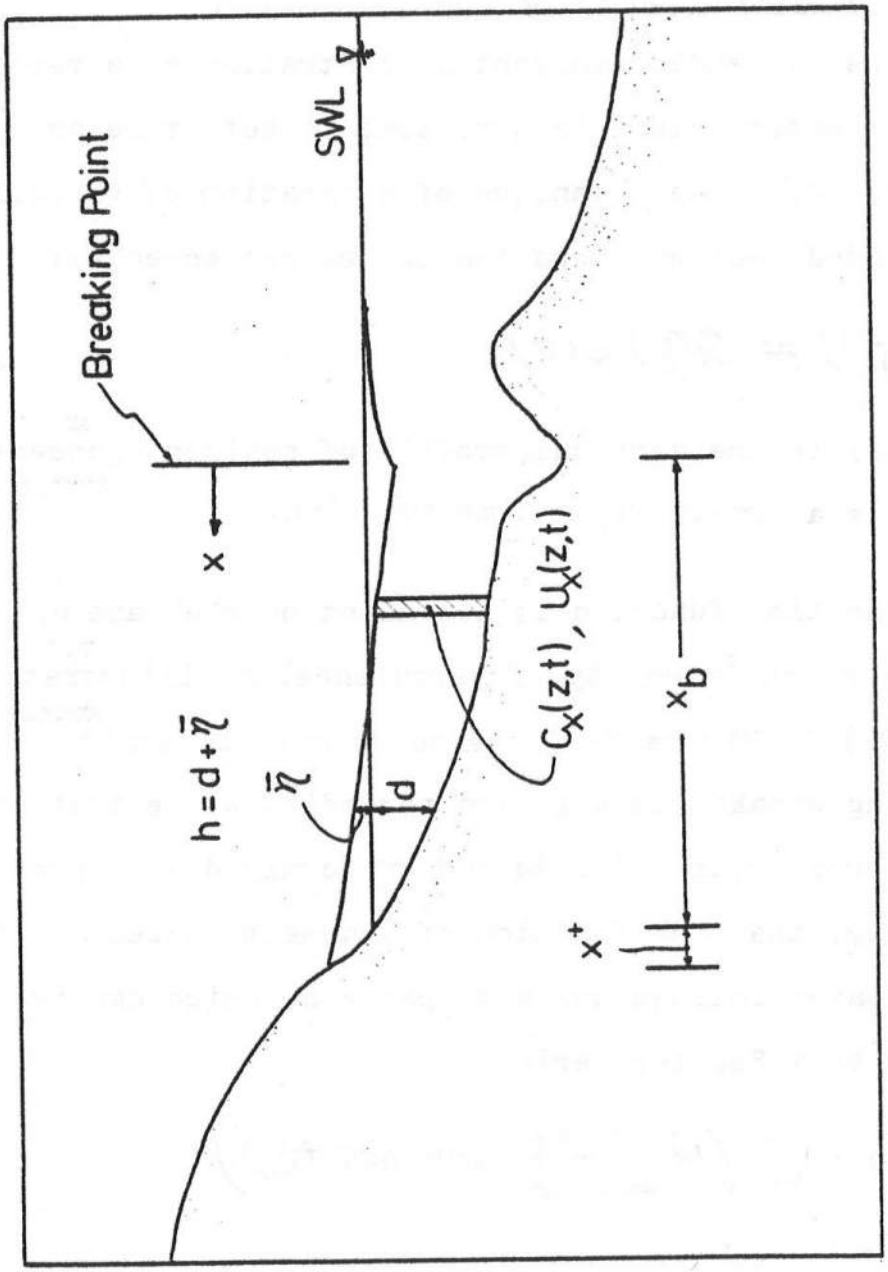

Figure 3-8 Schematic of Coordinate System and Water Depth in Transport Equation

$$\frac{U(t)+\bar{U}_R}{k\sqrt{g(d+\bar{\eta})}\,(1+\bar{\eta}/d)} = \sum_{n=1}^{\infty} \beta_n \sin(n\sigma t+\gamma_n)$$

SUSPENDED SEDIMENT CONCENTRATION

The suspended sediment concentration at a vertical section of water column in surf zone is both time and height dependent. Using the technique of separation of variables, the suspended sediment equation can be expressed as:

$$C_x(z,t) = G(z)\,C(t) \qquad (3\text{-}29)$$

where $C_x(z)$ is the vertical profile of sediment concentration and $C(t)$ is a non-negative time function.

The time function is dependent on the rate of dissipation and intensity of turbulence. As illustrated by Dean (1977) in Figure 3-9, the turbulence intensity of plunging breaker is high and periodic, while that of spilling breaker is moderate and uniformly distributed. Accordingly, the time function of sediment suspension by breaking waves follows the same pattern, which can be expressed by a Fourier Series:

$$C(t) = \bar{C}_c \left(1+\sum_{n=1}^{\infty} \frac{b_n'}{\bar{C}_c} \sin(n\sigma t+\theta_n)\right) \qquad (3\text{-}30)$$

where $\bar{C}_c$ and b_n' are Fourier constants, σ is the fundamental frequency, θ_n is the harmonic phase angle. Combining

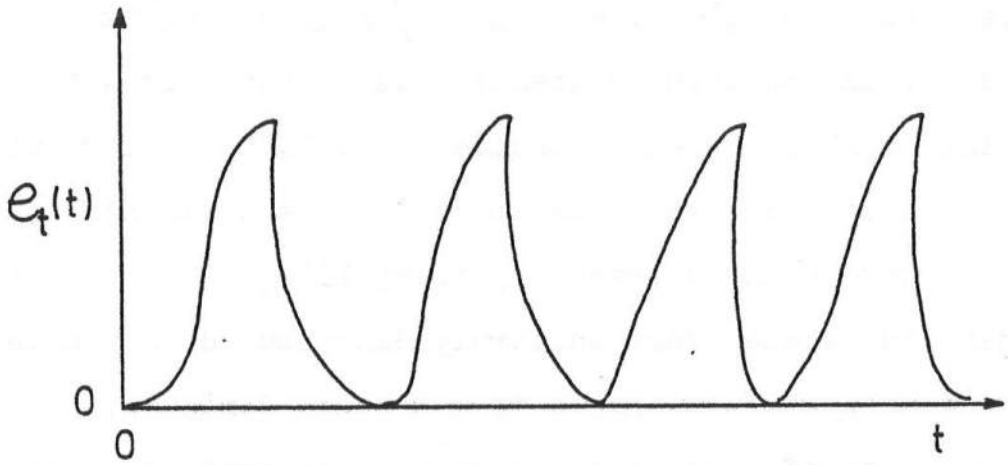

(A) TURBULENCE ENERGY DENSITY, $e_t(t)$
FOR LARGE DECAY (PLUNGING)

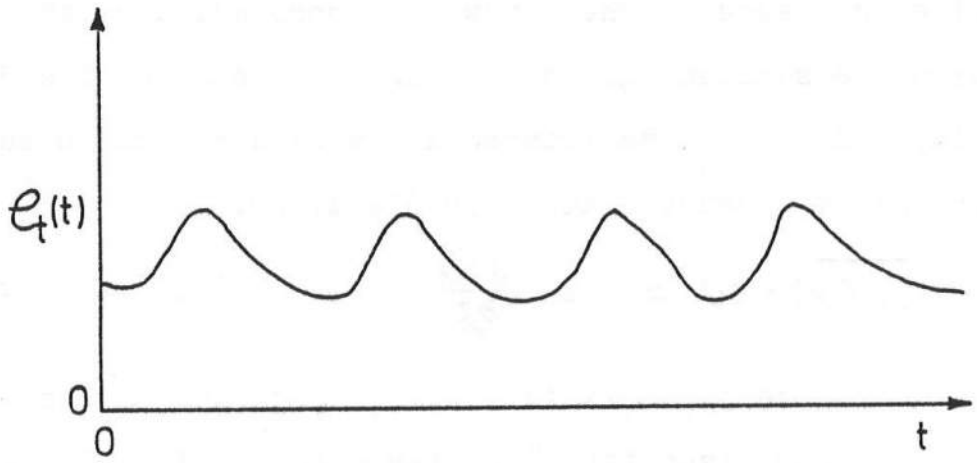

(B) TURBULENCE ENERGY DENSITY, $e_t(t)$
FOR SMALL DECAY (SPILLING)

Figure 3-9 Turbulence Energy Density for Large and Small Decay

Equations 3-29 and 3-30 yields

$$C_x(z,t) = \overline{C_x(z)}\left(1 + \sum_{n=1}^{\infty} b_n \sin(n\sigma t + \theta_n)\right) \qquad (3\text{-}31)$$

where $\overline{C_x(z)} = C_x(z) \cdot \overline{C_c}$, and $b_n = b_n' / \overline{C_c}$. For plunging breakers, the sediment suspension is periodic with the passing breaking waves as indicated by ISCMS test results and the periodic term in Equation 3-31 is dominant. As the breaker type changes gradually to spilling, the sediment suspension becomes more uniformly distributed in a wave cycle and the time averaged term becomes dominant. The measurements of suspended sediment concentration in surf zone supports this phenomenum as illustrated in Figure 3-10 and in Appendix D.

The time averaged vertical sediment concentration profile is, based on the classical approach, a balance between the sediment grain falling through a section due to gravity and the grains transported upward due to turbulent mixing and the concentration gradient, or,

$$\overline{C_x(z)} \cdot \omega = -\varepsilon \frac{\partial C_x}{\partial z} \qquad (3\text{-}32)$$

where ω is the particle falling velocity and ε is the kinematic eddy viscosity. For open channel flow, Rouse (1949) derived the concentration profile as:

$$C_x(z) = C_m(x) \, EXP\left[-a_\varepsilon \omega (z - z_m)/(k \cdot \sqrt{\tau/\rho})\right] \qquad (3\text{-}33)$$

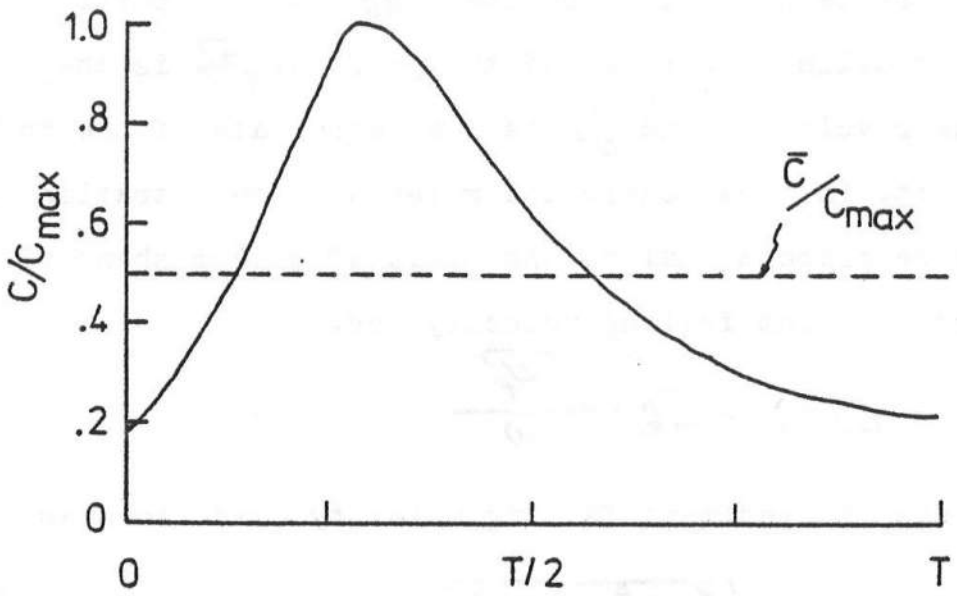

(A) PLUNGING WAVE CONDITION

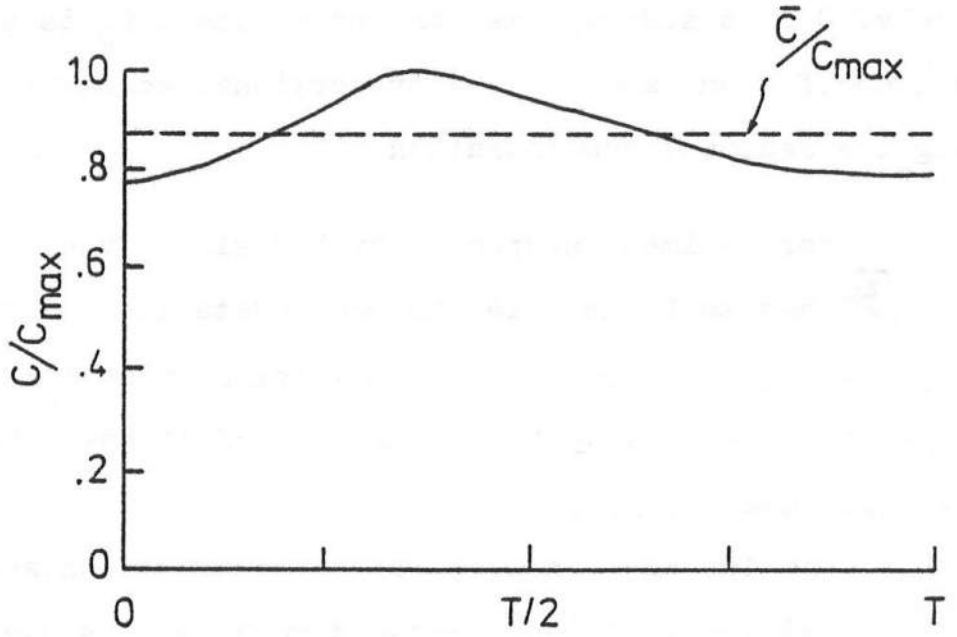

(B) SPILLING WAVE CONDITION

Figure 3-10 Averaged Instantaneous Suspended Sediment Concentration in One Wave Cycle

where $C_m(x)$ is the sediment concentration measured at a reference point from bottom, a_E is a proportion constant controlling the shape of the profile, $\sqrt{\tau_b/\rho}$ is the bottom shear velocity and z_m is the coordinate of the reference point. In this model, the reference concentration is assumed to be proportional to the ratio of bottom shear velocity and sediment falling velocity, or,

$$C_m(x) = C_k \frac{\sqrt{\tau_b/\rho}}{\omega} \qquad (3\text{-}34)$$

where the sediment falling velocity is defined as:

$$\omega = \sqrt{\frac{4}{3}\left(\frac{\rho_s-\rho}{\rho}\right)\frac{g D_{50}}{C_D}} \qquad (3\text{-}35)$$

where ρ_s and ρ are sediment and fluid densities respectively, D_{50} is sediment median grain size , C_D is particle drag coefficient and C_k is a proportional constant controlling the sediment concentration.

For sediment suspended by breaking waves, both a_E and $\sqrt{\tau_b/\rho}$ has to be modified to accomodate the nature of turbulence in the surf zone. In general, there are two quantities which determine the amount of sediment entrained into the water column:

(1) The wave-induced bottom shear stress,and

(2) The turbulence induced shear stress due to breaking waves.

In surf zone, the second mechanism is dominant.

Based on the derivation of Dally and Dean (1980), the turbulence induced shear stress velocity can be expressed as:

$$\sqrt{\tau/\rho} = \left[\frac{-2k}{\rho H_b \sqrt{gh}} \cdot \frac{\partial E \cdot C_g}{\partial x}\right]^{1/2} \qquad (3-36)$$

where $\frac{1}{h}\frac{\partial EC_g}{\partial x}$ is the rate of energy dissipation per volume. Considering steady conditions when averaging over a wave period and utilizing small amplitude shallow water wave relationship, Dean (1977) found that,

$$\frac{\partial E C_g}{\partial x} = \frac{\gamma}{8}\sqrt{g}\, K^2 \frac{\partial}{\partial x} h^{3/2} \qquad (3-37)$$

where $\gamma = \rho g$ and K is the breaking wave height to depth ratio. Combining Equations (3-33), (3-34), (3-36), (3-37), the time averaged suspended sediment concentration equation can be expressed as:

$$\overline{C(z)} = C_k \frac{\sqrt{kg}}{2w}\sqrt{\frac{\partial h}{\partial x}}\, EXP\left[-2a_c \frac{w}{\sqrt{kg}} \frac{1}{\sqrt{\frac{\partial h}{\partial x}}} \cdot \left(\frac{z - z_m}{h}\right)\right] \qquad (3-38)$$

The constants were calibrated with both laboratory and field data measured in surf zone by numerous investigators as summarized on Table 3-3.

Based on the data on Table 3-3, the average maximum sediment concentration in surf zone is approximately

Table 3-3 Summary of the maximum suspended sediment concentration measured in the fields and laboratories

	Investigator	C_m(ppm)	Z_m/h	Reference
FIELDS	Noda	1-10	0.07-0.1	14th JCCE
	Shimada et al.	$1\text{-}10^2$	0.04-0.1	21st JCCE (A)
	Irie et al.	$1\text{-}10^3$	0.14-0.22	22nd JCCE
	Fairchild	$10^3\text{-}10^4$	-	13rd ICCE
	Tanaka	$10^3\text{-}10^4$	0.08	22nd JCCE (B)
	Kana	$10^3\text{-}10^4$	0.08-0.33	16th ICCE
LABORATORIES	Homa et al.	$10^3\text{-}10^4$	0.014-0.05	11st JCCE
	Noda	$5\text{x}10^2\text{-}10^3$	0.03-0.1	14th JCCE (A)
	Hosoi	10^4	0.017	20th JCCE
	Nakato et al.	10^4	0.04	ASCE Vol. 103, WW1
	Kuruhara et al.	10^4	0.3	3rd JCCE
	Hosoi et al.	10^4	0.1	20th JCCE (B)
	Sawagaki	10^4	0.1	unpublished

Notes:
(1) C_m is maximum suspended sediment concentration
(2) Z_m is height from the bottom where C was measured
(3) h_m is water depth
(4) data in column (A) were measured in the offshore region, (B) were measured in surf zone
(5) ICCE means Proceedings of the International Conference on Coastal Engineering
(6) JCCE means Proceedings of the Japanese Conference on Coastal Engineering

$1x10^4$ ppm in the laboratory and $1x10^3$ ppm in the field. The median sand sizes observed were 0.2 mm and the average beach slopes were 1/10 in the laboratory and 1/25 in the field. The above average data were used to calibrate the proportional constants in Equation (3-38). The constant C_ϵ was found to be approximately $1x10^{-2}$ gram/cm^3 for laboratory condition and $2x10^{-3}$ gram/cm^3 for field condition. The vertical profile constant a_ϵ was also calibrated with laboratory and field data measured in surf zone by Wang (1979), Kurihara et. al. (1956), Tanaka (1975), and Sawaragi (1979). The calibrated results showed that $a_\epsilon \approx 2.5$ for laboratory condition and $a_\epsilon \approx 1.0$ for field condition. The suspended sediment concentration and profile used in the numerical model is shown in Figure 3-11. The measured data are also shown in the figure.

TRANSPORT EQUATION

Combining Equations (3-27), (3-28), (3-31) and time-averaging over one wave period, the suspended sediment transport equation in a vertical water column can be expressed as:

$$Q_x(t) = -\bar{U}_R \int_{-h}^{0} \bar{C}_x(z)dz + K\sqrt{gh}\left(\frac{h}{d}\right)\cdot\int_{-h}^{0}\bar{C}_x(z)dz$$
$$\cdot\left(\sum_{n=1}^{\infty}\beta_n \sin(n\sigma t+\gamma_n)\cdot\sum_{n=1}^{\infty}b_n \sin(n\sigma t+\phi_c)\right) \quad (3\text{-}39)$$

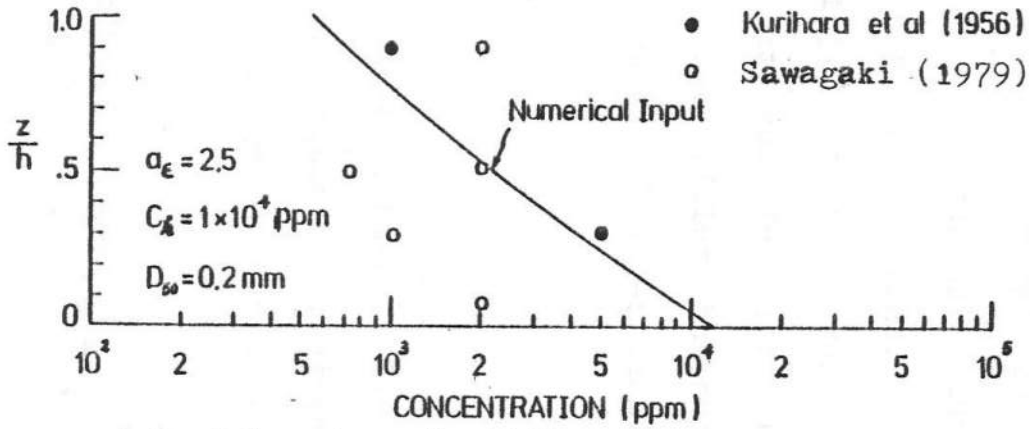

(a) Laboratory Condition

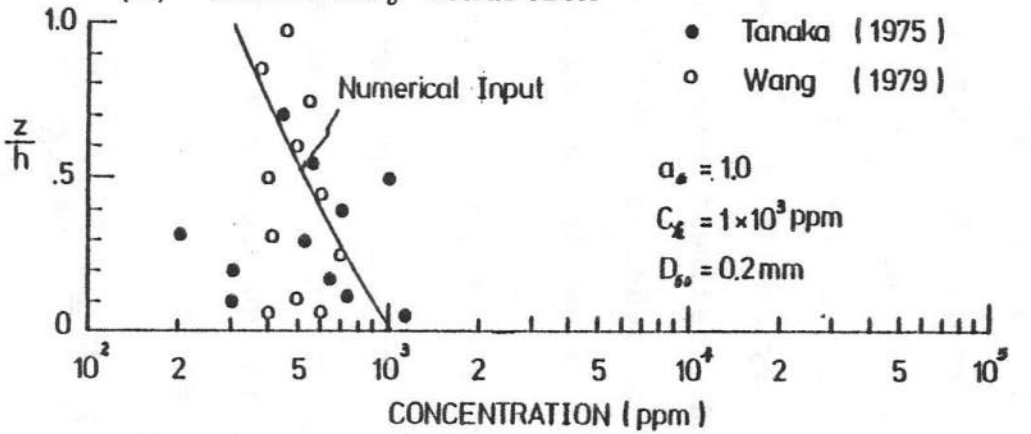

(b) Field Condition

Figure 3-11 Suspended Sediment Concentration Profile Used in the Numerical Model

where $\overline{(\ )}$ denotes $\frac{1}{T}\int_0^T (\ )dt$, the time-mean quantity.

The first term in Equation (3-39) is the contribution of mean suspended sediment convected by the second and higher order horizontal velocity, which was found to be always in offshore direction. The second term in the equation is the contribution of periodic sediment suspension convected on or offshore by the fluctuating first order horizontal velocity.

For plunging breaker, the mean return flow strength is weak and the sediment suspension is in phase with the first order velocity. Therefore, the fluctuating term is dominant and transport is onshore. As the breaker type gradually changes to spilling, the periodic term of suspended sediment becomes relatively unimportant while the time mean term becomes dominant. Therefore, the direction of sediment transport gradually reverses from onshore to offshore. Since the present knowledge is limited to the mean suspended sediment condition, the present transport equation is only valid for spilling breaker condition with $I_w > 0.9$, in which the periodic term can be neglected and the transport direction is exclusively offshore.

By integrating the transport equation over water depth, Equation (3-39) becomes:

$$Q_x(t) = \left(\frac{K_2 C_k}{4 a_c \omega^2}\right) h \left(-\frac{\partial h}{\partial x}\right)\left(1 - EXP\left[-2a_c\left(\frac{\omega}{\sqrt{kg}}\right)\left(\frac{1}{\sqrt{1-\frac{\partial h}{\partial x}}}\right)\right]\right)\cdot \bar{U}_R \quad (3\text{-}40)$$

CONTINUITY EQUATION

Assuming straight and parallel bottom contour on beach, a two-dimensional equation that governs the change in water depth with time can be derived based on the continuity equation for solids as:

$$\frac{dh}{dt} = \frac{1}{\rho_s (1-\lambda_p)} \cdot \frac{\partial Q_x}{\partial x} \quad (3\text{-}41)$$

where the coordinate system is shown in Figure 3-12, ρ_s is the sediment density, and λ_p is the void ratio of sediment. For quartz sand, ρ_s =2.65 gram/cm^3 and λ_p=0.45. Combining Equations (3-40) and (3-41) yields

$$\frac{dh}{dt} = \frac{.025}{\rho_s(1-\lambda_p)} \cdot \left(\frac{K_2 C_k}{4 a_c \omega^2}\right)\left(1 - EXP\left[2a_c\left(\frac{\omega}{\sqrt{kg}}\right)\left(\frac{1}{\sqrt{1-\frac{\partial h}{\partial x}}}\right)\right]\right)\frac{\partial}{\partial x}\left[h\cdot\left(-\frac{\partial h}{\partial x}\right)\sqrt{gh}\right] \quad (3\text{-}42)$$

Equation (3-42) implies that the change in water depth with time in surf zone, as well as the sediment transport rate, are depth-controlled. Starting with steeper initial slope, the beach erosion begins with higher rate. As the beach slope becomes milder, the transport rate slows down in water depth's 3/2 power. Theoretically, the winter or storm profile would reach equilibrium as the beach

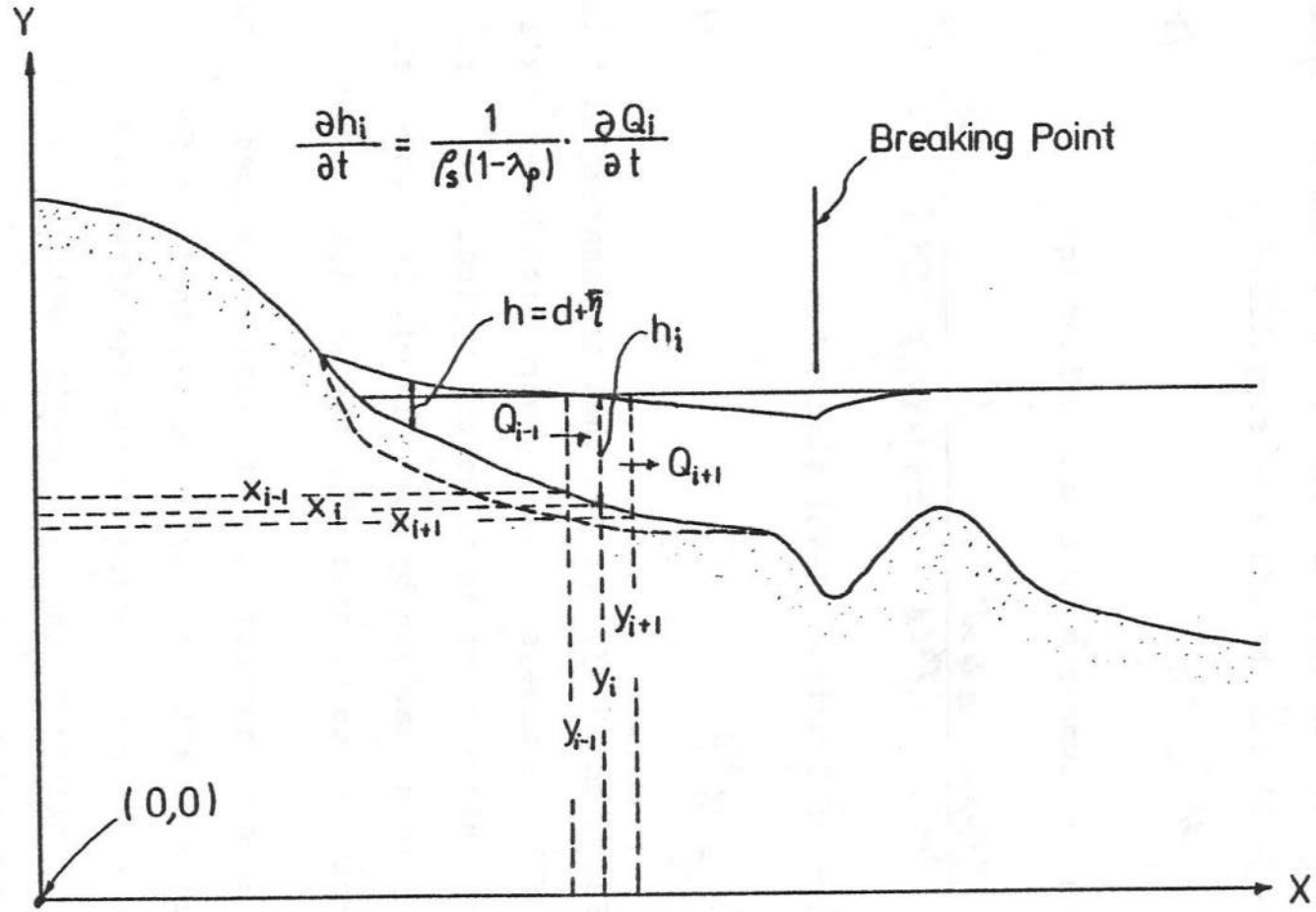

Figure 3-12 Schematic of Coordinate System for Numerical Calculation

slope in surf zone becomes flat ($-\frac{\partial h}{\partial x}=0$).

As the beach profile approaches equilibrium, both $\frac{\partial h}{\partial t}$ and $-\frac{\partial h}{\partial x}$ can be approximated by small constants ϵ_1 and ϵ_2. Equation (3-42) can therefore be simplified to

$$\frac{\partial}{\partial x} h^{3/2} = A \qquad (3\text{-}43)$$

where A is the lump-sum constant defined as:

$$A = \frac{\rho_s(1-\lambda_p)}{0.25} \frac{4a_b W^2}{K g^{1/2} C_b^2} \cdot \frac{1}{1-EXP\left[2a_b\left(\frac{W}{\sqrt{gh}}\right)\left(\sqrt{\frac{h}{2x}}\right)\right]} \cdot \frac{\epsilon_1}{\epsilon_2} \qquad (3\text{-}44)$$

Integration of Equation (3-43) yields

$$h = A\, x^{2/3} \qquad (3\text{-}45)$$

Equation (3-45) implies that the near-equilibrium beach profile is always concave upward with h being x's 2/3 power. This was proved to be the typical equilibrium beach profile summarized by Dean (1977). Therefore, the present model is consistent with the equilibrium shape.

Based on conservation of mass, the eroded sediment in surf zone is artificially deposited in the offshore region seaward from breaking point. The offshore bar is created asymmetric to the surf profile which is very similar to the laboratory condition.

3.3.2 NUMERICAL COMPUTATION

Due to the complexity of the governing equation, a finite difference numerical model was utilized to evaluate the beach evolution and erosion rate developed in Section 3.3.1. To compute the beach evolution, the surf zone was divided into several small cells with equal width Δx . The change of water depth was computed in each cell every n wave periods, or, $\Delta t = nT$. The bottom profile was smoothed every Δt with a moving average subroutine expressed as:

$$h_i = \frac{1}{4} h_{i-1} + \frac{1}{2} h_i + \frac{1}{4} h_{i+1} \qquad (3-46)$$

in order to simulate the natural smoothing mechanism due to bottom shear stress. The cell width used were 2.5 cm for laboratory beach simulation and 25 cm for field simulation.

The information required to start the model included the breaking wave conditions (H_b , T, K, breaking position), the median sediment grain size (D_{50}), and the initial beach slope. The initial foreshore profile for each numerical run was set in a concaved upward shape with desired average initial slope. The wave set-up prediction was based on the equations derived by Longuet-Higgins:

$$h = -\frac{\tan\alpha}{1 + \frac{3K^2}{8}} + h_b$$

$$\text{and} \quad h_b = \frac{d_b}{1 + \frac{K^2}{16}} \qquad (3-47)$$

The total volume of sand eroded at time t was the summation of the volume change in each cell within the eroding period. The eroded material was located offshore of the breaking point asymmetric to the surf zone profile to simulate an offshore bar. During the numerical beach evolution, the surf zone profile was always concave upward. The model would stop automatically when the foreshore slope is flat, indicating that equilibrium condition has reached. A flow chart illustrating the numerical procedures is shown in Figure 3-13.

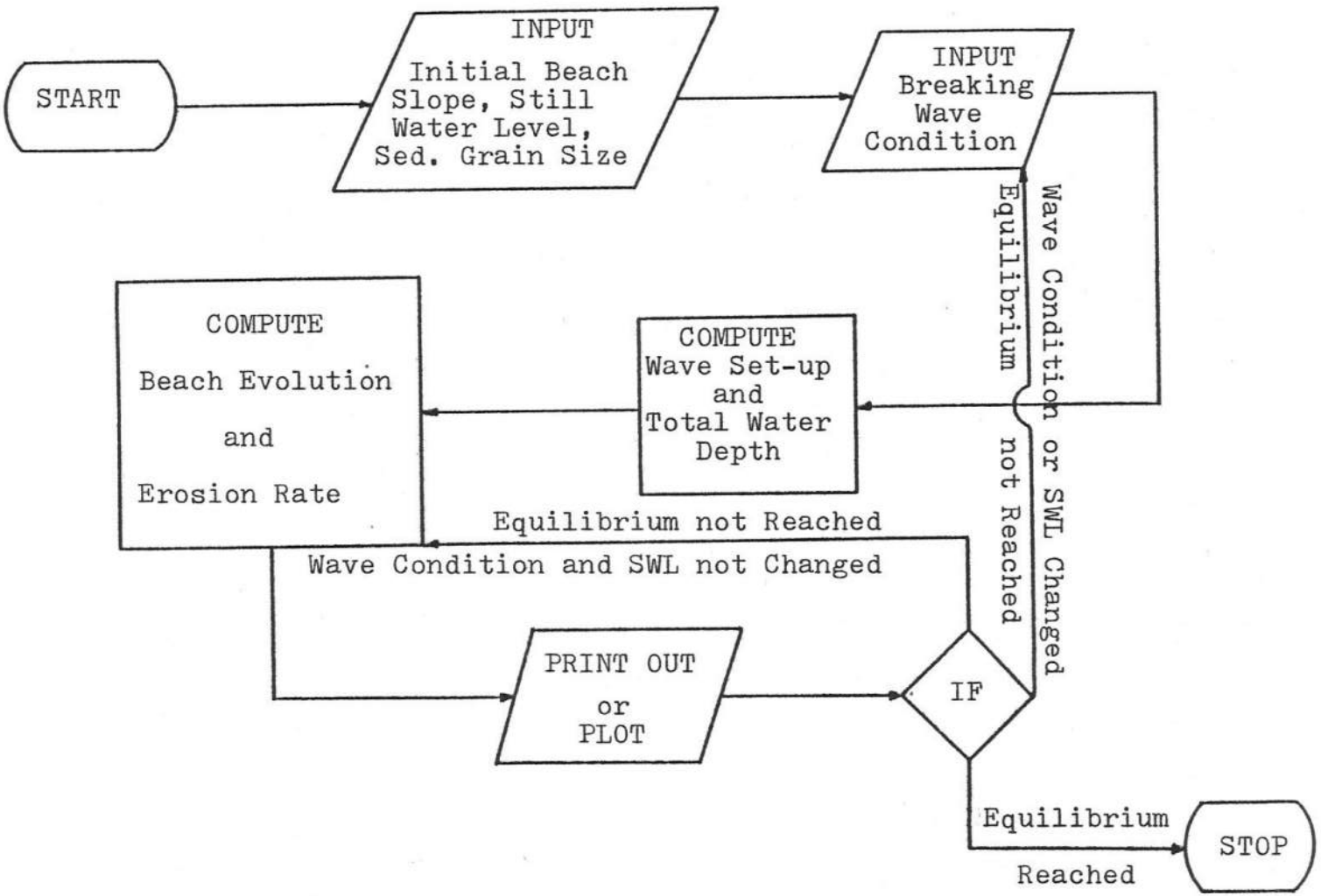

Figure 3-13 Flow Chart for Numerical Calculation

CHAPTER 4

LABORATORY EXPERIMENTS

Two sets of laboratory tests were conducted. The first set of experiments was designed to obtain the similarity constants and the mean return flow strength as developed in Section 3.2. In the second set of experiment the instantaneous suspended sediment concentration in surf zone was measured for various wave conditions.

All laboratory experiments were conducted in the wave tank located in the Civil Engineering laboratory. The wave tank is 24 inches wide and 52 inches deep with an overall length of 70 feet as shown in Figure 4-1. The portion of wave tank under study was 50 feet in length from the wave generator paddle to a plywood partition. The partition was used to provide a vertical backing against which a plywood plane beach or a sand beach could be formed and was posioned in order that the major portion of the profile could be viewed through the glass observation panel. Except for the 20 feet long observation panel on the side of the tank only, the tank is constructed of steel.

The Scotch Yoke type wave generator is powered by a

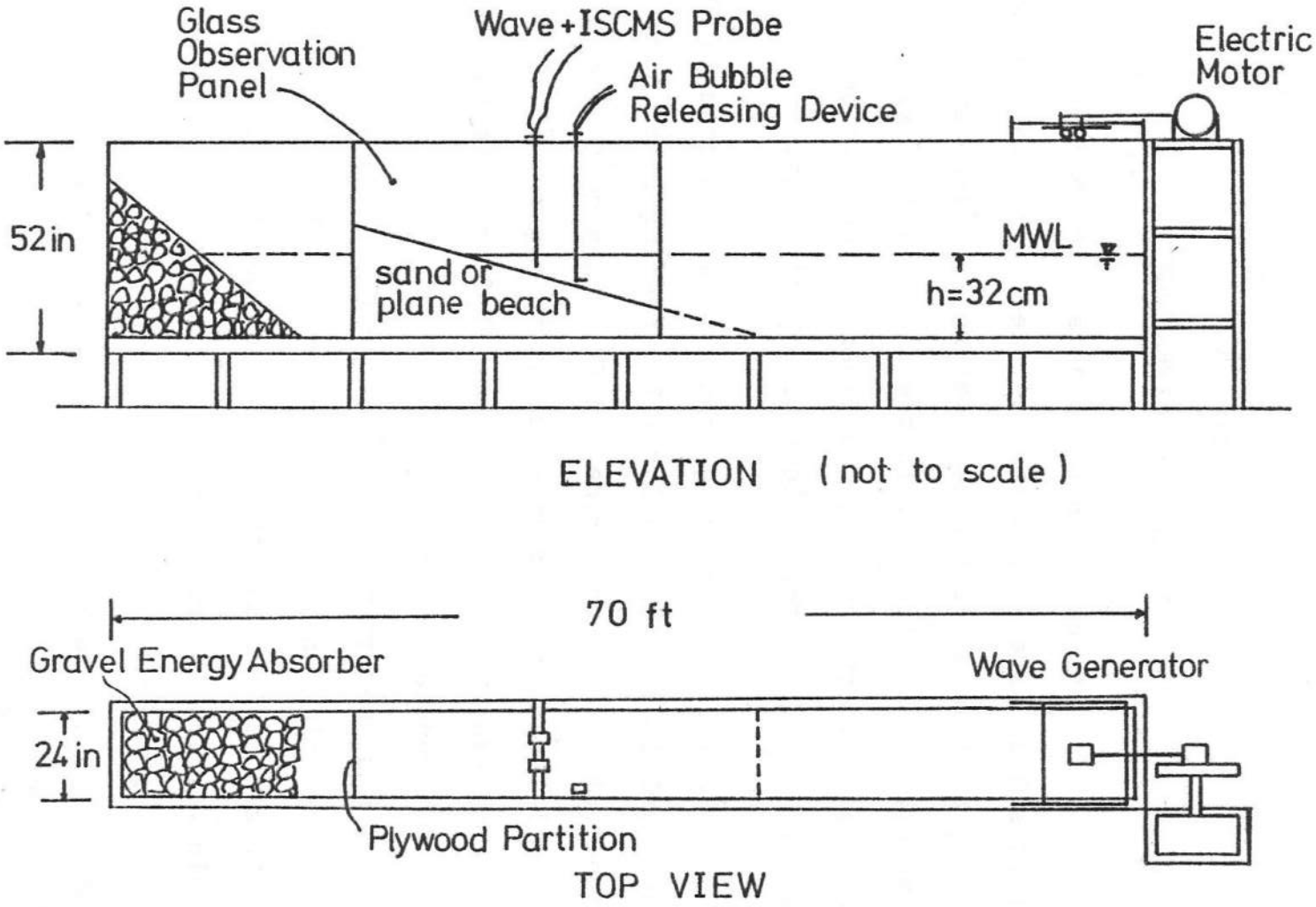

Figure 4-1 Laboratory Wave Tank Setup

1750 rpm, 7.5 Horse Power electric motor. The wave period is varied by varying the angular velocity of the rotating drive arm. The wave height is primarily a function of the rotating drive arm offset but is also related to the wave period. The steel wave paddle travels in a vertical plane on rollers mounted horizontally on top of the wave tank.

Two types of beaches were used in the experiments. The plane beach was made of plywood with 1 on 10 slope and 15 feet horizontal length. The plywood beach face was painted with polyurethane glass coating to reduce bottom effect. The sand beach material used in the experiments was graded construction sand with median diameter of 0.18 mm. The grain size distribution of the beach material is shown in Figure 4-2. This beach material is predominantly composed of quartz with a minor portion of dark minerals.

The experimental procedures and the arrangement of tests are discussed for each set of tests. The apparatus used in the present laboratory study is discussed in Section 4.1.

4.1 Discussion of Apparatus

The apparatus used in the present laboratory studies included the air bubble releasing device, the photographic equipments and the sediment concentration measuring instruments.

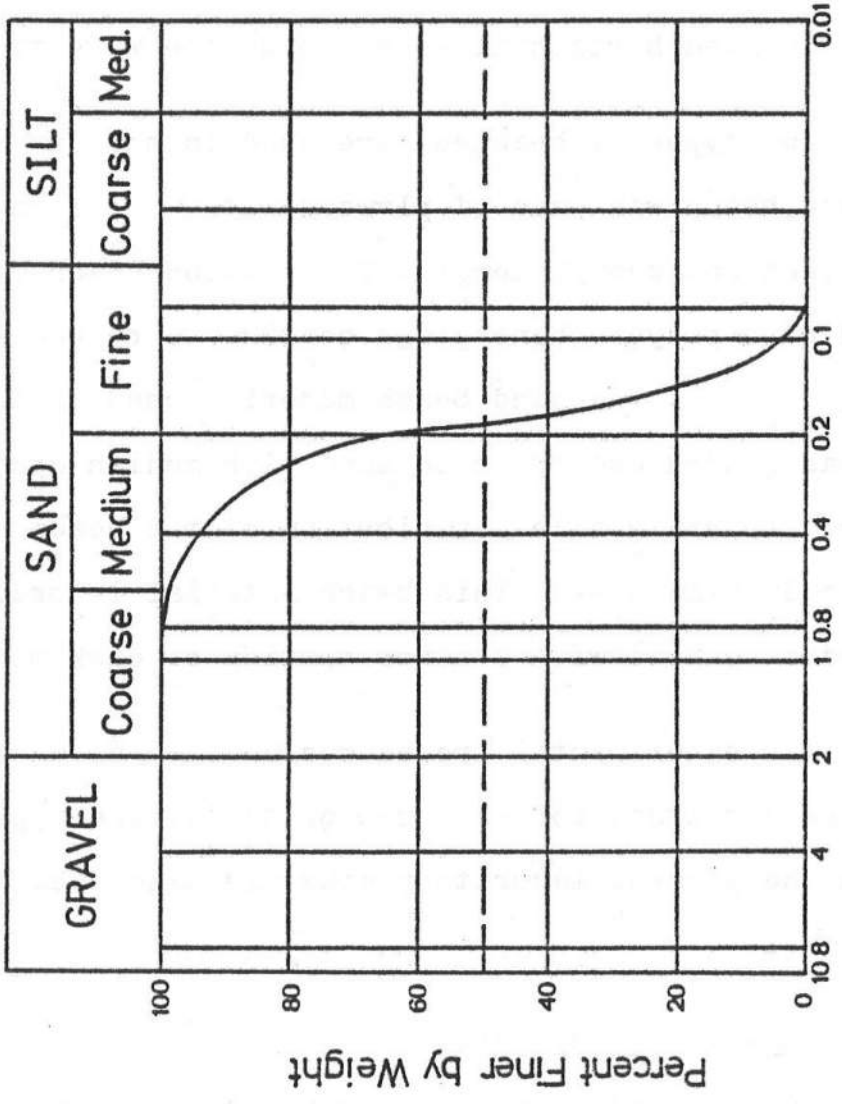

Figure 4-2 Grain Size Distribution of Laboratory Beach Material

The air bubble releasing device included pitot tubes and compressed air releasing system. The opening tips of the pitot tubes ranged from 0.3 to 0.5 mm. Compressed air was released from a high pressure steel tank through a rubber tube. The size of the released air bubble in water can be adjusted to a visible size by adjusting the releasing air pressure. The sizes of air bubble in water ranged from 1.0 mm to 1.5 mm during the tests.

The photographic equipments included a Paillard Bowlex 16 mm movie camera equipped with close-up lenses. The film shooting speed ranged from 12 to 62 frames per second. Kodak Tri-X reversal 16 mm B&W movie film was used. The motion pictures were analyzed with Model 224A photo-optical Data Analyzer. The data analyzer is a 16mm movie projector with variable film projecting speed ranging from 2 to 24 frames per second. Films can also be projected on the screen frame by frame similar to a slide projector.

The Iowa Sediment Concentration Measuring System is a complete system for measuring mean and statistical properties of particle concentration in sediment suspensions. The ISCMS probe consists of a gallium-arsenide light source, 0.062 inch long, 0.092 inch in diameter and a silicon planar diode with approximately the same dimensions. They were mounted on supports with their axes co-lined and a clear distance of 0.125 inch between them. The emmision

spectrum of the light source was concentrated at 0.9 microns where the light sensor is much wider, although it peaks at approximately 0.9 microns. The optimum bias voltage of the sensor is -20 to -5 volts, and thus it has a very large output impedence which causes signal attenuation by the cable connecting the transducer to the instrument. Different calibration curves should be prepared for each sand sample. The light attenuation is proportional to the sediment surface area per unit volume of suspended material. These apparatus are shown in Photo 1.

4.2 Water Elevation and Horizontal Velocity Measurement

The purpose of this set of experiments were to carlibrate the similarity proportional constants developed in section 3.2. A total of 10 runs were conducted in the wave tank. The incident wave conditions were arranged such that the breaker types gradually changed from plunging to spilling, while the the flow patterns also varied from oscillatory to circulatory. The wave periods were adjusted such that they evenly distributed in between 1.0 second and 2.0 second. The breaking wave heights were also tested in a wide range from 7.5 cm to 14.0 cm. The laboratory wave conditions for the 10 runs are shown in Table 4-1.

In each run both water elevation and horizontal fluid velocity were measured at various stations of different water depths. The stations were pre-marked with yellow

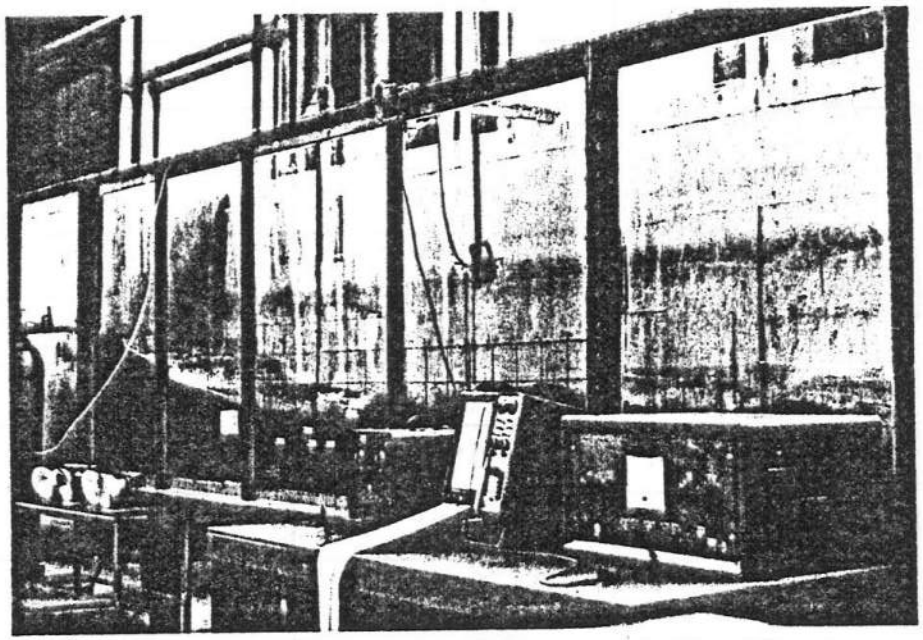

Photo 1 Laboratory set up of wave probe, ISCMS probe and air bubble releasing system

Table 4-1 Lab. Wave Condition for Similarity Study

Run No.	Incident Wave Height, H_c (cm)	Breaking Wave Height, H_b (cm)	Wave Period T, (sec)	$\frac{H_b^{1/2}}{g^{1/2}T\cdot\tan\alpha}$
PB-1	9.5	11.5	2.0	.54
PB-2	11.0	14.0	1.8	.66
PB-3	11.0	14.0	1.6	.75
PB-4	13.5	14.0	1.4	.85
PB-5	10.0	11.5	1.2	.90
PB-6	11.0	12.5	1.0	1.13
PB-7	10.5	11.5	1.0	1.08
PB-8	9.0	10.0	1.0	1.01
PB-9	8.0	9.0	1.0	.96
PB-10	6.0	7.5	1.0	.88

tape for the convenience of data reducing. The scaling grids were also pre-marked on the glass panel with 10 cm equal spacing. Measurements were made at stations 190, 210 and 230. The distance between each station was 20 cm. The water level was kept constant at 32 cm level in the wave tank and the still water depths at the three stations were 3.0, 5.0 and 7.0 cm respectively. The measuring stations and water depths are shown schematically in Figure 4-3.

The water elevations and horizontal fluid velocities for each run were recorded on movie film at 1 to 3 stations depending on the flow conditions in surf zone.The measuring techniques and detailed procedure for water elevation and horizontal fluid velocity testing are discussed in the following sub-sections.

4.2.1 Water Elevation Measurement

The photographic method was used for water elevation measurement. For each run the instantaneous water elevation evolution were recorded on movie film at various stations. The movie films were then projected on the engineering paper which was taped on a flat wall. The water elevations were marked frame by frame on the engineering paper and later scaled to actual length. Water elevations were always measured up to the solid water line while the white foam on top of the wave crest was neglected.

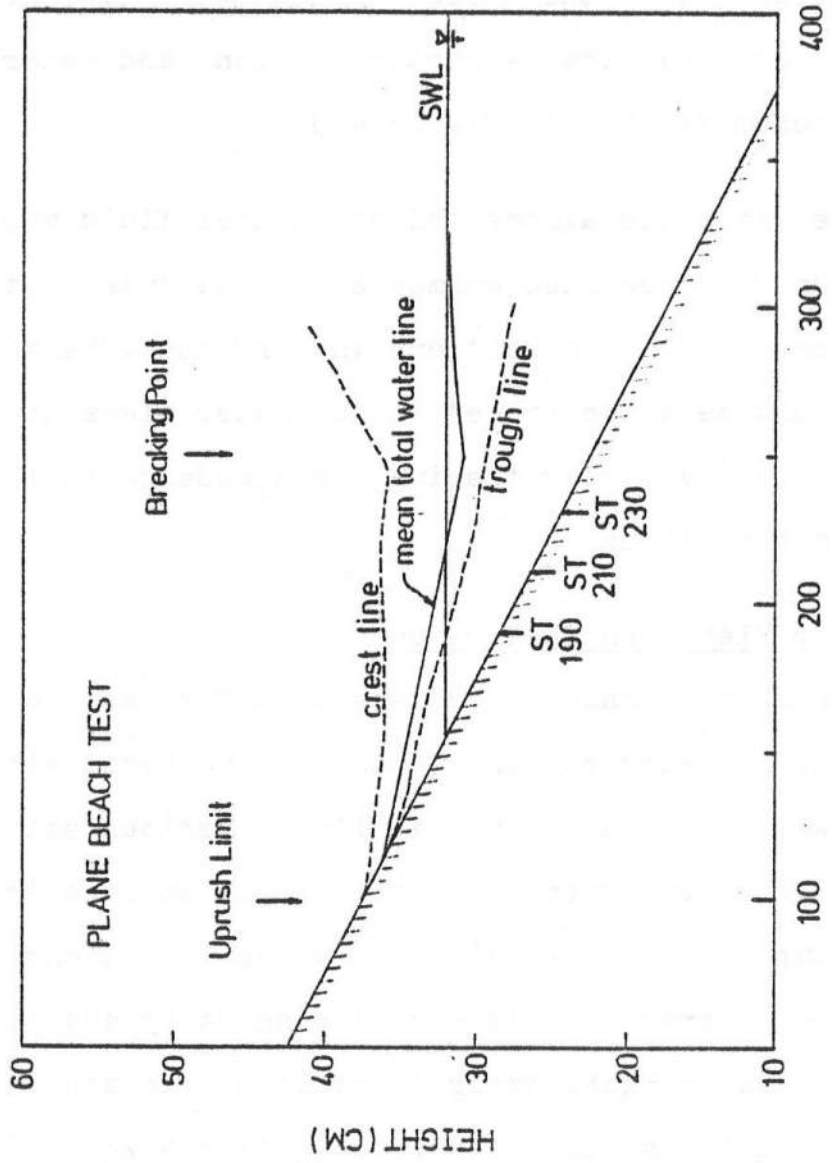

Figure 4-3 Measuring Stations and Definition of Water Level

Due to a partial reflection effect on plane beach, the measured water elevations were averaged over several wave cycles to avoid biased data. Based on the preliminary test runs, it was found that the instantaneous water elevation measured for this study can be represented by averaging the data over six wave cycles. The averaged water elevations were non-dimensionalized by the local water depth $h=(d+\bar{\eta})$ as presented in Appendix A. A total of 20 wave elevations were measured for the 10 runs.

4.2.2 Horizontal Fluid Velocity Measurement

The air bubble releasing technique was applied in this study. Pitot tubes were placed at various stations in surf zone. The tip of pitot tube was placed approximately 0.5 mm above the plywood beach floor and approximately 2.0 cm away from the glass observation panel. The purpose of this arrangement was to minimize the effect of bottom and side friction.

Due to the limited width of wave tank, the breaking waves in surf zone was approximately straight and parallel. Therefore, it is a reasonable assumption that both water elevation and horizontal fluid velocity are uniformly distributed across the beach, or, there is no lateral variation of flow field in surf zone. Consequently, the films obtained through the glass panel would well represent the flow at this section.

The film shooting speed was adjusted such that there would be 22 to 28 frames recorded in one wave cycle. Since the wave periods studied ranged from 1.0 to 2.0 second, the film shooting speed was adjusted from 14 frames per second to 22 frames per second.

The principle of air-bubble measuring technique is explained in the following paragraphs. As we release a tiny air bubble through the tip of pitot tube, the bubble in fluid would reach a terminal rising velocity shortly after it emerged in the fluid. The constant rising speed of the air bubble through water column of uniform stream would form a straight path line. If the air bubble rising velocity (U_b) were known, the flow rate of the uniform stream can be obtained by measuring the slope of the air bubble in fluid. Let m be the slope of the air bubble line measured from the vertical cross-sectional line, the flow speed would be mU_b.

If the air bubbles were released continuously, the consecutive rising air bubbles would form a straight line in a uniform stream as illustrated in Photo 2. For unsteady flow, the bubble lines would be sweeping back and forth in response to an oscillating flow field.

Assuming that the fluid flow is in Stoke's range, that is, the air bubble moves as the same speed with fluid

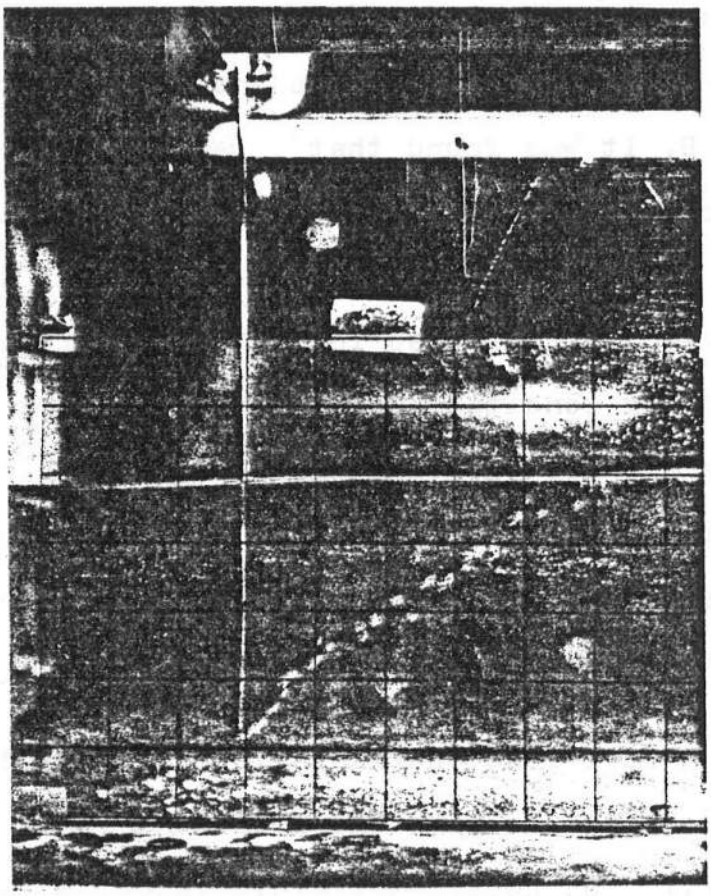

Opening of pitot tube : 0.5 mm

Flow rate in open channel : 0.25 m/sec

Grade system on glass panel : 1"x1"

Photo 2 Calibration of Air Bubble Rising Velocity

particle, the pathlines of air bubble would represent the surrounding fluid flow.

A dynamic analysis of air bubble in unsteady wave field was made to study the response of air bubble in unsteady flow. Details of this analysis is presented in Appendix B. It was found that , based on linear wave theory, the error of measured fluid velocity using air bubble technique is less than 20% at still water level due to vertical acceleration. It was also found that the released air bubble in laboratory condition would reach terminal velocity in approximately 0.04 second, which is 2 to 4% of the testing wave periods. In theory, the released air bubbles would travel less than 10% of the total water depth before reaching the terminal velocity.

In surf zone where shallow water condition applies, it is reasonable to make the following assumptions:

(1) The horizontal fluid velocity is uniformly distributed over water depth,

(2) The vertical component of fluid velocity can be neglected during measurement.

The instantaneous mean horizontal velocity is then the product of the air bubble rising velocity and the slope of bubble line at that same instant. Figure 4-4 is sample bubble lines reduced from a test run. The approximate

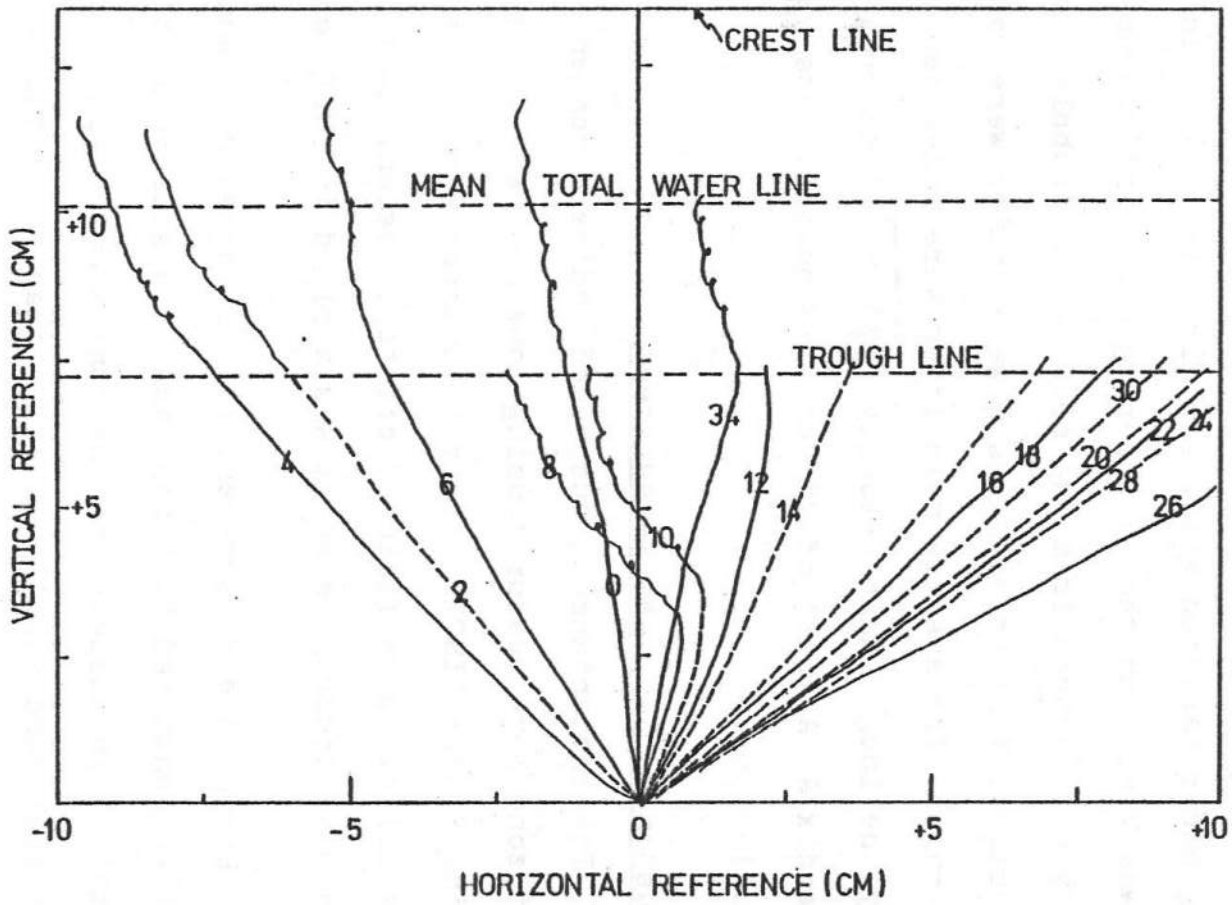

Note: The numbers denote the order of air bubble lines reduced in one wave period

Figure 4-4 Air Bubble Lines in Breaking Wave Field

straight lines substantiated the validity of air bubble releasing technique.

To obtain an instantaneous horizontal fluid velocity, the movie films were projected frame by frame on the engineering paper taped on wall. The air bubble lines in each frame was traced on the engineering paper and the horizontal velocity was reduced from the slope of the bubble line at that instant. Velocities for six wave cycles were reduced and averaged. The average velocities were non-dimensionalized by the local phase velocity ($\sqrt{g(d+\bar{\eta})}$) and presented in Appendix A. A total of 20 velocity measurements were made for the 10 runs.

4.3 Suspended Sediment Measurement

The instantaneous suspended sediment concentrations in surf zone were measured using Iowa Sediment Concentration Measuring System (ISCMS). This instrument was applied successfully in wave field of offshore region. Some difficulties were confronted as it was applied in surf zone.

During the measurement in surf zone, dirt and other impurities contained in beach sand were stirred in the fluid and remained in suspension. The contaminated fluid introduced higher concentration reading than the actual amount. This kind of error can be minimized by constant washing of beach sand. The zero reading in clear water kept changing

from time to time due to the rise and fall of water temperature. In consequence, zero readings had to be adjusted for each set of measurement.

There were air bubble intrusion in the water column due to wave breaking. The response of air bubbles in the probe sensing column was extra light reflected on the light sensor, causing a high frequency fluctuation superimposed on the true concentration reading. This high frequency noise was removed by using a built-in analog filter with time constant 0.058 second (17.24 Hz).

The calibration curve of ISCMS output voltage vs. sediment concentration was also obtained. During the calibration, sand sample from wave tank was put in a cylindrical pyrex glass container with 8 inch diameter and 18 inch height. An electric motor driven propeller was located approximately 1 inch above the bottom of the container. With adjusted motor speed and various amount of sand in the container, the suspended sediment concentration also varied.

The ISCMS voltage reading was recorded at the same time while suspended sediment sample was drained through a side wall of container into the 50 ml sampler. Sediment concentration was obtained by weighing the dry weight of the sample. The sediment concentrations were plotted against the corresponding ISCMS voltage reading as shown in Figure 4-5.

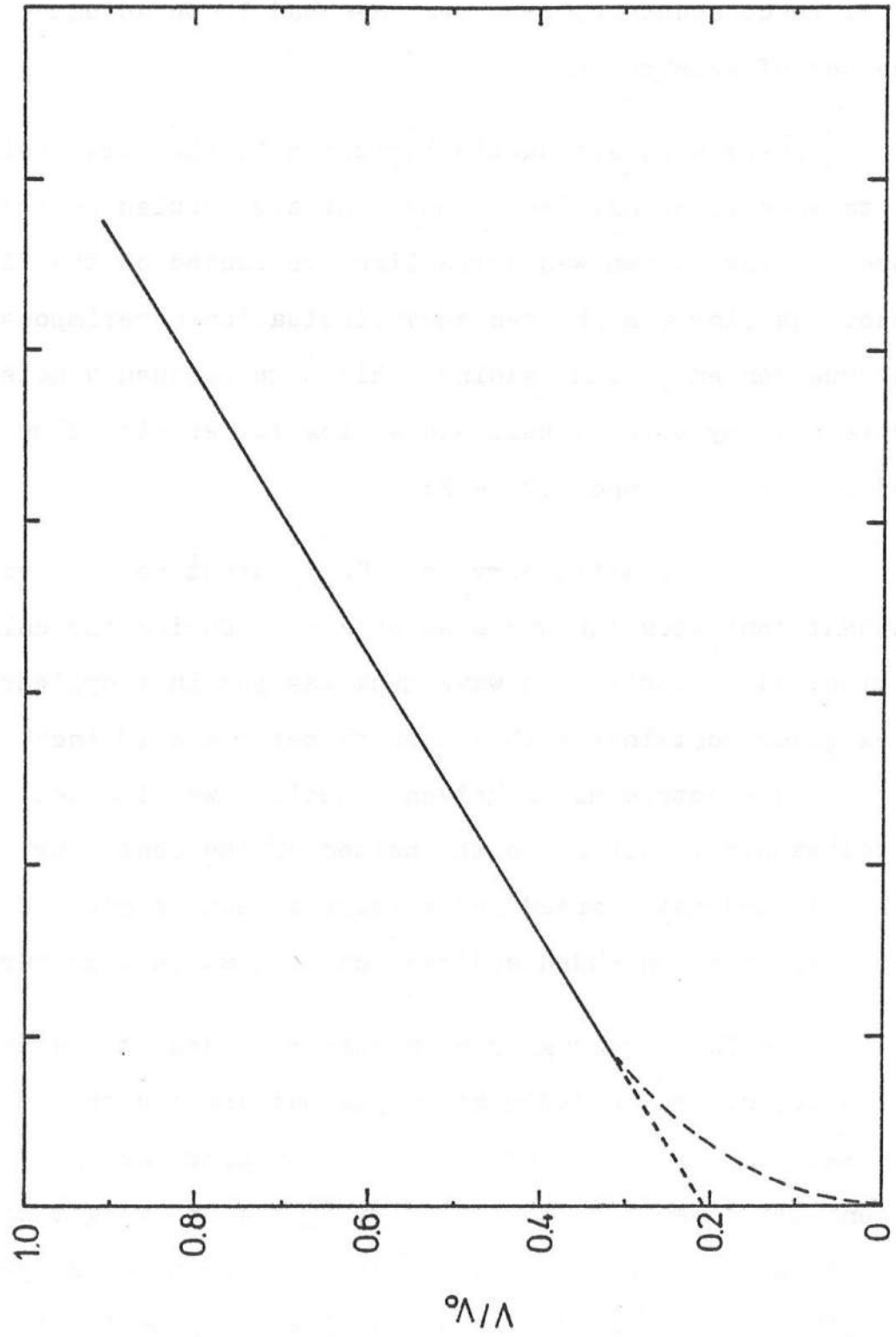

Figure 4-5 Calibration Curve of ISCMS Probe

The calibration curve indicated that a linear relationship existed when the suspended sediment concentration was greater than 20 gram/liter.

During wave tank measurement, both ISCMS probe and the capacitance wave probe were located in parallel, approximately 5 mm above sand bed. Synchronized sediment concentration and water elevation outputs were recorded on a two-channel HP chart recorder. The incident wave heights, breaking wave heights and wave periods were also recorded. A total of four runs were conducted. The arrangement of wave conditions are summarized on Table 4-2. The measured results are presented in Appendix C.

Table 4-2 Lab. Wave Conditions for Suspended Sediment Concentration Measurement

Run Number	Incident Wave Height, H_c (cm)	Breaking Wave Height, H_b (cm)	Wave Period T (sec)	Breaker Type
1	14.0	16.0	1.7	Spilling
2	16.0	18.0	1.5	Spilling
3	12.0	15.0	1.9	Plunging
4	10.0	13.0	1.2	Spilling

CHAPTER 5

RESULTS

In this chapter the data analysis procedures and the results are presented. The calibrated empirical formula are applied in the on/offshore sediment transport model to predict the beach profile evolution. Section 5.1 presents the calibrated results of breaking wave similarity model. The experimental data of previous researchers are analyzed using the same procedures and compared with the present results. The physical implication and the region of validity of the similarity model are discussed. In Section 5.2 the suspended sediment concentration data are analyzed using spectral analysis and data averaging techniques. Physical importance of the analyzed data is discussed while no quantitative conclusions are made. Section 5.3 presents the numerical results of on/offshore model developed in Section 3.3. Both beach profile evolutions and erosion rates are predicted for various wave and beach conditions. The numerical results are compared with the laboratory results of both the author and the previous researchers.

5.1 Breaking Wave Similarity

The 20 sets of laboratory water elevation and horizontal fluid velocity data measured as shown in Appendix A are analyzed. Detailed data analyzing procedures and results are discussed in the following paragraphs.

In the first step, the local water depths, including sea water level and wave set-up,were reduced from the movie film together with the water elevation measurement. The depths obtained at each station were used to non-dimensionalize the measured water elevation and velocity data. Due to the importance of total water depth for similarity model, the measured set-ups at different wave conditions were compared with the theoretical results by Longuet-Higgins and Stewart (1963). Wave set-up values from Runs 5,6 and 7 were compared with the theoretical predictions as shown in Figures D-1, D-2 and D-3 in Appendix D. The definition sketch, experimental results and the equations used for wave set-up prediction are also included in Appendix D. Since the measured set-ups were in good agreement with Longuet-Higgins prediction, it was applied in the on/offshore transport model.

For similarity analysis, the harmonic amplitudes and phase angles were obtained through Fourier Series analysis. The principle of Fourier Analysis is explained briefly as follows. In theory, any periodic function can be expressed by the Fourier Series defined as:

$$f(t) = a_0 + \sum_{n=1}^{\infty} \left(a_n \cos\frac{2\pi n}{T} t + b_n \sin\frac{2\pi n}{T} t\right)$$

where f(t) is the periodic function, t is the independent variable indicating time, T is the 1st harmonic period and a_0, a_n, b_n are Fourier Coefficients defined as follows:

$$a_0 = \frac{1}{T}\int_0^T f(t)\,dt$$

$$a_n = \frac{2}{T}\int_0^T f(t)\cos\frac{2\pi n}{T} t\,dt$$

$$b_n = \frac{2}{T}\int_0^T f(t)\sin\frac{2\pi n}{T} t\,dt$$

These Fourier Coefficients can also be expressed in numerical form as:

$$a_0 = \frac{1}{M}\sum_{n=0}^{m-1} f(n\cdot\Delta t)\cdot\Delta t$$

$$a_n = \frac{2}{M}\sum_{n=0}^{m-1} f(n\cdot\Delta t)\cos\left(\frac{2\pi n}{T} t\right)\cdot\Delta t$$

$$b_n = \frac{2}{M}\sum_{n=0}^{m-1} f(n\cdot\Delta t)\sin\left(\frac{2\pi n}{T} t\right)\cdot\Delta t$$

where $M\cdot\Delta t = T$ and M is the data points in one wave cycle. In this study the data points ranged from 22 to 27 depending upon the wave period and film speed.

Based on Equation (3-21), the non-dimensional water elevation can be expressed as:

$$\frac{\eta(t)}{(d+\bar{\eta})} = \sum_{n=1}^{\infty} \alpha_n \sin(n\sigma t + \phi_n) \qquad (5\text{-}2)$$

The non-dimensional water elevations can also be expressed in Fourier Series as:

$$\frac{\eta(t)}{(d+\bar{\eta})} = \sum_{n=1}^{\infty} (a_n \cos n\sigma t + b_n \sin n\sigma t) \qquad (5\text{-}3)$$

Since the mean water level of each set of data was set at $d+\bar{\eta}$,or, MWL=0, the time-mean Fourier Coefficient is zero ($a_0 = 0$). To obtain the Fourier Coefficients of the non-dimensional water elevation and velocity functions, data points of these functions were digitized in a constant time interval. The data points were then Fourier Transformed with computer program for desired Fourier Coefficients. The amplitude coefficients and phase angles were determined based on the trapezoid rule and Equations (5-2) and (5-3):

$$\alpha_n = \sqrt{a_n^2 + b_n^2} \qquad (5\text{-}4)$$

$$\phi_n = \tan^{-1} \frac{a_n}{b_n} \qquad (5\text{-}5)$$

The Fourier analysis of horizontal velocity was based on Equation (3-27):

$$\frac{u(t)+\bar{u}_R}{k\sqrt{g(d+\bar{\eta})}\,(1+\frac{\eta}{4})} = \sum_{n=1}^{\infty} \beta_n \sin(n\sigma t + \gamma_n) \qquad (5\text{-}6)$$

Before applying Fourier Analysis, the proportion constant k in Equation (5-6) was determined. Physically, the value $k\sqrt{g(d+\bar{\eta})}$ is the phase velocity of breaking wave in surf zone. The constant k varies with different types of breakers.

For plunging breaker without interference of breaking waves in surf zone and the ratio of H_b/d is high, a high k value is expected. On the other hand, a low k value is expected for spilling breaker, since breaking waves are interacting with each other and the ratio of H_b/d is low.

In laboratory measurement, the phase velocity of the breaking wave is the sum of maximum onshore horizontal velocity and the mean return flow speed. The mean return flow is just the numerical average of the horizontal velocity over one wave period, which is always in the offshore direction. The experimental results of the mean return flow strength and the constant k are shown in Figures 5-1 and 5-2 respectively. It appears that the mean return flow strength increases with increasing I_w but gradually reaches a constant in the spilling breaker region. The k value, on the other hand, decreases with increasing I_w. Since k is actually the ratio of wave celerity and $\sqrt{g(d+\bar{\eta})}$, the results are the consequence that spilling breakers travel slower than plunging breakers.

The wave amplitude coefficients, α_n , and wave phase coefficients, ϕ_n , of the first five harmonics obtained for the 10 runs are shown on Table 5-1. These values were plotted against the surf zone parameter as shown in Figure 5-3. The phase angles were adjusted so that $\phi_1=0$. These data are quite scattered but the trend is clear. Both α and ϕ become

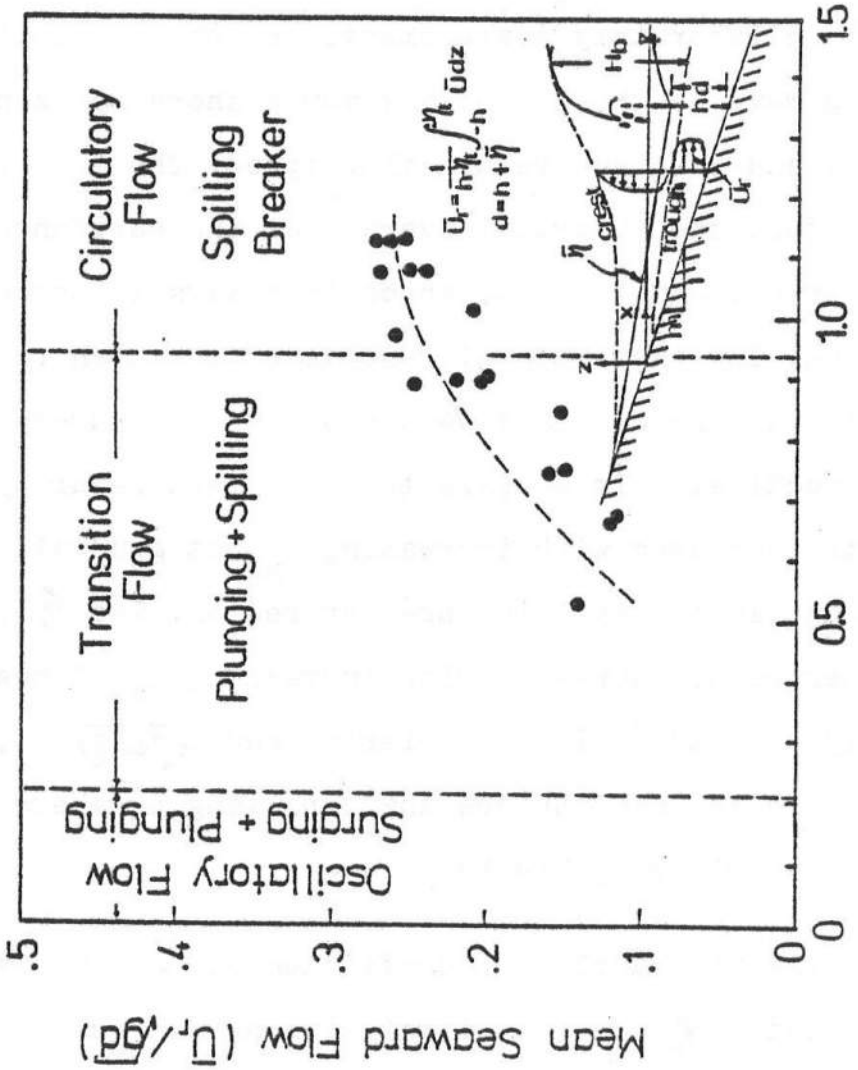

Figure 5-1 Return Flow vs. I_w

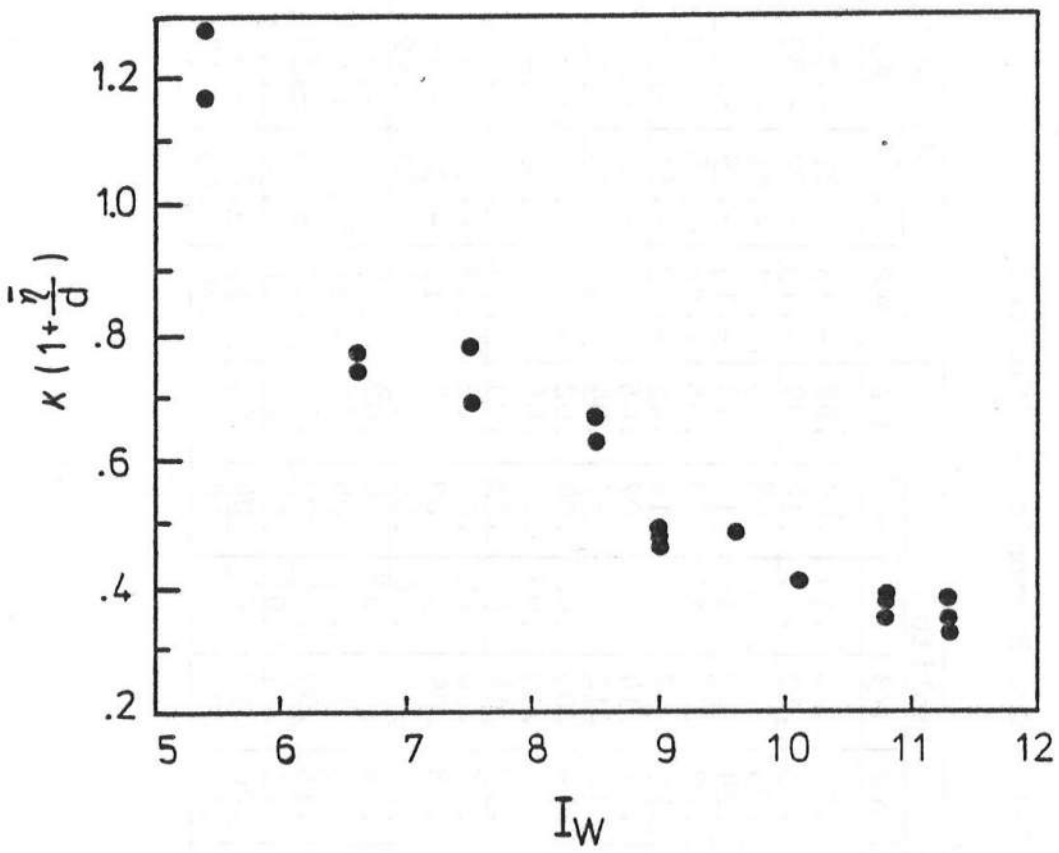

Figure 5-2 κ vs. I_w

Table 5-1 Wave Harmonic Coefficient

Run No.	Station	Amplitude						Phase (π)				
		α_1	α_2	α_3	α_4	α_5	α_6	ϕ_2	ϕ_3	ϕ_4	ϕ_5	ϕ_6
PB-1	190	.43	.22	.16	.10	.09	.08	-.13	-.21	-.35	-.41	-.56
	210	.41	.23	.15	.13	.12	.09	-.13	-.22	-.33	-.46	-.60
PB-2	190	.37	.23	.15	.11	.08	.05	-.17	-.41	-.53	-.82	-.96
	210	.39	.24	.20	.14	.12	.10	-.15	-.29	-.48	-.68	-.86
PB-3	190	.46	.27	.17	.10	.09	.05	-.26	-.48	-.62	-.82	-1.00
	210	.44	.28	.17	.15	.10	.08	-.27	-.51	-.72	-.80	-1.12
PB-4	190	.39	.22	.14	.10	.07	.05	-.13	-.32	-.35	-.51	-.61
	210	.37	.18	.12	.08	.07	.04	-.12	-.19	-.36	-.48	-.53
PB-5	190	.34	.19	.09	.06	.04	.02	-.08	-.22	-.39	-.43	-.70
	210	.30	.22	.13	.08	.07	.06	-.09	-.24	-.40	-.50	-.62
	230	.32	.18	.14	.07	.05	.03	-.14	-.25	-.41	-.51	-.65
PB-6	190	.32	.15	.10	.07	.04	.02	-.13	-.34	-.41	-.61	-.73
	210	.32	.18	.09	.06	.03	.03	-.19	-.36	-.46	-.57	-.79
	230	.30	.14	.10	.06	.04	.03	-.12	-.30	-.42	-.58	-.69
PB-7	190	.28	.18	.12	.06	.04	.02	-.23	-.46	-.77	-.79	-.98
	210	.32	.15	.10	.07	.04	.04	-.21	-.39	-.54	-.71	-.81
	230	.31	.15	.09	.06	.05	.03	-.19	-.33	-.59	-.64	-.97
PB-8	190	.31	.20	.11	.06	.06	.04	-.21	-.36	-.58	-.64	-.80
PB-9	190	.31	.20	.12	.08	.04	.03	-.11	-.29	-.44	-.67	-.66
PB-10	190	.40	.18	.09	.07	.04	.02	-.30	-.43	-.57	-.80	-1.18

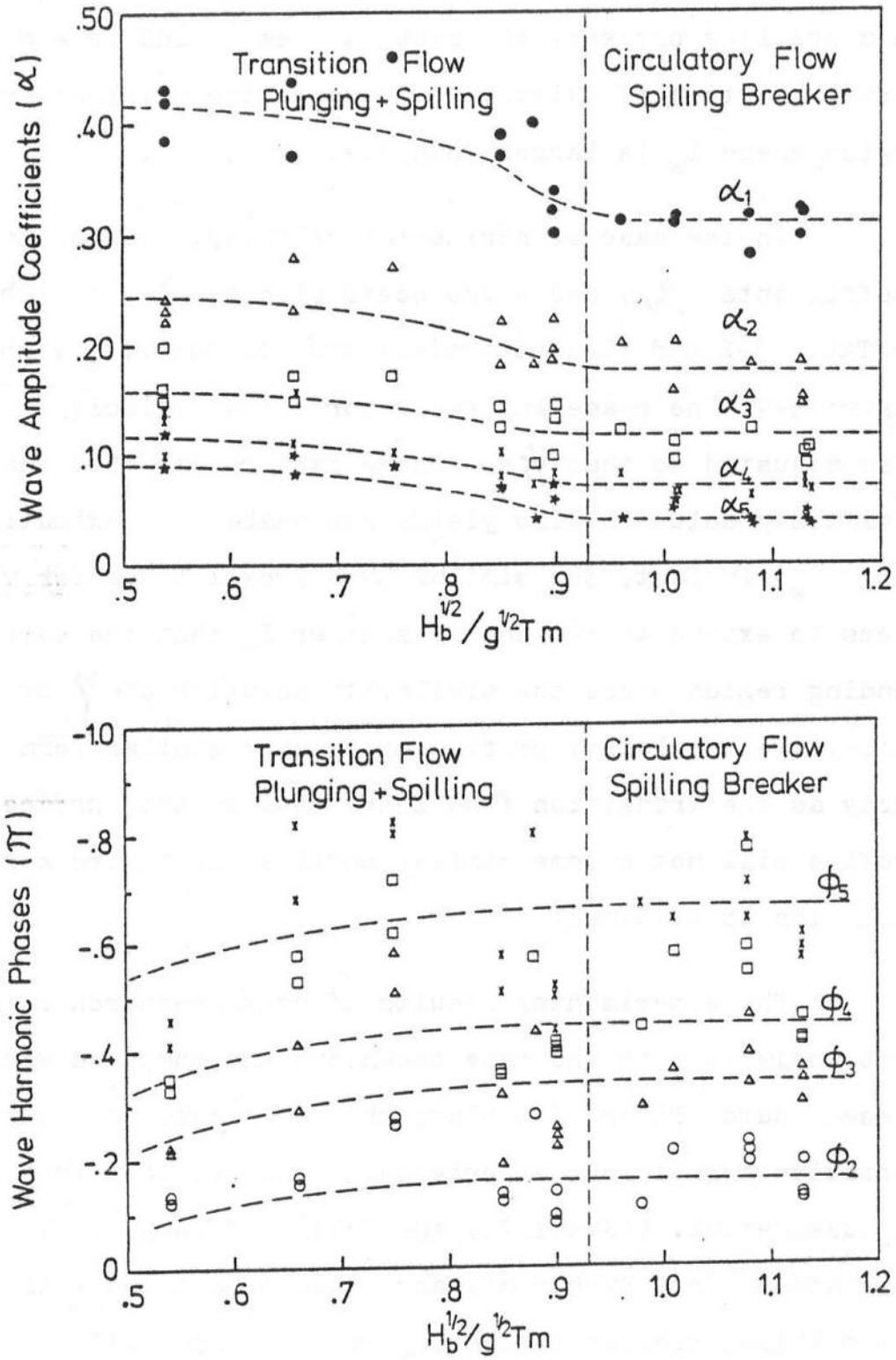

Figure 5-3 Wave Amplitude Coefficients and Phase Coefficients vs. I_w

constant when I_w becomes large. Since a large I_w corresponds to a spilling breaker, the results seem to indicate a similarity solution, if exists, would be in the spilling breaker region where I_w is larger than 0.9.

In the case of horizontal velocity, the amplitude coefficients, β_n, and phase coefficients, γ_n, are shown on Table 5-2 and plotted against the parameter, I_w, shown in Figure 5-4. The phase angles of horizontal velocity were also adjusted so that $\gamma_1 = 0$. These data reveal that the similarity solution also yields reasonable approximations for large I_w. In fact, the similarity approximations for velocity seems to extend to regions of smaller I_w than the corresponding region where the similarity solution of η becomes valid, i.e., velocity profile approaches similar form as early as the transition flow zone, whereas the surface profile will not become similar until spilling breaker condition is attained.

The experimental results of other researchers are also analyzed with the same technique and compared with the present data. Figure 5-5 plots the non-dimensional surface variation for various experients. In there, data from Svendsen et.al. (ISVA,1978) and Sakai and Iwagaki (1978) are also shown. Both Svendsen's and Sakai's data are well within the spilling breaker region (I_w ranging from 1.12 to 2.27). Their test conditions are listed in Table 5-3.

Table 5-2 Velocity Harmonic Coefficient

Run No.	Station	Amplitude						Phase (π)		
		β_1	β_2	β_3	β_4	β_5	β_6	ψ_2	ψ_3	ψ_4
PB-1	190	.56	.25	.17	.12	.04	.04	-.01	-.06	-.07
	210	.54	.31	.18	.10	.06	.04	-.04	.10	.07
PB-2	190	.70	.43	.13	.06	.02	.008	.11	.14	.15
	210	.72	.40	.12	.05	.02	.02	.04	.01	.08
PB-3	190	.76	.39	.15	.02	.01	.05	.08	.17	.03
	210	.75	.37	.11	.02	.03	.01	.05	.07	.41
PB-4	190	.90	.24	.11	.06	.01	.04	.01	.05	-.03
	210	.76	.29	.14	.08	.04	.02	.05	.00	.09
PB-5	190	.96	.35	.06	.07	.06	.02	.21	.78	.90
	210	.91	.29	.08	.14	.09	.05	.21	.99	1.03
	230	.92	.25	.05	.08	.06	.04	.22	.90	1.14
PB-6	190	.86	.33	.14	.02	.004	.02	.14	.01	.21
	210	.86	.29	.07	.04	.02	.009	.10	.00	1.11
	230	.81	.30	.05	.04	.03	.02	.07	.17	1.13
PB-7	190	.61	.42	.15	.03	.05	.07	.04	.01	.40
	210	.85	.29	.09	.02	.03	.01	.09	-.13	.99
	230	.84	.32	.03	.04	.05	.009	.12	.22	.19
PB-8	190	.86	.32	.03	.05	.06	.02	.18	.27	.91
PB-9	190	.83	.23	.05	.05	.02	.04	.10	.19	1.24
PB-10	190	.78	.25	.04	.06	.02	.05	.19	-.30	.81

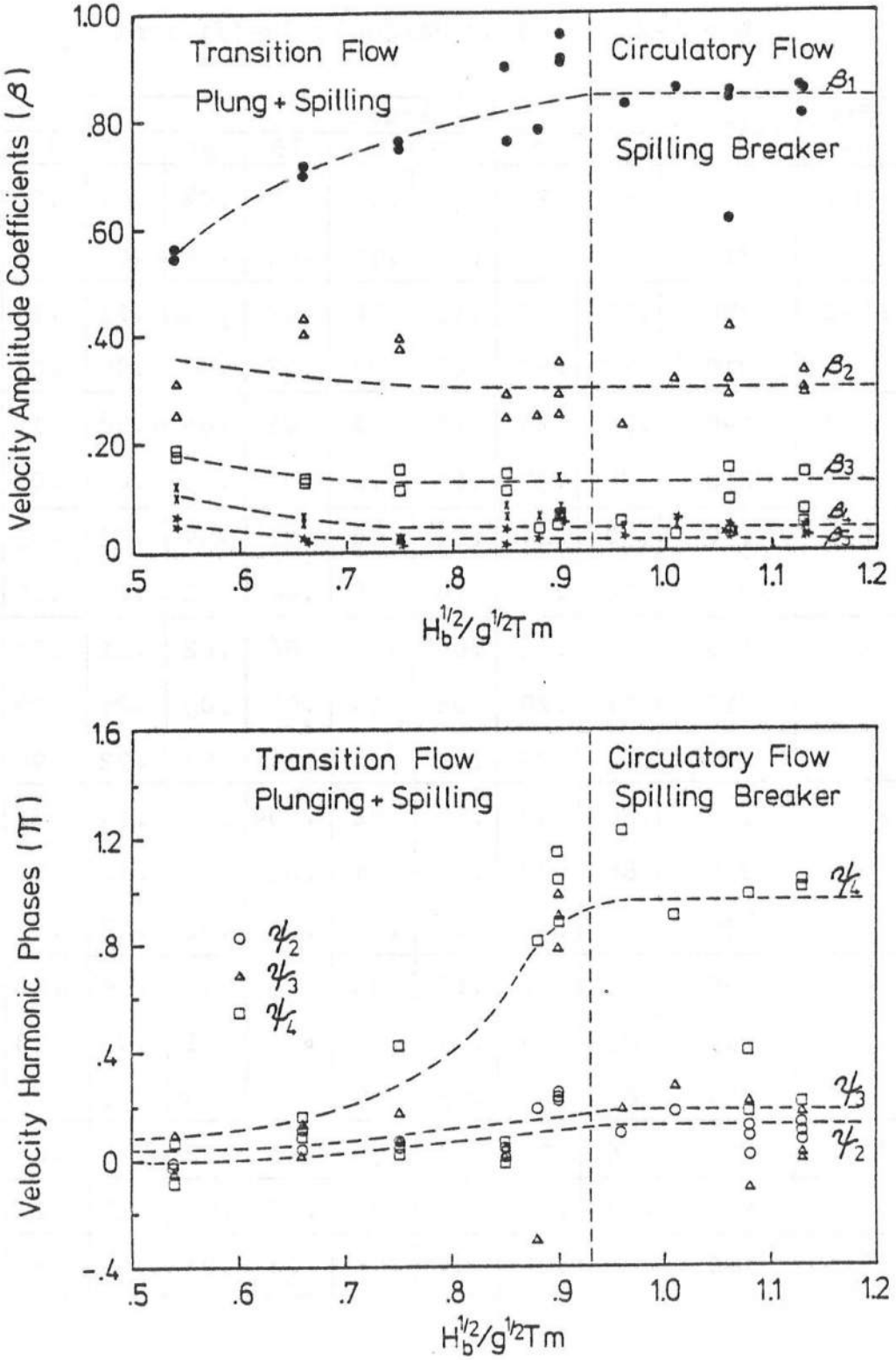

Figure 5-4 Velocity Amplitude Coefficients and Phase Coefficients vs. I_w

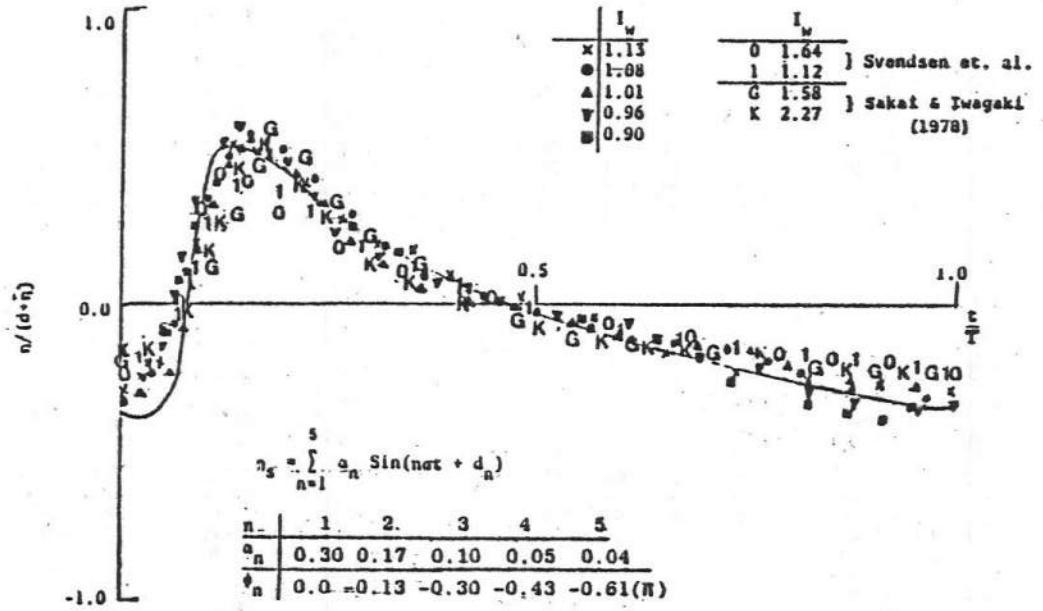

Figure 5-5 Non-dimensional Surface Profiles

Table 5-3 Test Conditions of Svendson's and Sakai and Iwagaki's

Lab. Conditions (ISVA) 1978

Run No.	Breaking Wave Height, H_b (cm)	Wave Period T (sec)	$\frac{H_b^{1/2}}{g^{1/2}T \cdot \tan\alpha}$
070703	4.12	1.43	1.50
070705	4.43	1.43	1.64
451015	5.25	2.22	1.12
451018	4.95	2.22	1.09

Lab. Conditions (Sakai and Iwagaki) 1978

Run No.	Breaking Wave Height, H_b (cm)	Wave Period T (sec)	$\frac{H_b^{1/2}}{g^{1/2}T \cdot \tan\alpha}$
2-2-2	9.4	1.24	1.58
3-2-1	11.5	1.24	2.27

All the data sets seem to exhibit a gross similarity feature. A closer examination of these profiles reveals that the fine features of similarity vary for data sets obtained by different investigators. These variations can best be explained with the aid of Table 5-4 where the statistics of the coefficients in the similarity solution are tabulated. First of all, the standard deviations of the amplitude coefficients are all very small (no more than 4% from the mean), which means the similarity solution is good in the region specified. On the other hand, the absolute value of α's are different. The present laboratory value and Sakai and Iwagaki's values are very close. They both differ somewhat from ISVA's values.

The relative importance of each harmonic component can be assessed from the values listed under $\alpha/\Sigma\alpha$. For instance, the fundamental component has a value of 0.4 to 0.5. The total contribution due to harmonics higher than third is usually less than 20%. In terms of wave height, the effect of these higher harmonics is insignificant because of the phase shift. In terms of energy, their contributions are even less. The relative importance of the first three harmonic components is quite consistent among the three sets of data.

The results of phase angle are somewhat unexpected. All the data show that the second harmonic leads the first

Table 5-4 Statistics of Wave and Velocity Harmonics

AMPLITUDE HARMONICS

Source	Amplitude (α)				Phase (ϕ)			No. Exps.
		Mean	σ	$\alpha/\Sigma\alpha$		Mean	σ	
Delaware	α_1	0.30	0.038	0.41	ϕ_1	-	-	9
	α_2	0.17	0.022	0.22	ϕ_2	-0.13π	0.027	
	α_3	0.10	0.011	0.15	ϕ_3	-0.30π	0.22	
ISVA	α_1	0.23	0.035	0.47	ϕ_1	-	-	32
	α_2	0.11	0.016	0.22	ϕ_2	-0.14π	0.08	
	α_3	0.07	0.012	0.14	ϕ_3	-0.28π	0.14	
Sakai and Iwagaki	α_1	0.32	-	0.48	ϕ_1	-	-	2
	α_2	0.15	-	0.23	ϕ_2	-0.25π	-	
	α_3	0.09	-	0.13	ϕ_3	-0.40π	-	

VELOCITY HARMONICS

Source	Amplitude (β)				Phase (ψ)			No. Exps.
		Mean	σ	$\beta/\Sigma\beta$		Mean	σ	
Delaware	β_1	0.81	0.078	0.63	ψ_1	-	-	8
	β_2	0.30	0.054	0.23	ψ_2	0.05π	0.09	
	β_3	0.08	0.043	0.06	ψ_3	0.07π	0.15	

σ : standard deviation

harmonic and the third harmonic leads both first and second. One would expect the other way around as the higher harmonics should have smaller phase velocities. The values of phase coefficients are very close for the Delaware and ISVA data. They both differ from Sakai and Iwagaki's value. This point is further examined later.

Figure 5-6 presents the non-dimensional velocity profiles. The statistics of velocity harmonics are also tabulated in Table 5-4. In here, the fundamental component lags the successive lower component as expected. However, these phase lags are all very small. The combined effects of dominant fundamental components and small phase shift result in a more symmetric profile than that of wave forms. The same kind of results have been obtained by Flick (1978) and Iwagaki (1970). A tentative explanation has been offered on the reasoning that the bottom and internal friction tend to dampen the higher wave components at a faster rate. The experimental data also show that the peak horizontal velocity always lags the peak water surface variation such as illustrated by an example in Figure 5-7.

As the wave breaks on a slope, the motion appears to be quite disorderly. When the breaking wave proceeds upslope, it gradually regains its regular appearance. The question is how far shoreward from the breaking point can the similarity solution be considered

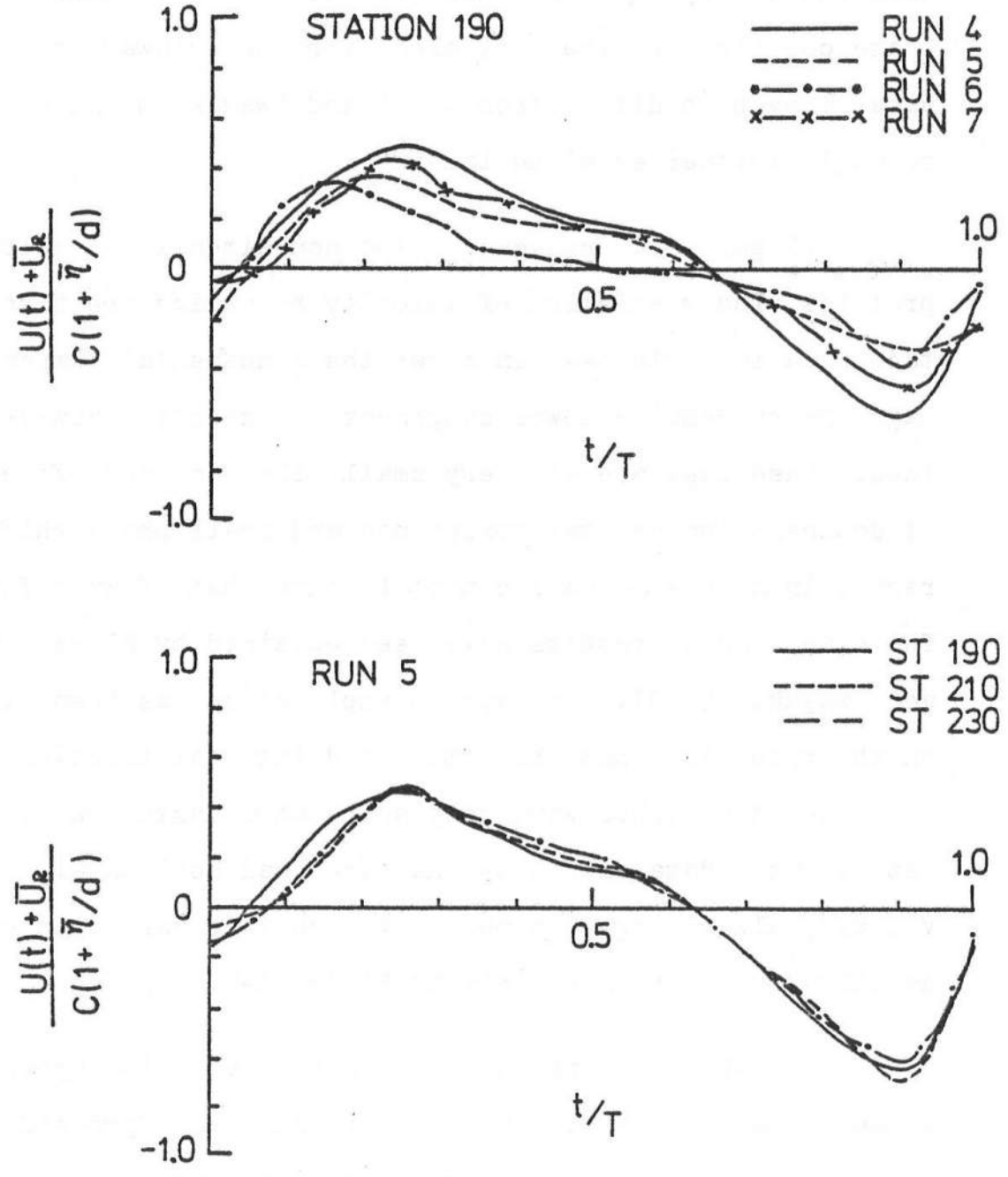

Figure 5-6 Non-dimensional Velocity Profiles

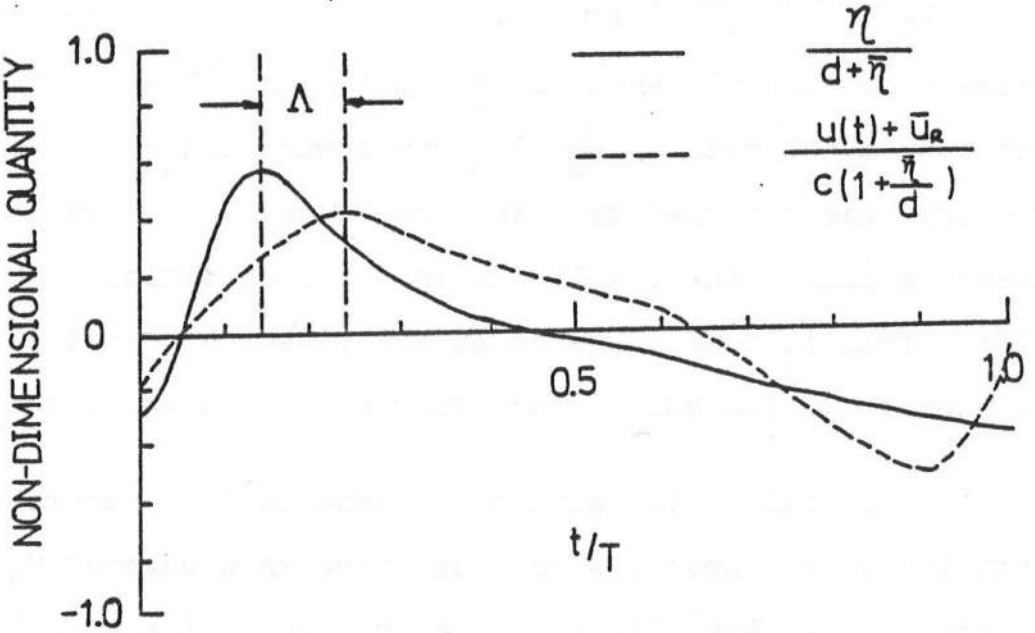

Figure 5-7 Comparison of Surface Profile and Velocity Profile

adequate. For this purpose, the phase angles are plotted against the non-dimensional depth d/d_b with d_b the depth at the breaking point. Four sets of data from different investigators are shown in Figure 5-8. In here, the phase coefficients are defined in terms of COSINE phase lag, i.e.,

$$\eta = \sum_{n=1}^{\infty} \alpha_n \cos(n\sigma t + \xi_n) \qquad (5\text{-}7)$$

The relationship between ξ_n and ϕ_n, which is defined as the SINE phase lag, is

$$\xi_n = (n-1)\frac{\pi}{2} + \phi_n \qquad (5\text{-}8)$$

These phase coefficients are shown to vary slowly with d/d_b and approach limits at $\frac{\pi}{2}$ intervals when $d/d_b \to 0$. Since the profiles measured by Sakai and Iwagaki are near the breaking point, the results in this figure explain why they differ from that of the present experiment and that of ISVA; both were carried out in the inner surf zone where $d/d_b < 0.7$.

To utilize the similarity equations to describe the breaking wave properties one must have knowledge of $\bar{U}_R$ and k as appeared in Equation (5-6). At present, we are unable to predict either. The experimental results of these quantities are, however, shown in Figures 5-1 and 5-2 respectively. It appears that the return flow strength increases with increasing I_w but gradually reaches a constant in the spilling breaking region. The k value, on the other hand, decreases with increasing I_w. Since k is actually the ratio of wave

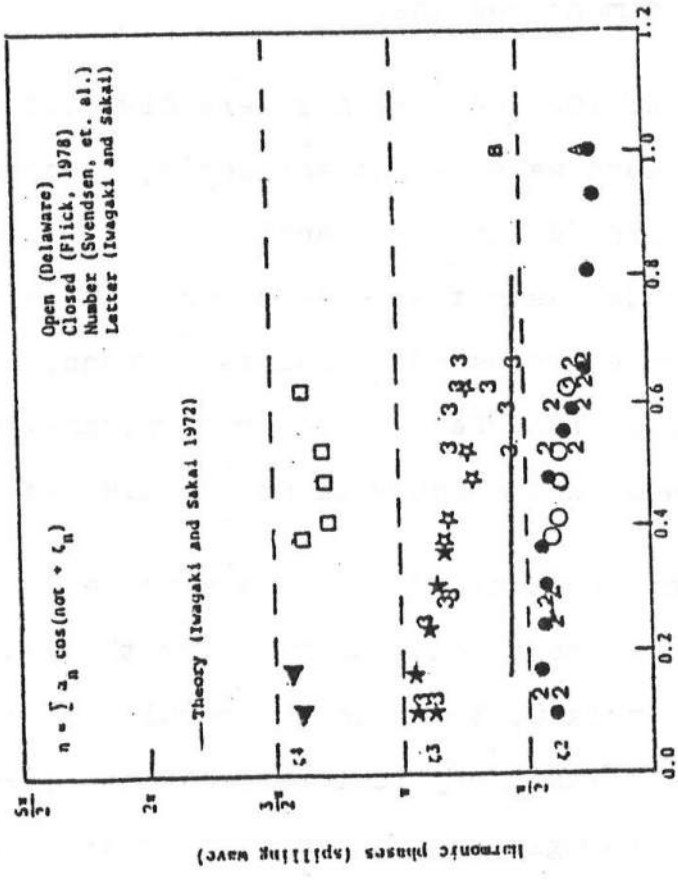

Figure 5-8 Variations of Phase Coefficients as a Function of d/d_b

celerity and $\sqrt{gd}$, the results are the consequence that spilling breakers travel slower than plunging breakers.

5.2 Suspended Sediment Concentration

Both spectral analysis and signal averaging techniques were used in analyzing the measured suspended sediment data. The purpose of this analysis was to determine statistically the correlation of breaking wave and the corresponding sediment suspension.

A total of 1024 data points were digitized from the strip charts of both wave height and sediment concentration records of each run for spectral analysis. The time increment between data points was set at 0.04 second, therefore, approximately 22-33 wave cycles were analyzed depending upon the wave period of each run. Details of spectral analysis procedures are well known and will not be discussed here.

The power spectral of incident wave height, breaking wave height and sediment concentration for the four runs are presented in Appendix C. Based on the results of spectral analysis, some important physical implications are discussed. For all runs, the single and concentrated peak of incident wave spectrum indicated a periodic, long crested wave. For breaking wave spectrum, more peaks appeared at $2f_c$, $3f_c$, ... where f_c is the fundamental wave frequency. This result substantiate the harmonic transfer process of shoaling waves

as discussed in section 3.2. The sharp lowering of peak amplitude with higher frequency component also indicated that the contribution of higher wave harmonic decreases quickly. There were also multiple peak in the sediment concentration spectrum, indicating a multiple suspension process exists in one wave cycle. The major sediment suspension appeared to be corresponding to the fundamental frequency f_c and the secondary suspension corresponding to $2f_c$. This phenomenum was more pronounced for plunging breaker as indicated by the results of Run 3. The double peak sediment concentration spectra were also reported by previous researchers such as Brenninkmeyer (1973) and Thornton (1970). The secondary peak was reasoned to be the backward movement of the same sediment cloud due to the breaking wave suspension.

The measured instantaneous sediment concentrations were a random process. In order to obtain a mean sediment suspension formula, the signal averaging technique was used. The analog ISCMS outputs up to 120 wave cycles were first converted into digital data points with fixed sampling interval Δt. The digital data were then averaged at each instant of one wave cycle. The sampling interval was set at 0.01 second and the number of digital points ranged from 125 to 190 in one wave cycle depending upon the wave period.

The results of averaged sediment concentrations over

20, 40, 60, 80 wave cycles for spilling and plunging conditions are shown in Figures 5-9 and 5-10 respectively. The averaged curves became stable after averaging over 60 wave cycles. The curves stabilize faster in Figure 5-10, indicating a more regular suspension process for plunging breaker. The averaged concentration curves for 60 wave cycles are presented in Appendix C. These average concentration curves can be expressed as:

$$\frac{\bar{C}}{\bar{C}_{max}} = \frac{C_0}{2} + \sum_{n=1}^{\infty} C_n \sin(n\omega t + \theta_n) \qquad (5\text{-}9)$$

where $C_0/2$ is the mean concentration , c_n is the harmonic concentrations and θ_n is the phase angle.

It was found that the mean concentration term is predominant for spilling breaker while the periodic concentration term is predominant for plunging breaker. The results of $\bar{C}_{max}$ for each run are compared with the corresponding breaking wave heights and spectral energies as shown on Table 5-5. Due to the uncertainty of ISCMS application in surf zone the measured and analyzed data were not applied in the on/offshore sediment model.

5.3 On/offshore Sediment Transport Model

A computer program was developed to predict the sediment transport rate. An outline of the computer program is presented in Appendix E. A total of 11 numerical runs

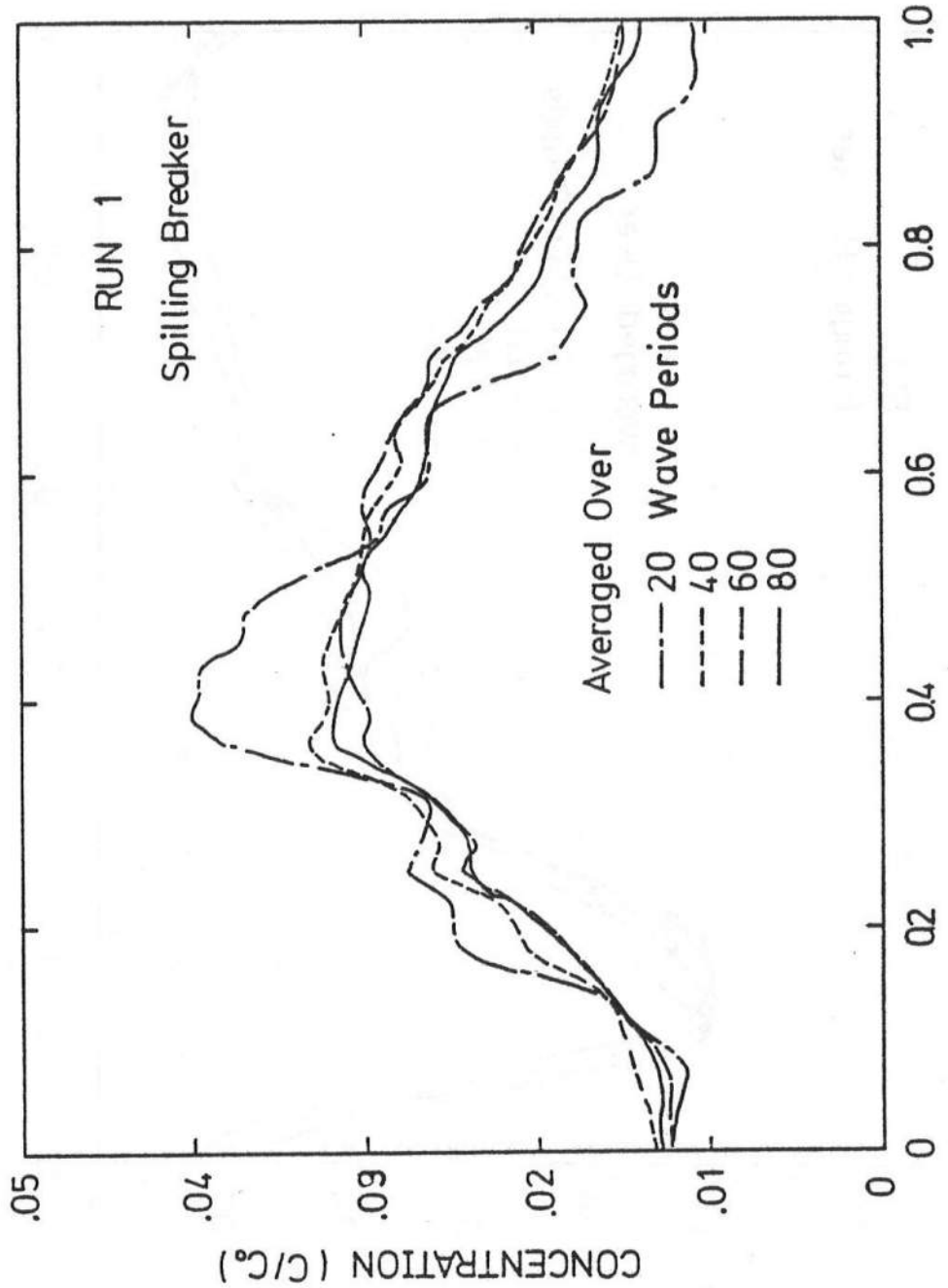

Figure 5-9 Instantaneous and Averaged Suspended Sediment Concentration for Spilling Breaker

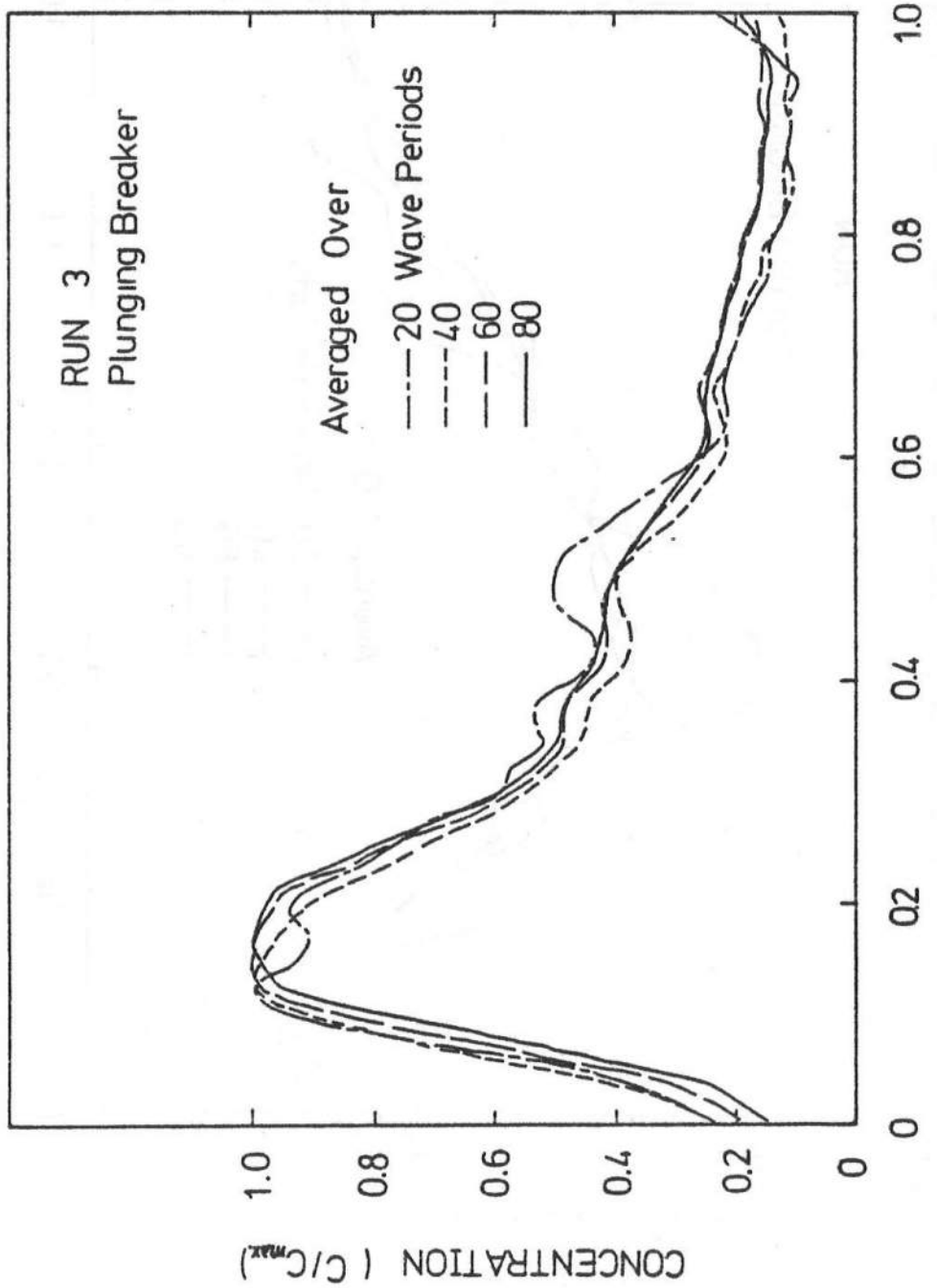

Figure 5-10 Instantaneous and Averaged Suspended Sediment Concentration for Plunging Breaker

Table 5-5 Test Results of Lab. Suspended Sediment Concentration

Run Number	Breaking Wave Height, H_b (cm)	Breaking Wave Spectral Energy in Surf Zone (cm^2-sec)	Averaged Max. Sed. Concentration (ppm)
1	16.0	15.1	6.0×10^3
2	18.0	16.8	2.0×10^4
3	15.0	13.9	3.6×10^4
4	13.0	18.9	2.0×10^3

were conducted as summarized on Table 5-6. Three runs were made to compare with the laboratory results conducted by the authors, Sunamura and Horikawa (1974) and Saville (1957). Six runs were made to demonstrate the effect of erosion rate changes due to variations of breaking wave height, sediment grain size, and beach slope. One run was made to simulate the effect of profile change due to Sea Water Level change, and one run was made to simulate the erosion process in field condition.

Both predicted beach profile evolution and transport rate were compared with the author's laboratory data as shown in Figures 5-11 and 5-12. The results indicated that for short term beach erosion, the transport model compared well with experimental data. Figure 5-12 showed that the numerical prediction was in good agreement with measured beach profile evolution in surf zone, although it was not successful in predicting the shape of offshore bar. Since the short term beach erosion is predominantly suspended sediment transport within surf zone, the present numerical model is proved to be well representing this process.

Numerical runs were also made to simulate the laboratory conditions of Sunamura and Horikawa (1974). The comparisons of beach profile evolution and erosion rate are shown in Figures 5-13 and 5-14 respectively. The results indicated that the present numerical model is in good agreement with

Table 5-6 Summary of Numerical Runs

Run Number	Input Conditions				Remarks
	H_b (cm)	T(sec)	D_{50} (mm)	tan α	
1	14.5	1.0	0.2	1/10	Simulation of Author's Lab. Results
2	9.1	1.0	0.2	1/10	Simulation of Sunamura and Horikawa's Lab. Results
3	140.5	11.3	0.2	1/15	Simulation of Saville's Small Scale Lab. Results
4	12.0	1.0	0.2	1/10	Examing the Effect of H_b Change
5	15.0	1.0	0.2	1/10	Examing the Effect of H_b Change
6	9.1	1.0	1.0	1/10	Examing the Effect of D_{50} Change
7	9.1	1.0	2.0	1/10	Examing the Effect of D_{50} Change
8	9.1	1.0	0.2	1/15	Examing the Effect of tanα Change
9	9.1	1.0	0.2	1/20	Examing the Effect of tanα Change
10	9.1	1.0	0.2	1/10	Examing the Effect of SWL Change
11	9.1	3.2	0.2	1/20	Examing the Erosion Rate in Field Condition

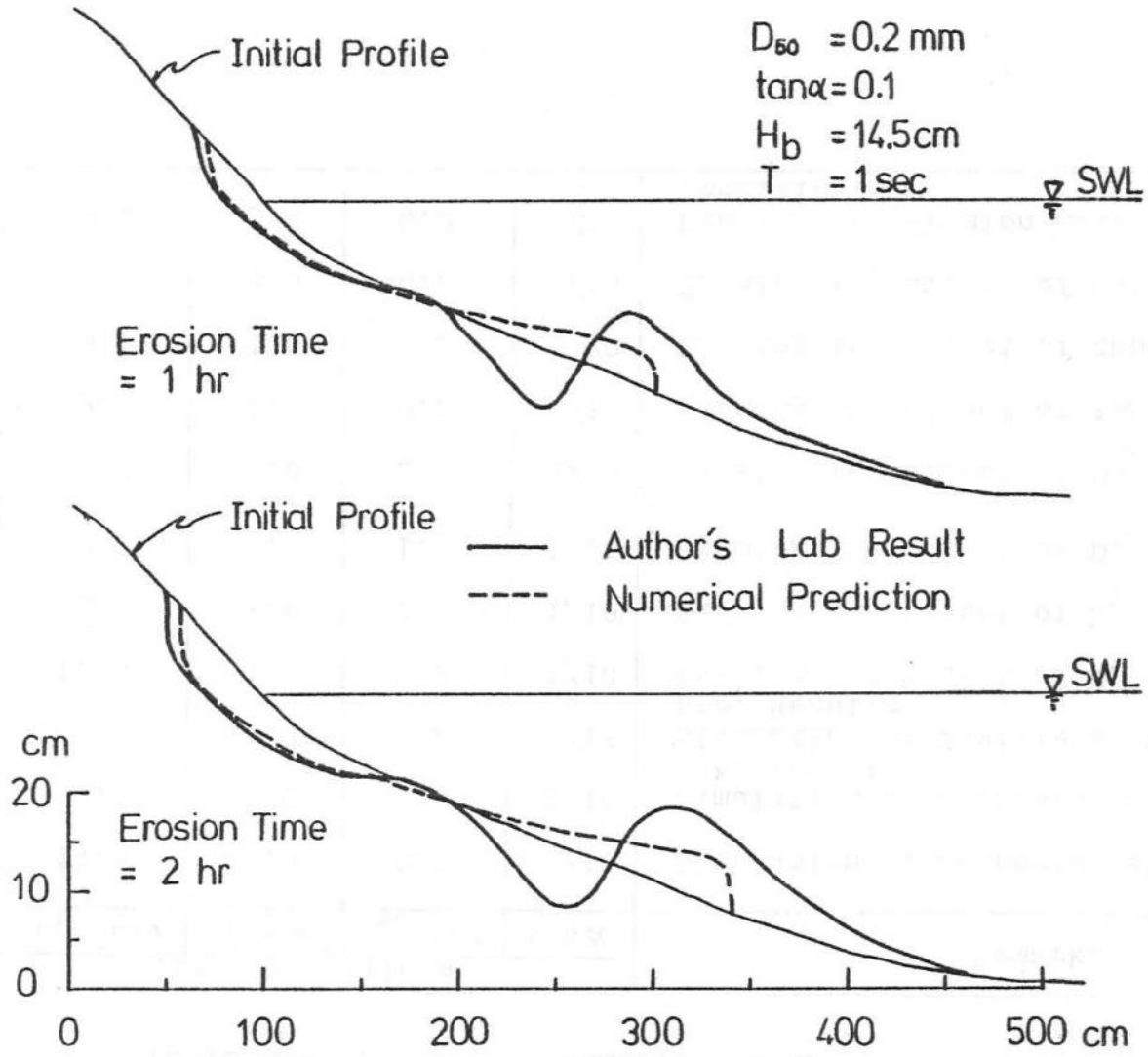

Figure 5-11 Comparison of Beach Profile Evolution with Author's Results

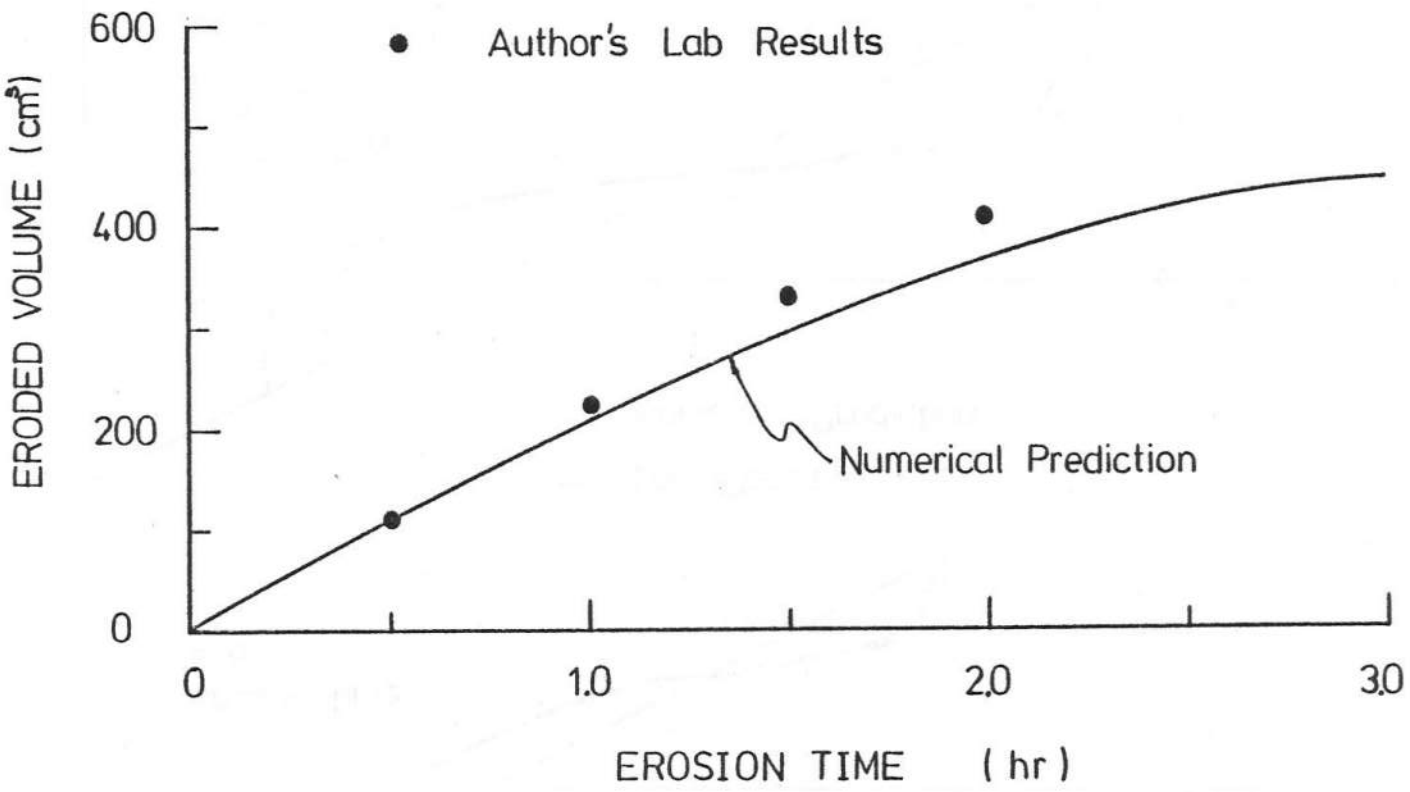

Figure 5-12 Comparison of Erosion Rate with Author's Results

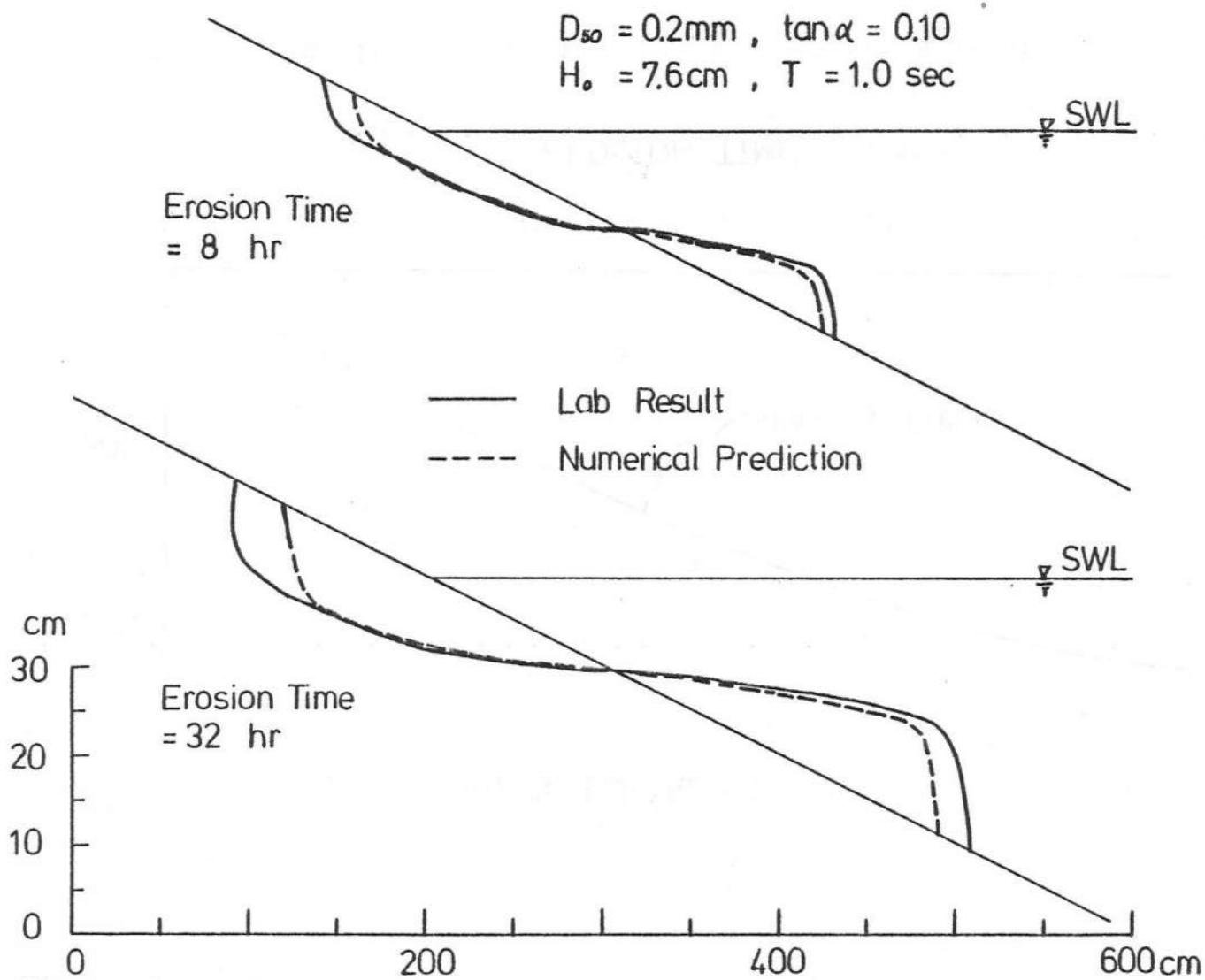

Figure 5-13 Comparison of Beach Profile Evolution with Sunamura and Horikawa's Results

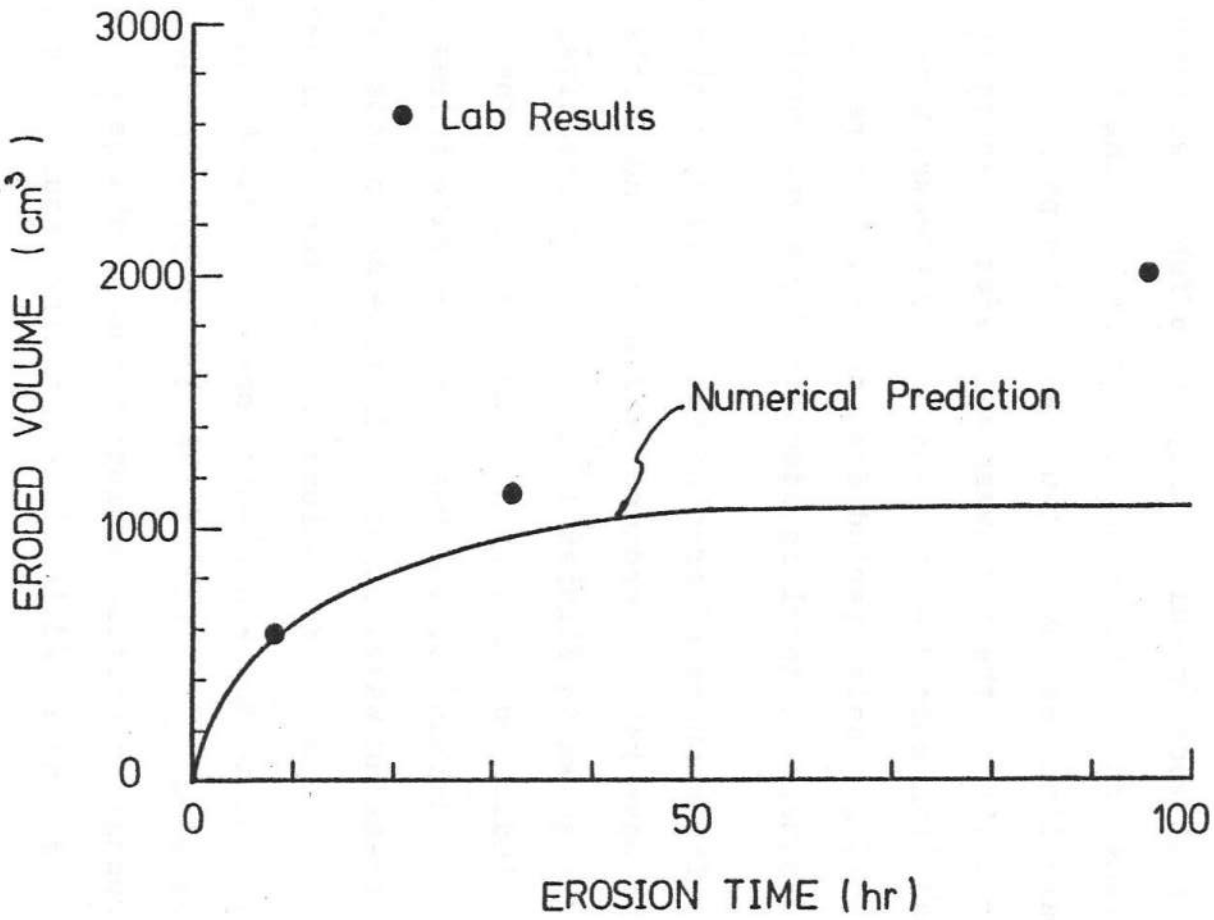

Figure 5-14 Comparison of Erosion Rate with Sunamura and Horikawa's Results

laboratory data within 50 hour initial eroding period. The numerical profile reached equilibrium by the end of this period while the laboratory profile kept eroding up to 160 hours. The reason for this deviation was due to the fact that the present model predicts only the offshore suspended sediment transport in surf zone (i.e. from breaking point to shoreward limit of wave set-up) while the physical model further included the the swash zone erosion which is mostly bed load transport due to bottom shear stress. Since an extreme long erosion period does not exist in reality, the present numerical model is adequate for storm conditions.

The changes of erosion rate due to variation of breaking wave height, sediment grain size and initial beach slope are shown in Figures 15,16 and 17 respectively. The results indicated that, by holding the rest of the initial conditions unchanged, the beach erosion rate increased with higher breaking wave, finer grain size and steeper initial slope. The final eroded volume was greater for higher breaking wave due to the wider surf zone involved. A change of wave period does not affect the erosion rate in the model. The response of profile evolution due to change of water level is demonstrated in Figure 18. The results showed that, by adding the still water level, the breaking point would be shifted further onshore and more foreshore beach material would be eroded.

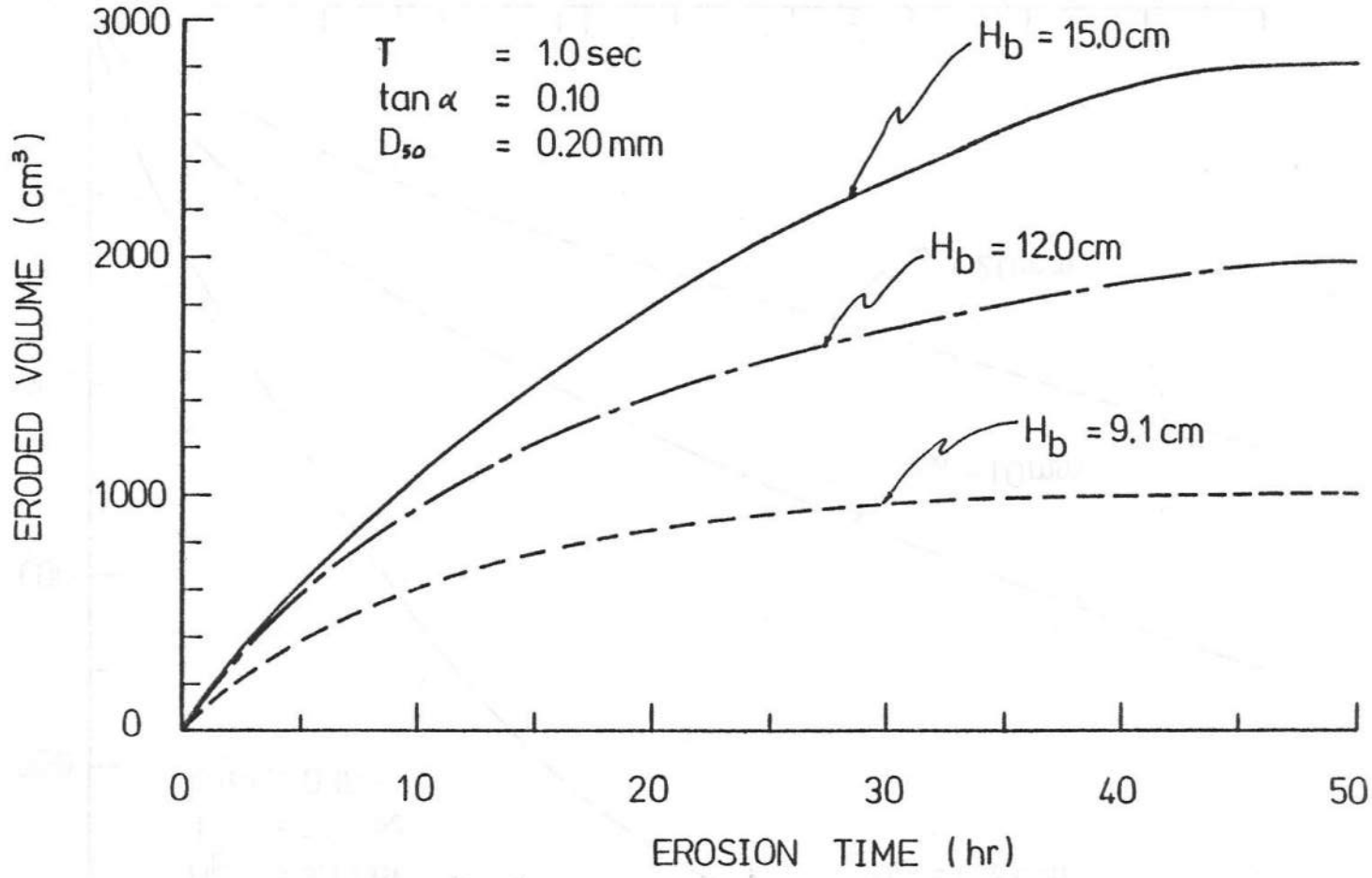

Figure 5-15 Effect on Erosion Rate due to Breaking Wave Height Variation

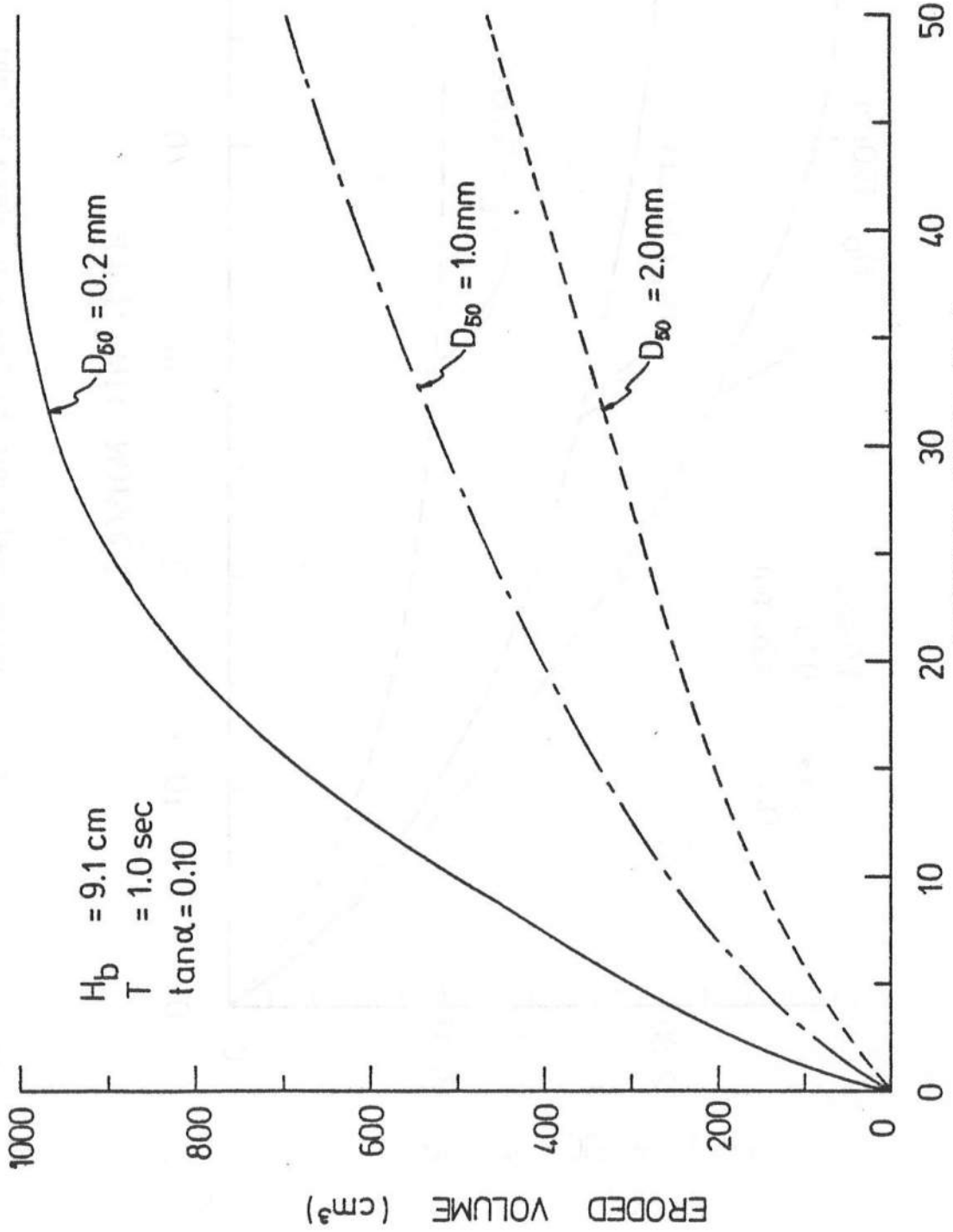

Figure 5-16 Effect on Erosion Rate due to Sediment Grain Size Variation

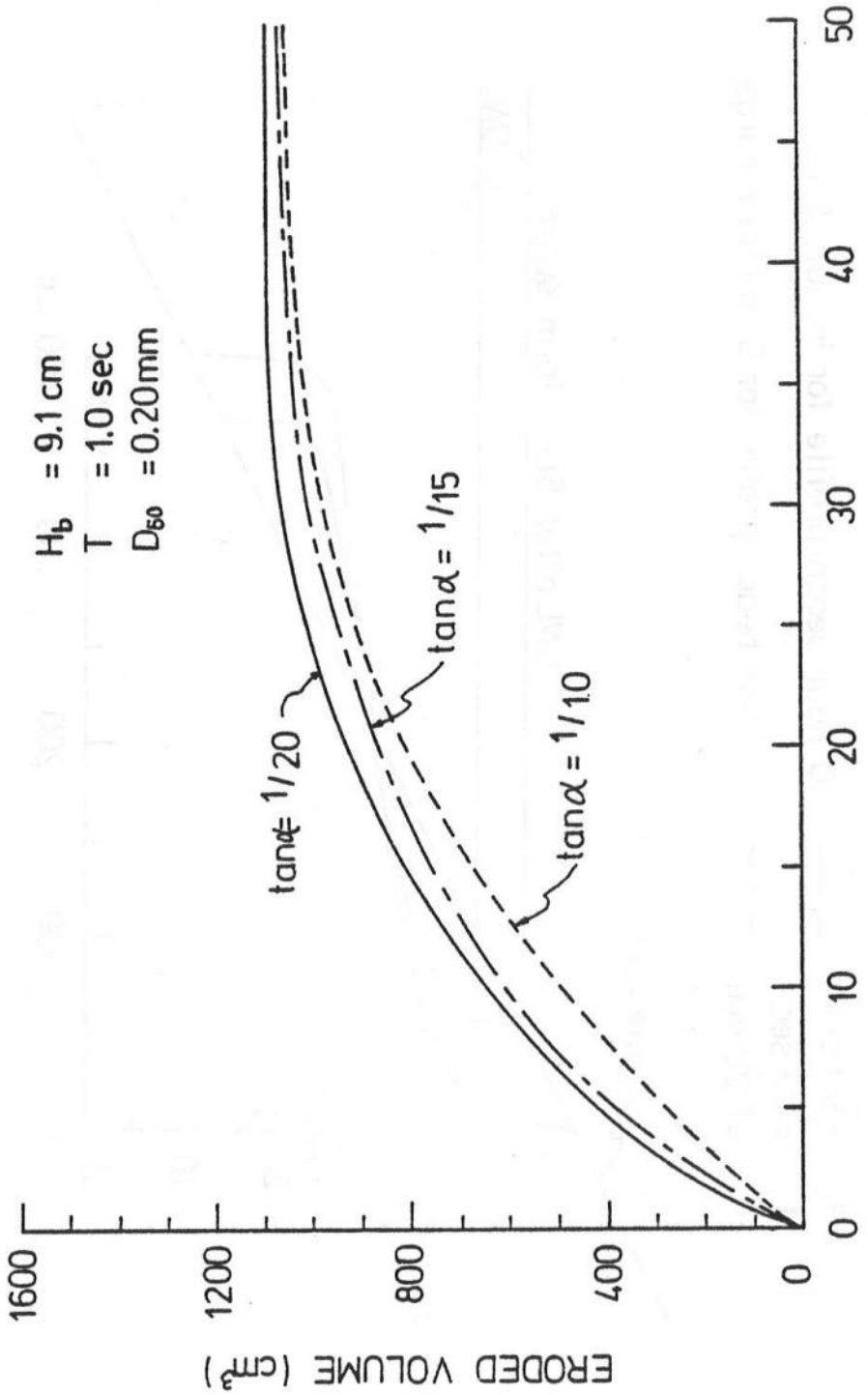

Figure 5-17 Effect on Erosion Rate due to Initial Beach Slope Variation

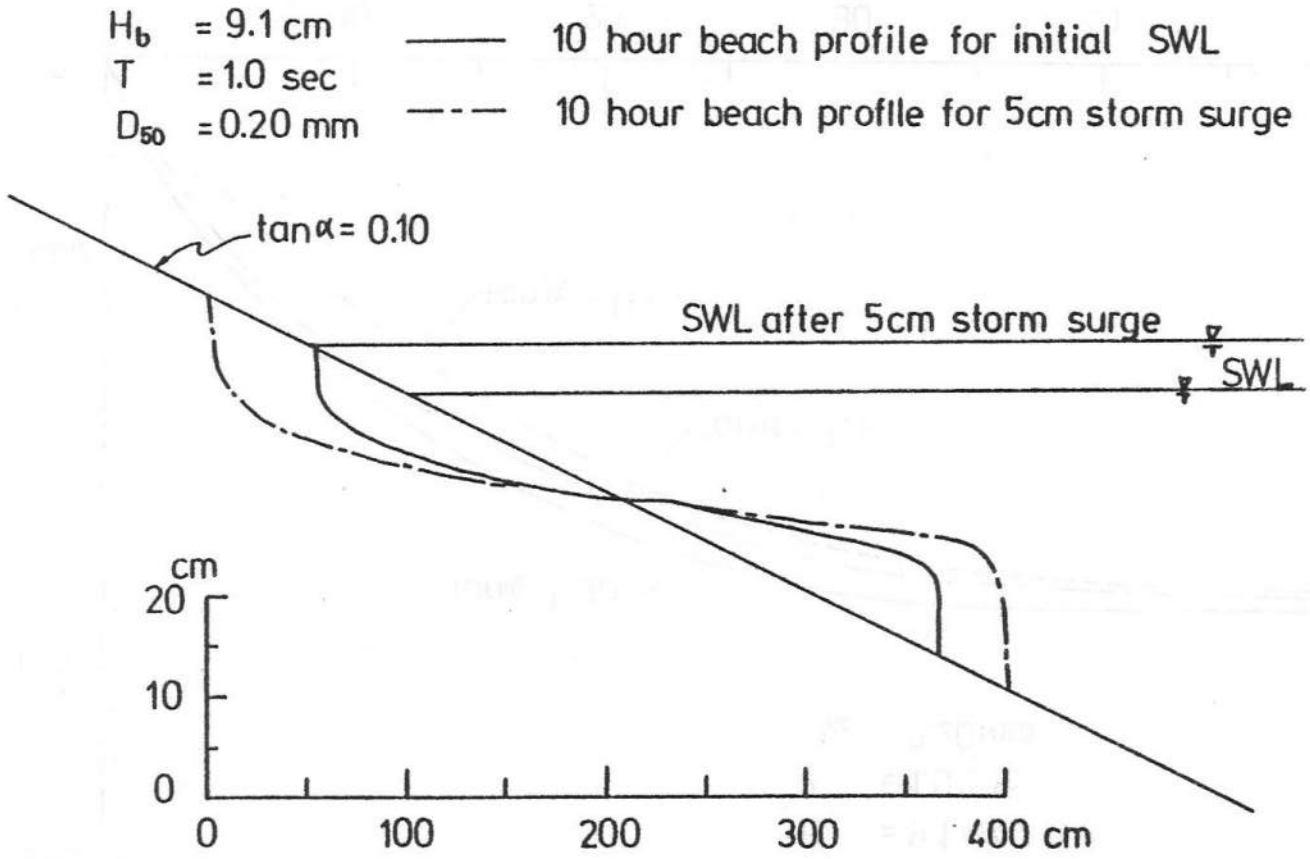

Figure 5-18 Effect on Profile Evolution due to Sea Water Level Variation

Two numerical runs were made to simulate the prototype wave and beach conditions. The first run was designed to simulate the large wave tank condition conducted by Saville. Comparisons of beach profile evolution and erosion rate are shown in Figures 5-19 and 5-20 respectively. The results indicated fair agreement between the experimental and predicted data. The lower predicted erosion rate is due to the use of prototype suspended sediment constant, which is probably too low for large wave tank condition. Figure 5-21 demonstrates the numerical erosion rates under laboratory and prototype conditions. the erosion rates were non-dimensionalized by the eroded volume at equilibrium condition. The results indicated a lower prototype erosion rate, which is probably due to less suspended sediment concentration in the field and the scale effect of physical model in the laboratory.

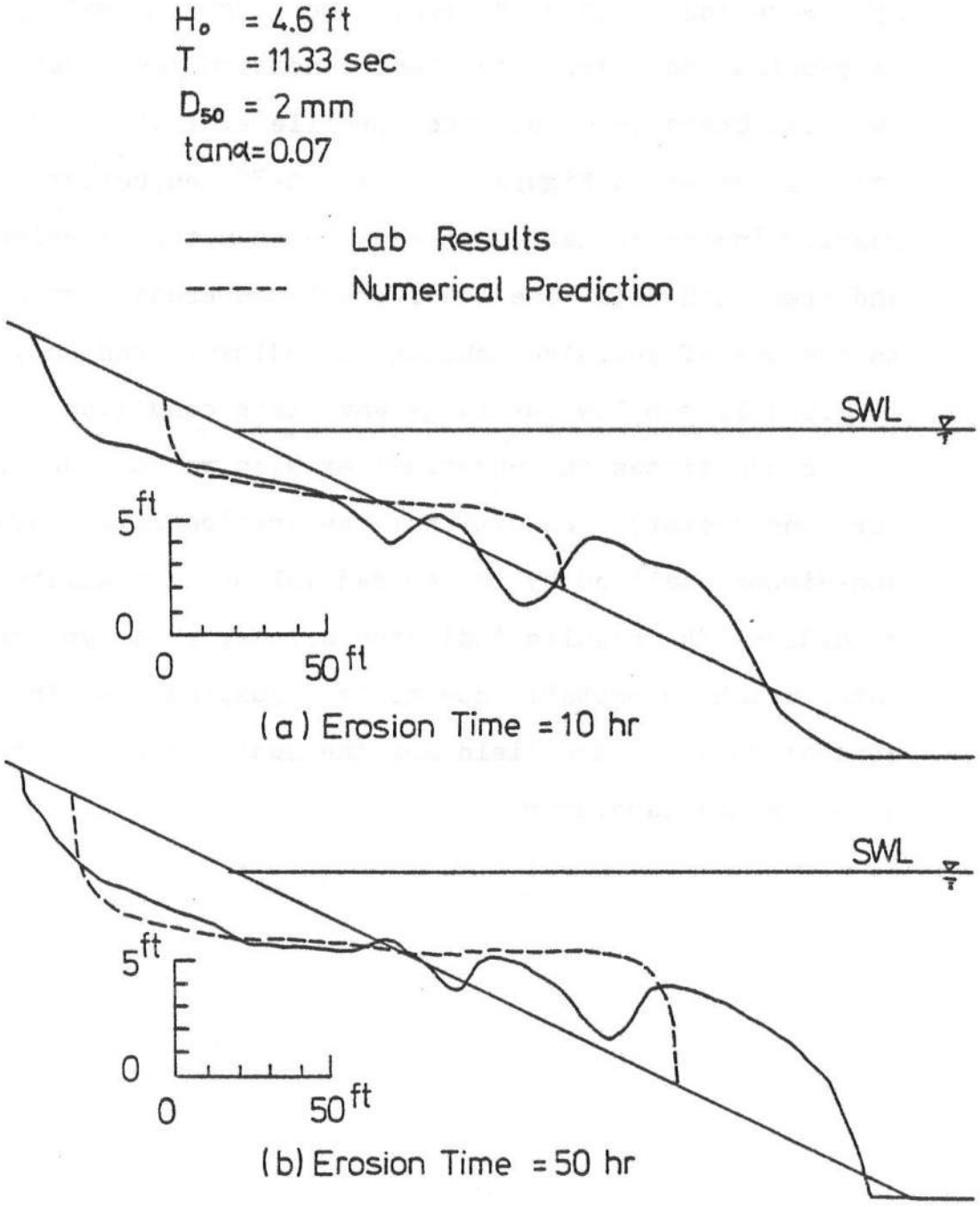

Figure 5-19 Comparison of Beach Profile Evolution with Saville's Results

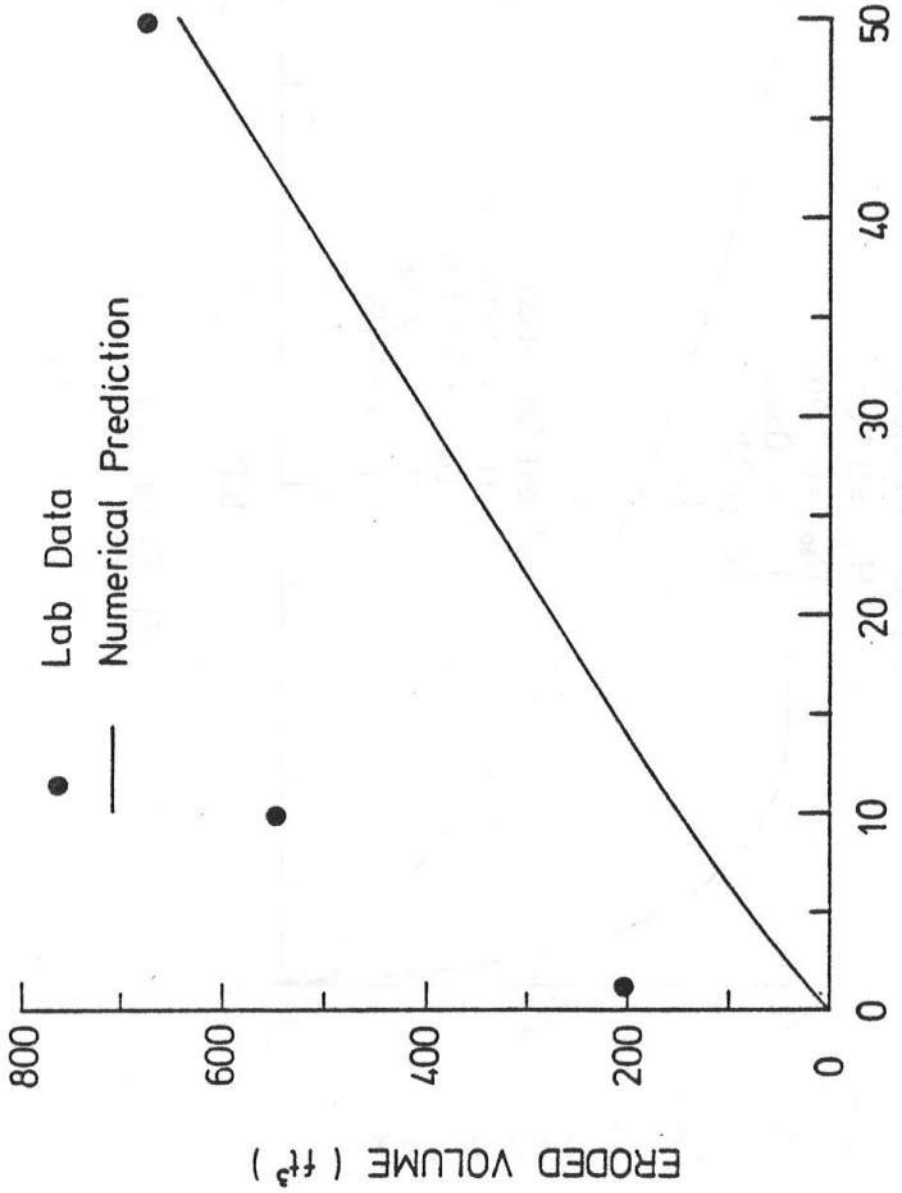

Figure 5-20 Comparison of Erosion Rate with Saville's Results

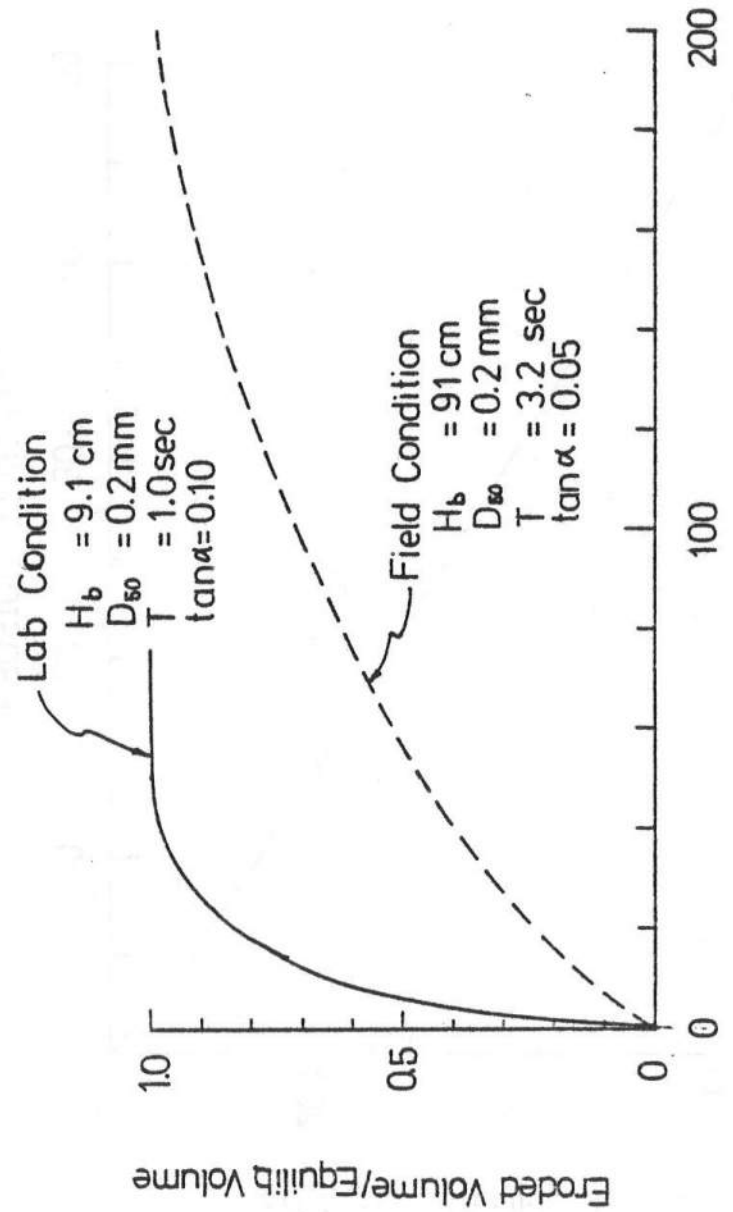

Figure 5-21 Comparison of Erosion Rates under Laboratory and Prototype Conditions

CHAPTER 6

CONCLUSIONS

Based on a swash model of breaking waves on constant slope, a surf zone parameter was derived. This non-dimensional parameter was defined as the ratio of the natural swash period of a single long-crested wave breaking on a constant slope to the incident wave period, or, $I_w = \frac{H_b^{1/2}}{g^{1/2} T \tan\alpha}$. Physically, this parameter implied the number of breaking waves in surf zone, and therefore, served as a wave interference index.

The surf zone parameter could be rearranged as the ratio of the square root of breaking wave steepness to beach slope. The new form was similar to the inverse of the previously proposed parameter if the incident wave height was replaced by the breaking wave height. The surf zone parameter derived from a theoretical basis offered an explanation as to why this parameter is important to classify the breaking wave properties. In addition, this parameter characterized the flow field and defined the similarity property in the surf zone. The derived transition values from surging to plunging and from plunging to spilling

breaker types were found to be consistent with Galvin's laboratory results.

Assuming both the water surface variations and the depth-averaged horizontal particle velocities in the surf zone could be expressed by the summation of Fourier components, similarity solutions were proposed in this study. These solutions were based on a pair of rather restrictive conditions, namely, both the amplitude and the phase velocity of each harmonic component were depth limited. The solutions, however, offered the advantage of being simple and completely defined by a few local flow parameters. Laboratory data from a number of investigators including those obtained at the present study were used to test the validity of the proposed solutions.

The results seem to suggest that the similarity solution is not universally applicable. However, if the wave is of the spilling type and is far inshore in the inner breaker zone, the similarity solution become suitable to describe the mean flow characteristics. These conditions can be defined in terms of the surf zone parameter I_w and the relative depth parameter d/d_b. The region of suitability is found to be when $I_w > 0.9$ and $d/d_b < 0.6$. In this region, both surface profile and horizontal velocity can be adequately described by the first three harmonics. The

velocity profile is found to be less asymmetric than the surface profile. For surface profile, the higher harmonics lead the lower ones whereas the contrary is true for the velocity profile.

The results of analyzed suspended sediment concentration data indicate two physical significances. The multiple peaks in the sediment concentration spectrum implies that multiple suspension process exists in one wave cycle. The peaks are more pronounced during spilling wave condition resulting in the uniform distribution of sediment concentration in one wave cycle. The averaged instantaneous sediment concentration profile is periodic and is in phase with the velocity profile for plunging breaker. The concentration profile for spilling breaker is more uniformly distributed with its peak lags the velocity peak. The difference in sediment suspension pattern is found to be the controlling factor of on/offshore transport direction.

As part of an attempt to simulate the on/offshore transport phenomena in the nearshore region, the present numerical model is successful in predicting the offshore sediment transport both qualitatively and quantitatively. Given any initial conditions including breaking wave height, sediment grain size and beach slope, the model is able to predict erosion rate and profile evolution in surf zone provided that the breaker is of spilling type.

A suspended sediment transport equation is applied in the model. The transport equation is obtained by coupling the horizontal particle velocity with the suspended sediment concentration. Due to the limited knowledge of sediment suspension in surf zone, the present model is only able to predict the mean condition, which is the offshore transport case. The model is highly depth-controlled. The erosion rate reduces sharply as the beach slope becomes milder. The equilibrium condition would be reached as the beach slope in surf zone is flat.

The numerical model can be applied to both laboratory and field conditions by using the proper proportional constants which are calibrated with either laboratory or field data. The present model predictions are found to be in good agreement with all laboratory results within 50 hour erosion period. Beyond this period, berm crest erosion takes place due to eroded unstable foreshore slope. This erosion process should be included in future model study.

Although the present laboratory measuring techniques offer sufficient engineering estimates of the flow field in surf zone, a more sophisticated velocity measuring technique is desirable for future study. The water elevation and velocity measurements should be conducted for various beach slopes and with both plane and sand beaches. More

detailed laboratory investigation of sediment suspension in surf zone is necessary for a complete on/offshore sediment transport model.

BIBLIOGRAPHY

Akyurek, M.,"Sediment Suspension by Wave Action Over a Horizontal Bed," M.S.Thesis, University of Iowa, 1972.

Bagnold,R.A.,"Beach Formation by Waves; Some Model Experiments in Wave Tank," Journal of the Institution of Civil Engineers, Vol.15, No.5237, Nov. 1940, pp. 27-52.

Bagnold,R.A.,"Sand Movement by Waves, Some Small Scale Experiments with Sand of very Low Density," Journal of the Institution of Civil Engineers, Vol.8, 1947 pp.441-455.

Battjes, J.A.,"Surf Similarity," Proceedings, 14th Coastal Engineering Conference, June, 1974, pp.466-477.

Bhattacharya,P.,"Sediment Suspension in Shoaling Waves," Ph.D. Dissertation, University of Iowa, 1971.

Bowen,A.J.,Inman,D.L., and Simmons,V.P.,"Wave Set-down and Set-up," Journal Geophysical Research, Vol.73, No.3, April, 1968, pp.2569-2577.

Bowen,A.J.,"Rip Currents, I-Theoretical Investigations," Journal Geophysical Research, Vol.74, pp.5467-5478.

Bonefille,R.,"L'utilization des Parametres A Dimensionnels dans l'Etude de l'Hydrodynamique des Sediments," Deuxieme These, Docteures Sciences, Grenoble, 1968.

Brenninkmeyer,S.J.,"Surf Zone Sedimentation Patterns," Ph.D. Dissertation, University of Southern California, 1973.

Carrier,G.F.and H.P.Greenspan,"Water Waves of Finite Amplitude on a Sloping Beach," Journal Fluid Mechanics, Vol.14, 1958, pp.97-107.

Dally, W. and R.G.Dean,"A Numerical Model for Beach Profile Evolution," Master's Thesis, University of Delaware,1980

Dalrymple,R.A.,"Wave Induced Mass Transport in Water Waves," Journal of Waterways Harbors and Coastal Engineering, May, 1976.

Dean,R.G.,"Heuristic Models of Sand Transport in the Surf Zone," Conference on Engineering Dynamics in the Coastal Zone, Australia, May, 1973.

Dean,R.G.,"Beach Erosion: Causes, Processes and Remedial Measures," CRC Critical Reviews in Environmental Control Vol.6,Issue 3, 1976.

Dean,R.G.,"Equilibrium Beach Profiles: U.S.Atlantic and Gulf Coast," Ocean Engineering Report No.12, Department of Civil Engineering, University of Delaware, January,1977.

Eagleson,P.S.,B.Glenne and J.A.Dracup, "Equilibrium Characteristics of Sand Beaches," Journal Hydraulic Division, ASCE HY1, 1967, pp.35-57.

Fleming,C.A. and Hunt, J.N., "Application of a Sediment Transport Model," Proceedings, 15th Coastal Engineering Conference, 1976, pp. 1184-1202.

Fox, W.T. and Davis, R.A., "Simulation Model for Storm Cycles and Beach Erosion on Lake Michigan," G.S.A., Bul., Vol.84, No.5, 1973, pp. 1769-1790.

Galvin, C.J., "Breaker Type Classification on Three Laboratory Beaches," Journal Geophysical Research, Vol.73, 1968, pp. 3651-3659.

Galvin, C.J.,"Wave Breaking in Shallow Water," Waves on Beaches and Resulting Sediment Transport, Edited by R.E. Meyer, Academic Press, New York, 1972, pp. 413-456.

Glover, J.R., P.K. Bhattacharya and J.F. Kennedy, "An Electro-Optical System for Measurement of Mean and Statistical Properties of Sediment Transport," IIHR Report 120, University of Iowa, October, 1969.

Goda, Y. "Wave Forces on a Vertical Cylinder: Experiments and a Proposed Method of Wave Force Computation," Report of Port and Harbor Technical Research Institute, No.8, 1964, pp. 74

Hattori,M.,"The Mechanics of Suspended Sediment Due to Standing Waves," Coastal Engineering in Japan, 12, 1969

Hom-ma,M. and K. Horikawa, "A Laboratory Study on Suspended Sediment Due to Wave Action," Proceedings, Xth Congress of the IAHR, London, 1963

Hunt,I.A.,"Design of Seawalls and Breakwaters," Journal of Waterway, Harbor and Coastal Engineering Division, Vol.85, WW3, September,1959, pp.123-152.

Inman, D.L. and W.H. Quinn, "Currents in the Surf Zone," Proceedings, Second Coastal Engineering Conference, Concil on Wave Research, Berkeley, California, 1951

Ippen, A.T., "Estuary and Coastline Hydrodynamics," Engineering Society Monograph, McGraw Hill Book Company 1966

Iribarren, C.R. and C. Nogales, "Protection des Ports," Section II, Comm.4, XVIIth International Navigation Congress, Lisbon, 1949, pp.31-80.

Iwagaki, Y. and H. Noda, "Laboratory Study of Scale Effects in Two-Dimensional Beach Processes," Proceedings, 8th Coastal Engineering Conference, 1962, pp.194-210.

Iwagaki, Y. and T. Sakai, "Horizontal Water Particle Velocity of Finite Amplitude Waves," Proceedings, 12th Coastal Engineering Conference, 1970, pp.309-325.

Johns, B., "On the Mass Transport Induced by the Oscillatory Flow in a Turbulent Boundary Layer," Journal Fluid Mechanics, Vol.43, 1970, pp.177-185.

Kana, T.W., "Suspended Sediment in Breaking Waves," Technical Report No.18-CRD, University of South Carolina, April, 1979.

Kemp, P.H., and D.T. Plinston, "Beaches Produced by Waves of Low Phase Difference," Journal of the Hydraulics Division, ASCE, September, 1968.

Lee, A.,C.A. Grated and T.S. Durrani, "Velocities under Periodic and Random Waves," Proceedings, 14th Coastal Engineering Conference, 1974, pp.558-574.

Levi-Civita, T., "Determination Rigoreuse des Ondes Permanentes d'Ampleur Finie," Math. Annalen, Vol.93, 1925, pp.247-257.

Liang, S.S. and H. Wang, "Sediment Transport in Random Waves," Technical Report 26, College of Marine Studies, University of Delaware.

Longuet-Higgins, M.S.,"Mass Transport in Water Waves," Phil, Trans. Royal Society, Vol.245, 1953, pp.535-581.

Longuet-Higgins, M.S., "A Note on Wave Set-up," Journal of Marine Research, April, 1963.

Meyer, R.D., "A Model Study of Wave Action on Beaches," M.S. Thesis, Department of Engineering, University of California, 1936.

Mogridge, G.R. and Kamphius, J.W., "Experiments and Ripple Formation Under Wave Action," Proceedings 13th Coastal Engineering Conference, 1972, pp.1123-1142.

Munk and Wimbush, "A Rule of Thumb for Wave Breaking Over Sloping Beaches," Oceanography, Vol.9, 1969, pp.56-59.

Noda, E.K., "Equilibrium Beach Profile Scale-Model Relationship," Journal of the Waterways Harbors and Coastal Engineering Division, WW4, ASCE, November 1972, pp.511-528.

Paul, M.J., J.W. Kamphuis and A. Brebner, "Similarity of Equilibrium Beach Profiles," Proceedings, 13th Coastal Engineering Conference, 1972, pp.1217-1236.

Paul, M.J., "Similarity of Bed Evolution and Sediment Transport in Mobile Bed Coastal Models," Ph.D. Thesis, Queen's University, 1972.

Sakai, T. and Y. Iwagaki, "Estimation of Water Particle Velocity of Breaking Waves," Proceedings, 16th Coastal Engineering Conference, 1978, pp.551-568.

Saville, T., "Scale Effects in Two-dimensional beach Studies," Trans. 7th Meet. Int. Assoc. of Hydraulic Research, Lisbon, 1957, A3-1.

Shinohara, K. et.al., "Sand Transport Along a Model Sandy Beach by Wave Action," Coastal Engineering in Japan, Vol.1, 1958.

Stokes, G.G., "On the Theory of Oscillatory Waves," Trans. Cambridge Phil. Soc., Vol.8,1847, pp.441-455.

Sunamura, T. and K. Horikawa, "Two-dimensional Beach Transformation Due to Waves," Proceedings, 14th Coastal Engineering Conference, 1974, pp.920-938.

Svendson, I.A., P.A. Madsen and J.B. Hansen, "Wave Characteristics in the Surf Zone," Proceedings, 16th Coastal Engineering Conference, 1978, pp.520-539.

Swart, D.H., "Offshore Sediment Transport and Equilibrium Beach Profiles," Delft Hydraulic Laboratory Publiction No. 131, 1974.

Thompson, W., "A Study of Equilibrium Beach Profiles," M.S. Thesis, University of Delaware, 1976.

Thornton, E.B., et.al., "Kinematics of Breaking Waves," Proceedings, 15th Coastal Engineering Conference, 1976

Tsuchiya, Y. and M. Yamaguchi, "Horizontal and Vertical Water Particle Velocities Induced by Waves," Proceedings, 13th Coastal Engineering Conference, 1972, pp.555-568.

Valembois, J., "Etude Sur la Modeledu Transport Littoral: Conditions de Similitude," Proceedings, 7th Coastal Engineering Conference, 1961, pp.277-307.

Waddel, E., "Dynamics of Swash and Implication to Beach Response," Technical Report No.139, Coastal Studies Institute, Louisianna State University, 1973.

Wang, H., R.A. Dalrymple and J.C. Shiau, "Computer Simulation of Beach Erosion and Profile Modification Due to Waves," Modeling Symposium, Vol.2, 1975, pp. 1369-1384.

Wiegel, R.L., "Oceanographical Engineering," Prentice Hall, Englewood Cliffs, N.J. 1964, pp.175.

Winant, C.D., D.L. Inman and C.E. Nordstrom, "Description of Seasonal Beach Changes Using Empirical Eigenfunctions," Journal Geophysical Research, Vol.80, No.15, May, 1975, pp. 1979-1986.

Yalin, M.S., "Theory of Hydraulic Models," MacMillan, London 1971.

APPENDIX A

WATER ELEVATION AND HORIZONTAL VELOCITY DATA

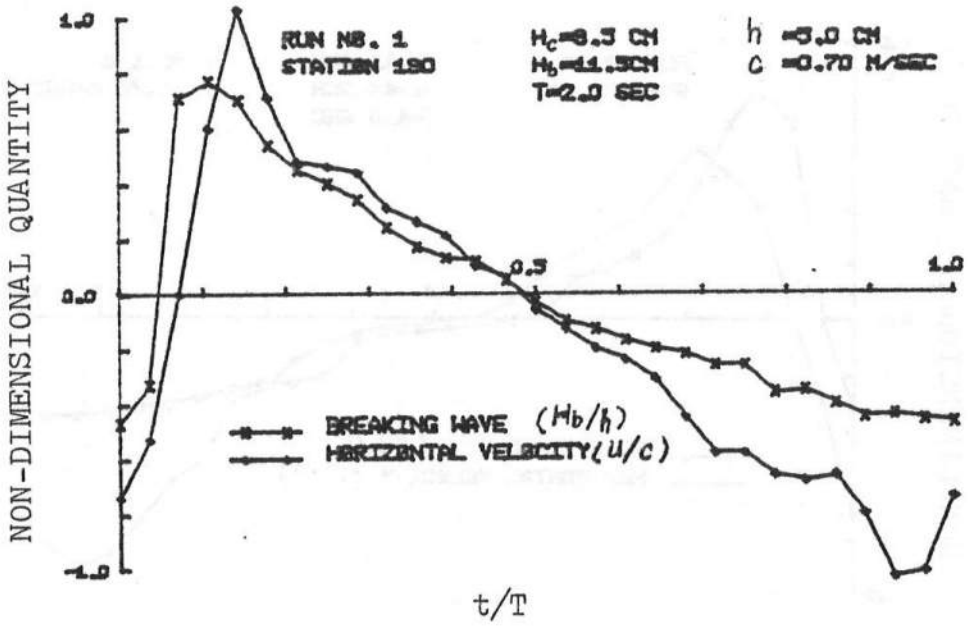
RUN NO. 1
STATION 190
H_c=8.3 CM
H_b=11.3CM
T=2.0 SEC
h =5.0 CM
c =0.70 M/SEC
BREAKING WAVE (H_b/h)
HORIZONTAL VELOCITY(u/c)
NON-DIMENSIONAL QUANTITY
t/T
1.0
0.5
0.0
-1.0

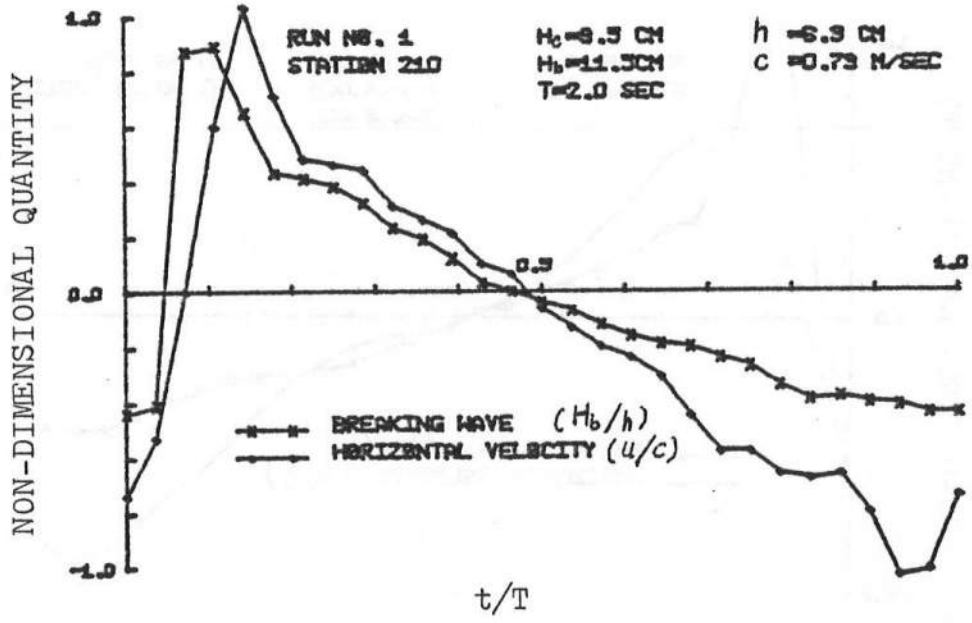
RUN NO. 1
STATION 210
H_c=8.3 CM
H_b=11.3CM
T=2.0 SEC
h =6.3 CM
c =0.73 M/SEC
BREAKING WAVE (H_b/h)
HORIZONTAL VELOCITY (u/c)
NON-DIMENSIONAL QUANTITY
t/T
1.0
0.5
0.0
-1.0

Figure A-1

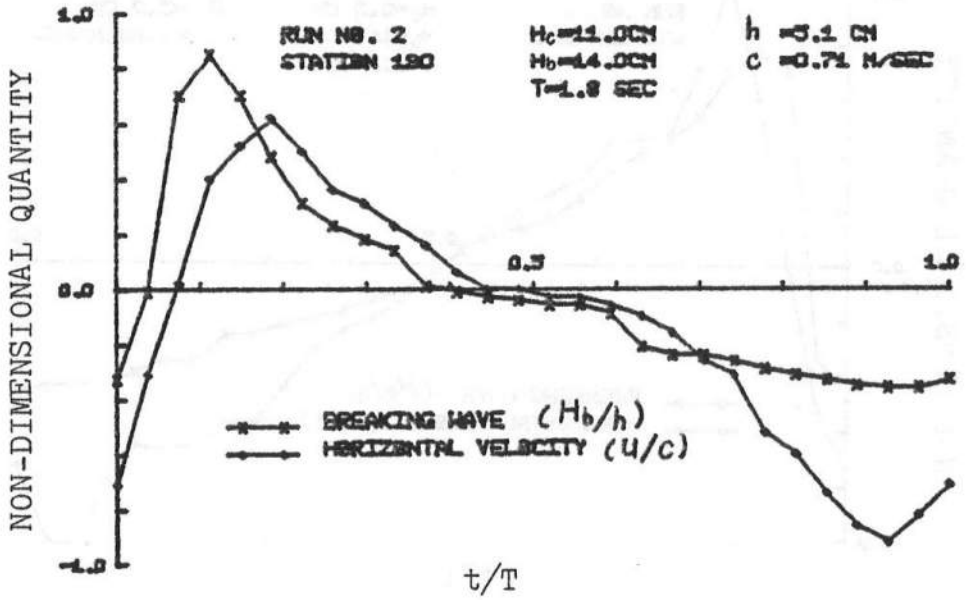
RUN NO. 2
STATION 190
Hc=11.0CM
Hb=14.0CM
T=1.8 SEC
h =5.1 CM
c =0.71 M/SEC
NON-DIMENSIONAL QUANTITY
1.0
0.0
-1.0
0.5
1.0
BREAKING WAVE (Hb/h)
HORIZONTAL VELOCITY (u/c)
t/T

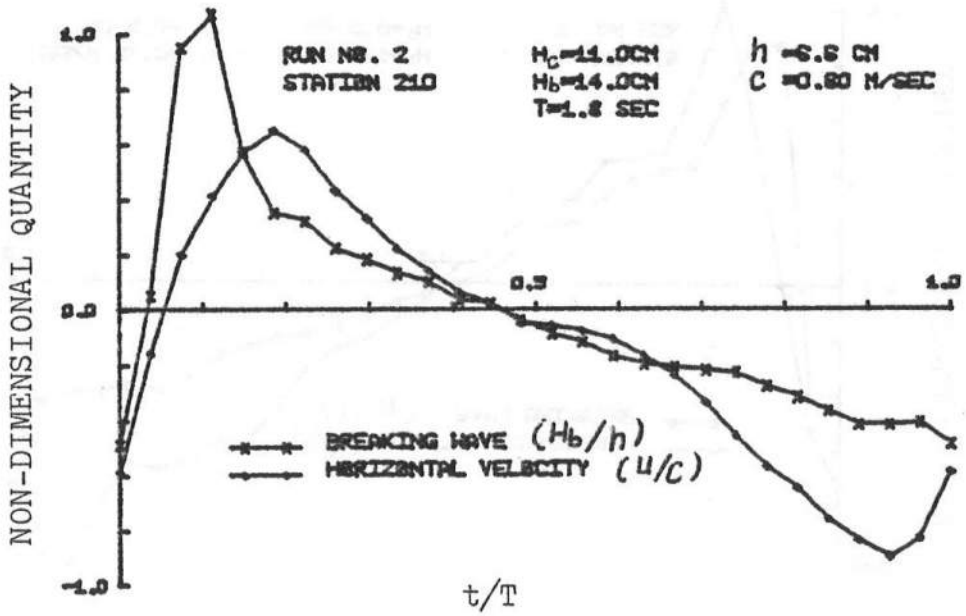
RUN NO. 2
STATION 210
Hc=11.0CM
Hb=14.0CM
T=1.8 SEC
h =6.6 CM
c =0.80 M/SEC
NON-DIMENSIONAL QUANTITY
1.0
0.0
-1.0
0.5
1.0
BREAKING WAVE (Hb/h)
HORIZONTAL VELOCITY (u/c)
t/T

Figure A-2

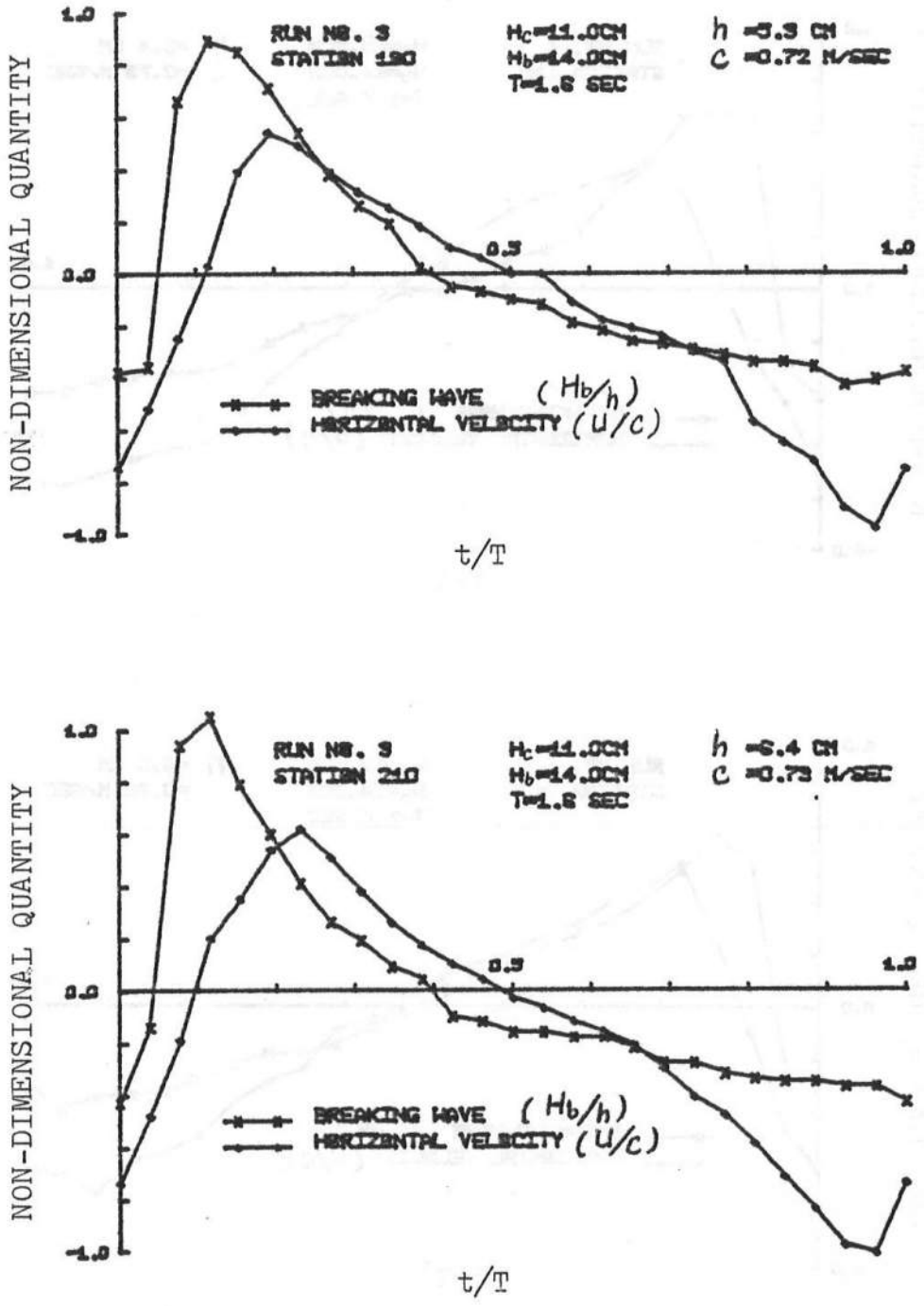
RUN NO. 3
STATION 180
Hc=11.0CM
Hb=14.0CM
T=1.6 SEC
h =5.3 CM
c =0.72 M/SEC
1.0
0.5
0.0
-1.0
NON-DIMENSIONAL QUANTITY
BREAKING WAVE (Hb/h)
HORIZONTAL VELOCITY (u/c)
t/T
RUN NO. 3
STATION 210
Hc=11.0CM
Hb=14.0CM
T=1.6 SEC
h =6.4 CM
c =0.73 M/SEC
1.0
0.5
0.0
-1.0
NON-DIMENSIONAL QUANTITY
BREAKING WAVE (Hb/h)
HORIZONTAL VELOCITY (u/c)
t/T

Figure A-3

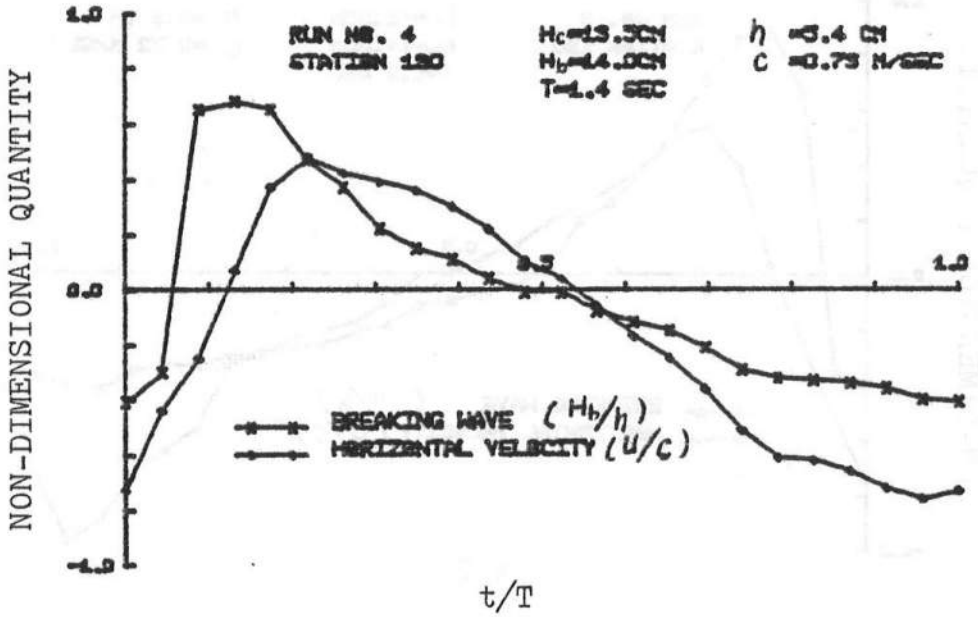
RUN NO. 4
STATION 180
Hc=13.3CM
Hb=14.0CM
T=1.4 SEC
h =5.4 CM
c =0.73 M/SEC
1.0
0.0
-1.0
0.5
1.0
BREAKING WAVE (Hb/h)
HORIZONTAL VELOCITY (u/c)
NON-DIMENSIONAL QUANTITY
t/T

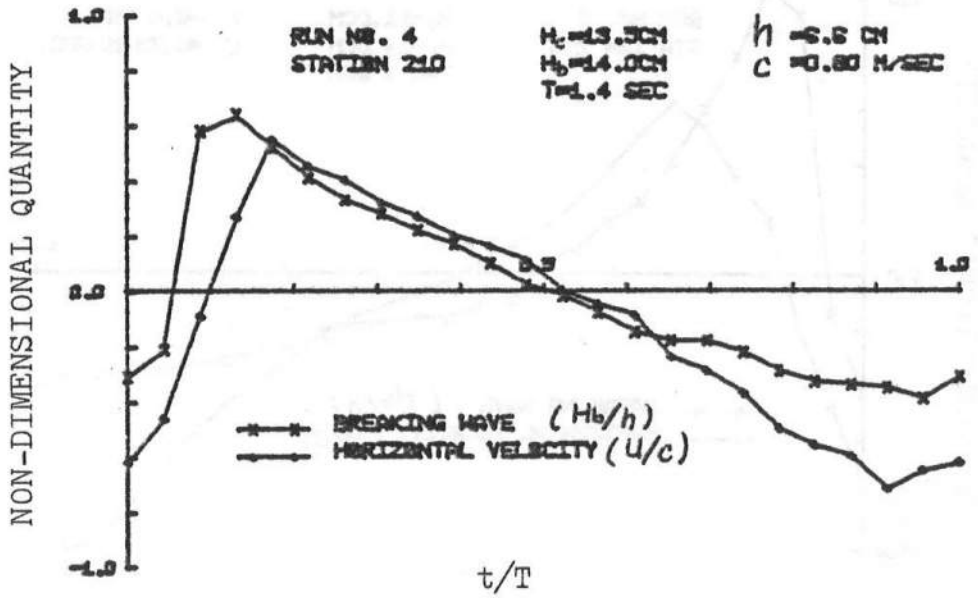
RUN NO. 4
STATION 210
Hc=13.3CM
Hb=14.0CM
T=1.4 SEC
h =5.6 CM
c =0.80 M/SEC
1.0
0.0
-1.0
0.5
1.0
BREAKING WAVE (Hb/h)
HORIZONTAL VELOCITY (u/c)
NON-DIMENSIONAL QUANTITY
t/T

Figure A-4

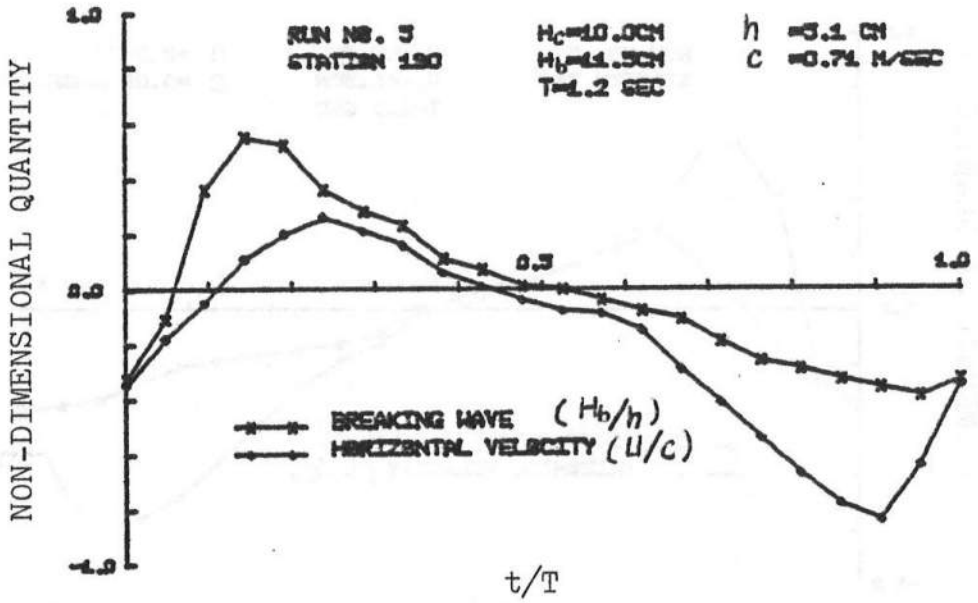
RUN NO. 5
STATION 190
H_c=10.0CM
H_b=11.3CM
T=1.2 SEC
h =3.1 CM
c =0.71 M/SEC
1.0
0.0
-1.0
0.5
1.0
BREAKING WAVE (H_b/h)
HORIZONTAL VELOCITY (u/c)
NON-DIMENSIONAL QUANTITY
t/T

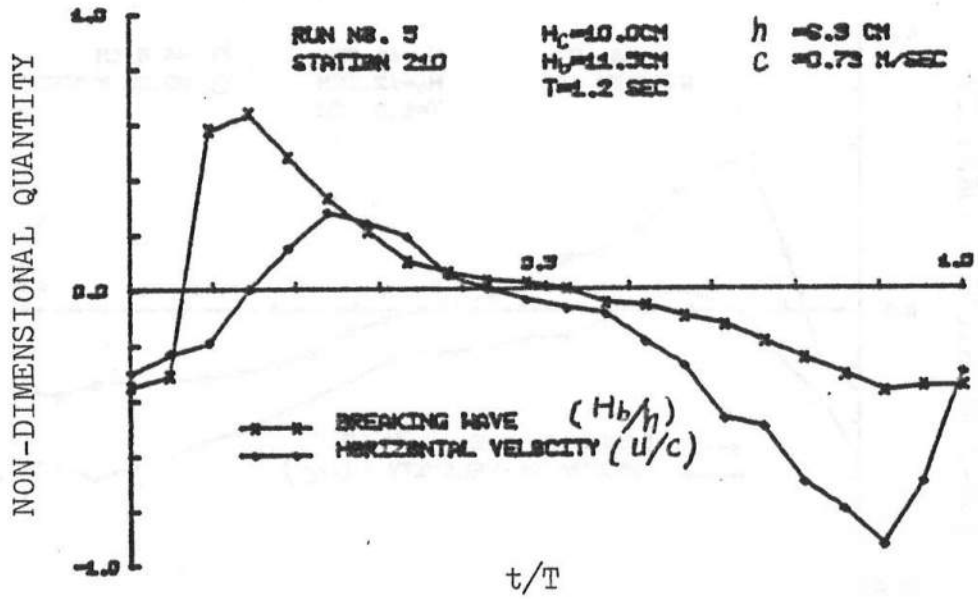
RUN NO. 5
STATION 210
H_c=10.0CM
H_b=11.3CM
T=1.2 SEC
h =2.3 CM
c =0.73 M/SEC
1.0
0.0
-1.0
0.5
1.0
BREAKING WAVE (H_b/h)
HORIZONTAL VELOCITY (u/c)
NON-DIMENSIONAL QUANTITY
t/T

Figure A-5

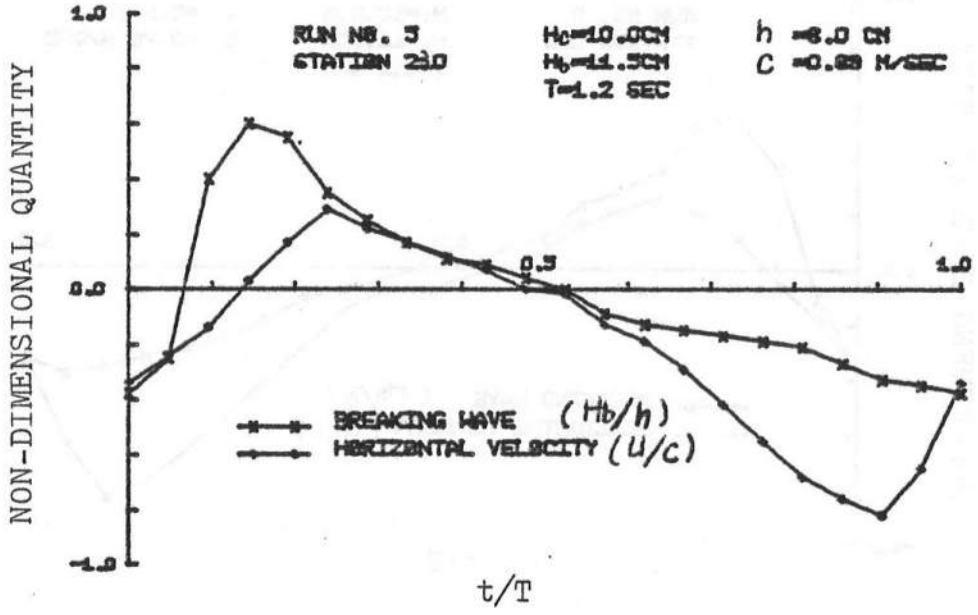
RUN NO. 5
STATION 23.0
Hc=10.0CM
Hb=11.5CM
T=1.2 SEC
h =8.0 CM
C =0.89 M/SEC
1.0
0.5
0.0
-1.0
BREAKING WAVE (Hb/h)
HORIZONTAL VELOCITY (u/c)
NON-DIMENSIONAL QUANTITY
t/T

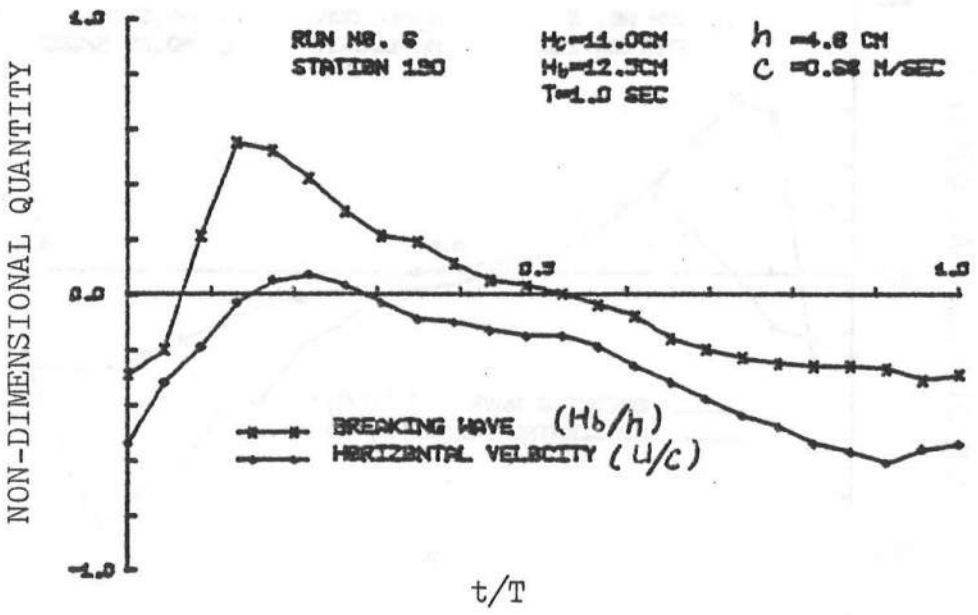
RUN NO. 6
STATION 19.0
Hc=11.0CM
Hb=12.3CM
T=1.0 SEC
h =4.8 CM
C =0.58 M/SEC
1.0
0.5
0.0
-1.0
BREAKING WAVE (Hb/h)
HORIZONTAL VELOCITY (u/c)
NON-DIMENSIONAL QUANTITY
t/T

Figure A-6

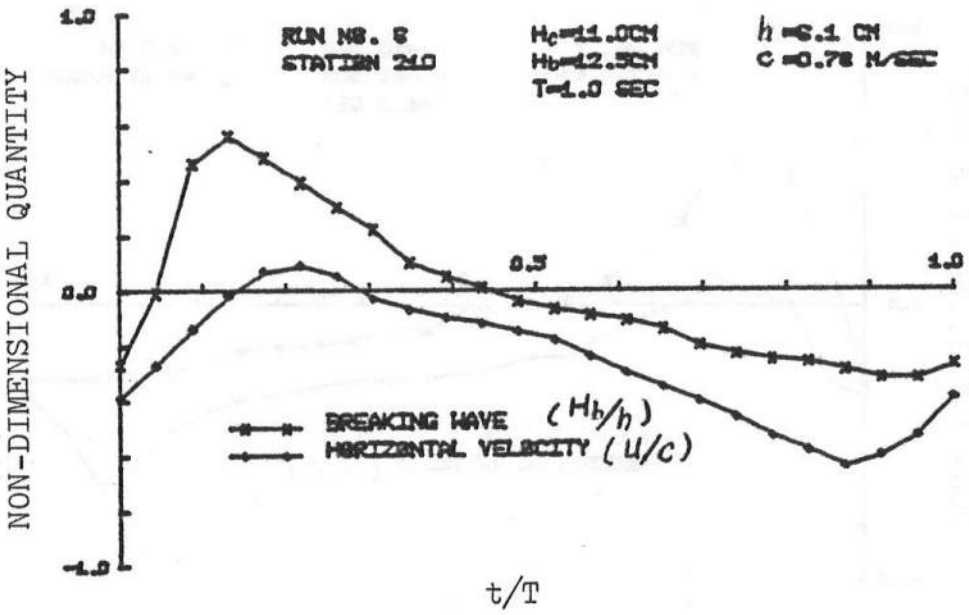
RUN NO. 6
STATION 210
Hc=11.0CM
Hb=12.3CM
T=1.0 SEC
h =6.1 CM
c =0.78 M/SEC
1.0
0.5
0.0
-1.0
NON-DIMENSIONAL QUANTITY
BREAKING WAVE (Hb/h)
HORIZONTAL VELOCITY (u/c)
t/T

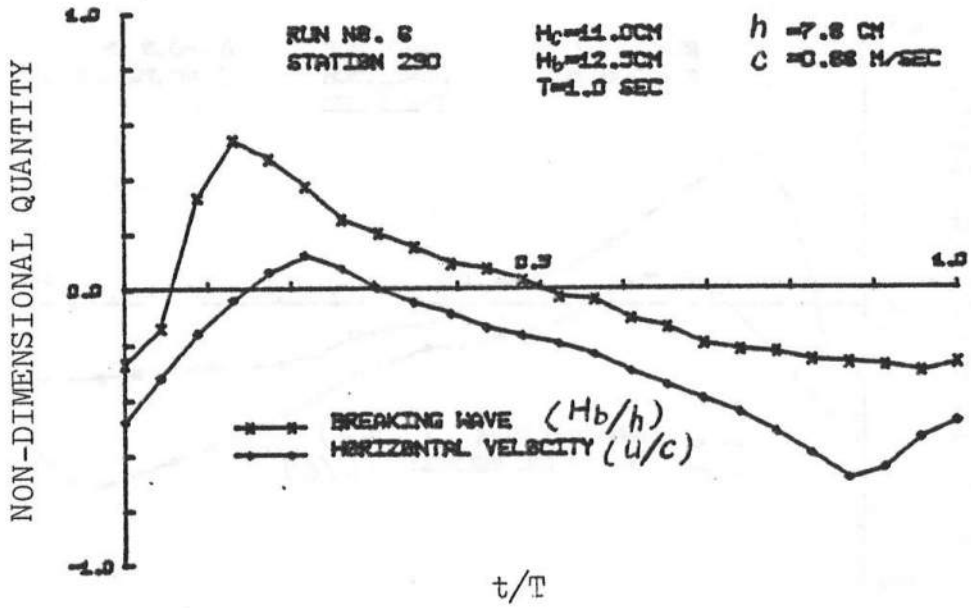
RUN NO. 6
STATION 230
Hc=11.0CM
Hb=12.3CM
T=1.0 SEC
h =7.6 CM
c =0.68 M/SEC
1.0
0.5
0.0
-1.0
NON-DIMENSIONAL QUANTITY
BREAKING WAVE (Hb/h)
HORIZONTAL VELOCITY (u/c)
t/T

Figure A-7

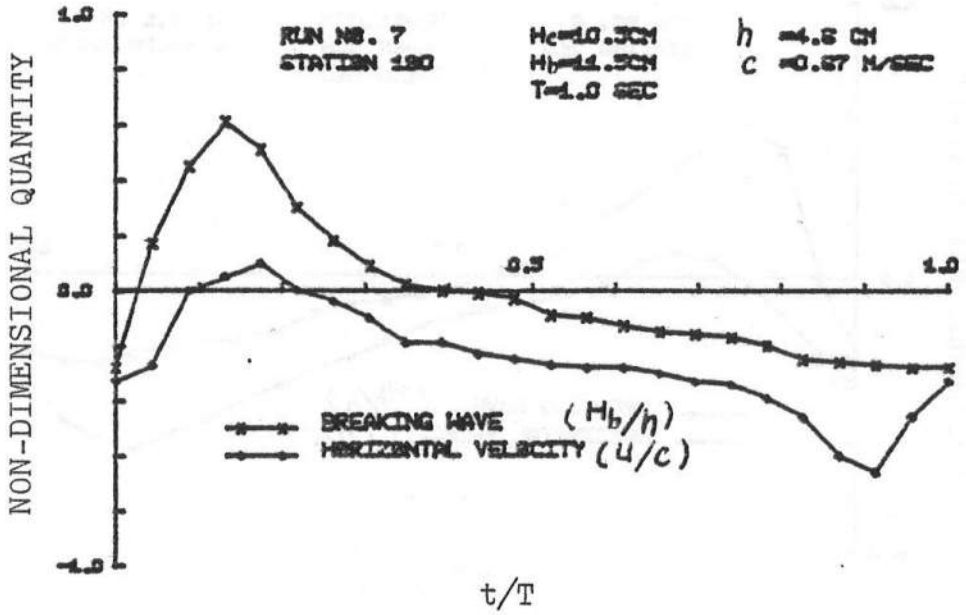
RUN NO. 7
STATION 180
Hc=10.3CM
Hb=11.3CM
T=1.0 SEC
h =4.6 CM
c =0.67 M/SEC
1.0
0.5
-1.0
0.5
1.0
NON-DIMENSIONAL QUANTITY
BREAKING WAVE (Hb/h)
HORIZONTAL VELOCITY (u/c)
t/T

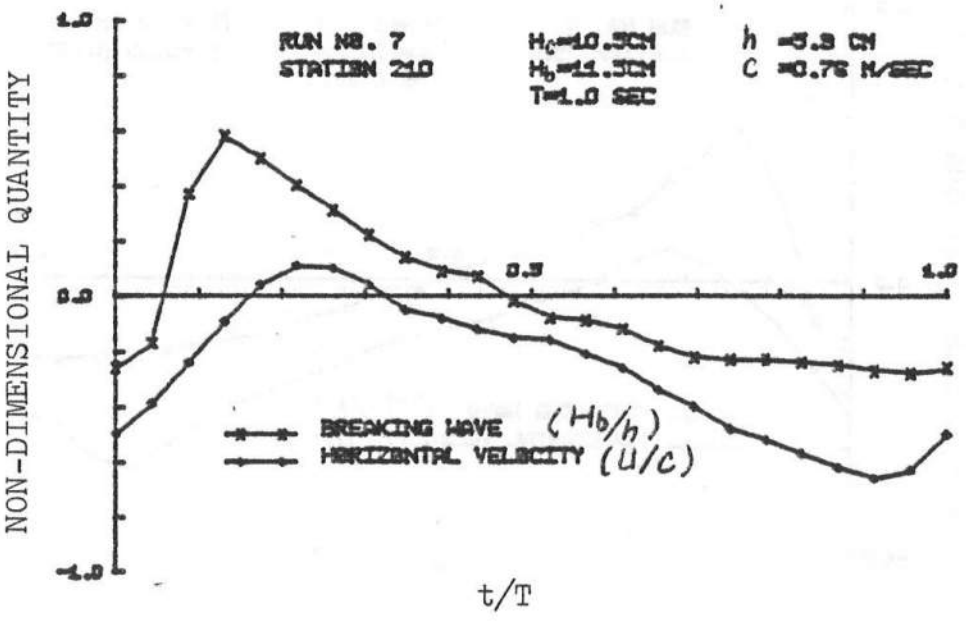
RUN NO. 7
STATION 210
Hc=10.3CM
Hb=11.3CM
T=1.0 SEC
h =5.3 CM
c =0.76 M/SEC
1.0
0.5
-1.0
0.5
1.0
NON-DIMENSIONAL QUANTITY
BREAKING WAVE (Hb/h)
HORIZONTAL VELOCITY (u/c)
t/T

Figure A-8

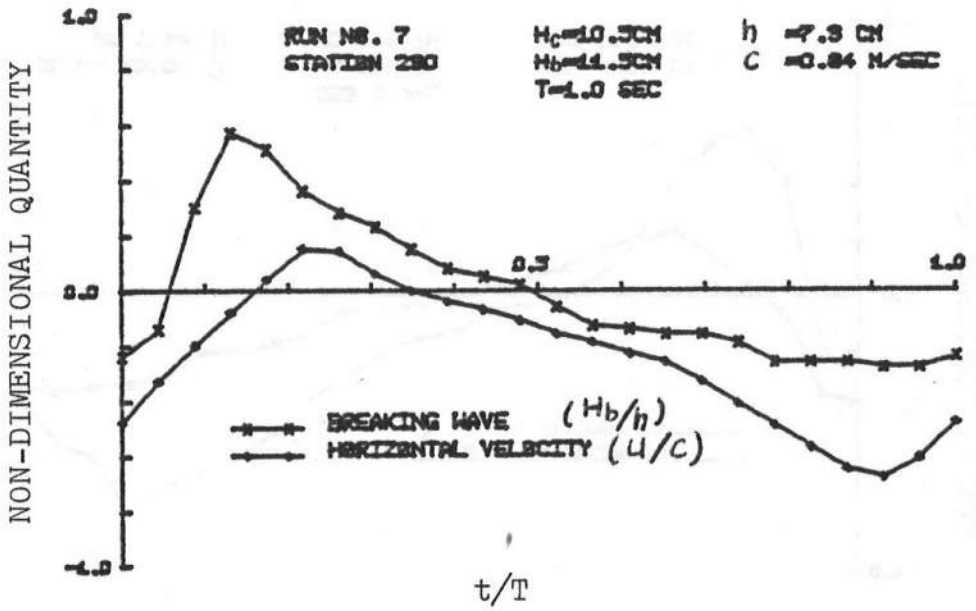
RUN NO. 7
STATION 280
H_c=10.3CM
H_b=11.3CM
T=1.0 SEC
h =7.3 CM
C =0.84 M/SEC
1.0
0.5
1.0
0.0
-1.0
BREAKING WAVE (Hb/h)
HORIZONTAL VELOCITY (u/c)
NON-DIMENSIONAL QUANTITY
t/T

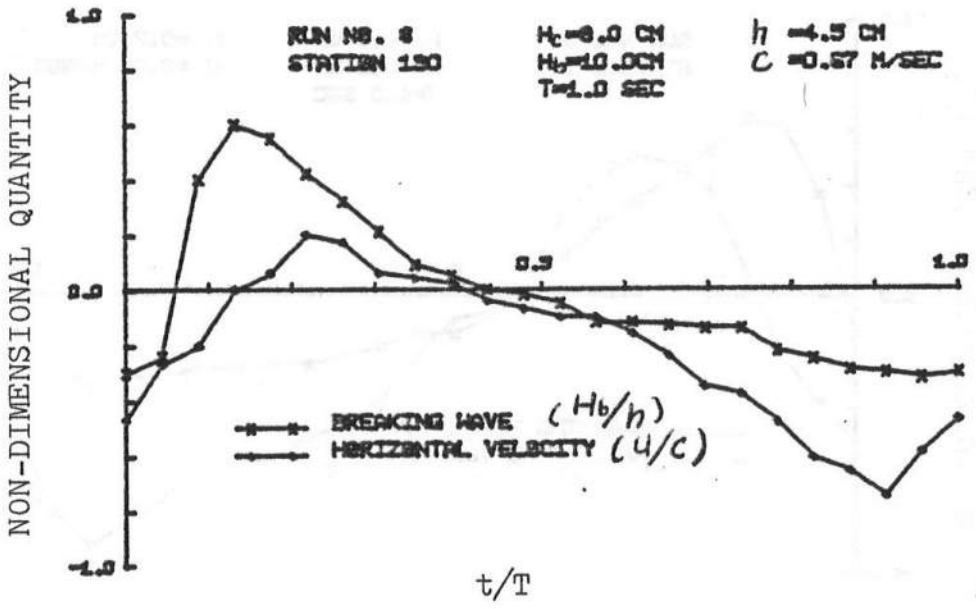
RUN NO. 8
STATION 130
H_c=8.0 CM
H_b=10.0CM
T=1.0 SEC
h =4.5 CM
C =0.67 M/SEC
1.0
0.5
1.0
0.0
-1.0
BREAKING WAVE (Hb/h)
HORIZONTAL VELOCITY (u/c)
NON-DIMENSIONAL QUANTITY
t/T

Figure A-9

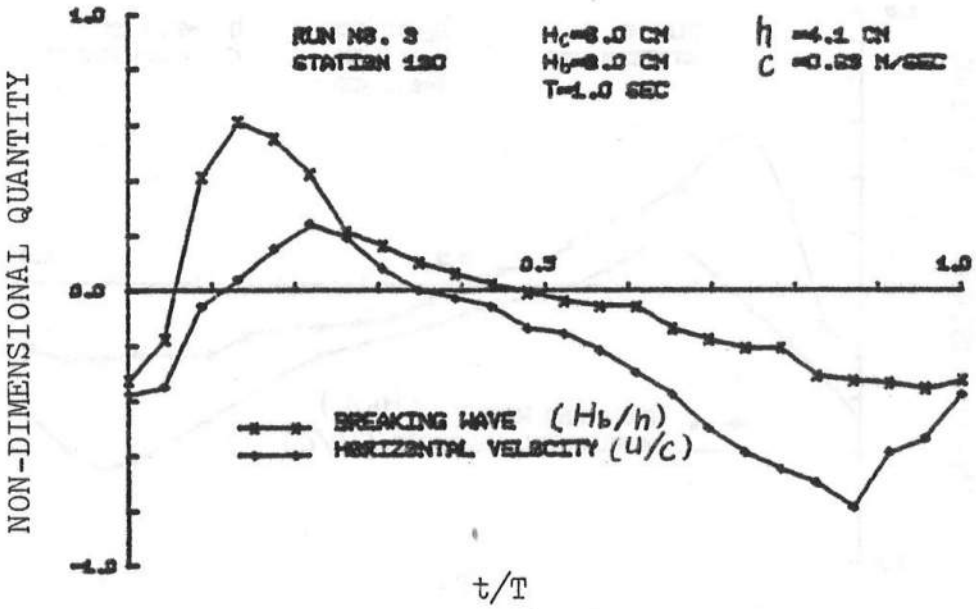
RUN NO. 9
STATION 130
H_c=8.0 CM
H_b=8.0 CM
T=1.0 SEC
h =4.1 CM
c =0.89 M/SEC
1.0
0.0
-1.0
0.5
1.0
BREAKING WAVE (H_b/h)
HORIZONTAL VELOCITY (u/c)
NON-DIMENSIONAL QUANTITY
t/T

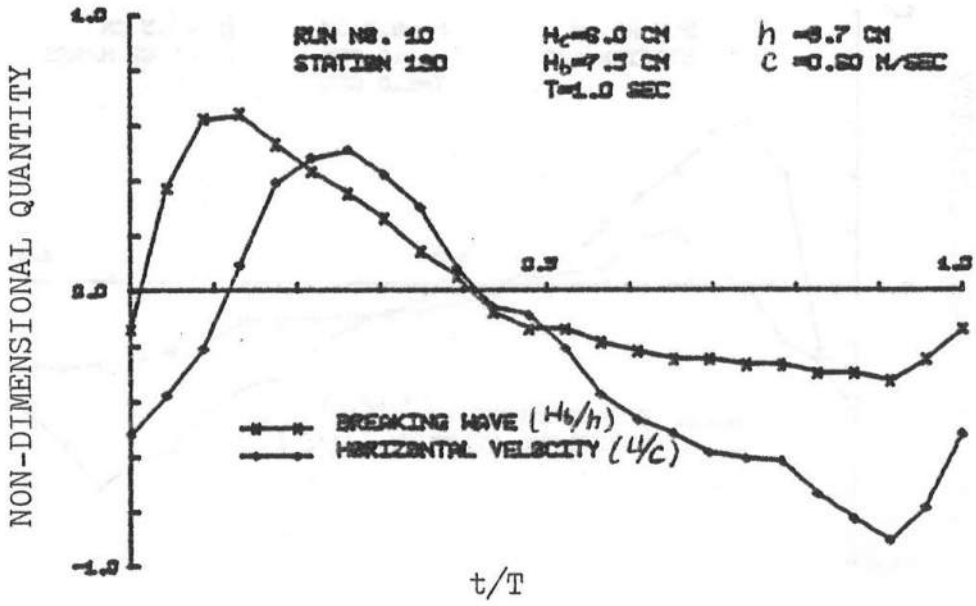
RUN NO. 10
STATION 130
H_c=8.0 CM
H_b=7.5 CM
T=1.0 SEC
h =8.7 CM
c =0.80 M/SEC
1.0
0.0
-1.0
0.5
1.0
BREAKING WAVE (H_b/h)
HORIZONTAL VELOCITY (u/c)
NON-DIMENSIONAL QUANTITY
t/T

Figure A-10

APPENDIX B

DYNAMICS OF AIR BUBBLE IN UNSTEADY WAVE FIELD

The coordinate system for the equation of motion of air bubble in fluid environment is defined as follows:

x-y coordinate for fluid field

ξ-η coordinate for air bubbles

The two coordinates are shown schematically in Figure B-1.

The vertical equation of motion of air bubble can be expressed as:

$$\rho_a \forall_p \ddot{\eta} = C_D A_p \rho_w (\dot{\chi} - \dot{\eta})^2 + \rho_w \forall_p \ddot{\chi} + m_a (\ddot{\chi} - \ddot{\eta}) + \forall_p g (\rho_w - \rho_a) \qquad (B\text{-}1)$$

where ρ_a is air density

ρ_w is fluid density

$\forall_p$ is air bubble volume

A_p is the project area of air bubble

C_D is drag coefficient

m_a is the added mass of air bubble

For a sphere shaped air bubble with diameter D, its volume, project area and added mass can be expressed as:

$$\forall_p = \frac{1}{6}\pi D^3$$

$$A_p = \frac{1}{4}\pi D^2$$

$$m_a = \frac{1}{2}\rho_w \forall_p$$

Equation (B-1) is a non-linear second order differential equation. Assuming that the flow field is in Stokes' range, the non-linear term in Equation (B-1) can be simplified to:

$$C_D A_p \rho_w (\dot{y}-\dot{\eta})^2 \approx C_{DL} A_p \rho_w (\dot{y}-\dot{\eta}) \qquad (B\text{-}2)$$

where

$$C_{DL} = C_D |\dot{y}-\dot{\eta}|$$

Substituting Equation (B-2) in Equation (B-1) and dividing each term in the equation by V_p, Equation (B-1) becomes:

$$\rho_a \ddot{\eta} = \frac{3}{2}\frac{C_{DL}}{D}\rho_w (\dot{y}-\dot{\eta}) + \rho_w \ddot{y} + \frac{1}{2}\rho_w (\ddot{y}-\ddot{\eta}) + g(\rho_w-\rho_a) \qquad (B\text{-}3)$$

Equation (B-3) can be rearranged to:

$$(\rho_a+\tfrac{1}{2}\rho_w)\ddot{\eta} + \frac{3}{2}\frac{C_{DL}}{D}\rho_w \dot{\eta} = \frac{3}{2}\rho_w \ddot{y} + \frac{3}{2}\frac{C_{DL}}{D}\rho_w \dot{y} + g(\rho_w-\rho_a) \qquad (B\text{-}4)$$

Since $\rho_a \ll \rho_w$, we can set ρ_a =0. Dividing both sides of Equation (B-4) with ρ_w yields:

$$\ddot{\eta} + 3\frac{C_{DL}}{D}\dot{\eta} = 3\ddot{y} + 3\frac{C_{DL}}{D}\dot{y} + 2g \qquad (B\text{-}5)$$

For air bubble releasing from bottom, the initial condition can be expressed as:

$$\dot{\eta} = 0 \quad \text{at} \quad t = 0$$

For a sinusoidal fluid particle velocity in the vertical direction, we define

$$\dot{y} = v_m \cos \omega t \qquad (B\text{-}6)$$

where v_m is the maximum amplitude of vertical velocity

ω is the wave frequency

Integration of Equation (B-5) applying the initial condition and Equation (B-6) yields:

$$\dot{\eta} = U_b\left[1 - \left(1 + \frac{a^2+3\omega^2}{a^2+\omega^2}\frac{v_m}{U_b}\right)e^{-at}\right] + \frac{a^2+3\omega^2}{a^2+\omega^2}v_m \cos\omega t - \frac{2a\omega}{a^2+\omega^2}v_m \sin\omega t \qquad (B\text{-}7)$$

where U_b is the terminal rising velocity of air bubble defined as $U_b = \sqrt{\frac{2}{3}g\frac{D}{C_{DL}}}$ and $a = 3\frac{C_{DL}}{D}$

Equation (B-7) can be simplified to

$$\dot{\eta} = U_b\left[1 - \left(1 + \frac{a^2+3\omega^2}{a^2+\omega^2}\frac{v_m}{U_b}\right)e^{-at}\right] + \frac{\sqrt{(a^2+3\omega^2)^2+(2a\omega)^2}}{a^2+\omega^2}v_m \cos(\omega t + \epsilon) \qquad (B\text{-}8)$$

where

$$\epsilon = \tan^{-1} \frac{2a\omega}{a^2+\omega^2}$$

The horizontal equation of motion of air bubble can be expressed as:

$$\rho_a \forall_p \ddot{\xi} = C_D A_p \rho_w (\dot{x}-\dot{\xi})^2 + \rho_w \forall_p \ddot{x} + m_a(\ddot{x}-\ddot{\xi}) \qquad (B\text{-}9)$$

Equation (B-9) can be simplified by assuming $\rho_a \approx 0$:

$$\ddot{\xi} + 3\frac{C_{DL}}{D}\dot{\xi} = 3\ddot{x} + 3\frac{C_{DL}}{D}\dot{x} \qquad (B\text{-}10)$$

For a sinusoidal horizontal fluid partical velocity, we define:

$$\dot{x} = U_m \sin \omega t \qquad (B\text{-}11)$$

where U_m is the maximum amplitude of horizontal velocity. The initial condition can be defined as:

$$\dot{\xi}(0) = 0 \qquad \text{at } t = 0$$

Integration of Equation (B-10) applying the initial condition and Equation (B-11) yields:

$$\dot{\xi} = U_m \left[\frac{\sqrt{(a^2+3\omega^2)^2+(2a\omega)^2}}{a^2+\omega^2} \sin(\omega t+\epsilon) - \frac{2a\omega}{a^2+\omega^2} e^{-at} \right] \qquad (B\text{-}12)$$

The analytical solutions of vertical and horizontal air bubble velocities are discussed in the following paragraphs:

Letting $\alpha = \frac{\sqrt{(a^2+3\omega^2)^2+(2a\omega)^2}}{a^2+\omega^2}$, $\beta = \frac{2a\omega}{a^2+\omega^2}$, $\gamma = \frac{a^2+3\omega^2}{a^2+\omega^2}$,

The vertical and horizontal air bubble velocities in Equations (B.-8) and (B.-12) becomes:

$$\dot{\eta} = U_b\left[1-\left(1+\gamma\frac{V_m}{U_b}\right)e^{-at}\right]+\alpha V_m \cos(\omega t+\epsilon) \qquad (B\text{-}13)$$

$$\dot{\xi} = U_m\left[\alpha \sin(\omega t+\epsilon)-\beta e^{-at}\right] \qquad (B\text{-}14)$$

For small air bubble,

$$a = 3\frac{C_{DL}}{D} \gg 0 \quad \text{and} \quad \left(\frac{\omega}{a}\right)^2 \approx 0$$

$$\alpha = \frac{\sqrt{1+3\left(\frac{\omega}{a}\right)^2+4\left(\frac{\omega}{a}\right)^2}}{1+\left(\frac{\omega}{a}\right)^2} \approx 1$$

$$\beta = \frac{2\frac{\omega}{a}}{1+\left(\frac{\omega}{a}\right)^2} \approx 2\frac{\omega}{a} \qquad (B\text{-}15)$$

$$\gamma = \frac{1+3\left(\frac{\omega}{a}\right)^2}{1+\left(\frac{\omega}{a}\right)^2} \approx 1$$

$$\epsilon = \tan^{-1}\frac{2a\omega}{a^2+\omega^2} \approx \frac{2\omega}{a}$$

Therefore, for a small air bubble rising through calm water, the vertical and horizontal velocities can be expressed as:

$$\dot{\eta} = U_b\left(1-e^{-at}\right)$$
$$\dot{\xi} = 0 \qquad (B\text{-}16)$$

The traveling time of air bubble in calm water as a function of the size factor "a" is illustrated graphically in Figure B-2.

For the present laboratory condition, the air bubble reached terminal velocity in approximately 0.06 seconds.

For the case of air bubble in unsteady wave field, the vertical and horizontal velocities of air bubbles after they reached terminal velocities are:

$$\dot{\eta} = U_b + \alpha v_m \cos(\omega t + \epsilon)$$
$$\dot{\xi} = \alpha v_m \sin(\omega t + \epsilon) \qquad (B\text{-}17)$$

The numerical values of α and ϵ are plotted against wave period "T" for various "a" values as shown in Figure B-3. It can be seen that for longer wave period and/or small bubble size, $\alpha \approx 1$ and $\epsilon \approx 0$. The results imply that for smaller bubble size and/or longer wave period, the better the fluid particle velocity can be represented by air bubble velocity.

In order to find the maximum error imposed during the velocity measurement, a correction factor "CF" was introduced. Referring to Figure B-4, the measured mean horizontal velocity can be expressed as:

$$U = \tan\beta \left[U_b + \alpha v_m \cos\phi \right] \qquad (B\text{-}18)$$

where $\phi = \omega t + \epsilon$

Letting the maximum bubble line slope measured be m, the bubble line slope at any instant in one wave cycle can be expressed as $\tan\beta = m\sin\phi$ and

$$\frac{U}{U_b} = m\sin\phi + \frac{\alpha}{2}\frac{\bar{v}_m}{U_b}\sin 2\phi \qquad (B\text{-}19)$$

Physically, for small phase error "ϵ", $m\sin\phi$ is the true horizontal velocity at that instant and $\frac{\alpha}{2}\frac{\bar{v}_m}{U_b}\sin 2\phi$ is the error introduced by vertical fluid velocity. The maximum error imposed is then $\frac{\alpha}{2}\frac{\bar{v}_m}{U_b}$ as shown in non-dimensional form. The correction factor is defined as

$$CF = \frac{\alpha}{2}\frac{\bar{v}_m}{U_b} \qquad (B\text{-}20)$$

The correction factor was plotted against different water depths, wave heights and wave periods as shown in Figures B-5 and B-6. The results indicated that at wave trough, CF ranged from 0.3 to 0.4 for deep water condition, 0.2 to 0.3 for shallow water condition. For fluid particle velocity in surf zone the error is further reduced due to weak vertical fluid velocity. Therefore, the maximum error introduced using air bubble velocity measuring technique would be less than 20%.

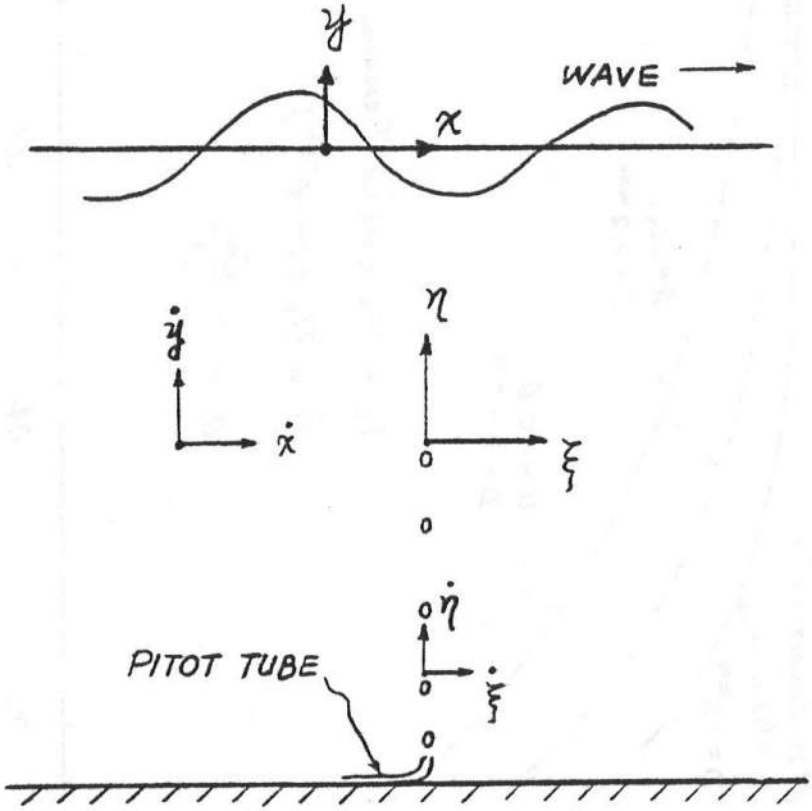

Figure B-1 Coordinate System for Air Bubble and Fluid Particle

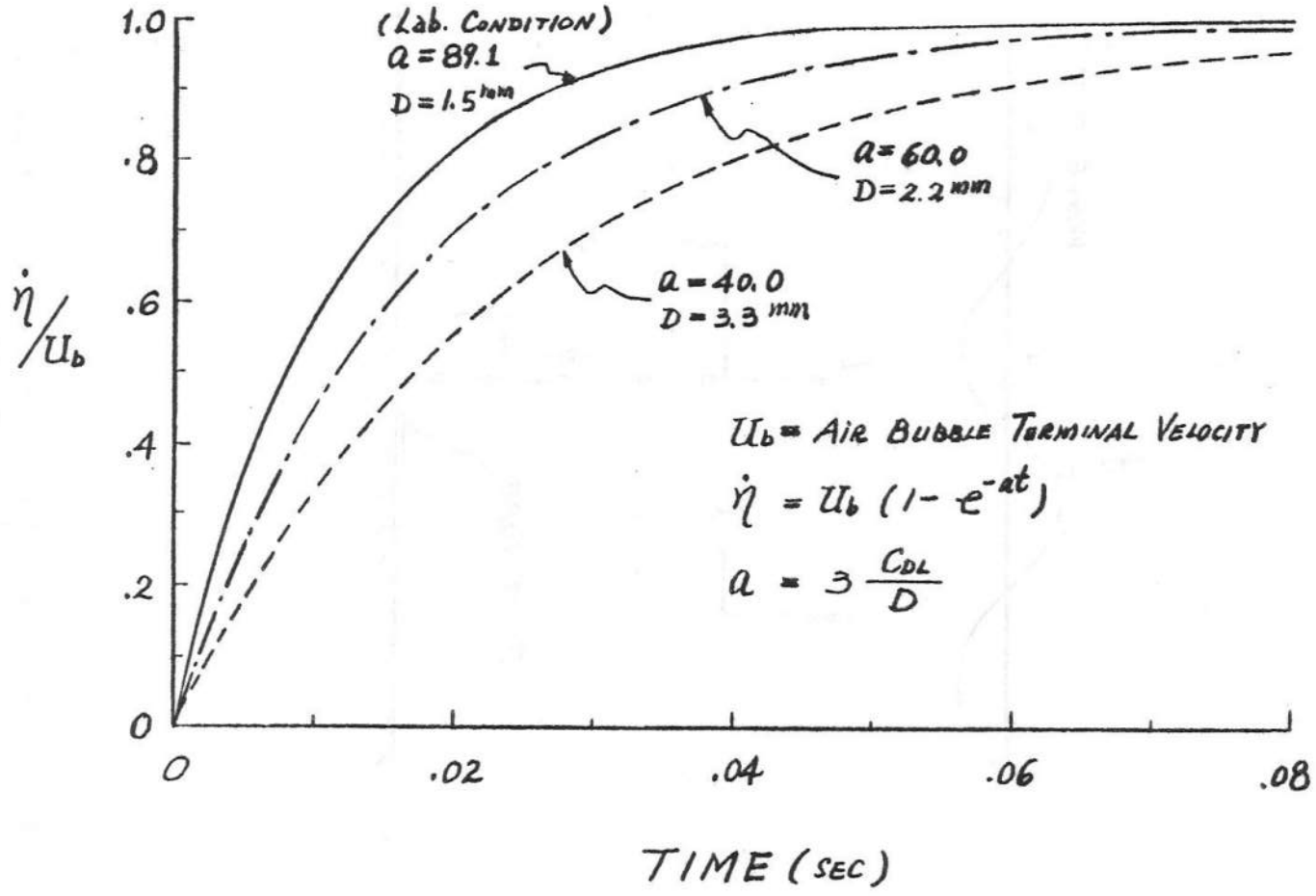

Figure B-2 Time Required to reach Rising Terminal Velocity

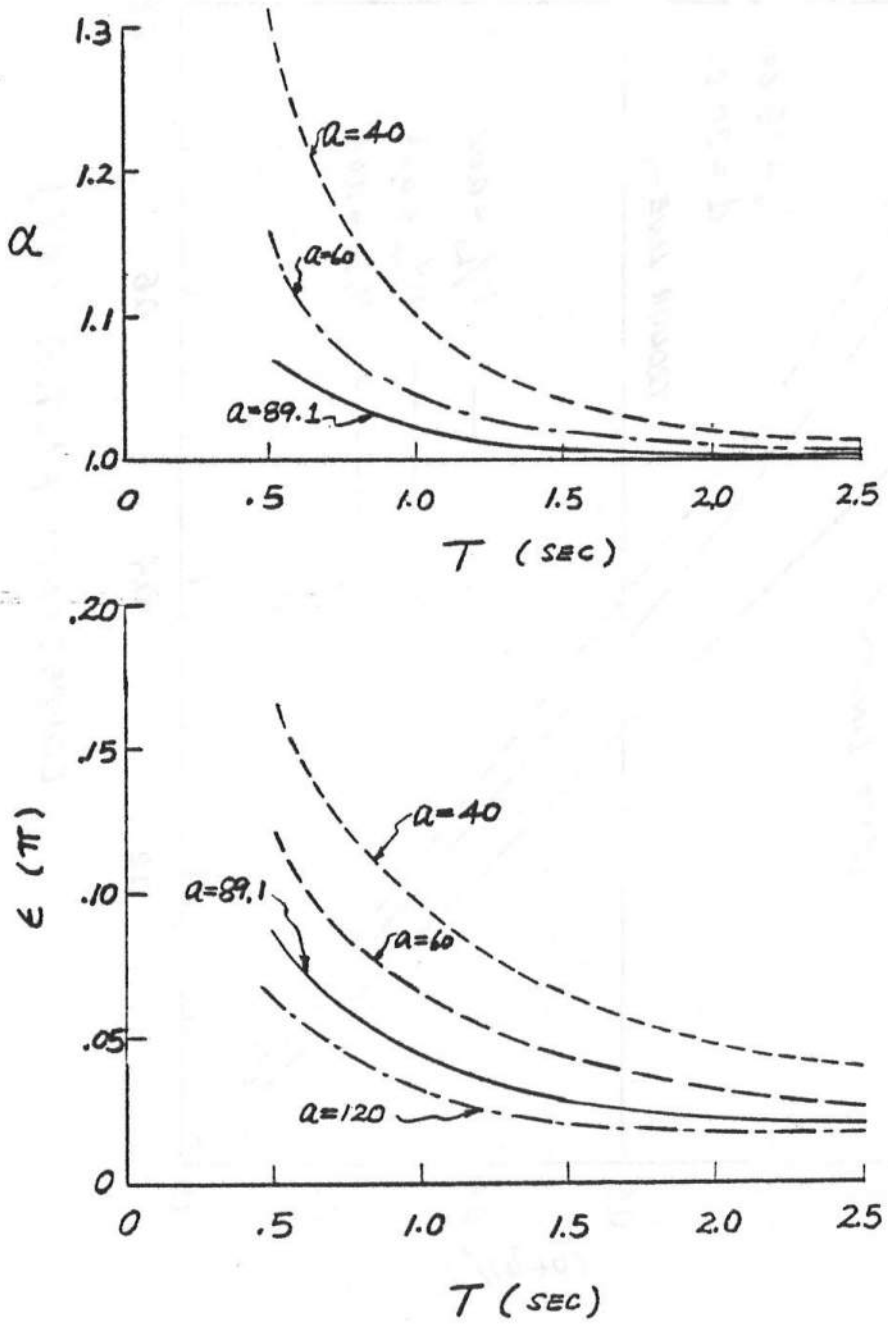

Figure B-3 α and ϵ vs. Wave Period

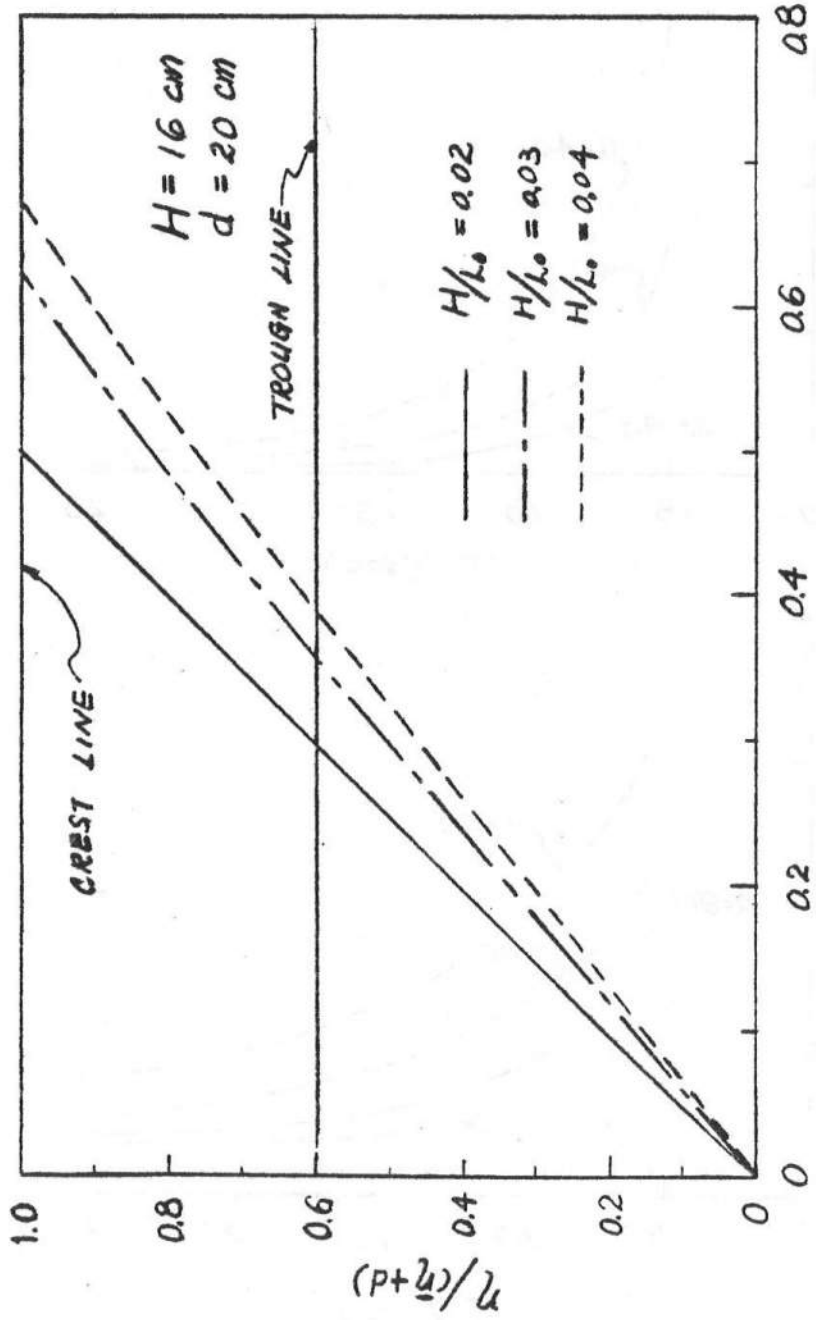

Figure B-4 Correction Factor vs. Total Water Depth

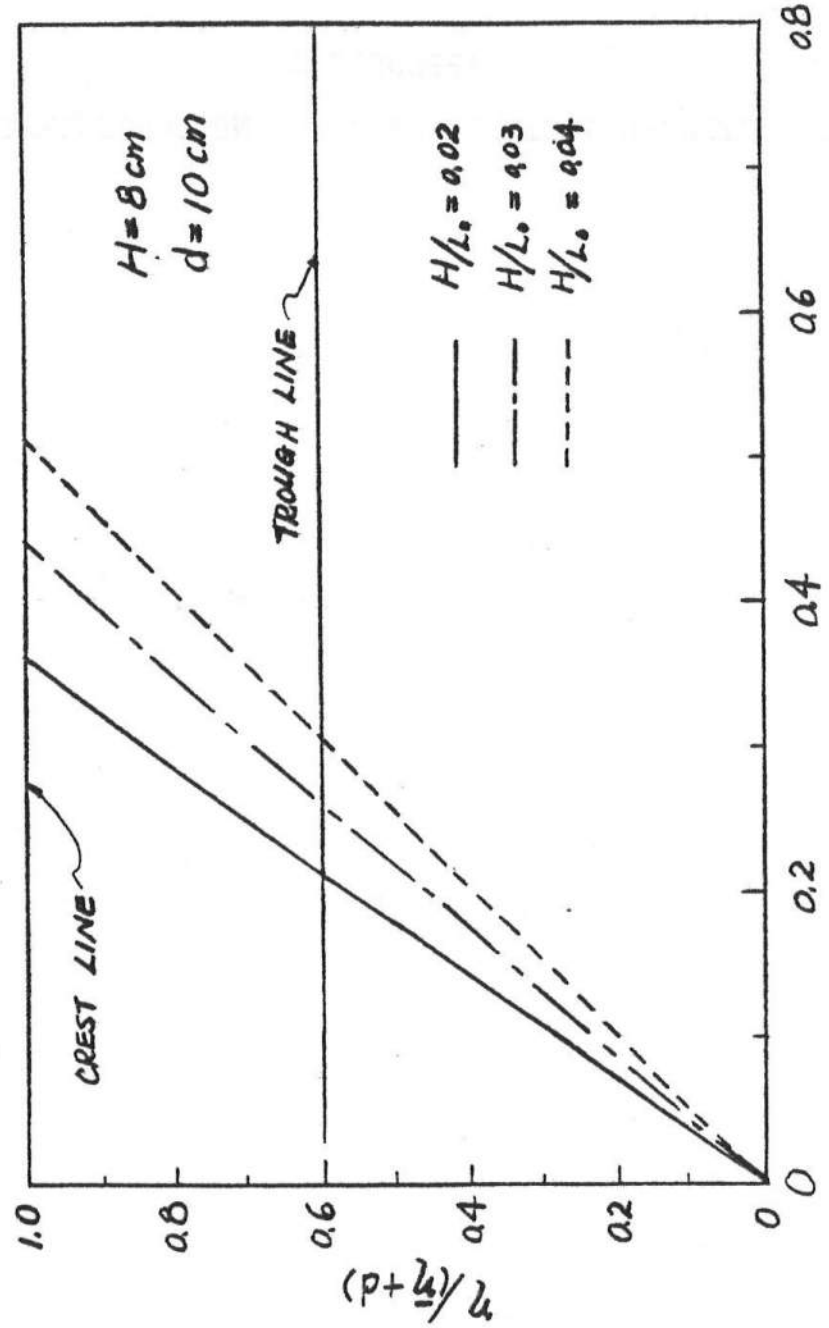

Figure B-5 Correction Factor vs. Total Water Depth

APPENDIX C

WAVE AND SUSPENDED SEDIMENT SPECTRA AND CONCENTRATION DATA

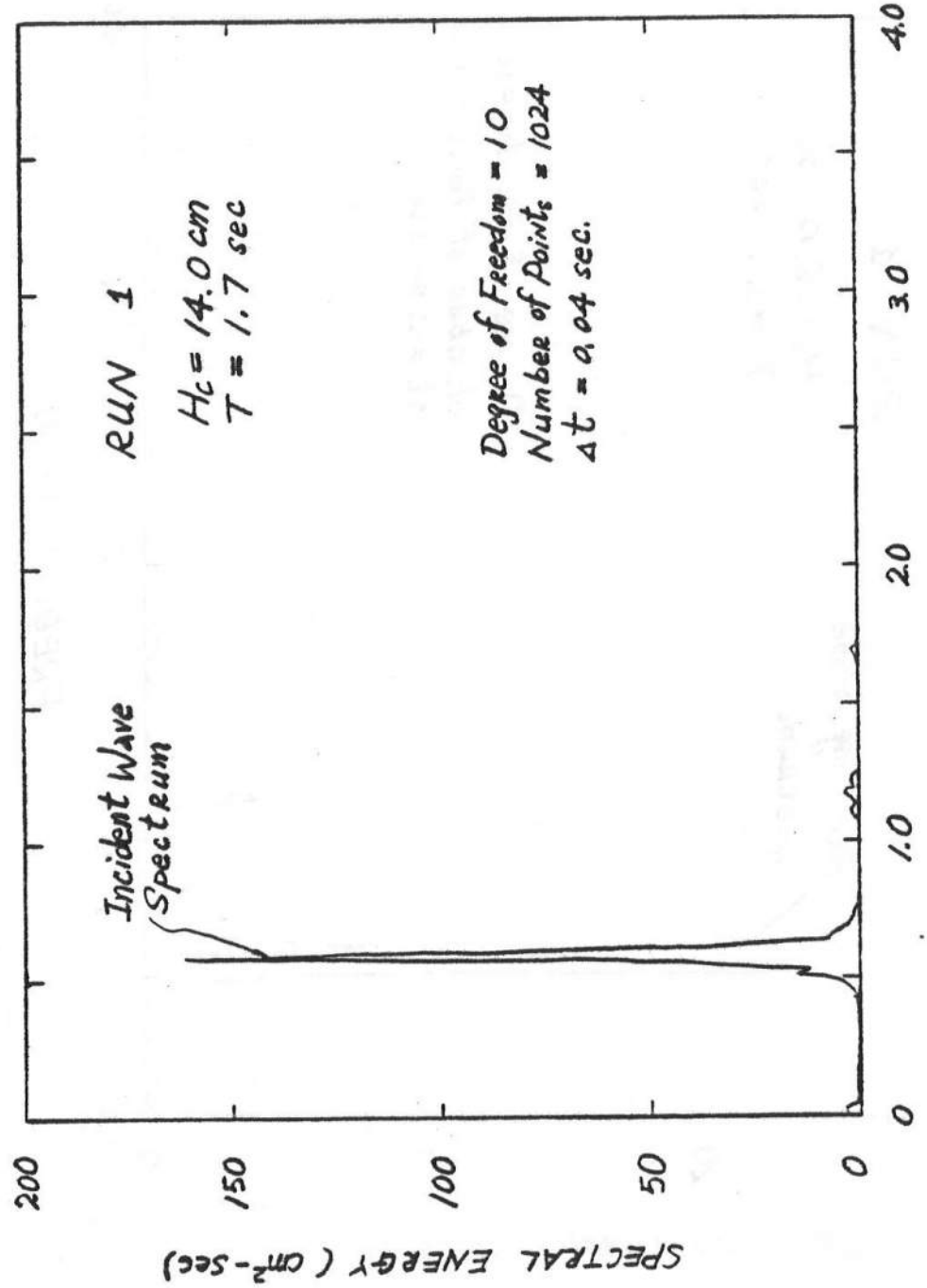

Figure C-1 Incident Wave Spectrum for Run 1

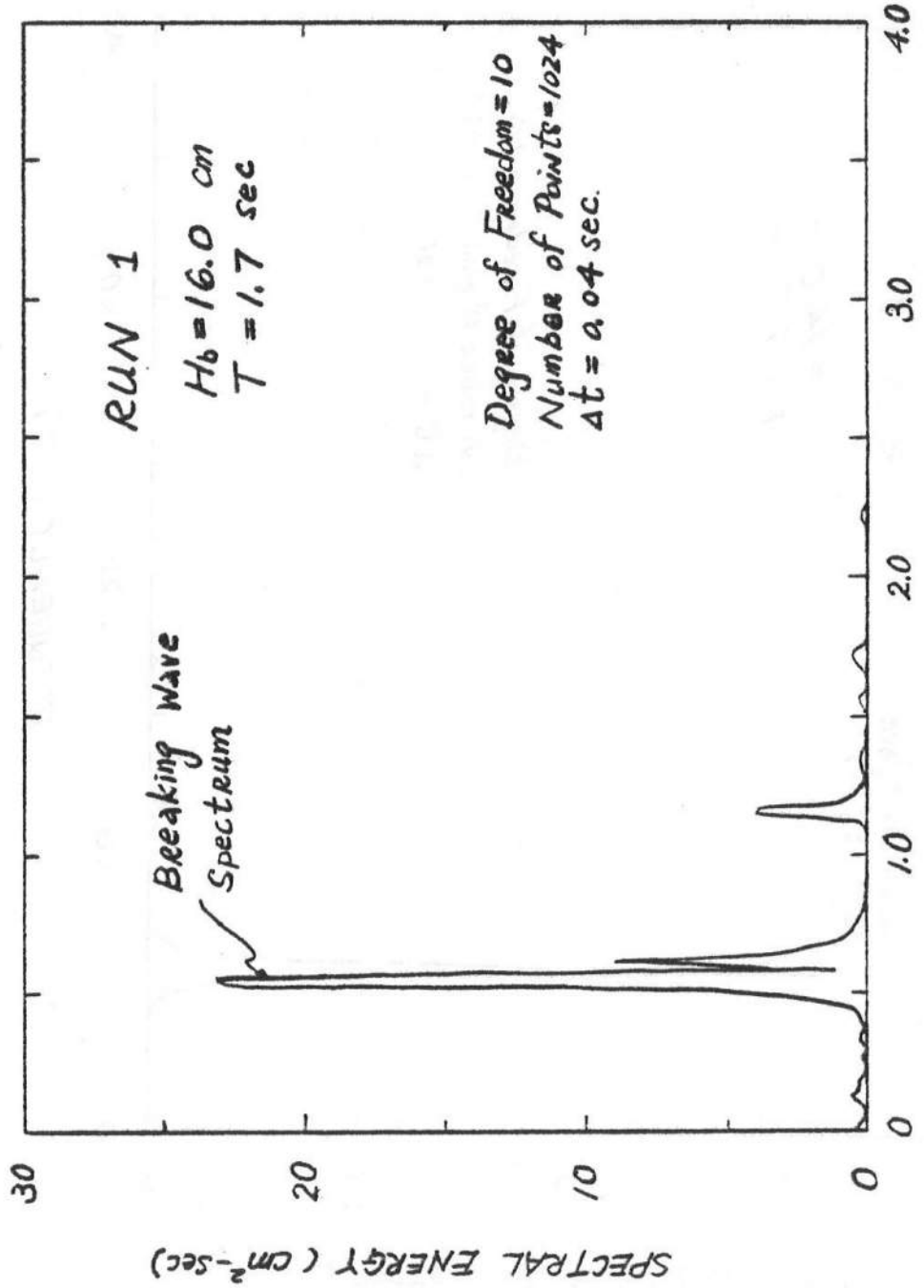

Figure C-2 Breaking Wave Spectrum for Run 1

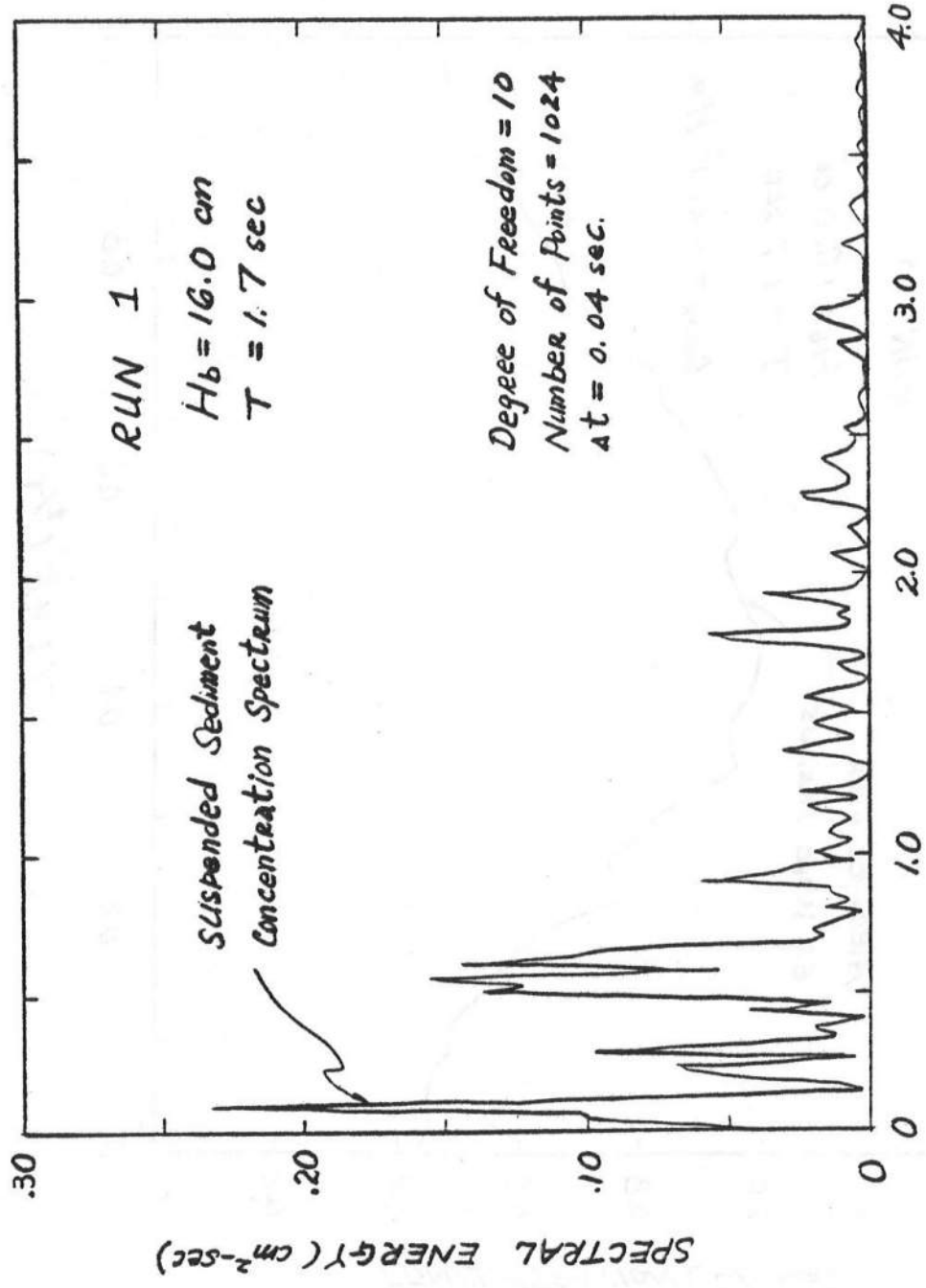

Figure C-3 Suspended Sediment Concentration Spectrum for Run 1

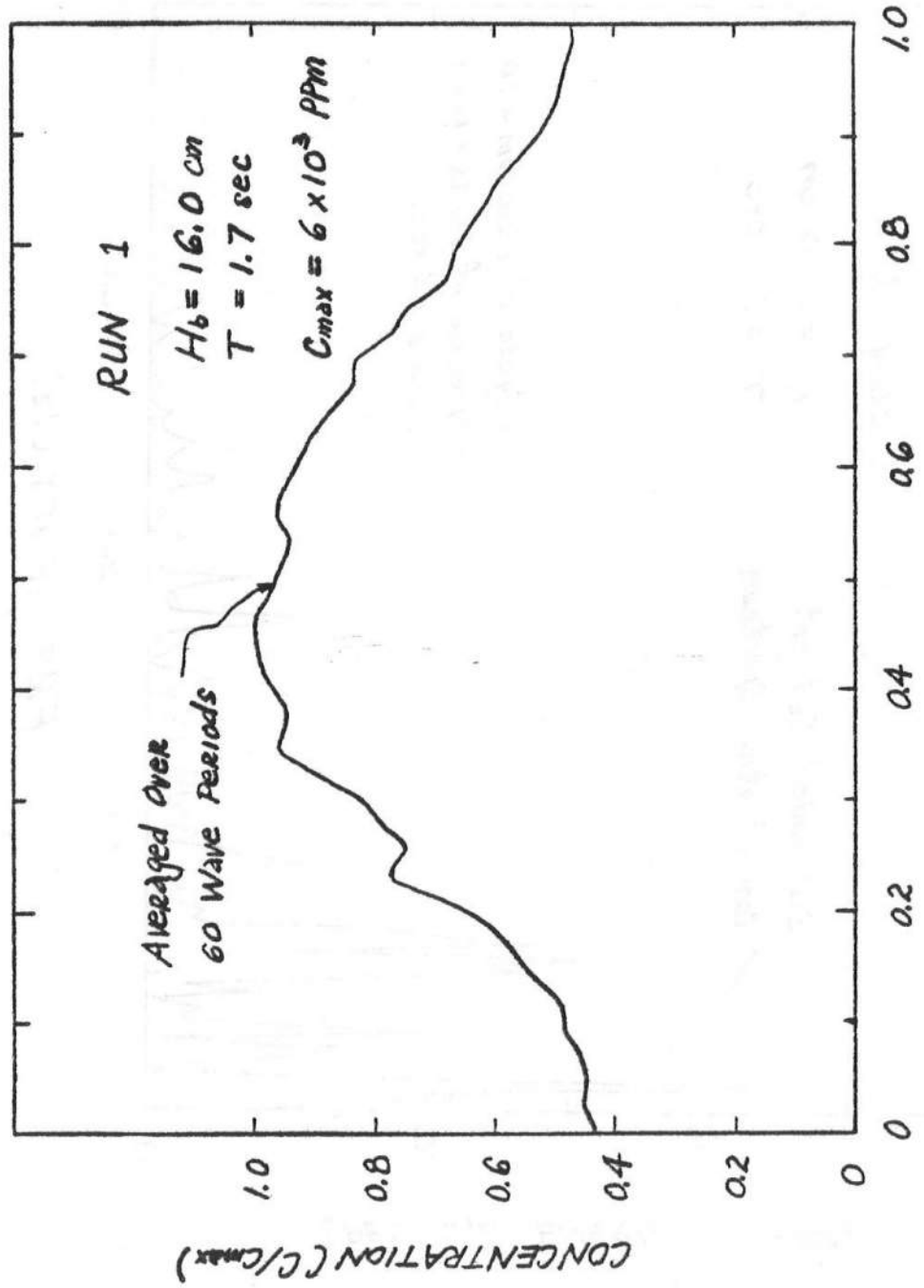

Figure C-4 Average Suspended Sediment Concentration for Run 1

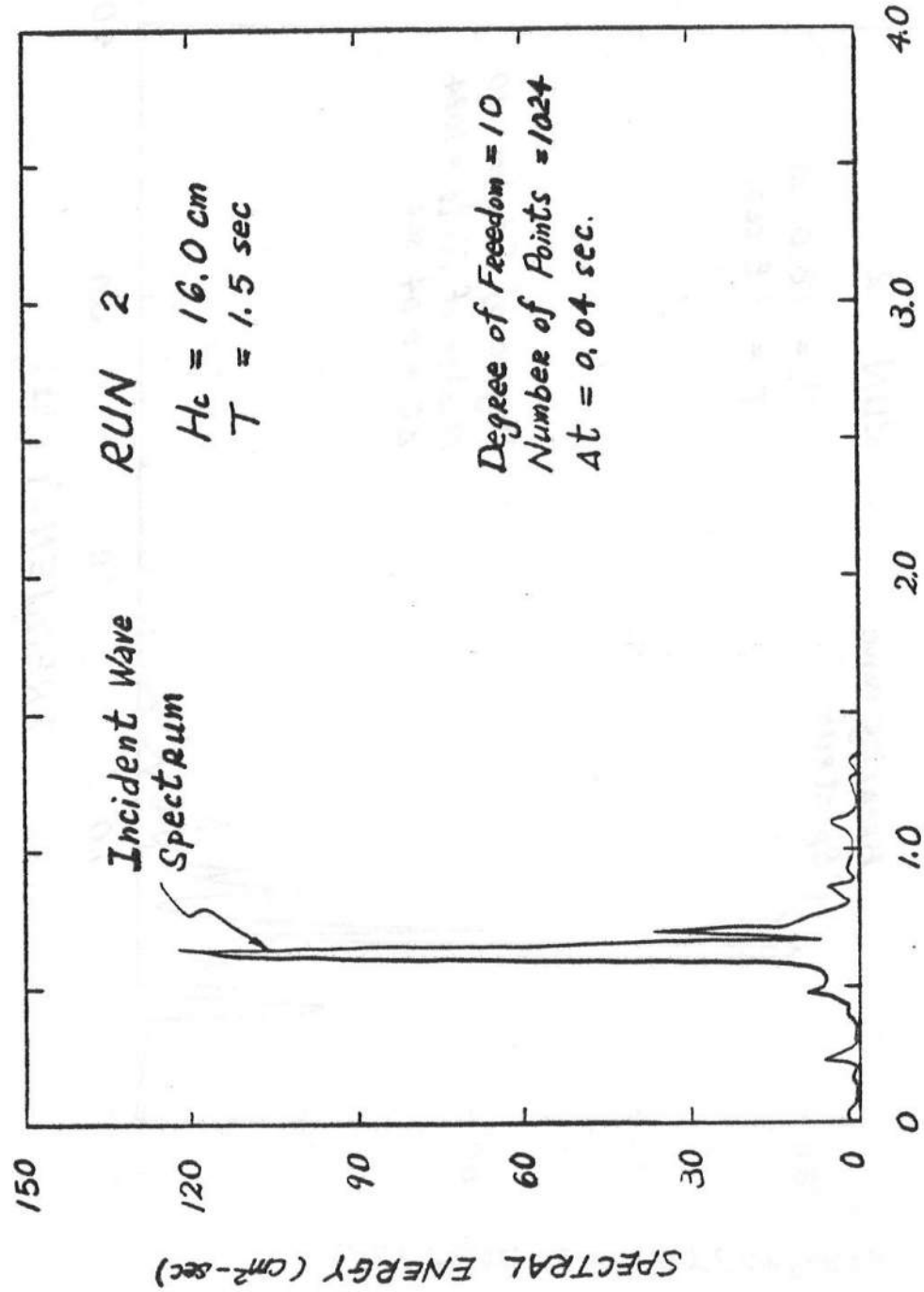

Figure C-5 Incident Wave Spectrum for Run 2

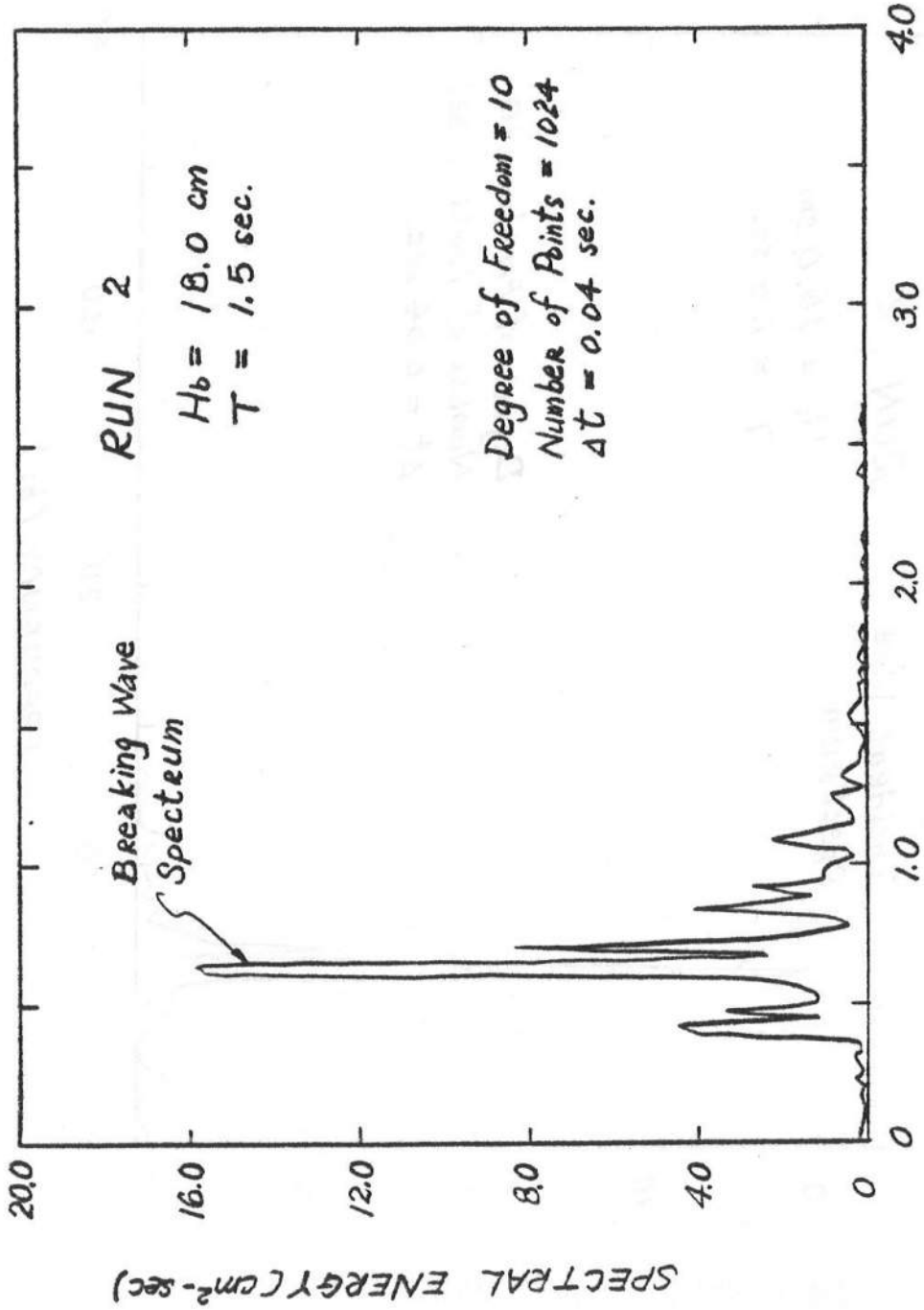

Figure C-6 Breaking Wave Spectrum for Run 2

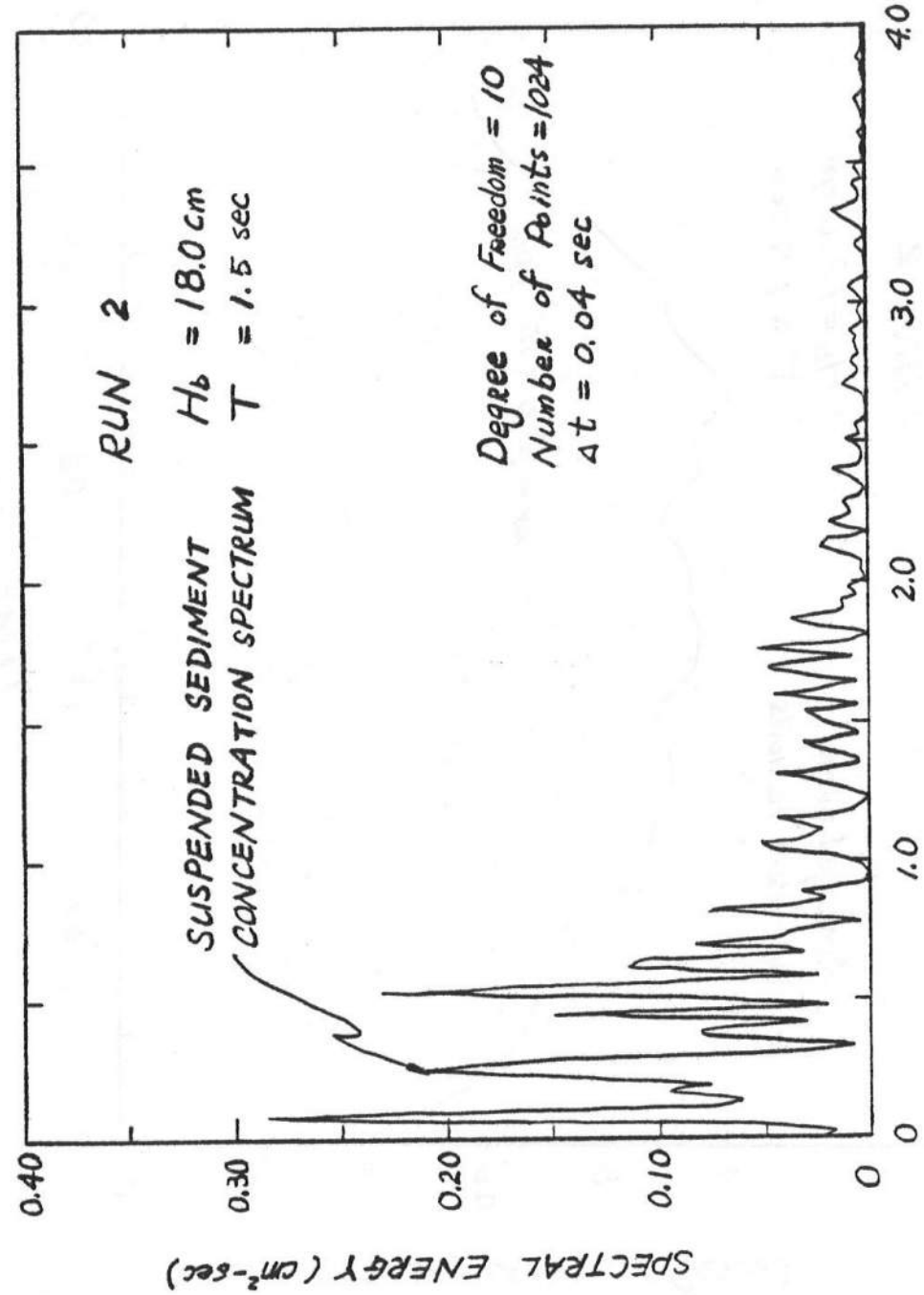

Figure C-7 Suspended Sediment Concentration Spectrum for Run 2

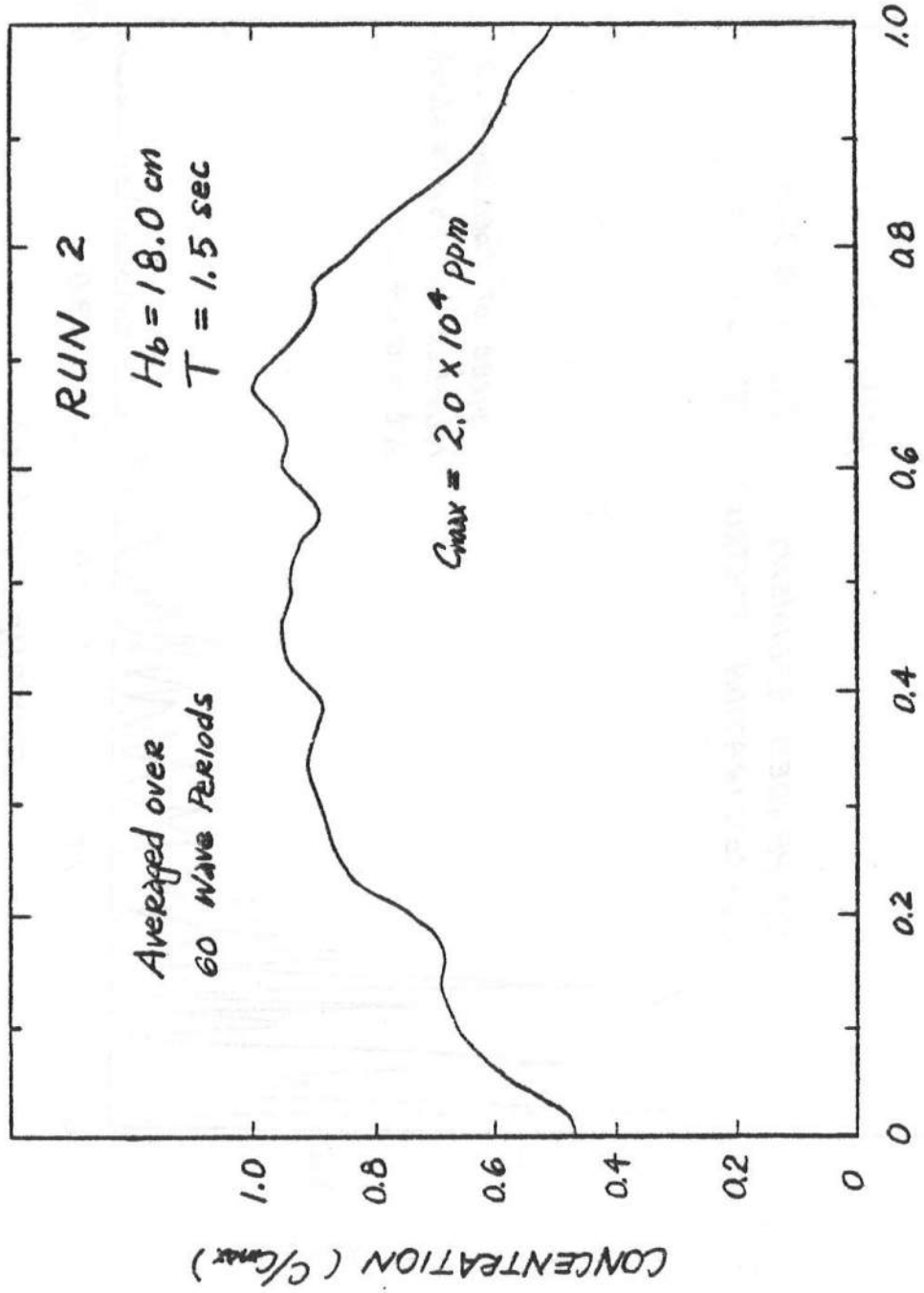

Figure C-8 Averaged Suspended Sediment Concentration for Run 2

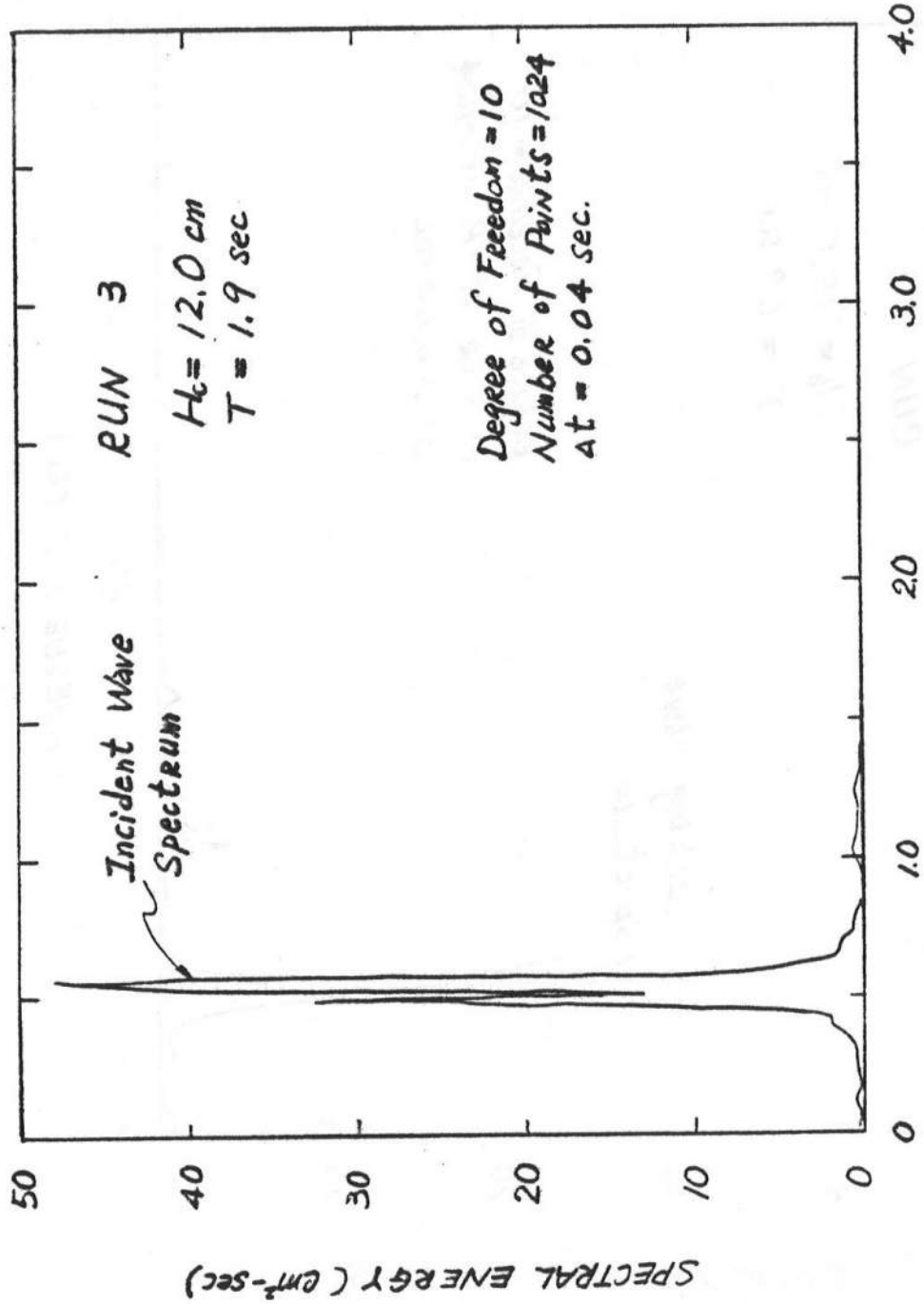

Figure C-9 Incident Wave Spectrum for Run 3

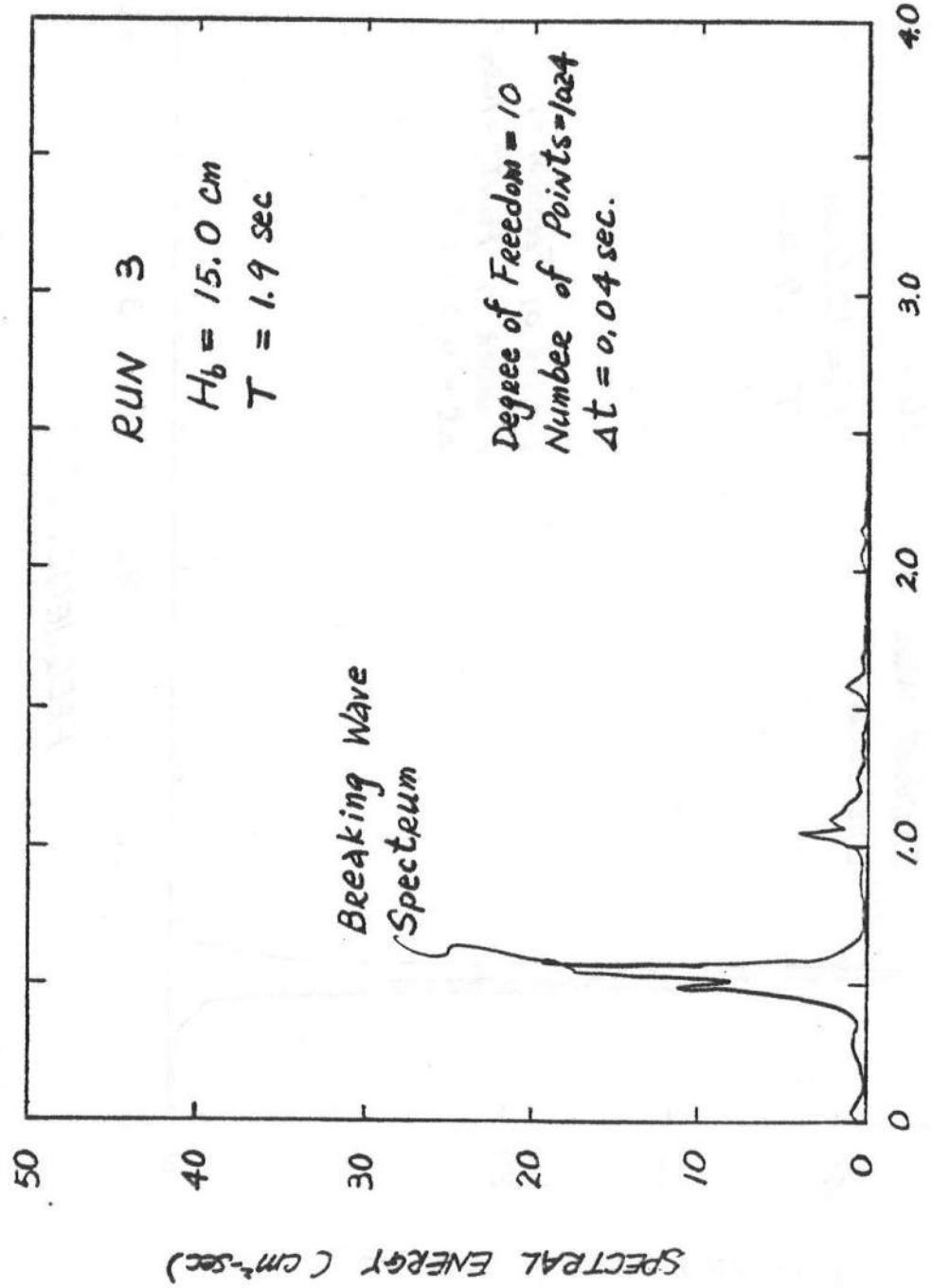

Figure C-10 Breaking Wave Spectrum for Run 3

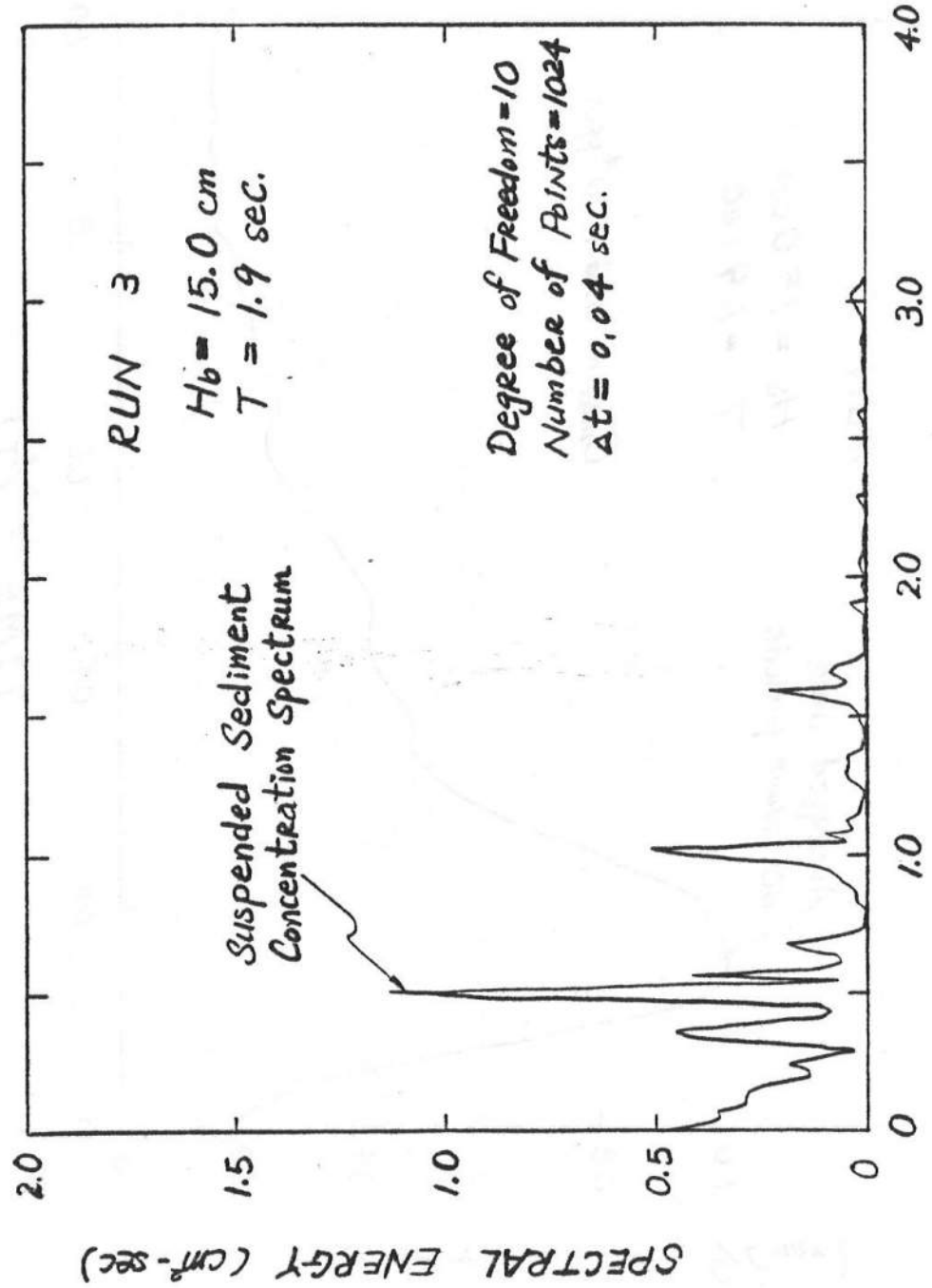

Figure C-11 Suspended Sediment Concentration Spectrum for Run 3

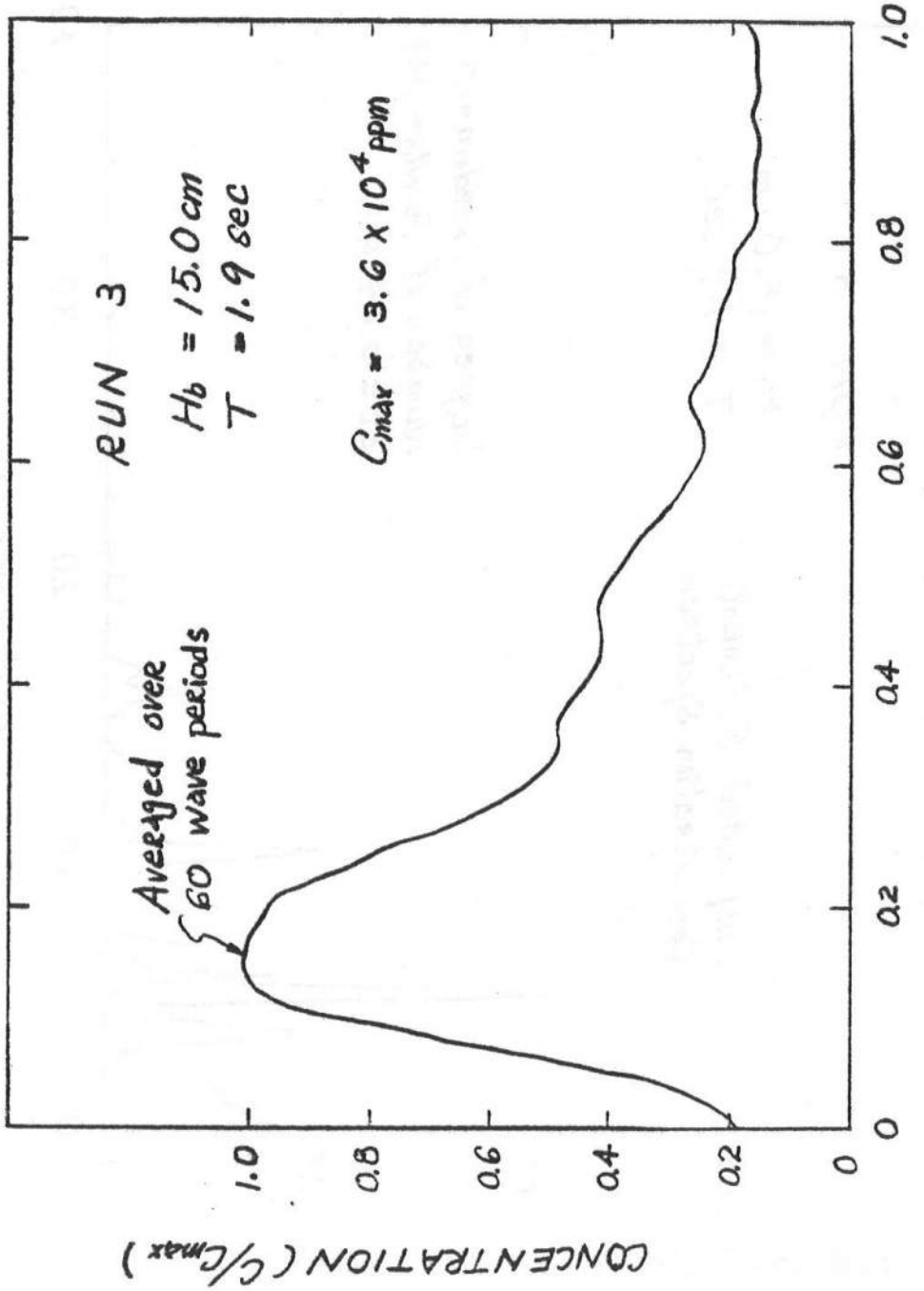

Figure C-12 Averaged Suspended Sediment Concentration for Run 3

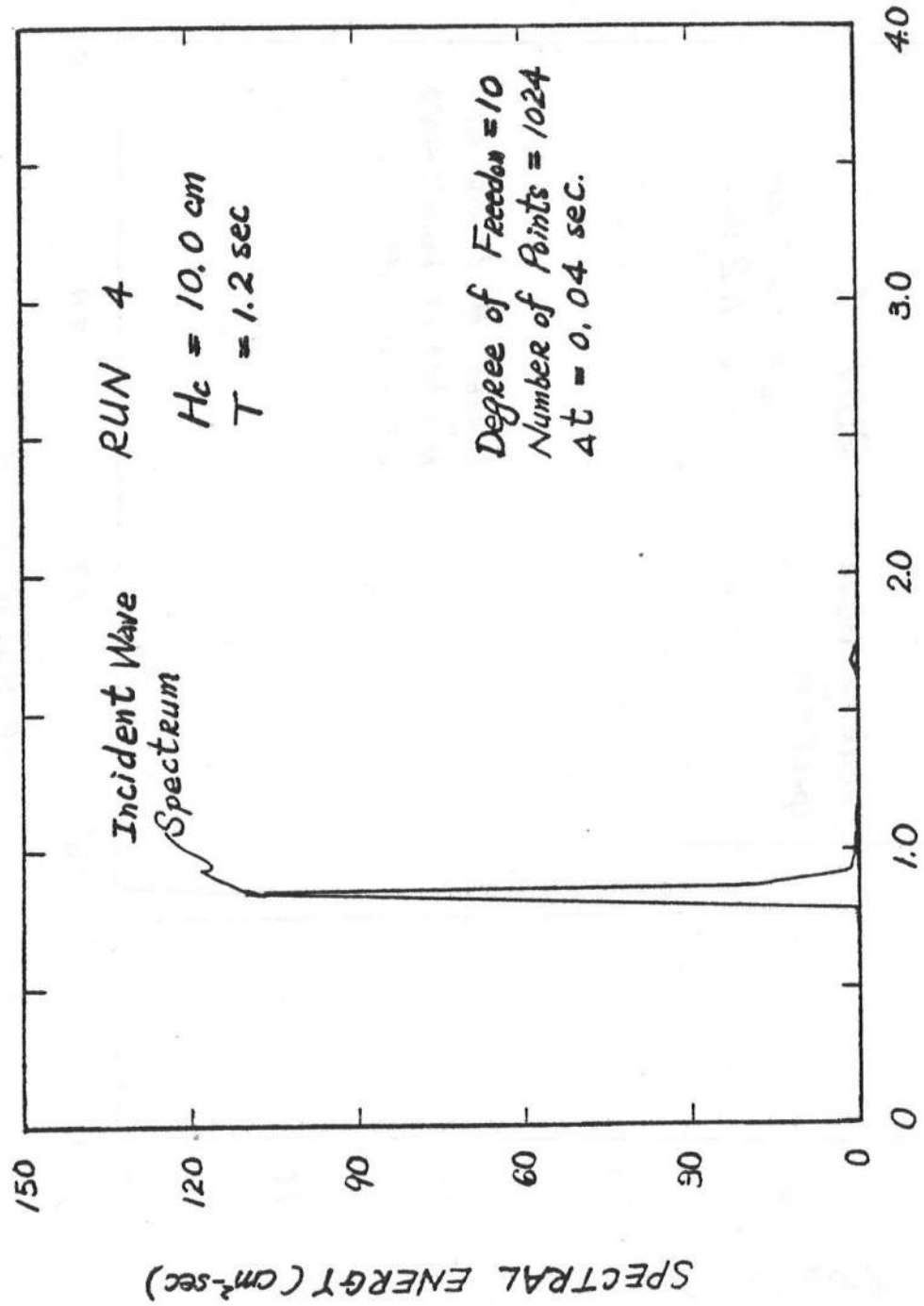

Figure C-13 Incident Wave Spectrum for Run 4

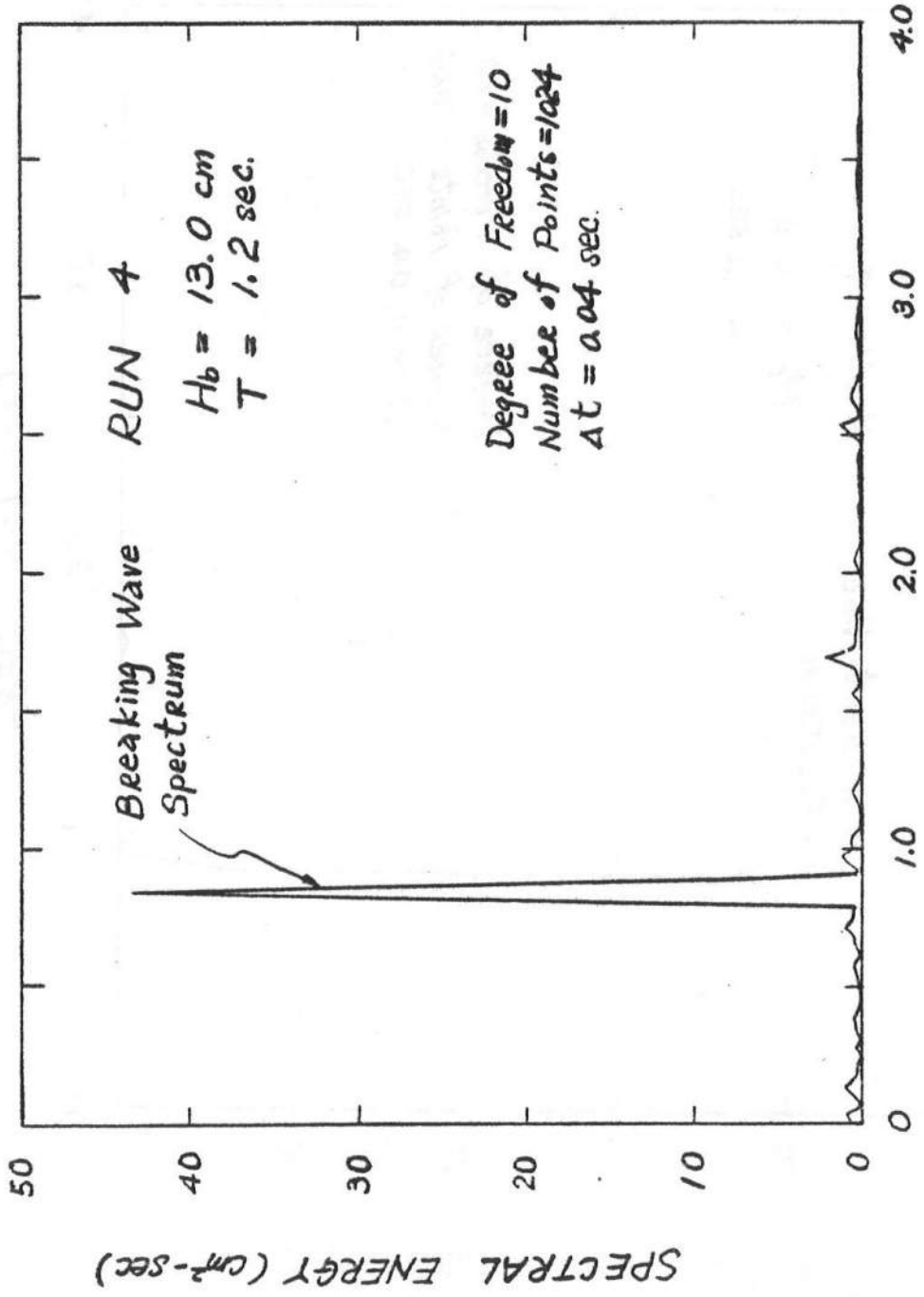

Figure C-14 Breaking Wave Spectrum for Run 4

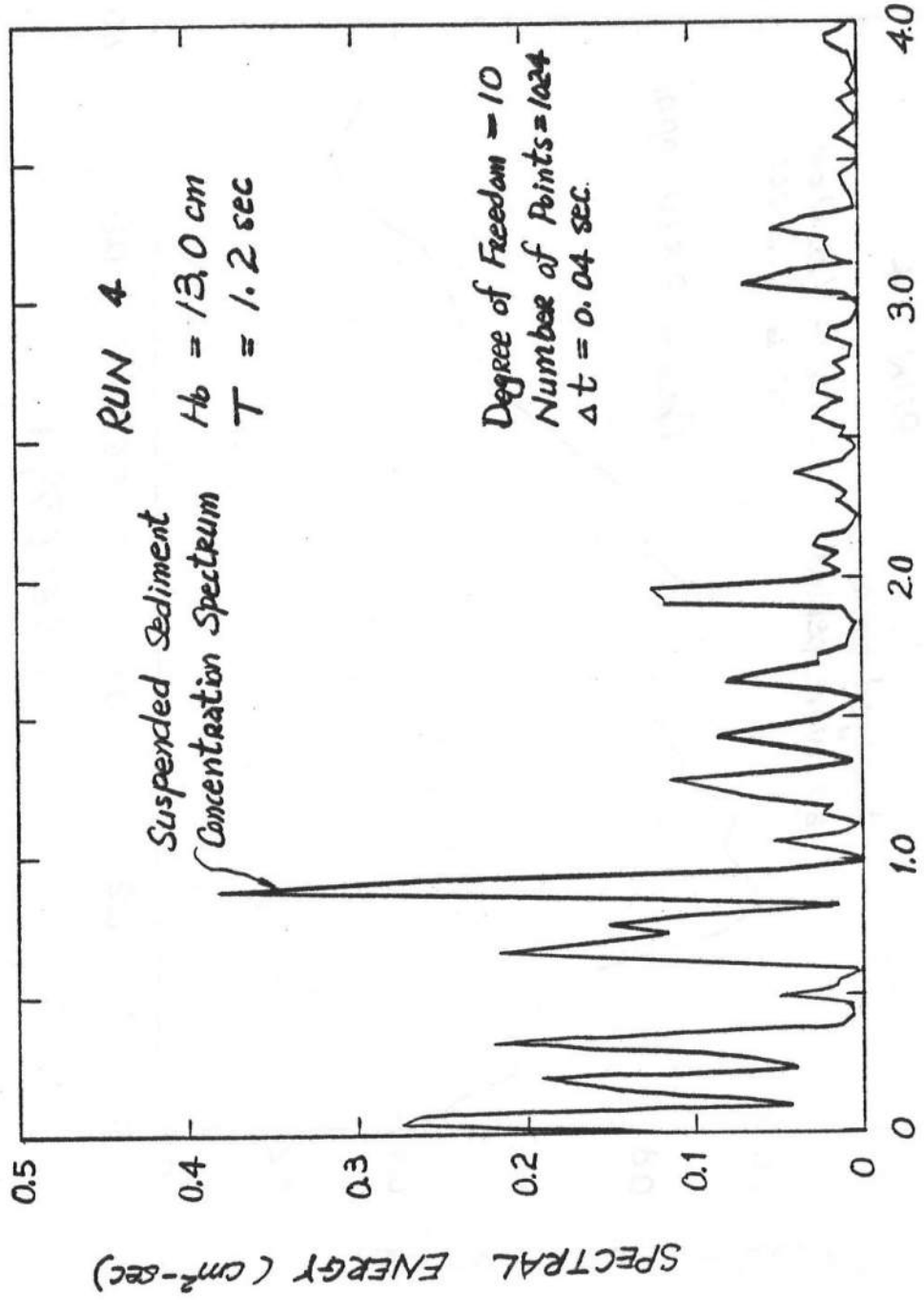

Figure C-15 Suspended Sediment Concentration Spectrum for Run 4

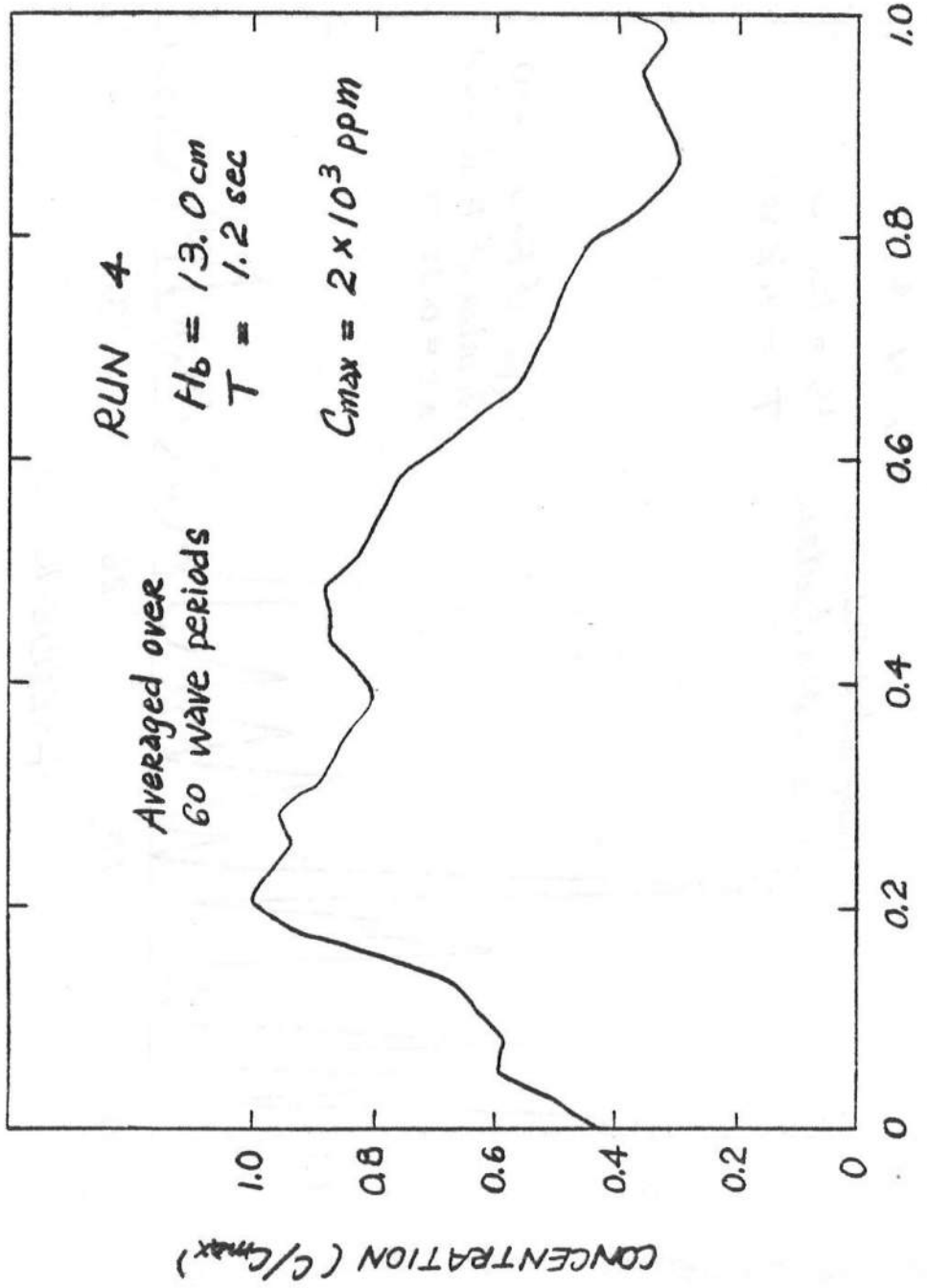

Figure C-16 Averaged Suspended Sediment Concentration for Run 4

APPENDIX D

WAVE SET-UP ON PLANE BEACH-
THEORY AND LABORATORY DATA

A. Set-Up Equations

Based on Longuet-Higgins (1963), the set-up equation can be expressed as:

$$\frac{\partial h}{\partial x} = \frac{-m}{1+3K^2/8} \qquad (D\text{-}1)$$

$$h = \frac{-m}{1+3K^2/8}x + h_b \qquad (D\text{-}2)$$

where $H_b = K h$ for spilling breaker and $h = d + \bar{\eta}$ (see Fig.D-1).

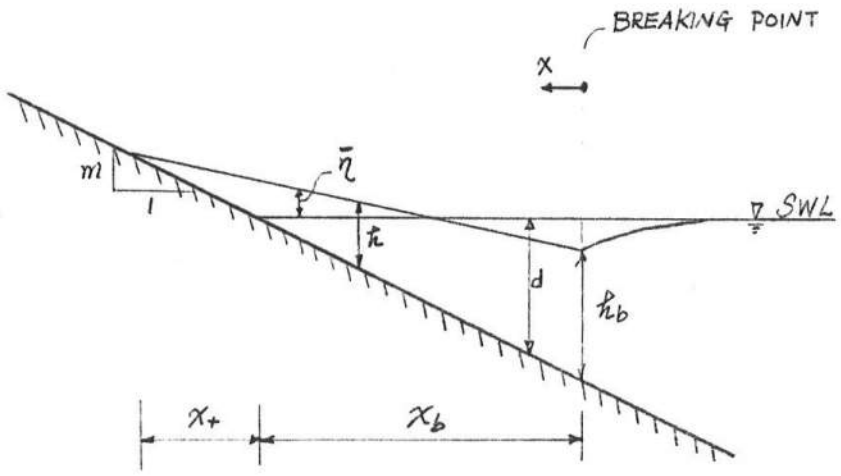

Figure D-1 Definition Sketch of Wave Set-up

At breaking point, x=0, we have

$$h = h_b$$

At still water level, $x=x_b$, we have

$$h_o = \frac{-m x_b}{1+3K^2/8} + h_b \qquad (D-3)$$

$$h_b = d_b - \frac{K^2 h_b}{16}, \text{ OR, } h_b = \frac{d_b}{1+K^2/16} \qquad (D-4)$$

$$h_o \approx d_b \left(\frac{1}{1+K^2/16} - \frac{1}{1+3K^2/8} \right) \approx d_b \left[\frac{5K^2}{16} \left(1 - \frac{5K^2}{16}\right) \right] \pm O(K^4)$$

OR, for the first approximation, (D-5)

$$h_o \approx h_b \cdot \frac{5K^2}{16} \left(1 - \frac{5K^2}{16}\right)$$

$$= \frac{5K^2}{16} \cdot H_b \left(1 - \frac{5K^2}{16}\right) \qquad (D-6)$$

B. Laboratory Data

Three sets of laboratory wave set-up data were reduced from the water elevation data, corresponding to Run No. 5,6,7 in Table 4-1. The wave and beach conditions of these three runs represent typical spilling breaker. The measured set-ups are summarized in Table D-1 and compared with the theoretical predictions shown in Figures D-2, D-3 and D-4.

Table D-1 Laboratory Wave Set-up Data

Run No.	Wave Condition			Local Water Depth (d+), cm		
	H_c(cm)	H_b(cm)	T(sec)	ST.190	ST.210	ST.230
5	10.0	11.5	1.2	5.1	6.3	8.0
6	11.0	12.5	1.0	4.8	6.1	7.8
7	10.5	11.5	1.0	4.6	5.9	7.3

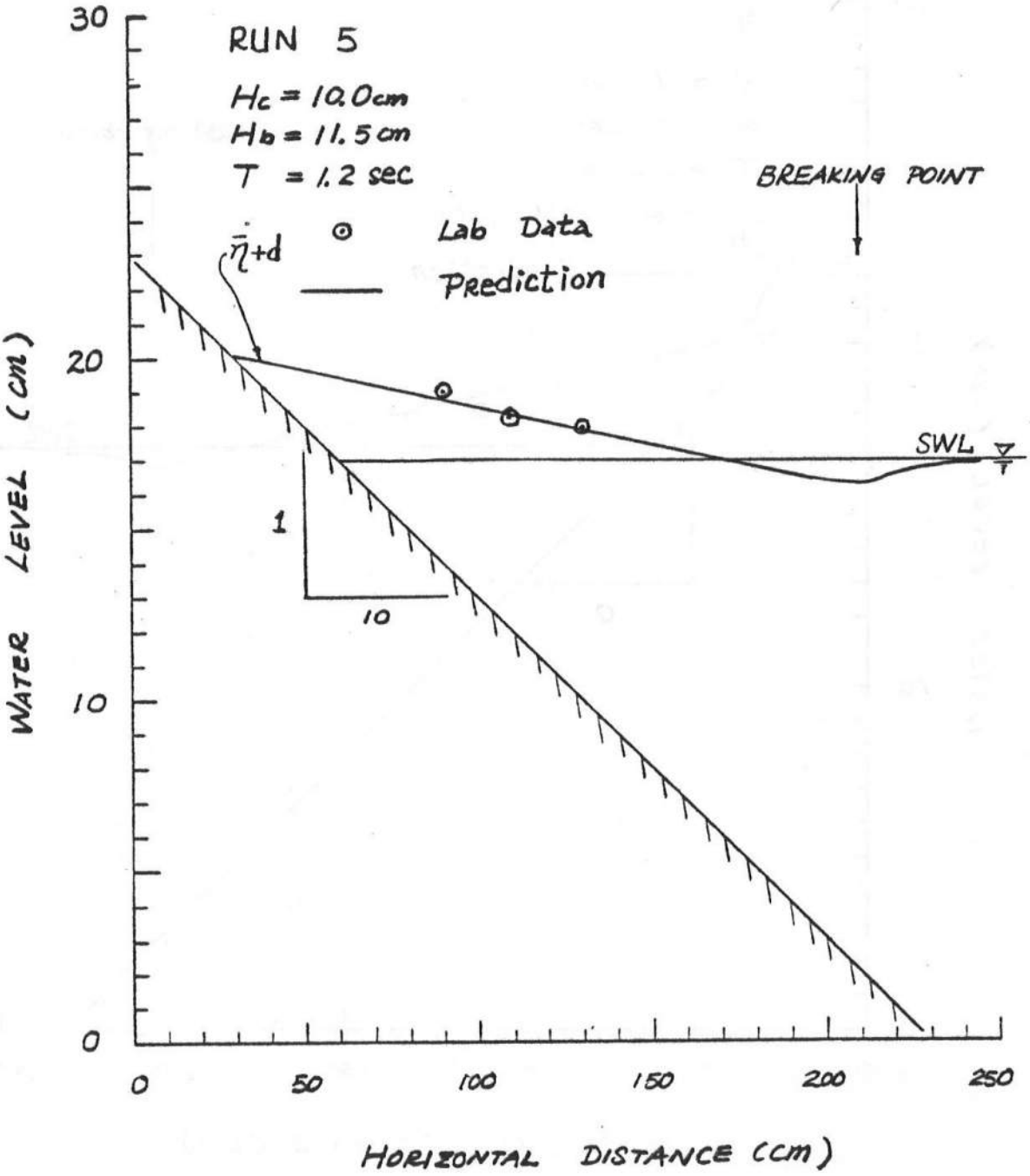

Figure D-2 Wave Run-up Data for Run 5

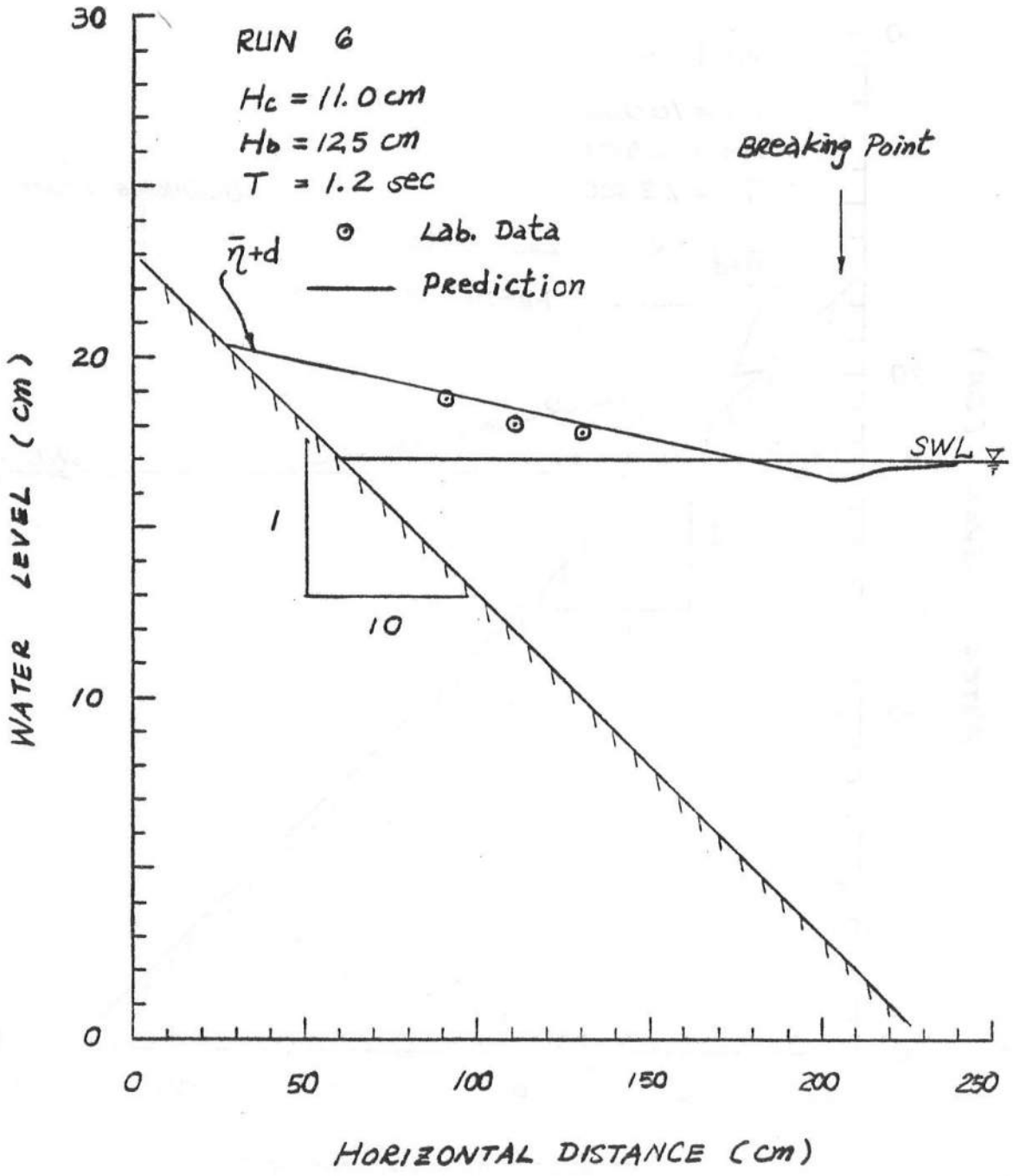

Figure D-3 Wave Run-up Data for Run 6

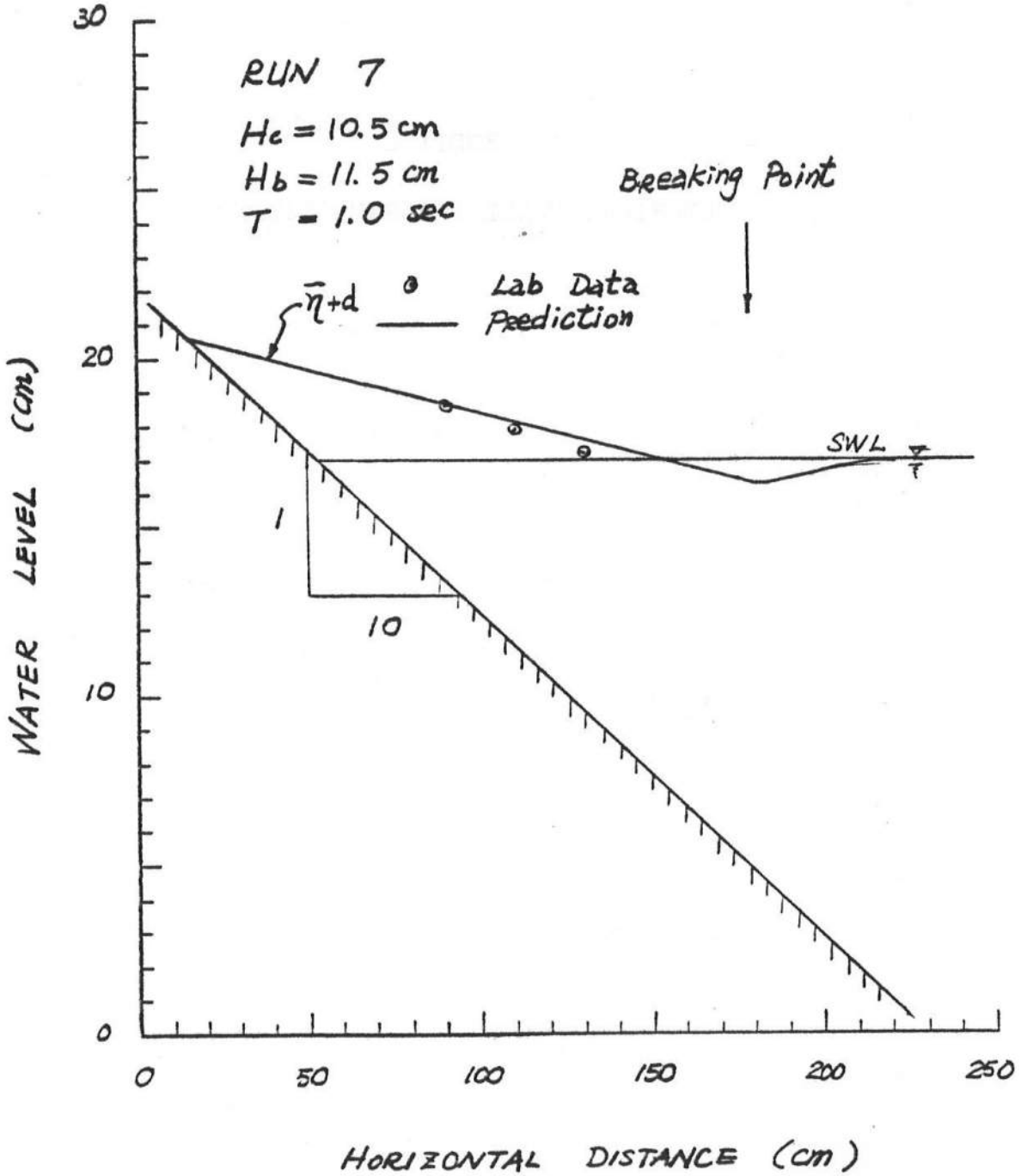

Figure D-4 Wave Run-up Data for Run 7

APPENDIX E

NUMERICAL MODEL PROGRAM LISTING

```
100 $RESET FREE
110 $SET AUTOBIND
120 FILE  6(MAXRECSIZE=22)
130       DIMENSION C(20),T(20),XP(20)
140       COMMON X(2001),Y(2001,20),N
150       COMMON/B1/G,PI,PI2
160       COMMON/B2/XB,YB,XWL,AY0,XPL,YPL
170       COMMON/B3/IPL,IB,IWL,SWL,CKAP
180       COMMON/B4/GS,PO,DM
190       COMMON/B5/WML(2001,20),Q(20)
200 C***
210 C***  INPUT NUMERICAL CONSTANTS
220 C***
230       G=980.62
240       PI=3.1416
250       PI2=2.*PI
260       GS=2.65
270       PO=0.45
280 C*    G=GRAVITATIONAL ACCELERATION (CM/SEC**2)
290 C*    GS=SEDIMENT GRAIN DENSITY (GRAM/CM**3)
300 C*    PO=SEDIMENT POROSITY
310 C***
320 C***  INPUT X,Y COORDINATE AND INITIAL SLOPE
330 C***
340       DX=2.5
350       YMAX=60.
360       WRITE(6,602)
370 602   FORMAT(1X,"TYPE 1 FOR 1/10 SLP,2 FOR 1/15 SLP,
380      1       3 FOR 1/20 SLP")
390       READ(5,/) ISLP
400       IF(ISLP.EQ.1) GO TO 1
410       IF(ISLP.EQ.2) GO TO 2
420       IF(ISLP.EQ.3) GO TO 3
430 1     XMAX=600.
440       SWL=30.
450       SLP=1./10.
460       N=XMAX/DX
470       DO 11 I=1,N
480 11    Y(I,1)=YMAX-0.8*(DX*(I-1))**0.6667
490       GO TO 5
500 2     XMAX=700.
510       SWL=35.
520       SLP=1./15.
530       N=XMAX/DX
540       DO 12 I=1,N
550 12    Y(I,1)=YMAX-0.7*(DX*(I-1))**.6667
560       GO TO 5
570 3     XMAX=800.
580       SWL=40.
590       SLP=1./20.
600       N=XMAX/DX
```

```
      DO 13 I=1,N
13    Y(I,1)=YMAX-0.6*(DX*(I-1))**0.6667
5     CONTINUE
      DO 14 I=1,N
      X(I+1)=X(I)+DX
14    Y(I,2)=Y(I,1)
C*    YMAX=MAXIMUM BEACH ELEVATION (CM)
C*    SWL=SEA WATER LEVEL (CM)
C*    N=NUMBER OF DISTANCE INCREMENTS
C***
C***  INPUT WATER LEVEL,SEDIMENT SIZE, EROSION TIME
C***
15    WRITE(6,604)
604   FORMAT(1X,"RN,","DM,","DT,","NDT,")
      READ(5,/)RN,DM,DT,NDT
C*    RN=RUN NUMBER, IF SWL CHANGED, RN ALSO CHANGE
C*    DM=MEDIAN GRAIN SIZE (MM)
C*    DT=DURATION OF TIME FOR BEACH EVO. (HOUR)
C*    NDT=NUMBER OF DT DESIRED
C***
C***  INPUT INCIPIENT WAVE INFORMATION
C***
      WRITE(6,606)
606   FORMAT(1X,"HB,","DB,","PER,")
      READ(5,/) HB,DB,PER
      CKAP=HB/DB
C*    HB=BREAKING WAVE HEIGHT AT BREAKING POINT (CM)
C*    DB=WATER DEPTH AT BREAKING POINT (CM)
C*    PER=INCIDENT WAVE PERIOD (SECOND)
C***
C***  COMPUTE BEACH EVOLUTION IN DT*NDT
C***
      YB1=SWL-DB
      CALL XYCORD(1,XB,YB1,IB,1)
      DO 20 J=3,NDT+2
C*    COMPUTE WAVE SET-UP
      J=J-1
      CALL WAVSUP(XB,AYB,AY0,XPL,J)
      XPL=XB-XPL
       XP(J)=XPL
       YB=YB1+AYB
C*     FIND N'TH INCREMENT AT SEA WATER LEVEL
       CALL XYCORD(1,XWL,SWL,IR,J)
       IWL=IR
C*     FIND N'TH INCREMENT AT RUN-UP LIMIT AND YPL
       CALL XYCORD(0,XPL,YIR,IR,J)
       YPL=YIR
       IPL=IR
       SUP=(YPL-YB)/(DX*(IB-IPL))
       J=J+1
       DO 25 I=IPL,IB
```

```
1120 25     WML(I,J)=YPL-SUP*DX*(I-IPL)
1130        DO 30 I=IB+1,N
1140 30     WML(I,J)=SWL
1150 C*     COMPUTE EROSION RATE IN DT
1160        CALL BEHEVO(J,N,DT,DX,PER)
1170        T(1)=0.
1180        T(J)=(J-2)*DT
1190 20     CONTINUE
1200 C*     OUTPUT TO PRINTER OR PLOTTER
1210        WRITE(6,608)
1220 608    FORMAT(1X,"TYPE 0 FOR PRINT OUT, 1 FOR PLOTTER")
1230        READ(5,/)ID
1240        IF(ID.EQ.1) GO TO 40
1250        WRITE(6,6010) RN
1260 6010   FORMAT(10X,"RUN NUMBER=",I3)
1270        WRITE(6,6020) HB
1280 6020   FORMAT(10X,"BREAKING WAVE HEIGHT (CM)=",F5.1)
1290        WRITE(6,6030) PER
1300 6030   FORMAT(10X,"WAVE PERIOD (SEC)=",F5.1)
1310        WRITE(6,6040) SLP
1320 6040   FORMAT(10X,"INITIAL SLOPE=",F5.2)
1330        WRITE(6,6050) DM
1340 6050   FORMAT(10X,"MEDIAN GRAIN SIZE (MM)=",F5.2)
1350        WRITE(6,6060)
1360 6060   FORMAT(10X,"ERODING TIME(HOUR)",2X,"ERODED VOL(CM)")
1370        WRITE(6,6070) ((T(J),Q(J)),J=3,NDT+2)
1380 6070   FORMAT(2F20.2)
1390        WRITE(6,/) (XP(J),J=2,NDT+2)
1400        DO 50 J=2,NDT+2
1410        WRITE(6,6080) T(J)
1420 6080   FORMAT(//,1X,"ERODING TIME=",I5,//)
1430        WRITE(6,6085) XP(J-1)
1440 6085   FORMAT(1X,"ERODING DIST.= ",F10.1,//)
1450        DO 50 K=IPL,IB,10
1460        WRITE(6,6090) (X(I),I=K,K+9)
1470 6090   FORMAT(1X,"X= ",10F7.1)
1480        WRITE(6,6100) (Y(I,J),I=K,K+9)
1490 6100   FORMAT(1X,"Y= ",10F7.1,/)
1500 50     CONTINUE
1510 40     CONTINUE
1520 C*     OPTION FOR SWL CHANGE
1530        WRITE(6,610)
1540 610    FORMAT(1X,"TYPE 0 FOR STOP, 1 FOR SWL CHANGE")
1550        READ(5,/) ISW
1560        IF(ISW.EQ.0) GO TO 60
1570        DO 70 I=1,N
1580        Y(I,1)=Y(I,J)
1590        Y(I,2)=Y(I,J)
1600 70     CONTINUE
1610        GO TO 15
1620 60     STOP
```

```
1630          END
1640  C***
1650  C***
1660          SUBROUTINE WAVSUP(XB,AYB,AY0,XPL,J)
1670  C***
1680  C***
1690  C*      THIS SUBROUTINE COMPUTES WAVE SETUP IN SURF
1700  C*      AYB=SETUP AT BREAKING POINT (ABOVE SWL)
1710  C*      AY0=SETUP AT SWL (ABOVE SWL)
1720  C*      XPL=X-CORD. AT RUNUP LIMIT
1730          COMMON X(2001),Y(2001,20)
1740          COMMON/B3/IPL,TR,TWL,SWL,CKAP
1750          CALL XYCORD(0,XB,YTR,TR,J)
1760          DB=SWL-YTR
1770          CALL XYCORD(1,XTRN,SWL,TR,J)
1780          S=DB/(XB-XTRN)
1790          AYB=S*(XB-XTRN)/(1.+CKAP**2/16.)
1800          AY0=AYB*(1.-5.*CKAP**2/16.)*(1.+CKAP**2/16.)
1810         1    *(5.*CKAP**2/16.)
1820          XPL=(XB-XTRN)*(1.+EXP(-0.6*(J-2))*5.*CKAP**2/16.)
1830          RETURN
1840          END
1850  C***
1860  C***
1870          SUBROUTINE  BEHEVO(J,N,DT,DX,PER)
1880  C***
1890  C***
1900  C*      THIS SUBROUTINE COMPUTES TRANSPORT RATES
1910  C*      AND BEACH EVOLUTION
1920          DIMENSION DQ(2001,20),DY(2001,20)
1930          COMMON X(2001),Y(2001,20)
1940          COMMON/B1/G,PI,PI2
1950          COMMON/B2/XB,YB,XWL,AY0,XPL,YPL
1960          COMMON/B3/IPL,TR,TWL,SWL,CKAP
1970          COMMON/B4/GS,PO,DM
1980          COMMON/B5/WML(2001,20),Q(20)
1990  C*      INPUT NUMBER OF WAVE PERIODS EACH ITERATION
2000          WRITE(6,612)
2010  612     FORMAT(1X,"NO. OF WAVE PERIODS EACH ITER.")
2020          READ(5,/) CIN
2030          NIT=INT(360.*DT/(PER*CIN))
2040          DO 10 I=1,N
2050  10      Y(I,J)=Y(I,J-1)
2060          DO 15 I=1,IPL-1
2070  15      WML(I,J)=Y(I,J)
2080  C*      COMPUTE TRANSPORT EQUATION
2090          AE=1.
2100          CK=0.01
2110          CU=0.25
2120          CD=1.5
2130          VF=SQRT(4.*G*(DM/10.)*(GS-1.)/(3.*CD))
```

```
2140          ACKH=(CK*CKAP*CU*G**1.5)/(4.*AF*VF**2)
2150          DO 20 K=1,NIT
2160          DO 20 I=IPL+1,IB-1
2170          ADH1=(Y(I-1,J)-Y(I+1,J))/(2.*DX)
2180          IF(ADH1.LE.0.) ADH1=0.00001
2190          ADH2=((WML(I+1,J)-Y(I+1,J))**1.5-(WML(I-1,J)
2200         1      -Y(I-1,J))**1.5)
2210          AEXP=EXP(-2.*AF*VF/SQRT(CKAP*G*ADH1))
2220          DQ(I,J)=0.5*ACKH*(1.-AEXP)*(ADH2*ADH1)*(CTN*PER)
2230          Q(J)=Q(J)+DQ(I,J)
2240          DY(I,J)=DQ(I,J)/(DX*GS*(1.-PO))
2250          Y(I,J)=Y(I,J)-DY(I,J)
2260          Y(IPL,J)=Y(IPL+1,J)
2270  C*      SMOOTH THE BEACH PROFILE USING HANNING WINDOW
2280          CALL SMOOTH(J)
2290  20      CONTINUE
2300  C*      SET UP OFFSHORE BAR ASYMMETRIC TO BEACH PROFILE
2310          IBP=IB-IPL-1
2320          DO 30 I=1,IBP
2330          DDY=Y(IB-I,J-1)-Y(IB-I,J)
2340          Y(IB+I,J)=Y(IB+I,J)+DDY
2350  30      CONTINUE
2360          RETURN
2370          END
2380  C***
2390  C***
2400          SUBROUTINE XYCORD(IND,XIR,YIR,IR,J)
2410  C***
2420  C***
2430  C*      THIS SUBROUTINE FINDS Y-CORD GIVEN X-CORD
2440  C*      AND VICE VERSA
2450  C*      IF IND=0,GIVEN X-CORD TO FIND Y-CORD
2460  C*      IF IND=1,GIVEN Y-CORD TO FIND X-CORD
2470          COMMON X(2001),Y(2001,20),N
2480          IF(IND.EQ.1) GO TO 30
2490          DO 10 I=1,N
2500          IF((XIR-X(I)).LE.0.) GO TO 20
2510  10      CONTINUE
2520  20      IR=I
2530          YIR=Y(IR,J)
2540          RETURN
2550  30      DO 40 I=1,N
2560          IF((YIR-Y(I,J)).GE.0.) GO TO 50
2570  40      CONTINUE
2580  50      IR=I
2590          XIR=X(IR)
2600          RETURN
2610          END
2620  C***
2630  C***
2640          SUBROUTINE SMOOTH(J)
```

Distribution

Office of Naval Research
Coastal Science Program
Code 42205
Arlington, VA 22217

Defense Documentation Center
Cameron Station
Alexandria, VA 22314

Director, Naval Research Lab.
ATTN: Technical Information Officer
Washington, D. C. 20375

Director
Office of Naval Research Branch Office
1030 East Green Street
Pasadena, CA 91101

Chief of Naval Research
Code 100M
Office of Naval Research
Arlington, VA 22217

Office of Naval Research
Operational Applications Division
Code 200
Arlington, VA 22217

Office of Naval Research
Scientific Liaison Officer
Scripps Institution of Oceanography
La Jolla, CA 92093

Director Naval Research Laboratory
ATTN: Library, Code 2628
Washington, D. C. 20375

ONR Scientific Liaison Group
American Embassy - Room A-407
APO San Francisco, CA 96503

Commander
Naval Oceanographic Office
ATTN: Library, Code 1600
Washington, D. C. 20374

Naval Oceanographic Office
Code 3001
Washington, D. C. 20374

Chief of Naval Operations
OP 987P1
Department of the Navy
Washington, D. C. 20350

Oceanographer of the Navy
Hoffman II Building
200 Stovall Street
Alexandria, VA 22322

Naval Academy Library
U. S. Naval Academy
Annapolis, MD 21402

Commanding Officer
Naval Coastal Systems Laboratory
Panama City, FL 32401

Director
Coastal Engineering Research Center
U. S. Army Corps of Engineers
Kingman Building
Fort Belvoir, VA 22060

Officer in Charge
Environmental Research Prodctn Felty.
Naval Postgraduate School
Monterey, CA 93940

Director
Amphibious Warfare Board
U. S. Atlantic Fleet
Naval Amphibious Base
Norfolk, Little Creek, VA 23520

Commander, Amphibious Force
U. S. Pacific Fleet
Force Meteorologist
Comphibpac Code 25 5
San Diego, CA 93155

Librarian, Naval Intelligence
Support Center
4301 Suitland Road
Washington, D. C. 20390

Commanding Officer
Naval Civil Engineering Laboratory
Port Hueneme, CA 93041

Chief, Wave Dynamics Division
USAE-WES
P. O. Box 631
Vicksburg, MS 39180

Commandant
U. S. Coast Guard .
ATTN: GECV/61
Washington, D. C. 20591

Office of Research and Development
%DS/62
U. S. Coast Guard
Washington, D. C. 20591

National Oceanographic Data
Center %D764
Environmental Data Services
NOAA
Washington, D. C. 20235

Prof. Dr. Fuehrboeter
Lehrstuhl F. Hydromechanik U. Kuestenw
Technische Hochschule Braunschweig
Beethovenstrasse 51A
D-3300 Braunschweig, West Germany

Prof. Dr. Walter Hansen
Direktor D. Instituts F. Meereskunde
Universitaet Hamburg
Heimhuderstrasse 71
D-2000 Hamburg 13, West Germany

Prof. Dr. Klaus Hasselmann
Institut F. Geophysik
Universitaet Hamburg
Schleuterstrasse 22
D-2000 Hamburg 13, West Germany

Coastal Studies Institute
Louisiana State University
Baton Rouge, LA 70803

Dr. Edward Thornton
Department of Oceanography
Naval Postgraduate School
Monterey, CA 93940

Dr. Douglas I. Inman
University of California A-009
Shore Processes Laboratory
La Jolla, CA 92093

Dr. Bruce Heyden
Dept. of Environmental Sciences
University of Virginia
Charlottesville, VA 22903

SECURITY CLASSIFICATION OF THIS PAGE (When Data Entered)

REPORT DOCUMENTATION PAGE		READ INSTRUCTIONS BEFORE COMPLETING FORM
1. REPORT NUMBER ONR TR. No. 12	2. GOVT ACCESSION NO.	3. RECIPIENT'S CATALOG NUMBER
4. TITLE (and Subtitle) Surf Zone Properties and On/Offshore Sediment Transport		5. TYPE OF REPORT & PERIOD COVERED 6. PERFORMING ORG. REPORT NUMBER
7. AUTHOR(s) Wei-Chong Yang and Hsiang Wang		8. CONTRACT OR GRANT NUMBER(s) N00014-81-K-0297
9. PERFORMING ORGANIZATION NAME AND ADDRESS		10. PROGRAM ELEMENT, PROJECT, TASK AREA & WORK UNIT NUMBERS
11. CONTROLLING OFFICE NAME AND ADDRESS Department of Civil Engineering University of Delaware, Newark, DE 19711		12. REPORT DATE June 1982 13. NUMBER OF PAGES 201
14. MONITORING AGENCY NAME & ADDRESS(if different from Controlling Office)		15. SECURITY CLASS. (of this report) 15a. DECLASSIFICATION/DOWNGRADING SCHEDULE

16. DISTRIBUTION STATEMENT (of this Report)

This report has been approved for public release and sale; its distribution is unlimited.

17. DISTRIBUTION STATEMENT (of the abstract entered in Block 20, if different from Report)

18. SUPPLEMENTARY NOTES

19. KEY WORDS (Continue on reverse side if necessary and identify by block number)

Surf zone, sediment transport, coastal process, nearshore modeling.

20. ABSTRACT (Continue on reverse side if necessary and identify by block number)

The surf zone properties and the on/offshore sediment transport rate were studied in the laboratory. A non-dimensional surf zone parameter defined as the ratio of the natural swash period to the wave period was found to be pertinent to a variety of surf zone phenomena. A similarity solution was proposed to describe the flow characteristics inside the surf zone. Finally, a numerical model was developed to predict on/offshore sediment transport.

DD FORM 1 JAN 73 1473 EDITION OF 1 NOV 65 IS OBSOLETE

Unclassified

SECURITY CLASSIFICATION OF THIS PAGE (When Data Entered)